MOLECULAR AND METABOLIC REGULATION OF CELL DEATH IN CD8$^+$ T CELL SUBSETS

by

Sasha E. Larsen Akins

Dissertation submitted to the Faculty of the
Emerging Infectious Diseases Graduate Program
Uniformed Services University of the Health Sciences
In partial fulfillment of the requirements for the degree of
Doctor of Philosophy 2016

UNIFORMED SERVICES UNIVERSITY, SCHOOL OF MEDICINE GRADUATE PROGRAMS
Graduate Education Office (A 1045), 4301 Jones Bridge Road, Bethesda, MD 20814

FINAL EXAMINATION/PRIVATE DEFENSE FOR THE DEGREE OF DOCTOR OF PHILOSOPHY
IN THE EMERGING INFECTIOUS DISEASES GRADUATE PROGRAM

Name of Student: Sasha Larsen

Date of Examination: April 4, 2016
Time: 1:30 PM
Place: C2015

DECISION OF EXAMINATION COMMITTEE MEMBERS:

	PASS	FAIL
Joseph Mattapallil, PhD DEPARTMENT OF MICROBIOLOGY AND IMMUNOLOGY Committee Chairperson	✓	
Andrew Snow, PhD DEPARTMENT OF PHARMACOLOGY AND MOLECULAR THERAPEUTICS Dissertation Advisor	✓	
Edward Mitre, MD DEPARTMENT OF MICROBIOLOGY AND IMMUNOLOGY Committee Member	✓	
Brian Schaefer, PhD DEPARTMENT OF MICROBIOLOGY AND IMMUNOLOGY Committee Member	✓	
Pamela Schwartzberg, PhD NIH Committee Member	✓	

UNIFORMED SERVICES UNIVERSITY, SCHOOL OF MEDICINE GRADUATE PROGRAMS
Graduate Education Office (A 1045), 4301 Jones Bridge Road, Bethesda, MD 20814

APPROVAL OF THE DOCTORAL DISSERTATION IN THE EMERGING INFECTIOUS DISEASES GRADUATE PROGRAM

Title of Dissertation: "Molecular and Metabolic Regulation of Cell Death in CD8+ T cell subsets"

Name of Candidate: Sasha Larsen
Doctor of Philosophy
April 4, 2016

DISSERTATION AND ABSTRACT APPROVED:

DATE:

Joseph Mattapallil, PhD — 4/4/16
DEPARTMENT OF MICROBIOLOGY AND IMMUNOLOGY
Committee Chairperson

Andrew Snow, PhD — 4/4/2016
DEPARTMENT OF PHARMACOLOGY AND MOLECULAR THERAPEUTICS
Dissertation Advisor

Edward Mitre, MD — 4/4/2016
DEPARTMENT OF MICROBIOLOGY AND IMMUNOLOGY
Committee Member

Brian Schaefer, PhD — 4/4/16
DEPARTMENT OF MICROBIOLOGY AND IMMUNOLOGY
Committee Member

Pamela Schwartzberg, PhD — 4-4-16
NIH
Committee Member

ACKNOWLEDGMENTS

Andrew Snow for his scientific wisdom, unparalleled optimism and constant faith in my ability to succeed. I am truly fortunate and eternally grateful to have had such excellent mentorship.

Gil Katz, Jeff Stinson, Swadhinya Arjunaraja and Kelsey Voss for such a wonderful work environment. A truly collegial and collaborative group is a rare thing and I'm thankful to have spent my time amongst such fine scientists.

My Committee: Joseph Mattapallil, Brian Schaefer, Ed Mitre, and Pamela Schwartzberg for their generosity of time, guidance and encouragement.

The USUHS BIC flow cytometry core, specifically Kateryna Lund for teaching me flow cytometry and the seemingly endless hours spent sorting rare populations of memory cells.

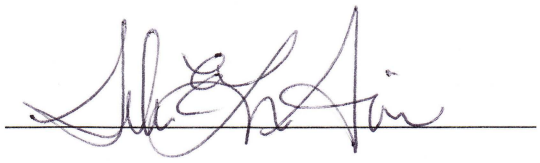
Cara Olsen for her expertise and patience while teaching me the proper methods and applications of statistical analysis.

DEDICATION

To Cole, for all of our grand adventures past present and future.

COPYRIGHT STATEMENT

The author hereby certifies that the use of any copyrighted material in the dissertation manuscript entitled: "Molecular and Metabolic regulation of cell death in $CD8^+$ T cell subsets" is appropriately acknowledged and, beyond brief excerpts, is with the permission of the copyright owner.



Sasha E. Larsen Akins

ABSTRACT

Dissertation:

Molecular and Metabolic Regulation of Cell Death in $CD8^+$ T cell Subsets

Sasha E. Larsen Akins, Doctor of Philosophy, 2016

Thesis directed by:

Andrew L. Snow, Ph.D.

Assistant Professor, Department of Pharmacology

Cellular $CD8^+$ T cell immunity is responsible for fighting intracellular pathogens and generating a long lasting memory pool for improved control of subsequent infections. During primary and secondary T cell responses, activated effector T cells rapidly proliferate to control an invading pathogen. However, T cell expansion must be constrained and counterbalanced through programmed cell death to cull excess cells and prevent unintended collateral damage to the host. Two major pathways of programmed cell death eliminate activated effector T cells: restimulation induced cell death (RICD) and cytokine withdrawal induced cell death (CWID). The primary focus of this work was to define new molecular and metabolic determinants of differential apoptosis sensitivity via comparative analysis of primary human $CD8^+$ T cells. First, we identify a critical role for diacylglycerol kinase α (DGKα) in modulating TCR signaling in SAP-deficient T cells, which we previously showed are resistant to RICD. Loss of the adaptor

protein SAP causes X-linked lymphoproliferative disease (XLP-1). Without SAP, we found that hyperactive DGKα depleted the key second messenger diacylglycerol, attenuating the TCR signal below the threshold required to induce expression of specific pro-apoptotic molecules of the nuclear-orphaned receptor family. Importantly, we showed that pharmacological inhibition of DGKα restored RICD sensitivity in primary XLP-1 patient T cells. This work offers a new therapeutic approach for reversing acute, often lethal $CD8^+$ T cell accumulation. Second, we describe here a direct influence for glycolytic metabolism on RICD sensitivity of $CD8^+$ effector T cells. Specifically, acute glucose availability and active glycolysis promoted *de novo* expression of Fas-ligand after TCR restimulation. For the first time, these data indicate an explicit role for metabolic reprogramming in licensing RICD in activated effector T cells. Those effector T cells that survive the contraction phase of an immune response make up the memory population reserved to provide long lasting immunity. Memory T cells are classified into distinct subsets based on the differential expression of cell surface molecules, anatomic location, and discrete functional capabilities. Lastly we show that greater effector T cell accumulation derived from central memory (CM) T cells is likely due to an autophagy-mediated resistance to CWID, compared to effector memory (EM) T cells. Overall, this dissertation work highlights the translational potential of controlling molecular and metabolic determinants of cell death sensitivity in order to manipulate the magnitude of a T cell response.

TABLE OF CONTENTS

LIST OF TABLES xi

LIST OF FIGURES xii

CHAPTER 1: Introduction 2

T cell homeostasis 2
Restimulation-induced cell death: RICD 5
Cytokine withdrawal-induced cell death: CWID 10
$CD8^+$ Memory T cells 14
Subsets of CD8+ Memory 16
Memory and Cell Death 20
T cell Metabolism 21
Summary 24

CHAPTER 2: Inhibition of diacylglycerol kinase α restores restimulation-induced cell death and reduces immunopathology in XLP1 26

Abstract 27
Introduction 28
Materials and Methods 31
Study Design 31
Cell Culture 31
siRNA transfections 32
Immunofluorescence experiments with primary T cells 32
Cytofluorimetry 33
Conjugation and live-cell imaging of Jurkat T-cells 33
Western Blotting 35
Quantitative RT-PCR 35
CTL assays for autologous T cells 35
Soluble FasL ELISA 36
Overexpression of DGKα/DGKζ in primary T cells 37
Mice and in vivo experiments 37
In vitro stimulation of mouse splenocytes 37
Assessment of tissue histology in LCMV-infected mice 38
Assessment of LCMV viral titers 38
Statistical analysis 39
Study approval 39
Results 40
DGKα inhibition rescues RICD in SAP-deficient T cells 40
Inhibition of DGKα rescues defective DAG polarization and signaling at the IS in SAP-deficient cells 48

NUR77 and NOR1 mediate the rescue of RICD that is induced by DGKα inhibition in SAP-deficient T cells 61
DGKα inhibition reduces $CD8^+$ T cell accumulation and activation in LCMV-infected Sh2d1a -/- mice 67
Discussion 78

CHAPTER 3: Sensitivity to restimulation-induced cell death is linked to glycolytic metabolism in human T cells 128

Abstract 128
Introduction 130
Materials and Methods 132
Isolation, activation and culture of primary human $CD8^+$ T cells 132
Apoptosis assays and flow cytometry 132
Western blotting 133
ELISA 134
Statistics 134
Results 135
Discussion 150

CHAPTER 4: Differential CWID sensitivity of effector T cells derived from distinct human $CD8^+$ memory subsets 152

Abstract 152
Introduction 153
Materials and Methods 156
Isolation, activation and culture of primary human CD8+ T cells 156
Apoptosis assays and flow cytometry 156
Western blotting 157
ELISA 158
Results 159
EmE T cells are more sensitive to CWID than CmE T cells 159
Differential CWID sensitivity is not due to differences in IL-2 production nor IL2R expression 164
Higher basal expression and induction of BIM in EmE T cells 168
Differential phosphorylation of S6 between CmE and EmE during IL-2 withdrawal 171
CmE T cells demonstrate greater protective autophagy during CWID than EmE T cells 175
Discussion 178

CHAPTER 5: Discussion 182

Discussion 182
Determinants of RICD 182
Molecular 182
Metabolic 184
Memory phenotypes linked to cell death sensitivities 188

Summary 191
REFERENCES 193

APPENDIX A: Ratio of memory subsets at the time of isolation predict subsequent RICD sensitivity in derived effector $CD8^+$ T cells. 206

Introduction 206
Materials and Methods 208
Isolation, activation and culture of primary human CD8+ T cells 208
Apoptosis assays and flow cytometry 208
Western Blotting 209
2-dimensional differential gel electrophoresis 210
Statistics 210
Results 211
Discussion 227

LIST OF TABLES

Table 1. $CD8^+$ Memory T cells defined by surface marker, location and defining feature(s). 19
Table S1. siRNA sequences. 83
Table S2. TaqMan gene expression arrays. 83
Table S3. Spot densitometry analysis for western blotting 84
Table S4. Statistical analysis 85
Table 2. MS-MS results from top 8 spots. 223

LIST OF FIGURES

Figure 1. DGKα silencing or inhibition restores RICD in XLP-1 patient T cells. 42
Figure 2. DGKα silencing or inhibition restores RICD in SAP-silenced T cells. 44
Figure S1. Activity of DGKα and DGKζ contributes to RICD resistance in T cells.... 46
Figure 3. DGKα silencing or inhibition restores synapse formation in SAP-deficient T cells. 49
Figure 4. DGKα silencing or inhibition restores PKCθ and RasGRP1 recruitment to the IS in SAP-deficient cells. 52
Figure S4. Major steps of the automated segmentation and fluorescence quantification algorithm. 54
Figure 5. DGKα silencing restores TCR-induced PKCθ and Ras-mediated signaling pathways to drive RICD in SAP-deficient cells. 57
Figure S2. DGKα silencing restores RICD in SAP-deficient cells through PKCθ and Ras-mediated signaling pathways. 59
Figure S3. DGKα blockade fails to rescue TCR-induced upregulation of pro-apoptotic mediators FASL and BIM in SAP-deficient cells. 62
Figure 6. Silencing or inhibition of DGKα restores RICD sensitivity in SAP-deficient T cells via induction of pro-apoptotic molecules NUR77 and NOR1. 65
Figure 7. R59022 DGK inhibitor reduces the numbers of activated virus- specific $CD8^+$ T cells in LCMV-infected *Sh2d1a*$^{-/-}$ mice. 69
Figure 8. R59022 DGK inhibitor reduces the numbers but not incidence of virus-specific activated $CD8^+$ cytokine producing cells in the spleens of LCMV infected *Sh2d1a*$^{-/-}$ mice. 72
Figure S5. DGKα inhibition enhances SAP-deficient CD8+ T cell cytotoxicity against autologous B cell targets. 74
Figure S6. R59022 DGKα inhibitor does not impair viral clearance in the livers and spleens of LCMV infected *Sh2d1a*$^{-/-}$ mice. 76
Figure S7. Gating strategies used in Fig 7 and Fig 8 are presented above. 82
Figure 9. Increased RICD sensitivity in glycolytic $CD8^+$ T cells. 136
Figure 10. Acute glucose availability governs RICD sensitivity 140
Figure 11. Cell cycle progression and differential effector function do not contribute to differential RICD sensitivity in Glu vs. Gal T cells RICD sensitivity in glycolytic $CD8^+$ T cells. 144
Figure 12. Glycolysis enhances RICD specifically by facilitating FASL induction after TCR restimulation. 148
Figure 13. Activated human CM $CD8^+$ T cells give ride to more effectors over time compared to EM T cells. 160
Figure 14. EmE are more sensitive to CWID than CmE. 162
Figure 15. Differential CWID sensitivity is not due to different IL-2R expression nor IL-2 autocrine signaling between CmE and EmE. 166
Figure 16. Higher basal expression and induction of BIM make EmE more susceptible to CWID. 169
Figure 17. Differential phosphorylation of S6 between CmE and EmE T cells during IL-2 withdrawal 173

Figure 18. CmE demonstrate greater protective autophagy during CWID than EmE.... 176
Figure 19. EmE T cells are more sensitive to RICD than CmE T cells. 212
Figure 20. CM:EM ratio predicts the difference in subsequent RICD sensitivity between memory-derived effector T cells. 215
Figure 21. Higher basal LCK activity and sustained TCR-induced LCK phosphorylation in EmE relative to CmE. 218
Figure 22. Higher GAPDH expression in restimulated EmE T cells. 221
Figure 23. Greater RICD sensitivity of EmE is linked to glycolytic metabolism. 225

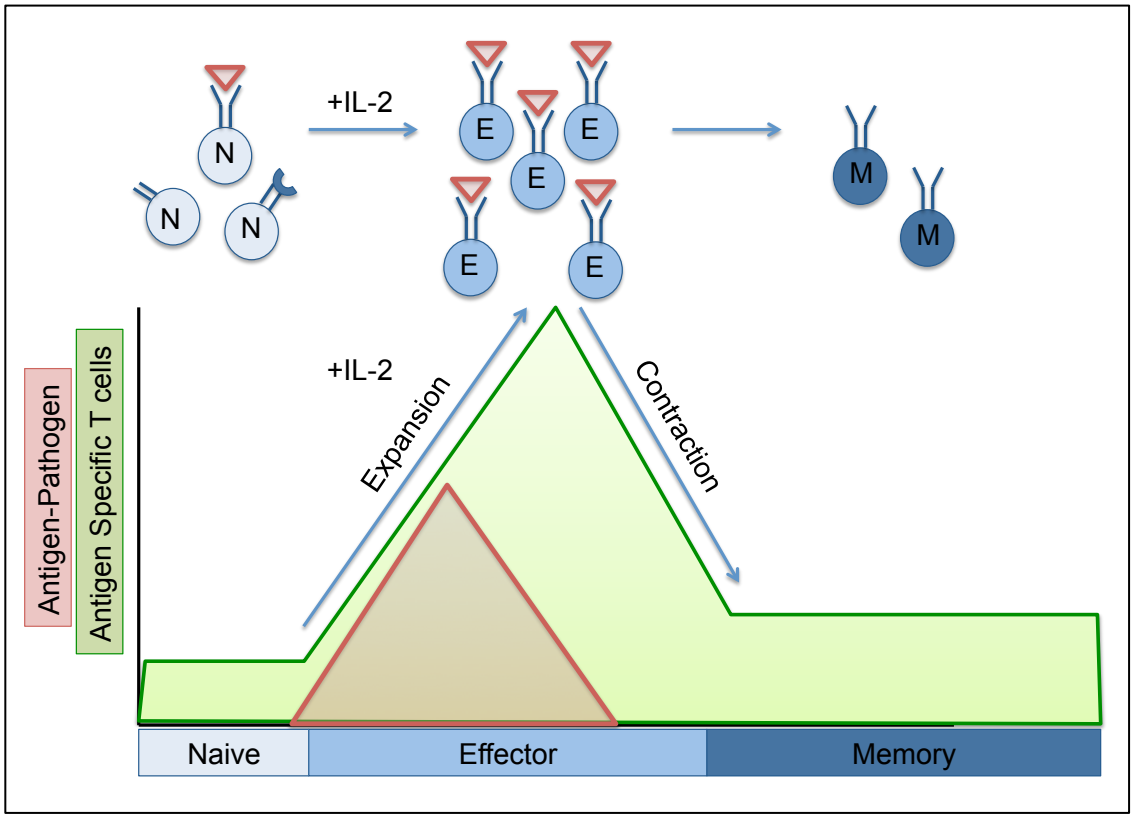
CHAPTER 1: Introduction

T CELL HOMEOSTASIS

The adaptive or acquired immune system is an integral component of the body's defense against foreign pathogens. Unlike the innate immune system that rapidly identifies general patterns or characteristics of pathogens (e.g. bacterial lipopolysaccharides), the adaptive immune system typically recognizes and responds to distinct, pathogen-derived protein antigen epitopes via clonal selection of lymphocytes bearing unique, highly specific antigen receptors. Additionally, the hallmark of a successful adaptive immune response is the generation of specific, lasting "memory" that can be sourced during a subsequent encounter to provide accelerated resolution of infection. The control and elimination of foreign organisms is achieved with humoral (antibody) responses and cell-mediated responses carried out by B and T lymphocytes, respectively. Whereas $CD4^+$ "helper" T cells orchestrate the adaptive response and provide assistance to other differentiating immune cells, $CD8^+$ cytolytic T lymphocytes (CTL) are specifically responsible for identifying and destroying cells infected with intracellular pathogens (e.g. viruses) and tumorigenic host cells.

During an intracellular infection, mature naïve $CD8^+$ T cells recognize specific pathogen-derived peptides presented on major histocompatibility complex I (MHC I) using their unique T cell receptor (TCR). Along with CD28 co-stimulation provided by antigen presenting cells, these $CD8^+$ T cells undergo activation and acquire potent effector functions used to control and eliminate the pathogen. Activated T cells receive a third signal from the autocrine/paracrine production of survival cytokine interleukin 2

(IL-2), which induces rapid proliferation and expansion of the activated effector pool. Activated effectors that subsequently encounter specific antigen on infected or tumorigenic cells will lyse that target cell in a contact-dependent manner. Generating a large effector population of T cells is critical for the control of foreign pathogens. However, it is equally necessary to restrain expansion and eventually contract the number of activated effectors as discussed below. Those cells that survive the contraction phase after the pathogen is cleared can transition into the memory pool, so that they can provide faster antigen specific responses to resolve future infections.



Along with activation and proliferation, cell death plays a critical role in shaping the cellular immune response and maintaining immune homeostasis. The majority of activated effector T cells need to be removed once an infection in cleared, and this occurs

through a cell death pathway known as apoptosis. Unlike necrosis, which involves unplanned cell damage and release of cellular contents that often results in inflammation, apoptosis is a systematic, genetically programmed process that results in tidy removal of dead cells via phagocytosis. In this manner, programmed cell death is a healthy ongoing process used for normal turnover of cells in the body. Apoptosis of T cells can be induced by either intrinsic (mitochondrial) or extrinsic (death receptor) signals, described in more detail below. Both types of stimuli ultimately induce activity of cysteine-aspartic acid protease (caspase) enzymes. Caspase cascade activity induces cleavage of nuclear proteins involved in chromatin condensation, as well as endonuclease activity and DNAse activity for ordered DNA fragmentation. Apoptosis results in the blebbing of small apoptotic bodies containing cellular contents that can be readily cleared in a non-inflammatory manner by phagocytes. Interestingly, not all effector T cells are equally sensitive and eliminated by programmed cell death; ideally a small pool of memory T cells survive contraction and confer long-lasting protection against a secondary infection.

Cell death sensitivity is often overlooked as a determinant of the magnitude and potency of a T cell response, overshadowed by proliferation rates and effector function profiles. However, well-studied disorders such as autoimmune lymphoproliferative syndrome (ALPS) demonstrate that defects in lymphocyte apoptosis can result in lymphoproliferation, autoimmunity and dysregulated control of effector T cell expansion (42; 54; 94). ALPS patients have mutations in the Fas death receptor signaling axis, which confers apoptosis resistance (42; 94; 134). Defects in apoptosis underscore the importance of T cell contraction to cull excess cells and prevent unintended “collateral damage” to the host. The two major pathways of programmed cell death that eliminate

activated effector T cells are restimulation induced cell death (RICD) and cytokine withdrawal induced cell death (CWID).

Restimulation-induced cell death: RICD

Restimulation-induced cell death (RICD), formerly known as activation-induced cell death (AICD), is defined as programmed death of effector T cells after second stimulation of the TCR by antigen. This phenomenon was initially described as a growth/cell cycle block in T cell hybridomas after antigen stimulation (7; 8). Subsequent studies in primary T cells showed that interleukin-2 (IL-2) was a critical component that 'predisposed' T cells to apoptosis (94). The initial studies of hybridomas were unable to detect this sensitivity dependence on IL-2, because the cells were immortalized and therefore not dependent on IL-2 to induce cell cycling. Researchers further examined the kinetics of cell death and determined that this antigen-induced death was a rapid process, detectible by cell shrinkage and DNA fragmentation as early as 3 hours post restimulation (196). Russell et al. showed that in a mixed T cell culture of different antigen specificities, stimulation with a single antigen only deleted those clones specific for the antigen with no bystander effects on the co-cultured clones (154). This suggested that the apoptotic program was only being induced in the cell specific for antigen, and not via indirect killing of neighboring cells. Additionally, researchers determined that this programmed cell death through TCR stimulation was specific for activated, cycling T cells, and did not apply to their naïve counterparts (154). Collectively, these early studies determined T cell RICD sensitivity has three requirements; 1) prior activation through the TCR, 2) cell cycle induction via IL-2, and 3) a subsequent strong restimulation through the TCR (174).

Execution of RICD is a multifactorial process that includes TCR-induced expression of death receptor ligand FASL, as well as the expression of pro-apoptotic B cell lymphoma-2 (Bcl-2) interacting mediator of cell death, BIM (19; 56; 175). While BIM targets mitochondrial membrane stability in order to induce cell death, surface expression of FASL is able to provide an extrinsic signal through the death receptor FAS and assembly of a death-inducing signaling complex (DISC)(19). Both signaling pathways converge upon the activation of downstream caspases, which in turn cleave many protein substrates for the execution of apoptosis. Stimulation through the TCR initiates signaling through proximal kinases like lymphocyte specific kinase (Lck) and the zeta-chain associated protein kinase 70 (Zap70), recruiting phospholipase C gamma 1(PLCγ1) to phosphorylated tyrosines in the integral membrane protein known as linker of activated T cells (LAT). Active PLCγ1 cleaves phosphadylinositol 4,5-biphosphate (PIP_2) in the plasma membrane, generating diacylglycerol (DAG) and inositol triphosphate (IP_3). DAG is a critical second messenger for protein kinase C theta (PKCθ) activation, which allows transcription factors like the nuclear factor in activated T cells (NF-AT) and nuclear factor kappa-light-chain enhancer of activated B cells (NF-κB) to enter the nucleus and likely enhance FASL transcription (86; 92; 105). Simultaneously, IP_3 allows release of Ca^{2+} from the endoplasmic reticulum which activates calcineurin to remove inhibitory phosphate groups on NF-AT (92). NF-AT, NF-κB and c-myc have all been identified as transcription factors that bind the FASL promoter and shown to be critical for expression of FASL (22; 86; 92; 105; 131). T cells from mice lacking PKCθ or NF-AT demonstrate significantly lower expression of FasL, and in the case of $PKC\theta^{-/-}$ also a reduction in RICD sensitivity compared to WT (92; 105). Conversely, FasL is

negatively regulated by nitric oxide and retinoic acid which preclude NF-AT from entering the nucleus (86). Importantly, only activated and not naïve T cells express FASL (59). BIM expression is similarly induced via TCR stimulation and requires PKCθ, calcineurin and NF-AT activity (158). Due to their important roles in promoting cell death, regulation of FASL and BIM have been extensively studied.

Although RICD was described over two decades ago (196), the molecular components that change the TCR signaling from pro-proliferative in naïve T cells to pro-apoptotic in restimulated effector T cells have yet to be fully defined. Initial studies of programmed cell death demonstrated that the induction of apoptosis is not limited to naïve T cell negative selection in the thymus, but also extends into the periphery (67; 196). So although early research was completed in an *in vitro* setting, these data were extrapolated into a probable role of RICD in peripheral tolerance. However, the physiological relevance of RICD *in vivo* is still actively being studied. Recent work from our lab and others suggests that in order to limit nonspecific inflammatory damage to the host, RICD sets an upper limit of expansion for effector T cells (174-176).

It has been demonstrated that when RICD is disrupted, severe immunopathology can occur. One example is X-linked lymphoproliferative disorder (XLP-1), caused by a deficiency in SLAM Associated Protein (SAP). Previous work demonstrated that the adaptor protein SAP increases TCR signal strength via positive signals through the NK,T and B antigen (NTB-A) receptor. Loss of SAP therefore results in attenuated TCR signal strength and a marked decline in RICD sensitivity in XLP-1 patient T cells (174). This defect in RICD manifests most dramatically during Epstein Barr virus (EBV) infection, where XLP-1 patients demonstrate uncontrolled T cell lymphoproliferation that causes

severe, non-specific inflammatory host damage and death in up to 65% of cases from "fulminant infectious mononucleosis" (FIM) (17; 118). Recent work from our lab has helped to resolve the mechanistic role of SAP in enhancing TCR signal strength. Specifically, after TCR ligation, SAP recruits lymphocyte specific protein kinase (LCK) to the SLAM family receptor NTB-A, while simultaneously displacing the inhibitory SH2-containing protein tyrosine phosphatase 1 (SHP-1). This facilitates a greater induction of proximal phosphorylation events at the immunological synapse and subsequent TCR signaling (84; 174). Our lab has also demonstrated that in the absence of SAP, production of TCR induced pro-apoptotic effector molecules (e.g. FASL, BIM) is diminished (174).

Many downstream signaling proteins are activated by TCR stimulation, including PKCθ. PKCθ activity is important for signaling the survival and proliferation of T lymphocytes, particularly through phosphorylation of caspase recruitment domain family member 11 (CARD11). Phosphorylated CARD11 oligomerizes with B cell lymphoma 10 (BCL10) and mucosa associated lymphoid tissue lymphoma translocation protein 1 (MALT1) to form the "CBM complex" and propagate downstream activation of NF-κB (20; 107). PKCθ is recruited to the membrane by DAG, a product of the hydrolysis of PIP_2 by PLCγ1. Notably, mice lacking SAP manifest a similar disease phenotype to XLP-1 patients, and have a reduction in PKCθ recruitment to the immune synapse (27). Signaling via the second messenger DAG is regulated in part by diacylglycerol kinases (DGKs), which convert DAG into phosphatidic acid (PA). Recent studies have demonstrated that SAP also negatively regulates DGKα activity, allowing sufficient DAG to recruit PKCθ to the membrane and potentiate a robust TCR signal. In the

absence of SAP, increased DGKα activity depletes DAG levels, in turn weakening TCR signal strength (9). Work detailed in Chapter 2 tested and confirmed the hypothesis that pharmacological inhibition of DGKα should prevent depletion of DAG to promote strong TCR signaling and restoration of RICD in XLP-1 SAP deficient T cells.

These data align well with the threshold model of RICD sensitivity. This model proposes that activated effector T cells that receive a relatively strong TCR stimulus are able to propagate a proportionally robust downstream signal for the *de novo* induction of pro-apoptotic molecules, whereas a relatively weak TCR stimulus (e.g. in the absence of SAP) will not be sufficient to induce apoptosis. At any given time, effector T cells may vary in their relative 'activation state' set point, determined by cumulative phosphorylation of tyrosine residues found in the CD3 complex (e.g. CD3ζ ITAMs) and TCR associated proximal signaling components, such as LCK. In addition to TCR signal strength, the 'activation state' of the cell may play a large role in influencing sensitivity. In a mouse adoptive transfer model, researchers demonstrated that 16-20 month rested memory T cells generated greater recall responses than memory $CD8^+$ T cells rested for just one month (147). It is possible that the long-term memory cells were more "rested down", while the recently generated memory still retained a higher 'activation status' closer to the RICD threshold. What remains unclear in this model is how this threshold of sensitivity varies from person to person and cell to cell. *In vitro* assays demonstrate substantial variability in the proportion of activated effector T cells between normal healthy donors, and/or within any single donor (30-80%), that will undergo apoptosis after a strong, polyclonal (e.g. anti-CD3 Ab) TCR stimulus. This suggests that there must be other molecular determinants of RICD sensitivity that either directly feed into the

TCR signal (e.g. SAP), or independently regulate the induction of key pro-apoptotic molecules. Work detailed in this dissertation provides new molecular insights into the molecular control of RICD sensitivity (Chapter 2), including a novel link between metabolic reprogramming in T cells and RICD (Chapter 3).

Understanding how RICD is regulated at the molecular level may inform strategies to better control activated T cells that have escaped apoptosis in autoimmune disorders and lymphoproliferative diseases. In this context, we would manipulate molecular components or regulators of RICD in order to 'dial up' RICD sensitivity, therefore decreasing the number of auto-reactive or non-specific T cells that would otherwise contribute to cytopathic immunopathology. Understanding the RICD mechanism may conversely be exploited to predict and potentially manipulate the magnitude of a T cell response for improving anti-tumor immunity and optimal vaccination/boosting strategies. In this context, we may wish to 'turn down' RICD in order to obtain more memory T cells, or prolong the survival of their derived effectors.

Cytokine withdrawal-induced cell death: CWID

While RICD sets an upper limit of effector expansion, CWID is the major pathway that helps contract the effector T cell pool after clearance of a pathogen. CWID is critical for terminating the immune response and returning to homeostasis. In contrast to RICD, CWID is an intrinsically activated apoptosis pathway mediated by gradual decline of the key survival factor IL-2 in the inflammatory milieu. Early studies demonstrated *de novo* protein expression after IL-2 withdrawal was critical for DNA fragmentation in activated T cells (47). In fact, signaling through the IL-2 receptor (IL-2R) helps to suppress expression of the pro-apoptotic protein BIM, while simultaneously

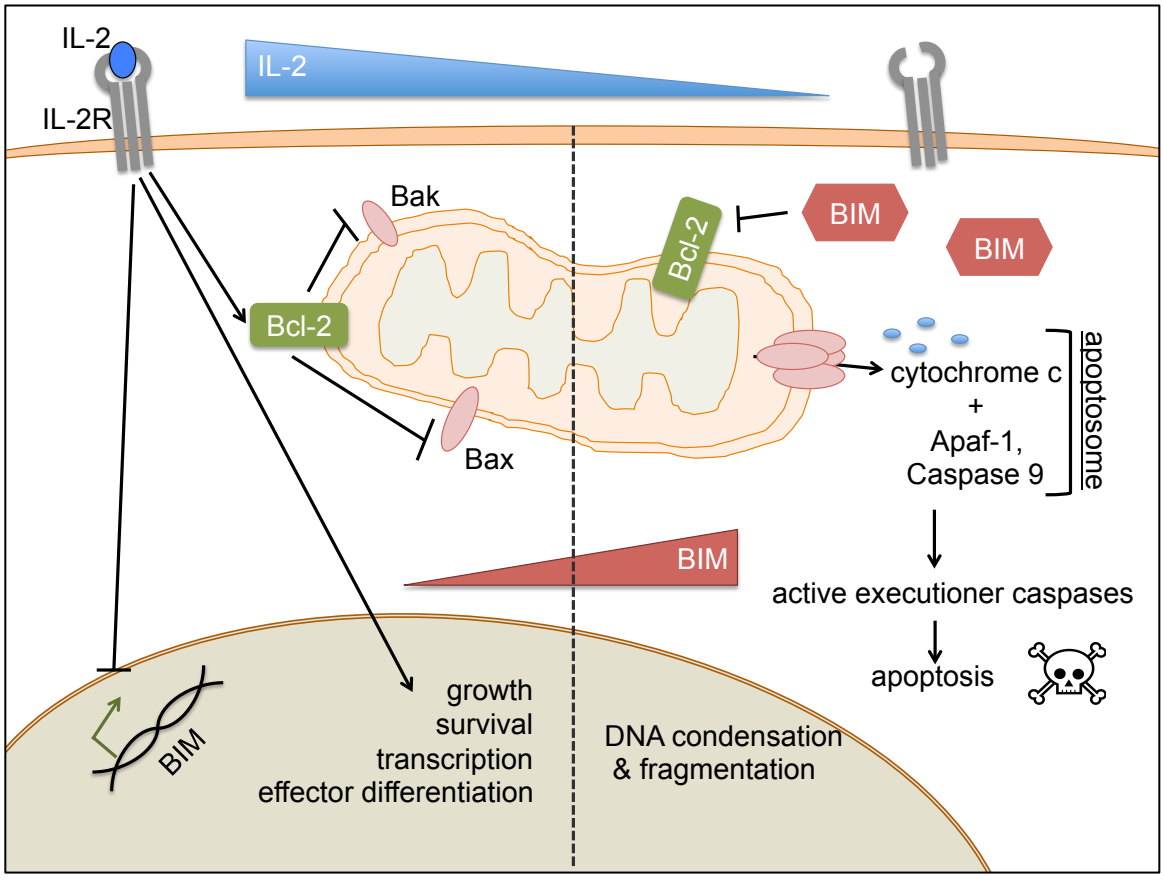
increasing the expression of anti-apoptotic protein B cell lymphoma-2 (Bcl-2) (29; 43; 71; 81; 87; 149; 200; 205).

The high affinity IL-2R is made up of three components, α (CD25), β (CD122), and common γ chain (CD132). IL-2 drives effector T cell expansion by promoting cell survival and proliferation. When IL-2 binds to the IL-2R, Janus family tyrosine kinases (JAK1/3) phosphorylate tyrosine residues in the IL-2Rβ chain, which serve as docking sites for signal transducer and activator of transcription 5 (STAT5a/b) and Src homology 2 domain containing adaptor (Shc) proteins (1; 51; 90). Phosphorylated STAT5 molecules form dimers, translocate to the nucleus, and serve as transcription factors for IL-2 responsive genes such as IL-2Rα (CD25), c-Myc, and Bcl-2 (98; 104). Recruitment of Shc results in downstream activation of the mitogen-activated protein kinase (MAPK) pathway via Ras, which further induces Bcl-2 (51; 58; 104). Shc association with the IL-2R also triggers the phosphatidylinositol-3-kinase (PI3K)-protein kinase B (Akt) signaling pathway (58). Both Akt and extracellular signal regulated kinase (ERK) phosphorylate critical transcription factors of the Forkhead-Box family, specifically FoxO3a. Phosphorylation of FoxO3a promotes degradation and precludes the transcription factor from entering the nucleus, preventing transcription of BIM mRNA (39; 150; 179). Akt activity is also known to repress expression of additional pro-apoptotic proteins, including Bcl-2 associated death promoter (BAD) (172). Akt is multipotent in its influence on cell death, not only repressing pro-apoptotic molecules but also helping to preserve survival proteins. In order to prevent degradation of anti-apoptotic myeloid cell leukemia-1 (Mcl-1) protein, Akt represses glycogen synthase kinase-3 (GSK-3) so it is unable to phosphorylate Mcl-1 (172).

Due to its significant role in promoting T cell apoptosis, it is not surprising that BIM expression is regulated in a variety of ways. These include the aforementioned transcriptional control via IL-2R signaling and epigenetic control by promoter methylation (172). In addition to repressing transcription, post-translational phosphorylation by ERK and AKT result in the degradation of BIM (122). BIM is also sequestered by Bcl-2 in order to suppress its pro-apoptotic activity. The complex regulation of BIM also occurs at the translational level. BIM mRNA translation is negatively regulated by microRNAs and a variety of RNA binding proteins (172). Furthermore, BIM mRNA undergoes alternative splicing in T cell to produce 3 main isoforms with differential pro-apoptotic potential; BIM_{EL} (extra long 196 a.a.), BIM_{L} (long 140 a.a.) and BIM_{S} (short 110 a.a.) (73; 172). While the BIM_{S} isoform is the most potent inducer of apoptosis, BIM_{EL} and BIM_{L} demonstrate complex interactions with autophagy. Interestingly, while BIM is itself degraded through autophagy (89), overexpression studies of BIM_{EL} and BIM_{L} have demonstrated a role for BIM in down regulating autophagy (172) and increasing apoptosis in T cells (73). Work in Chapter 4 further explores the connection between BIM, autophagy and CWID.

The relative ratio of Bcl-2 family proteins is the ultimate gatekeeper of survival versus apoptosis in any given T cell. The Bcl-2 family of proteins is made up of both pro- and anti-apoptotic factors that control mitochondrial membrane stability. Anti-apoptotic Bcl-2 and Bcl-xL are integral outer mitochondrial membrane (OMM) proteins which maintain membrane stability by preventing oligomerization of two critical pro-apoptotic Bcl-2 family members, Bcl-2 associated X (BAX) and Bcl-2 homologous antagonist/killer (BAK). As IL-2R signaling wanes, expression of pro-apoptotic BIM is

de-repressed (29; 43; 56; 71; 81; 166). Elevated expression of pro-apoptotic Bcl-2 homology 3 domain (BH3 only) proteins (e.g. BIM, Puma) tips the balance of Bcl-2 family proteins in favor of apoptosis. BH3 only proteins directly antagonize Bcl-2 and Bcl-xL, releasing BAX and BAK proteins to localize to the OMM and oligomerize to form a pore. This destabilization of the OMM releases cytochrome c from the intermembrane space, which complexes with cytosolic caspase-9 and apoptotic protease activating protein-1 (APAF-1) to form the "apoptosome". The apoptosome serves as a platform for caspase 9 activation, which further activates executioner caspases (-3,-6,-7) and downstream signaling events leading to programmed cell death (205).



Much like XLP-1 disease demonstrates the physiological importance of RICD, Ras-associated autoimmune leukoproliferative disorder (RALD) demonstrates the critical role CWID plays in human T cell homeostasis. These cases of gain-of-function Ras mutations lead to constitutive extracellular signal-regulated kinase (ERK) activity and continual repression of BIM, even in the absence of IL-2R signaling. Lymphocytes from individuals suffering from RALD are resistant to IL-2 withdrawal dependent apoptosis, resulting in leukocytosis, lymphoproliferation and autoimmunity (25; 170; 185). Similarly, genetically modified $BIM^{-/-}$ mice exhibit elevated numbers of circulating T cells that show increased *in vitro* survival compared to WT controls (18). Additionally, $BIM^{-/-}$ mice maintain increased numbers of plasma cells generating high levels of serum immunoglobulin, resulting in significant autoimmunity and immune complex glomerulonephritis (18). Taken together these studies demonstrate the profound and delicate influence cytokine signaling plays in cell death and lymphocyte homeostasis.

The role of CWID in contracting the primary immune response and associated molecular mechanisms are well studied. However, what remains unclear is how sensitivity to this pathway may differ among subsets of T cells, including recently defined memory T cell subsets. Work detailed in Chapter 4 tackles this question by comparing two distinct memory T cell subsets, as described in the next section. By default or design, memory T cells are ultimately those that have survived the contraction phase imposed by CWID.

$CD8^+$ Memory T cells

T lymphocytes provide specific and lasting responses to pathogens through selected antigen receptors and the generation of memory, respectively. Memory $CD8^+$ T

cells are critically important during the second encounter with antigen, as they are known to provide strong swift clearance of viral infections. This greater clearance is partly due to clonal selection of T cell receptors (TCR) that specifically recognized the pathogen upon first encounter. The memory T cell pool retains those TCRs best suited for specific recognition of immunodominant antigenic epitopes associated with a pathogen. As such, memory T cells are able to rapidly proliferate and perform effector functions when stimulated by their cognate antigen. The accelerated recall of memory T cells is partly due to a bioenergetic superiority over other cell types. Unlike antigen naïve cells, memory T cells retain a comparatively large mitochondrial mass for generating greater amounts of ATP. This enhanced mitochondrial mass and ATP generation enables secondary effectors, derived from memory, to proliferate more quickly, produce more effector cytokines and induce glycolysis (23; 188). Robust expansion of effector cells and their specificity for the pathogen are what make the secondary response more efficient than the first.

A typical adaptive immune response involves antigen stimulation of naïve T cells, effector expansion, and contraction. The transition into long-lived memory occurs after the contraction phase and resolution of the immune response. However, there are two models of memory T cell development. Some research suggests memory T cells are derived directly from effectors that survive contraction after an infection is controlled (125) ("linear model"), while more recent work supports a model where certain effector T cells are predetermined to become memory (80; 82; 132). The predetermined model suggests that after activation, effectors become either short-lived effector T cells (SLECs), defined as IL-7 receptor alpha (IL-7Rα)^{lo}, or memory precursor T cells

(MPECs) with high expression of IL-7Rα (76; 80; 132; 207). Indeed, lineage fate decisions can occur as early as the first cell division, termed 'asymmetric division' (3; 6; 96; 112), or be influenced later by environmental inflammatory cues (78; 208). Most recently, c-myc distribution and induction has been shown to influence differential metabolic reprogramming in TCR stimulated cells (191). Understanding the cellular programming that influences early fate decisions on the road to memory formation is critical when attempting to induce efficient lasting vaccine responses in the T cell pool. Long-lived memory T cells are essential for continued protection against many intracellular pathogens, and the mechanism behind their maintenance is well studied. During steady state conditions, memory T cells slowly turn over in the absence of antigen. Certain cytokines are essential; IL-7 provides survival signals to memory T cells (116; 117), while IL-15 promotes homeostatic division (11; 198; 203). In addition to cytokines, there is evidence that varying amounts of antigen at primary stimulation will influence the proportion and differentiation of memory subsets (159).

Subsets of CD8+ Memory

The $CD8^+$ memory T cell compartment is further parsed into subsets based on surface markers and effector phenotypes. The most well defined subsets include central memory (CM), effector memory (EM), stem-cell memory (SCM), and resident memory (RM) T cells. Each subset possesses unique phenotypes and together they represent a continuum of differentiation (151), discussed below in detail.

The two best-characterized memory $CD8^+$ T cell subsets are CM and EM. The homing and longevity of these two subsets are measurably different. CM T cells are longer lived *in vivo* and undergo more self-renewal than EM T cells (156; 157; 197).

High expression levels of CD62L on CM cells allows preferential homing to lymph nodes, although both CM and EM can be found in peripheral blood and splenic tissue. Memory cells are designed for robust effector T cell generation upon rechallenge; therefore, effectors derived from each subtype can also be studied. Interestingly, effectors derived from CM and EM cells show equivalent cytolytic activity as well as cytokine secretion capacity after adoptive transfer (156; 193; 197). However, these subsets demonstrate substantial differences in engraftment potential, as well as differential protective immunity after adoptive transfer and challenge (12; 147; 193; 197). It has been suggested that CM cells are more efficient at controlling viral infections because of a greater 'proliferative potential'. In one key example, Wherry and colleagues showed that adoptively transferred LCMV-specific CM cells gave rise to a larger effector pool compared to EM cells after viral rechallenge in mice. However, these CM-derived effector T cells had actually undergone fewer rounds of division than EM-derived effectors (197). Therefore, discrepancies in CM- versus EM- derived effector T cell numbers and corresponding infection control cannot be explained by proliferative capacity or effector function alone. Close examination of a mouse Sendai virus infection time course has revealed that EM effector responses dominate early, while CM derived effectors take over in number at later time points (147). This data accentuates the importance of acknowledging T cell accumulation as the end product of both proliferation and cell death. Detailed analysis of RICD and CWID sensitivity between CM and EM derived effectors may help clarify their differential abilities to control infection. Memory subset phenotyping is becoming increasingly important in T cell therapy decisions. As part of these phenotypic analysis, it is critical to also examine their

respective death sensitivities to apoptotic stimuli. Chapter 4 will delve into this issue directly.

Stem cell memory are true to their name and are most 'stem cell like' in that they have a high potential for self renewal, are the least-differentiated memory subset and preferentially home to lymph nodes (60; 61; 99). They are uniquely distinguished by their high expression of the Fas (CD95) death receptor despite their relative longevity *in vivo*, which may suggest inherent resistance to this death pathway. Indeed, under certain conditions Fas can actually promote survival rather than canonical pro-apoptotic signaling (127). In depth analysis of death sensitivity in SCM may help to further elucidate the seemingly opposing roles of the Fas death receptor. Despite sharing many properties with naïve T cells, SCM are antigen-experienced cells that can secrete effector cytokines (60; 88). Because they are the least differentiated, this multipotent subset can give rise to all other memory T cell subsets making them a particularly attractive option for adoptive T cell therapy (55; 88). A recent study demonstrated that retrovirally engineered SCM T cells could be detected in human recipients up to 12 years after infusion, and remarkably these cells maintained their precursor potential (14).

Early studies into the homing properties of memory T cells established a subset of EM-like cells, which did not circulate and preferentially resided in non-lymphoid tissue (13; 109; 163). These cells were later termed resident memory (RM) T cells. Early characterization of memory subsets focused mainly on peripheral blood samples; since RM T cells do not recirculate, they were missed. In fact, later studies including a parabiosis mouse model demonstrated that even enzymatic isolation from non-lymphoid tissue underestimates the broad distribution of tissue resident $CD8^+$ memory population

and each tissue type varies in proportion or number of RM (161; 163; 180). RM cells are particularly important for immune surveillance at mucosal barrier tissues and common infection routes (62; 169). Lymph node-sequestered CM T cells or circulating EM T cells are less likely to encounter a target cell immediately after infection, whereas RM T cells lie in wait at probable infection sites. RM function as early detectors that 'sound the alarm', so their effectiveness is not strictly limited to their cytolytic activity, but extends into their ability to express interferon-γ (IFN-γ) and bolster local inflammatory chemokines that recruit additional antigen experienced T cells (79; 114; 161; 162). Not only are RM T cells sensitive antigen detectors that express TCRs with up to 20 fold higher affinity than circulating effector T cells (57), they are also unique in their ability to be early sentinels of infection due to their location. An experimental infection of respiratory syncytial virus (RSV) showed that higher pre-infection numbers of RM in the airway correlated with fewer symptoms and a reduced viral load in human volunteers, suggesting RM provide early protection in the lung (79). As a newly defined subset, much work still remains to define the role of RM in different infections. Additionally it will be important to identify the unique mechanisms that allow RM T cells to persist in antigen rich environments for prolonged periods of time without inducing apoptosis or anergy.

Table 1. $CD8^+$ Memory T cells defined by surface marker, location and defining feature(s).

Subset	Surface Markers	Primary location	Defining feature
Stem Cell Memory (SCM)	$CD95^+$ $CD45RA^+$ $CD62L^+$ $CCR7^+$ $CD27^+$ $CD45RO^-$	Lymph node	Multipotent and self renewing

	$CD122^+$		
Central Memory (CM)	$CD45RO^+$ $CD62L^+$ $CCR7^+$	Lymph node	Some self renewal, longevity, high protective capacity
Effector Memory (EM)	$CD45RO^+$ $CCR7^-$	Peripheral Circulation	Early responder, Most differentiated
Resident Memory (RM)	$CD103^+$ $CD69^+$ $S1P_1^-$	Peripheral-nonlymphoid tissue and secondary lymphoid organs	Sentinel cells

Memory and Cell Death

A balance of proliferation and death directs the magnitude of a T cell response, but the question of how cell death shapes a secondary memory response remains unanswered. Indeed, unlike SLECs and MPECs whose relative longevity *in vivo* is actively being investigated, further differentiated memory T cell subsets have yet to be comprehensively evaluated for their sensitivities to specific cell death pathways, despite the important role of apoptosis in immune homeostasis.

Little is known about how death sensitivity may differ for effector T cells derived from specific memory T cell subsets like CM and EM. One report suggested that for human $CD4^+$ T cells, only effector T cells derived from the EM subset were sensitive to RICD, which was solely dependent on extrinsic apoptosis signaling through the Fas death receptor (142). However, RICD of $CD8^+$ T cells is not solely dependent on Fas (175), and the sensitivity of $CD8^+$ CM and EM cells to both extrinsic and intrinsic apoptosis stimuli has not been investigated previously. Another study demonstrated that although total

CD8+ T cell counts were reduced in antigen-rich pleural effusions from lung cancer patients, those cells with a memory phenotype predominated (137), suggesting a relatively lower sensitivity to cell death in the memory population. The mechanism by which memory T cells exhibit greater stability and longevity *in vivo* compared to effector T cells is still incomplete (147). Indeed, recent studies indicate that CM T cells from a mouse model of LCMV infection are able to tolerate higher expression of BIM than EM cells due to elevated levels of Bcl-2 (91), yet no additional studies have examined how these expression profiles would impact derived effector CWID sensitivity. Comprehensive apoptosis studies would offer new insight into why $CD8^+$ CM derived T cells display superior effector cell expansion, viral control and persistent memory responses *in vivo* compared to their EM counterparts. Evidence of greater caspase activity, a marker of early apoptosis commitment, in EM-derived effectors versus CM-derived effectors suggests that indeed apoptosis sensitivity between memory subsets is physiologically relevant (193).

There may be any number of mechanisms by which subsets of memory T cells are rendered differentially sensitive to cell death pathways, including: resting activation state (72; 74; 147), active metabolic network (4; 23; 46), imprinted differences in signaling pathways, or some as yet to be defined parameter.

T CELL METABOLISM

Over the past few years, immunologists have begun to characterize the rapid and dynamic changes in cellular metabolism that occur during the course of an effective $CD8^+$ T cell response. Recent reports demonstrate that changes in cellular metabolism over the course of a T cell response profoundly influence cell survival and differentiation,

including the generation of memory (4; 5; 63; 128; 135; 191; 199). Additionally the transition from naïve to effector T cell is dependent of the expression of c-myc and hypoxia inducible factor 1 α (HIF1α), which activate the glycolytic machinery required for effector T cell proliferation (191).

Similar to other somatic cells, naïve and memory T cells exist in a generally quiescent metabolic state and primarily utilize mitochondrial oxidative phosphorylation (OXPHOS) for ATP synthesis (23; 189). Following T cell receptor (TCR) stimulation, however, antigen specific T cells rapidly switch to using glycolysis even in the presence of oxygen (33; 63; 68; 100; 126; 128; 129). This phenomenon, 'the Warburg effect', was first described in cancer cells that preferentially used aerobic glycolysis (194), generating a net 2 moles ATP per 1 mole of glucose versus the more efficient OXPHOS which generates ~36 moles of ATP per 1 mole of glucose (70). Albeit less efficient for ATP generation, glycolysis also generates macromolecules such as amino acids, lipids, and nucleotides (70; 100). Synthesis of macromolecules is vitally important for rapidly dividing cells such as effector T cells. In addition to meeting the requirements for building new cells, aerobic glycolysis has also been directly linked to the ability of an activated T cell to acquire potent effector functions (e.g. IFN-γ production) (30; 33; 70; 126; 129). Interestingly, it is during this unique window of aerobic glycolysis usage that effector T cells are rendered competent for RICD. Chapter 3 explores this correlation directly. It is becoming more evident that metabolic programming plays a critical role in the activated effector phase of a $CD8^+$ T cell response.

Memory T cells switch back to OXPHOS and fatty acid oxidation (FAO) after infection resolution (130). The most important cytokine for establishing T cell memory,

IL-15, seems to play a role in this switch back into a quiescent metabolic program. In fact, it has been implied that memory T cells use FAO to preserve mitochondrial mass and machinery required for rapid recall upon rechallenge (129; 130; 188; 189). Additionally, failure to switch to FAO severely inhibits memory T cell formation (130). Both FAO and OXPHOS enable memory T cells to remain in a resting state of limited homeostatic proliferation while at the same time being exquisitely poised for rapid proliferation upon rechallenge.

Metabolic reprogramming has become a major target for influencing T cell responses *in vivo*. The mammalian target of rapamycin complex (mTORC) integrates many environmental and cellular cues that dictate T cell activation, glycolysis and differentiation choices, and as such is an ideal node for pharmacological manipulation (37; 110; 115; 135; 144). In contrast to memory T cell precursors, short-lived terminally differentiated effectors are predominantly glycolytic and have higher mTOR activity. This suggests mTOR may play an integral role during metabolic reprogramming and cell fate decisions. Indeed, treatment with the mTOR inhibitor rapamycin gave rise to five times more long-lived memory cells in an *in vivo* LCMV infection mouse model compared to untreated mice (69). Researchers determined that rapamycin-treated effectors T cells induce aerobic glycolysis upon TCR stimulation similar to untreated controls, but unlike controls they also upregulated their usage of OXPHOS (69). This model proposes that greater OXPHOS usage in MPEC T cells may help ensure their survival through the contraction phase. Potential correlations between CWID sensitivity and OXPHOS have yet to be examined in detail.

Although dynamic metabolism is critical for T cell activation, effector functions and memory development, what remains unclear is how these same metabolic changes may influence apoptotic sensitivities of T cell subsets. In a study of IL-15 transgenic mice, researchers were able to demonstrate that the abundant production of IL-15 effectively reduced IL-2 dependent RICD in $CD4^+$ T cells (106). Other studies have also demonstrated this dichotomy induced by IL-2 and IL-15, suggesting the metabolic state conferred by IL-15 exposure reduced caspase-3 activity and down-regulated downstream apoptosis (155). In addition to these data, the concurrent timing of RICD sensitivity with cellular dependence on glycolysis lends credence to the hypothesis that sensitivity to RICD may be dependent on metabolic programming, as described in Chapter 3. Naïve and memory T cells are not sensitive to RICD, previously thought to be due to the fact that they undergo only homeostatic division and are not perpetually in cycle like activated effectors exposed to IL-2, a requisite for RICD sensitivity (16; 94). However, the explosion of information relating metabolism to survival and cell fate decisions begs more investigation into whether sensitivity of activated effectors to RICD is dependent on glycolytic metabolism.

SUMMARY

The primary goal of this dissertation was to define novel molecular determinants of cell death sensitivity in $CD8^+$ T cells. This was accomplished by addressing the following three specific aims:

1. Characterize the SAP-DGKα signaling axis and determine if it is a viable therapeutic target for manipulating RICD sensitivity.

We hypothesize that inhibition and knockdown of DGKα will restore RICD sensitivity in SAP-deficient CD8$^+$ T cells.

2. Examine if metabolic programming directly influences RICD sensitivity.

   We hypothesize that glycolytic metabolism explicitly sensitizes effector CD8+ T cells to RICD.

3. Determine if effector T cells derived from distinct memory CD8$^+$ T cell subsets display differential apoptosis sensitivity.

   We hypothesize that central memory-derived effector T cells will be less sensitive to RICD and CWID than effector memory-derived effector T cells.

The work described herein critically examines the important role of cell death in CD8$^+$ T cell homeostasis and the various molecular mechanisms that govern sensitivity to apoptosis. Specifically, Chapter 2 continues the molecular exploration of how SAP potentiates RICD sensitivity via DGKα regulation. Chapter 3 exposes a novel connection between RICD sensitivity and metabolic programming in CD8$^+$ effector T cells. Lastly, Chapter 4 considers the role of differential apoptosis sensitivity in the hierarchy of protective capacity and longevity in the memory T cell compartment. This research was performed using expanded primary human T cells, providing a unique and applicable platform for the study of cell death sensitivity.

CHAPTER 2: Inhibition of diacylglycerol kinase α restores restimulation-induced cell death and reduces immunopathology in XLP1

Published as: **Elisa Ruffo[*], Valeria Malacarne[*], Sasha E. Larsen[*], Rupali Das[*], Laura Patrussi, Christoph Wülfing, Christoph Biskup, Senta M. Kapnick, Katherine Verbist, Paige Tedrick, Pamela L. Schwartzberg, Cosima T. Baldari, Ignacio Rubio, Kim E. Nichols[#], Andrew L. Snow[#], Gianluca Baldanzi[#], Andrea Graziani[#] . 2016.** Inhibition of diacylglycerol kinase α restores restimulation-induced cell death and reduces immunopathology in XLP-1. *Sci Transl Med*. 8(321).

* These authors contributed equally to this work
# These authors contributed equally to this work

This work was completed as a multi-lab collaboration, and as such was published with four co-first authors. As a co-first author, S E Larsen was responsible for determining the molecular mechanisms responsible for RICD sensitivity under DGKα inhibition in SAP-deficient T cells. Specifically implicating the nuclear-orphaned receptors to a previously unappreciated role in RICD sensitivity. Additionally, S E Larsen was responsible for completing all statistical analysis and was integral in generating data presented in supplemental figures used to address reviewer comments, including DGK overexpression data.

ABSTRACT

X-linked lymphoproliferative disease (XLP-1) is an often-fatal primary immunodeficiency associated with the exuberant expansion of activated $CD8^+$ T cells following Epstein-Barr virus (EBV) infection. XLP-1 is caused by defects in SAP, an adaptor protein that modulates T cell receptor (TCR)-induced signaling. SAP-deficient T cells exhibit impaired TCR restimulation-induced cell death (RICD) and diminished TCR-induced inhibition of diacylglycerol kinase alpha (DGKα), leading to increased diacylglycerol metabolism and decreased signaling through Ras and PKCθ. Here, we show that down-regulation of DGKα activity in SAP-deficient T cells restores diacylglycerol signaling at the immune synapse and rescues RICD via induction of the pro-apoptotic proteins NUR77 and NOR1. Importantly, pharmacological inhibition of DGKα prevents the excessive $CD8^+$ T cell expansion and IFNγ production that occur in Sap-deficient mice following Lymphocytic Choriomeningitis Virus infection without impairing lytic activity. Collectively, these data highlight DGKα as a viable therapeutic target to reverse the life-threatening EBV-associated immunopathology that occurs in XLP-1 patients.

INTRODUCTION

X-linked lymphoproliferative disease (XLP-1) is a heritable immune disorder caused by germline mutations in the *SH2D1A* gene, which encodes the Signaling Lymphocytic Activation Molecule (SLAM)-associated protein (SAP). SAP is a small SH2 domain-containing adaptor primarily expressed in T, natural killer (NK) and invariant NKT (iNKT) cells (119). XLP-1 is best recognized for the increased susceptibility of affected males to develop overwhelming lymphoproliferation following primary Epstein Barr virus (EBV) infection (186). Also known as fulminant infectious mononucleosis (FIM), this lymphoproliferative process is characterized by the massive accumulation of activated $CD8^+$ T cells, which infiltrate multiple organs and inflict severe tissue damage. FIM is the most common and clinically challenging manifestation of XLP-1, with up to 65% of patients dying despite the use of chemo-immunotherapy (17). Accordingly, alternative and more effective treatment strategies are sorely needed for XLP-1 patients who develop FIM.

T lymphocytes derived from XLP-1 patients exhibit multiple functional defects, including reduced cytotoxic activity (209) and impaired restimulation-induced cell death (RICD) (174). RICD is a self-regulatory apoptosis program triggered by repeated TCR stimulation that maintains peripheral immune homeostasis by constraining the accumulation of activated T cells (176). A similar death defect is present in the activated T cells of *Sh2d1a*$^{-/-}$ mice (35). It is proposed that defective RICD, combined with impaired clearance of EBV-infected B cells, sustains and amplifies the expansion of activated T cells that typifies FIM (174; 176).

SAP binds to immunotyrosine-based switch motifs (ITSMs) within the cytoplasmic domains of the SLAM-family receptors (SLAM-Rs) (136), thus competing with the binding of SH2 domain containing inhibitory lipid and tyrosine phosphatases such as SHIP and SHP-1/SHP-2 (171). In addition, SAP facilitates recruitment of kinases such as FynT and Lck to SLAM-Rs to promote optimal signaling within T, NK and NKT cells (32; 84). Indeed, RICD resistance in XLP patient T cells results in part from weak TCR signaling associated with excess SHP-1 activity and defective recruitment of Lck to the NTB-A receptor, which colocalizes with the TCR (84; 174). Although SAP links SLAM-R signaling to several downstream functions via activation of Src-family kinases (e.g. IL-4 secretion (27), iNKT cell development (121)), this signaling axis is not the only pathway in which SAP is involved for signal regulation. For example, the requirement for SAP in the provision of $CD4^+$ T cell-mediated "help" for B cell differentiation is Fyn-independent (139). To fully understand XLP-1 pathogenesis and develop more effective therapeutic interventions, the mechanistic characterization of signaling molecules involved in these "alternative" SAP-dependent signaling pathways is imperative.

We recently observed that following TCR stimulation, SAP selectively inhibits diacylglycerol kinase-alpha (DGKα) without requiring FynT or Lck (9). DGKα and DGKζ phosphorylate diacylglycerol (DAG) to generate phosphatidic acid, thereby modulating TCR signal strength by regulating DAG levels and downstream biochemical events (123; 210). In activated T cells, silencing SAP expression results in persistently active DGKα and thus impaired DAG signaling, leading to reduced-mediated PKCθ membrane recruitment, NFAT and ERK1/2 activation and interleukin 2 (IL-2) production (9). These data collectively suggest that upon antigen stimulation, SAP inhibits DGKα

activity to facilitate optimal DAG accumulation and full TCR signal strength, ultimately leading to cell activation.

Because TCR signal strength directly correlates with RICD sensitivity (167), we hypothesized that the reduced RICD of XLP-1 T cells might be linked to deregulation of DGKα in the absence of functional SAP. Consistent with this notion, we show herein that the loss of SAP in T cells results in reduced DAG polarization to the immune synapse (IS) and impaired TCR-induced DAG-dependent TCR signaling. Both of these events are due to persistent DGKα activity and contribute to RICD resistance. Consequently, the inhibition of DGKα in XLP-1 T cells restored DAG signaling and RICD by rescuing IS architecture and triggering a specific DAG-dependent apoptotic process mediated by the orphan receptors *NR4A1* (NUR77) and *NR4A3* (NOR1). Strikingly, *in vivo* inhibition of DGKα activity reduced the excessive $CD8^+$ T cell accumulation and IFNγ production that occur in *Sh2d1a*$^{-/-}$ mice infected with Lymphocytic Choriomeningitis Virus (LCMV), a murine model of FIM. Our findings illuminate the SAP/DGKα signaling axis as a key regulator of TCR-induced apoptosis. Importantly, these results highlight DGKα as a novel, druggable target for treating FIM by promoting RICD, reducing the accumulation of pathogenic, activated $CD8^+$ T cells and thus mitigating the life-threatening immunopathology that often occurs in EBV-infected XLP-1 patients.

MATERIALS AND METHODS

Study Design

This was a preclinical study to 1) determine if DGKα inhibition could rescue RICD in SAP-deficient T cells, and 2) assess the efficacy of a DGKα inhibitor in attenuating $CD8^+$ T cell lymphocytosis and immunopathology in LCMV-infected SAP-deficient mice, a model of FIM. Although *in vitro* experiments utilizing XLP-1 patient T cells were often constrained by limited sample availability, each RICD experiment was performed with at least 2 separate XLP patients and different control donors (e.g. Fig 1A-B). We also generated robust corroborating data using siRNA-mediated SAP knockdown in T cells from multiple human donors ($n \geq 3$ experiments each). Once we established that DGKα blockade restored RICD sensitivity in SAP-deficient T cells, we focused on delineating the biochemical mechanism that explains this phenomenon. For all *in vitro* data, the number of experiments (including technical replicates) is defined in each figure legend. For *in vivo* experiments, numbers of mice are outlined in each figure legend. All statistical analyses described below were verified by consultation with an experienced biostatistician (Cara Olsen, USUHS).

Cell Culture

Peripheral blood mononuclear cells (PBMCs) were isolated from normal controls or XLP-1 patients by Ficoll-Paque PLUS (GE Healthcare) density gradient centrifugation, washed, and resuspended at $2x10^6$ cell/ml in complete media (cRPMI): RPMI-GlutaMAX (Life Technologies) containing 10% heat inactivated FCS (Lonza), 2 mM glutamine, and 100 U/ml of penicillin and streptomycin (Life Technologies). T cells were activated with 1 μg/ml anti-CD3 (clone UCHT1) and anti-CD28 (clone CD28.2) antibodies. After 3

days, activated T cells were washed and cultured in cRPMI plus 100 IU/ml rhIL-2 (Peprotech) at $1.2x10^6$ cells/mL for ≥7 days before apoptosis assays were conducted (media changed every 2-3 days). Jurkat A3 cells were from ATCC, and 293FT from Life Technologies. Cells were cultured in RPMI or DMEM (Life Technologies) with 10% FCS and antibiotics/antimycotics (Sigma-Aldrich). DGK inhibitors R59949 and R59022 (Sigma-Aldrich) were dissolved in DMSO.

siRNA transfections

PBMCs were transfected with 200 pmol of Stealth Select siRNA or Stealth RNAi Negative Control Duplexes (Life Technologies). siRNA sequences are listed in Table S1. Transient transfections were performed using Amaxa nucleofector kits for human T cells (Lonza) and the Amaxa Nucleofector II or 4D systems (programs T-20 or EI-115). Cells were cultured in IL-2 (100 IU/ml) for 4 days to allow target gene knockdown. Knockdown efficiency was periodically evaluated by RT-PCR and Western blotting.

Immunofluorescence experiments with primary T cells

Human T cells were stimulated with soluble anti-CD3 and anti-CD28 (1 μg/ml) for at least 7 days and transfected with Amaxa Nucleofector™ Kit for human T Cells (Lonza) with control, SAP-specific and/or DGKα-specific siRNA. After 72 hours T cells were incubated with Raji B cells loaded with mixed SEE and SEB superantigens (1 μg/ml) for 15 min, fixed and stained for either PKCθ or RasGRP1. For some experiments, transfected T cells were pre-treated with R59949 (10 μM, 30 min 37°C) or DMSO before conjugation.

Cytofluorimetry

To examine RICD, activated T cells (10^5 cells/well) were plated in triplicate in 96-well round-bottom plates and treated with anti-CD3ε mAb OKT3 (1-100 ng/ml) in cRPMI + 100 IU/ml rhIL-2 for 24 hours. R59949 (5-10 μM), R59022 (5-10 μM), DAG (50 μM), U0126 (5 μM), FR180204 (10 μM) or Rottlerin (6 μM) inhibitors were added 30 minutes before restimulation. At 24 hours post-restimulation, cells were stained with 1 μg/ml propidium iodide and collected for 30 seconds per sample on FACScan or Accuri C6 flow cytometers (BD). Cell death was analyzed with CellQuest/CFlow software (BD) or Flowing software (Turku Bioimaging) as percentage of cell loss = (1 – [number of viable cells (treated) / number of viable cells (untreated)]) × 100 (174).

For AnnexinV assays, ~$1x10^6$ cells were treated with OKT3 (10 ng/ml) as above. Cells were stained 6-12 hours later with AnnexinV-PE (Biolegend) and analyzed on an Accuri C6. To evaluate CD25 expression, $1x10^6$ cells were stimulated with OKT3 (100 ng/ml) for 24 hours, fixed and stained with anti-CD25 plus anti-mouse AlexaFlour488. Stained cells were collected on a FACSCalibur.

Conjugation and live-cell imaging of Jurkat T-cells

Raji B cells were resuspended in RPMI 0% FCS + 5 μM of CellTracker Red CMPTX for 30 min at 37 °C and washed twice with RPMI + 10% FCS. Raji were resuspended in RPMI 10% FCS + 1 μg/ml SEE superantigen (1 hour, 37 °C), washed twice and resuspended in conjugation medium (RPMI, 0.2 % endotoxin low and fatty acid free BSA, 50 mM HEPES pH 7.5). Jurkat cells were resuspended in conjugation medium and mixed 1:1 with SEE-loaded Raji cells. The cell mixture was spun at 100 g for 1 min and incubated 10 min at 37°C. Cell conjugates were seeded on polylysine-coated glass-

bottom dishes. Live cell confocal imaging was performed with a Zeiss LSM 510 inverted laser scanning microscope (LSM) with a thermostated stage chamber and a C-Apochromat X63 water immersion objective lens (Zeiss). The confocal aperture was adjusted to give optical sections of 1 μm. LSM image files were processed using the Zeiss LSM image browser software (Version 3.1).

For DGKα inhibition experiments, Jurkat shSAP or shCNTRL cells were transfected with the appropriate expression plasmids using the DMRIE-C reagent (Life Technologies). Lifeact-GFP was a kind gift of Roland Wedlich-Soldner**,** GFP-tubulin was from Julian Downward and PKCθ-CRD was from Doreen Cantrell. After 48 hours, 10 μM R59949 was added 30 min prior to starting conjugate formation.

For DGKα knockdown experiments, 0.5 x 10^6 Jurkat shSAP or shCNTRL cells were microporated (Neon® Transfection System, Life Technologies) according to the manufacturers' instructions (1400V, 30 sec, 1 pulse) and incubated for 96 hours in 2 ml RPMI + 10 % FCS prior to conjugation experiments.

To quantify mean fluorescence intensities (MFIs) in the plasma membrane of T cells, we developed software in *MATLAB* (MathWorks), which segments the image automatically and creates two masks, one for the T cell plasma membrane at the interface with the Raji B cell and the other for the remaining T cell plasma membrane. MFI in either mask can be calculated. Major steps of the segmentation algorithm are shown in Fig. S4. In brief, in the filtered image gradients to neighboring pixels are calculated. Pixels with high gradients can help to identify edges such as the plasma membrane. For this analysis, the contact zone of the Jurkat cell was defined as the part of the plasma

membrane that is within a perimeter of 2 μm surrounding the plasma membrane of the Raji B cell.

Western Blotting

Lymphocytes (1-10x10^6 cells) were stimulated, lysed and subjected to SDS-PAGE and immunoblotting as described (9; 174). Immunoblot images were acquired and quantified using a Versadoc Model 4000 Imaging System (Bio-Rad) or ImageJ software (for film). Spot densitometry analyses are summarized in Table S3.

Quantitative RT-PCR

Activated lymphocytes (30x10^6 cell/ml) were stimulated in cRPMI with 10 μg/ml OKT3 for 4 hours. R59949 (5 μM) was added 30 minutes before restimulation. Cells were washed with cold PBS, and mRNA was extracted using a ChargeSwitch Total RNA Cell Kit (Life Technologies). RNA was reverse transcribed using High-Capacity cDNA Reverse Transcription Kits (Life Technologies), and cDNA targets quantified by RT-PCR (C1000 Thermal Cycler CFX96, Bio-Rad) using TaqMan gene expression assays (see Table S2), with *GUSB* as the housekeeping control (Life Technologies).

CTL assays for autologous T cells

To generate *in vitro* activated mouse CTLs, whole splenocytes from naïve WT or *Sh2d1a*-/- P14 mice were harvested and stimulated with 10 nM LCMV gp33 *(KAVYNFATM)* peptide (AnaSpec) for 3 days in 10% complete media (RPMI 1640 plus 10% FBS, 2mM L-glutamine, 50U/mL penicillin/streptomycin, and 50μM β-mercaptoethanol). Cells were then washed once and resuspended in complete media plus 10 IU/mL recombinant human IL-2 and seeded in fresh media plus rhIL-2 every 48

hours. All experiments were performed with CTLs 7 days after initial *in vitro* stimulation. Resting B cells were purified by negative selection with anti-CD43 microbeads (Miltenyi) and activated with 1μg/mL LPS from *E. coli* (Enzo Life Sciences) in 10% complete media for 2 days before use as targets in all assays.

In vitro cytolytic activity was evaluated using a FACS-based method. Targets were stained with 1μM Cell Trace Violet (CTV, Life Technologies) with 1μM A4Y (KAVANFATM) peptide for 1 hour at 37°C, washed twice, and resuspended in 10% complete media. Previously activated WT or *SH2D1A*-/- P14 CTLs were washed and added to 96 well round bottom plates and titrated in 10% complete media. Pulsed targets were added to wells with T cells to achieve indicated effector:target ratios, and additional wells set up with target cells alone to control for spontaneous target cell death. Plates were incubated at 37°C for 4 hours, spun down, and supernatents discarded. Cells were then stained with αCD8-APC (BD, clone 53.6.7) antibodies and LiveDead green (Life Technologies) for 20 minutes at 4C, and washed once with FACS buffer before analysis. For analysis, the CTV+ LiveDead+ population represents the target cells that have been killed, while the CTV+ LiveDead-population represents the remaining viable target cells in each well. Percent cytotoxicity was calculated as follows: % cytotoxicity = 100 – [(viable CTV+ cells in sample)/(viable CTV+ cells in control)] x 100, where CTV+ cells in sample are cells in experimental wells, and viable CTV+ cells in control are cells in wells without T cells.

Soluble FASL ELISA

Soluble FASL was measured in restimulated T cell supernatants using the Human FASL/TNFS6 Quantikine ELISA Kit (R&D Systems).

Overexpression of DGKα/DGKζ in primary T cells

Expression plasmids (pCMV6) encoding myc-tagged DGKa or DGKz were purchased from Origene. Activated T cells cultured in complete RPMI + 100U/ml IL-2 were transfected with 5 ug of each construct or a GFP control (pmax-GFP, Lonza) using an Amaxa Nucleofector 4D system (P3 solution, program EO-115). Apoptotic cells were removed 8 hours post-transfection using a Dead Cell Removal Kit (Miltenyi) prior to setting up RICD assays as previously described. To calculate % cell loss as described, PI stained cells were collected for 2 min constant time on an Accuri C6 flow cytometer (BD Biosciences).

Mice and in vivo experiments

Sh2d1a$^{-/-}$ mice were as described (40). C57BL/6 (B6) mice were purchased from Jackson Laboratories. To establish LCMV infection, mice received $2x10^5$ plaque-forming units (PFU) of LCMV-Armstrong by intraperitoneal (i.p) injection on day 0 and experiments were carried out until day +8 post-infection. Beginning at day 4, mice were given twice daily i.p injections of R59022 at a dose of 2 mg/kg body weight, dissolved in DMSO. Mice in all groups were sex and age matched.

In vitro stimulation of mouse splenocytes

Splenocytes were cultured at a concentration of $10x10^6$ cells/mL with or without gp33 peptide (0.4 ng/μL, AnaSpec) in the presence of monensin and fluorochrome conjugate anti-CD107α (BD Biosciences) for 5 hours. Cells were washed, fixed and permeabilized with cytofix/cytoperm (BD Biosciences) and stained for intracellular cytokines. Fluorochrome conjugated anti-mouse CD4, CD8, TCRβ, and IFNγ monoclonal antibodies were from BD Biosciences. Anti-mouse CD44 and TNFα antibodies were

purchased from eBioscience. APC- conjugated MHC-I restricted LCMV gp33 tetramer was provided by John Wherry (University of Pennsylvania). Data were collected on an LSRII flow cytometer (BD Biosciences) and analyzed using FlowJo software (Tree Star). Serum IFNγ levels were determined by enzyme linked immunosorbent assay (R&D Systems).

Assessment of tissue histology in LCMV-infected mice

Livers were fixed overnight in 10% formalin (w/v) (Fischer Scientific), embedded in paraffin, cut in 5 μm sections, and stained with hematoxylin and eosin. Images were captured using a Ni-/-n Eclipse 90i equipped with a Nikon DS-Fi1 camera and NIS-Elements BR 3.0 software (Nikon). For each sample, five random fields were captured at 20x magnification (Nikon Plan Apo 10x; NA 0.45) and subjected to computer-based quantification of inflammatory infiltrates using the BZ-II Analyzer Hybrid Cell Count software (Keyence). The average number of inflammatory foci (defined as clusters containing >8 lymphocytes) was determined for each treatment group, along with the area of the inflammatory infiltrate.

Assessment of LCMV viral titers

Vero cells were plated onto 6 well plates at $1x10^5$ cells/mL in MEM with 7% penicillin, 1% streptomycin, 1% L-glutamine and incubated overnight at 37°C. Cells were incubated with 200 μL of a 10-fold serial dilution of liver lysates for 1 hour at 37°C, then overlaid with a 1:1 mixture of 1% agarose and 2X 199 medium (Corning Life Sciences) with 10% FBS. Plates were incubated at 37°C for 4 days. Wells were then overlaid with 2 mL of a 1:1 mixture of 1% agarose and 2X 199 medium with 1:50 dilution of 1% neutral red.

Plates were incubated at 37°C for 12 more hours and plaques counted to determine the PFU/g tissue.

Statistical analysis

Evaluation of *in vitro* assays across multiple treatments (RICD, RT-PCR, ELISA), and *in vivo* experiments, were analyzed using two-way ANOVA (alpha: 0.05) with Sidak's multiple comparisons correction using GraphPad PRISM software. When comparing two groups (RT-PCR, $AnnV^+$ cells), a two-tailed paired Student's t-test was performed in Microsoft Excel. Error bars are described in figure legends as ± SEM or ± SD where appropriate. A single asterisk denotes significance of a p-value ≤0.05 in all experiments; p-values are included in Table S4.

Study approval

Blood samples were obtained with informed consent under protocols approved by the respective Institutional Review Boards (Cincinnati Children's Hospital Medical Center, National Institute of Allergy and Infectious Diseases, University of Piemonte Orientale). Experimental procedures on animals were approved by the Institutional Animal Care and Use Committee at The Children's Hospital of Philadelphia and St. Jude Children's Research Hospital.

RESULTS

DGKα inhibition rescues RICD in SAP-deficient T cells

To investigate whether reduced DAG signaling contributes to the T cell-driven pathologic manifestations of XLP-1, we examined whether silencing or inhibition of DGKα could restore the sensitivity of XLP-1 T cells to RICD. SAP-deficient XLP-1 T cells exhibit reduced RICD relative to control T cells following stimulation with increasing concentrations of the agonistic anti-CD3 Ab OKT3 (174) (Fig 1A-B). Remarkably, this defect in RICD was substantially rescued by the siRNA-mediated silencing of DGKα (Fig. 1A-C), or by pre-treatment with the DGKα inhibitors R59949 (Fig. 1D-E) or R59022 (Fig. 1F) (160). The rescue in RICD obtained upon DGKα inhibition was likely due to the induction of apoptosis, as indicated by an increased percentage of AnnexinV$^+$ cells (Fig. 1G). Conversely, the inhibition or silencing of DGKα had little effect on RICD in activated T cells from healthy subjects (Fig. 1-2). As patient-derived cells were limited, we repeated these assays using siRNA to knock down SAP expression in activated T cells from healthy donors (Fig. 2) (174). In agreement with our prior findings, SAP-silenced cells exhibited defective RICD that was rescued by concomitant silencing of DGKα (Fig. 2A-B), or by treatment with the DGKα inhibitors R59949 (Fig. 2C) or R59022 (Fig. 2D). This restoration of RICD in SAP-silenced T cells was associated with enhanced apoptosis, as indicated by increased AnnexinV staining (Fig. 2E). For other isoforms expressed in T cells, silencing of DGKζ, but not DGKδ, also partially rescued RICD in SAP silenced cells (Fig. S1A-D). Conversely, overexpression of DGKα or DGKζ conferred partial resistance to RICD in normal T cells (Fig. S1E-F). These findings suggest a link between the RICD resistance of SAP-deficient lymphocytes and unrestrained DAG depletion caused by enhanced

DGK activity. To explore this further, we supplemented cultures with the DAG analogue 1,2-dioctanoyl-sn-glycerol (C8-DAG), which is rapidly incorporated into the cell membrane and triggers DAG-dependent signaling (77). Indeed, C8-DAG treatment markedly enhanced RICD in SAP-silenced but not control T cells (Fig. 2F). Collectively, these data demonstrate that excessive DGKα activity contributes to RICD resistance in SAP-deficient T cells, and that this process can be reversed by inhibition of DGKα. These data suggest that SAP promotes TCR signal strength and RICD sensitivity by attenuating DAG metabolism carried out by DGKα in activated T cells (Fig. 2G).

Figure 1. DGKα silencing or inhibition restores RICD in XLP-1 patient T cells. (A-B) Activated T cells from normal donors (Ctrl) or indicated XLP-1 patients were transfected with control (cntrl) or DGKα-specific siRNA, then restimulated 4 days later with OKT3 Ab. After 24 hours, % cell loss was evaluated by PI staining. Data are mean ± SD of 2 experiments (A) or 1 experiment (B) performed in triplicate, representative of 2 independent experiments using different control donors. **(C)** DGKα relative expression (rel exp) in siRNA-transfected cells from (A) measured by qRT-PCR (upper panel, mean ± SEM, n=4) or by Western blotting, with tubulin as loading control (lower panel). (D-F) Ctrl or XLP patient T cells were restimulated with OKT3 Ab following pretreatment with DGK inhibitors R59949 or R59022 (5-10 μM), or DMSO. After 24 hours, % cell loss was evaluated by PI staining. Data are mean ± SD of 3 experiments (E), or 1 experiment (D, F) performed in triplicate representative of 2 independent experiments using different control donors. (G) Cells used in (D) were pre-treated with R59949 (10 μM) or DMSO and restimulated with OKT3 (100 ng/ml) for 0, 6 and 12 hours. The % of apoptotic cells was measured by AnnexinV staining. Representative histograms are shown; marker numbers denote % AnnexinV$^+$ cells. The net increase in AnnexinV$^+$ cells at 12 hours is shown at right. Data are mean ± SD of 6 independent experiments using 4 separate controls and 2 XLP patients. Asterisks denote statistical significance by two-way ANOVA with Sidak correction (A-B, D-F) or paired t-test (C, G).

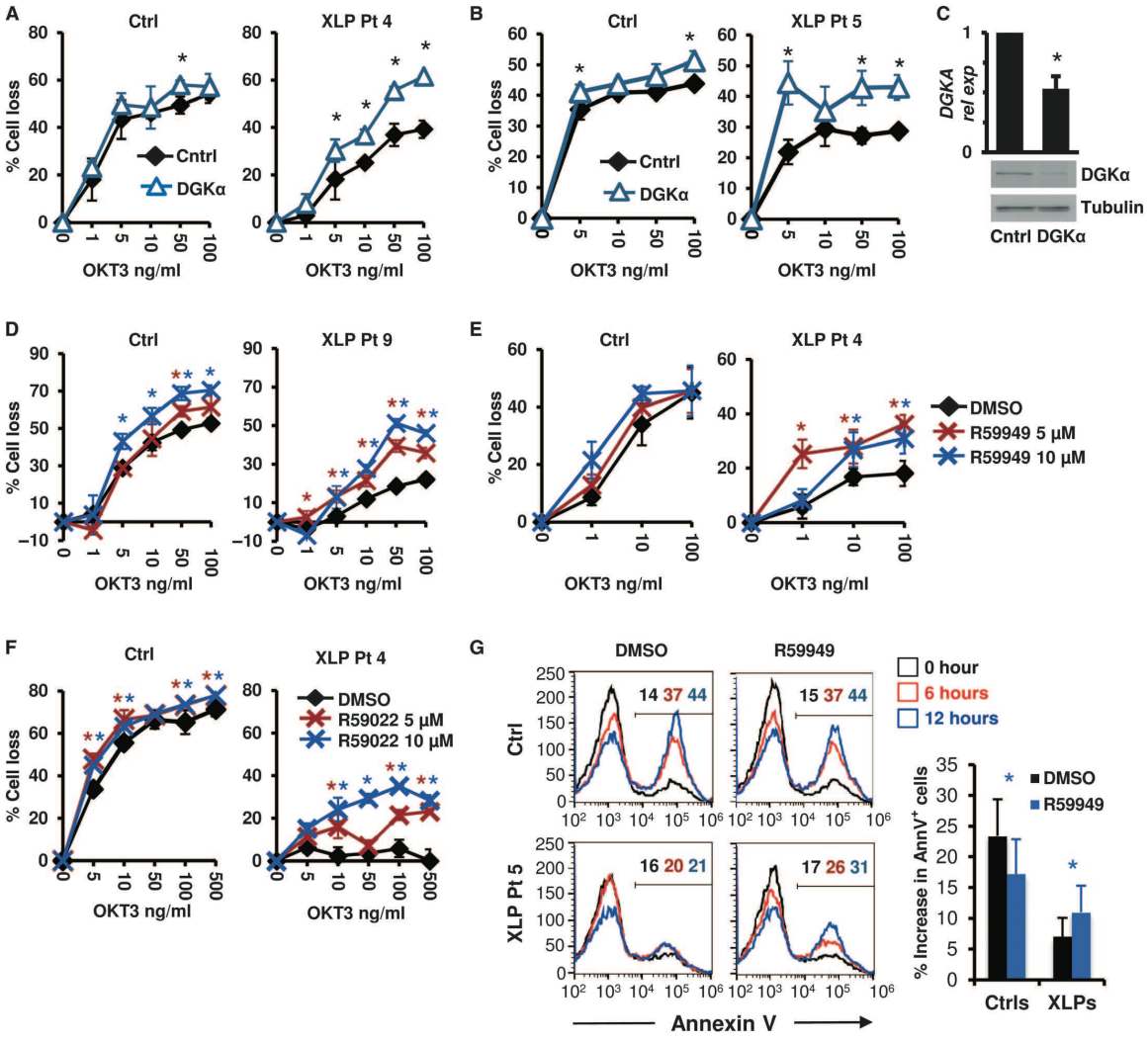

A
Ctrl
XLP Pt 4
% Cell loss
Cntrl
DGKα
OKT3 ng/ml
B
Ctrl
XLP Pt 5
C
DGKA rel exp
DGKα
Tubulin
Cntrl DGKα
D
Ctrl
XLP Pt 9
E
Ctrl
XLP Pt 4
DMSO
R59949 5 μM
R59949 10 μM
F
Ctrl
XLP Pt 4
DMSO
R59022 5 μM
R59022 10 μM
G
DMSO
R59949
0 hour
6 hours
12 hours
Ctrl
XLP Pt 5
14 37 44
15 37 44
16 20 21
17 26 31
Annexin V
% Increase in AnnV+ cells
Ctrls
XLPs

Figure 2. DGKα silencing or inhibition restores RICD in SAP-silenced T cells. (A) Activated normal donor T cells were transfected with control or SAP siRNA and restimulated 4 days later with OKT3 Ab. After 24 hours, % cell loss was evaluated by PI staining. Data are mean ± SEM of 3 experiments performed in triplicate. (B) SAP expression in siRNA-transfected T cells from (A) was measured by qRT-PCR (upper panel, mean ± SEM of 4 experiments) or by Western blotting, with actin as a loading control (lower panel). (C-D) siRNA-transfected cells (A) were restimulated with OKT3 Ab following pretreatment with DMSO, DGK inhibitor R59949 or R59022 (5-10 μM). After 24 hours, the % cell loss was evaluated by PI staining. Data are mean ± SEM of 5 experiments (C), or 5 (control) and 8 (SAP siRNA) independent experiments (D) performed in triplicate. (E) siRNA-transfected cells as in (A) were pretreated with DMSO or R59022 (10 μM) and restimulated with OKT3 (10 ng/ml). After 12 hours, the % apoptotic cells was evaluated by AnnexinV staining. Representative histograms are shown; marker numbers denote % AnnexinV$^+$ cells. The net increase in AnnexinV$^+$ cells at 12 hours is shown at right. Data are mean ± SD of 4 experiments. (F) siRNA-transfected cells (A) were treated with C8-DAG (50 μM) and restimulated with OKT3 Ab. After 24 hours, % cell loss was evaluated by PI staining. Data are mean ± SEM of 5 experiments performed in triplicate. Asterisks denote statistical significance by two-way ANOVA with Sidak correction (A,C,D-F) or paired t-test (B,E). (G) Schematic cartoon: pro-apoptotic TCR signaling is governed by DGKα inhibition in activated T cells.

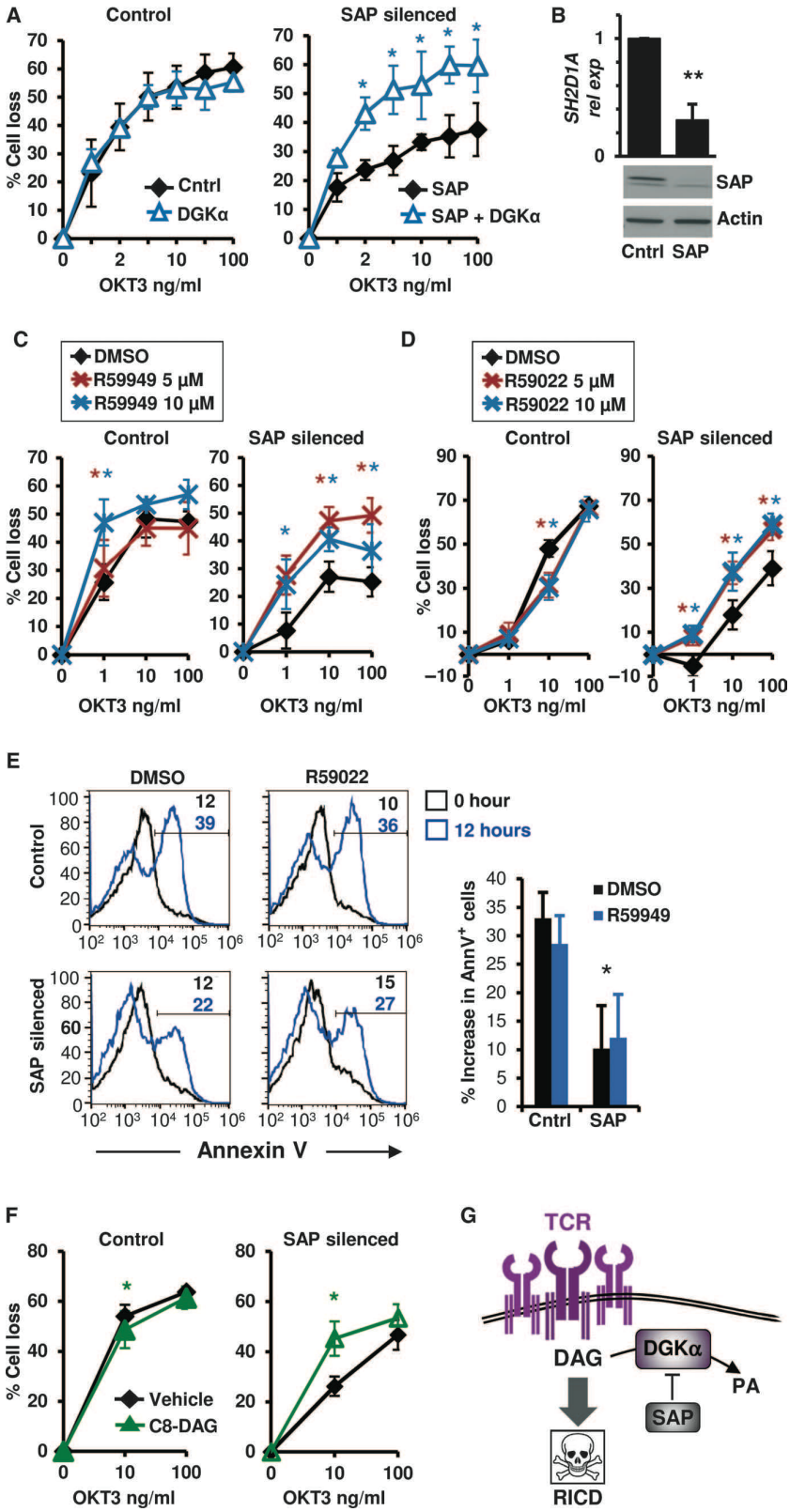
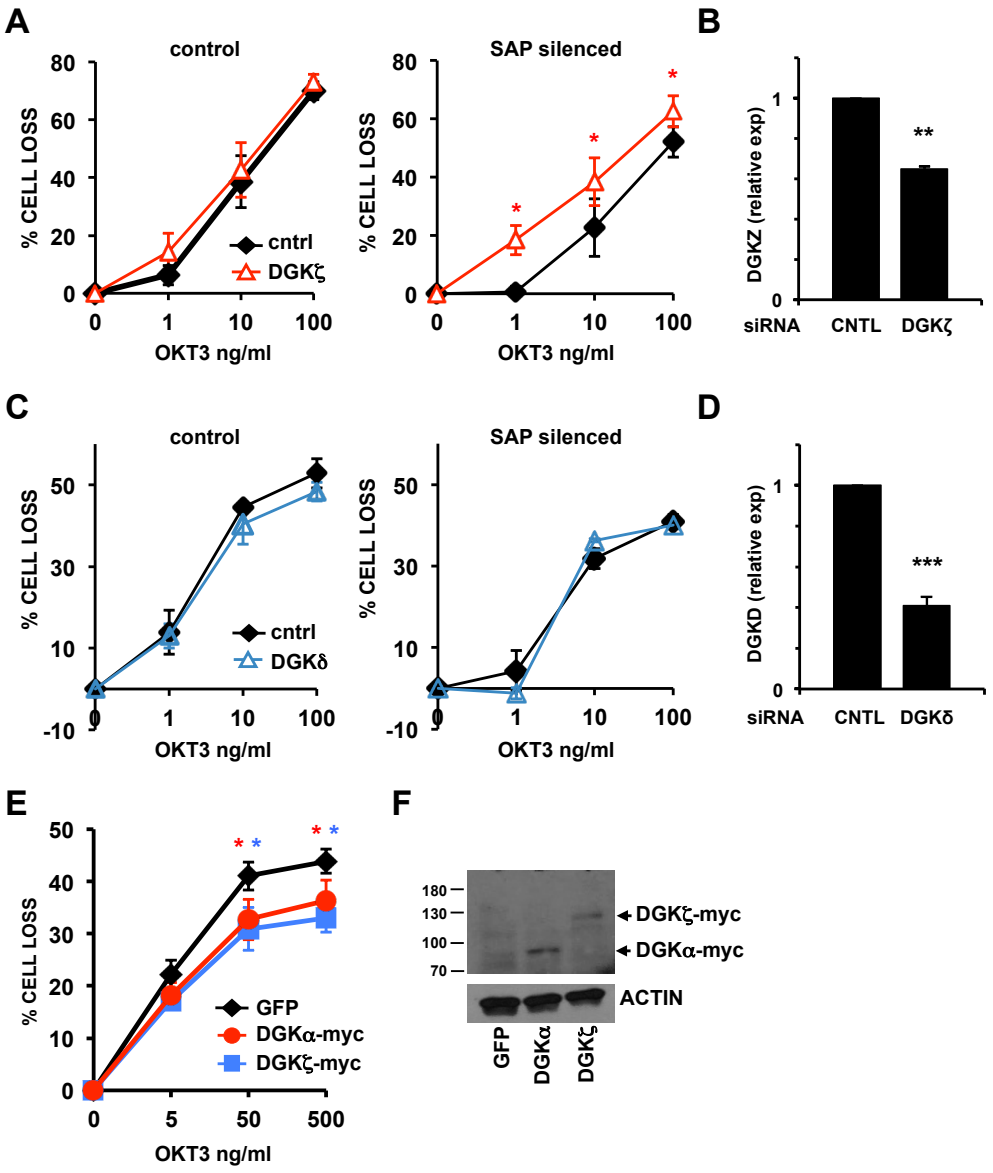

A
Control
SAP silenced
% Cell loss
OKT3 ng/ml
Cntrl
DGKα
SAP
SAP + DGKα
B
SH2D1A rel exp
SAP
Actin
Cntrl SAP
C
DMSO
R59949 5 μM
R59949 10 μM
D
DMSO
R59022 5 μM
R59022 10 μM
E
DMSO
R59022
Control
SAP silenced
0 hour
12 hours
12
39
10
36
12
22
15
27
Annexin V
% Increase in AnnV+ cells
DMSO
R59949
Cntrl SAP
F
Vehicle
C8-DAG
G
TCR
DAG
DGKα
PA
SAP
RICD

Figure S1. Activity of DGKα and DGKζ contributes to RICD resistance in T cells. (A-D) Activated normal donor T cells were transfected with control or SAP siRNA -/+ DGKz (A) or DGKd (C) siRNA and then restimulated 4 days later with OKT3. After 24 hours, % cell loss was evaluated by PI staining. Data are mean -/+ SEM of 8 (A) or 4 (C) independent experiments performed in triplicate. Knockdown of DGKZ (B) or DGKD (D) mRNA was assessed by quantitative RT-PCR; data are mean -/+ SEM for 3 experiments. (E) Activated normal donor T cells were transfected with expression plasmids encoding GFP or myc-tagged DGKa or DGKz. After 8 hours, cells were restimulated with OKT3; % cell loss was evaluated 24 hours later by PI staining. Data are mean -/+ SEM of 3 experiments; expression of myc-tagged DGKa and DGKz was assessed by immunoblotting.


A
control
SAP silenced
% CELL LOSS
OKT3 ng/ml
cntrl
DGKζ
B
DGKZ (relative exp)
siRNA
CNTL
DGKζ
C
DGKδ
D
DGKD (relative exp)
DGKδ
E
GFP
DGKα-myc
DGKζ-myc
F
DGKζ-myc
DGKα-myc
ACTIN
GFP
DGKα
DGKζ

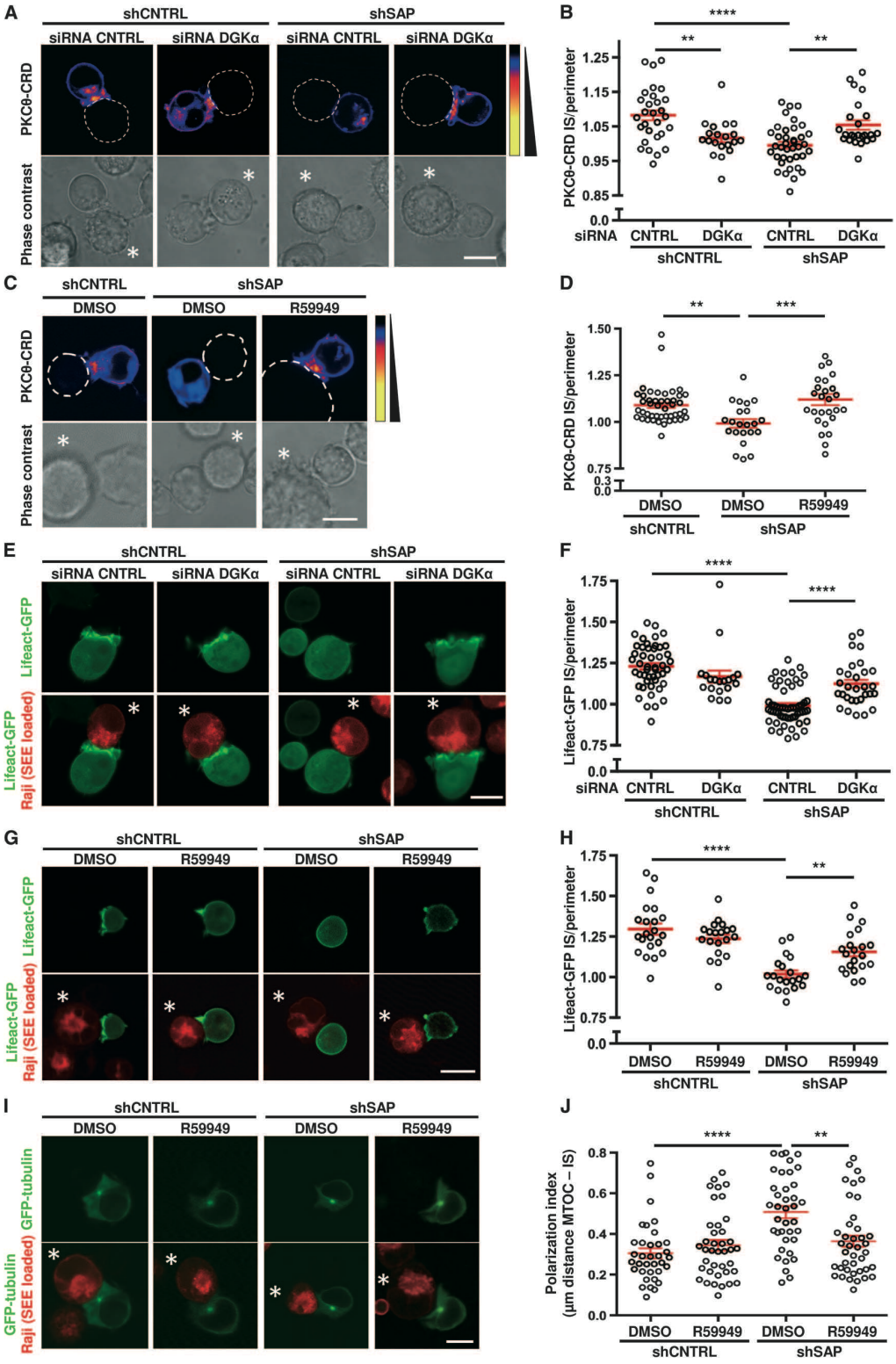
Inhibition of DGKα rescues defective DAG polarization and signaling at the IS in SAP-deficient cells

DAG generation and polarization at the IS are required for TCR-induced cellular responses (28). To investigate whether the deregulated DGKα activity caused by SAP deficiency affects DAG polarization toward the IS, we imaged DAG localization using a PKCθ-CRD-based biosensor (177). Following activation by superantigen-loaded Raji B cells, we observed that PKCθ-CRD polarization to the IS was strongly reduced in SAP-silenced versus control Jurkat cells (Fig. 3A-D). In contrast, co-silencing of DGKα (Fig. 3A, B) or pre-treatment with the DGK inhibitor R59949 (Fig. 3C, D) restored PKCθ-CRD polarization in SAP-silenced T cells. Consistent with the finding that DGKα shapes the DAG gradient at the IS (34), DAG polarization was also reduced in SAP-expressing, DGKα-silenced Jurkat cells (Fig. 3A, B).

Polarized DAG signaling triggers F-actin polymerization and microtubule organizing center (MTOC) orientation (141). Consistent with reduced DAG polarization, SAP-silenced T cells exhibited a strong defect in F-actin accumulation at, and MTOC orientation toward, the IS upon contact with superantigen-loaded Raji cells (Fig. 3E-J). Again, silencing or inhibition of DGKα partially restored these processes (Fig. 3E-J). These findings indicate that SAP regulates the architecture of the IS by inhibiting DGKα, thereby limiting DAG metabolism locally.

Figure 3. DGKα silencing or inhibition restores synapse formation in SAP-deficient T cells.

ShCNTRL or shSAP Jurkat T cells were transiently transfected as indicated. After 48 (C, D, G, H, I, J) or 96 (A, B, E, F) hours, T cells were challenged with SEE-loaded Raji B cells, and confocal live cell images were captured during T cell-APC conjugation. In (C, D, G, H, I, J) T cells were pretreated for 30 minutes with 10 μM R59949 or DMSO. (A, C) Top row: EGFP-tagged PKCθ-CRD (pseudo color) together with the perimeter of the APC (dotted line). Bottom row: phase contrast images with APC denoted by *. Scale bar 10 μm. (B, D) Quantification of EGFP-PKCθ-CRD accumulation at the IS. Mean ± SEM of >20 conjugates per condition from 3 experiments. (E, G) Top row: Lifeact-GFP (green). Bottom row also shows Raji B cells stained with CellTracker Red CMTPX (red). Scale bar 10 μm. (F, H) Quantification of Lifeact-GFP accumulation at the IS. Mean ± SEM of >20 conjugates per condition from 3 experiments. (I) Top row: GFP-tubulin (green). Bottom row also shows Raji B cells stained with CellTracker Red CMTPX (red). Scale bar 10 μm. (J) Quantification of MTOC polarization index. Mean ± SEM of >35 conjugates per condition from 2 experiments. Asterisks in all panels denote statistical significance by one-way ANOVA with Sidak correction.


A
shCNTRL
shSAP
siRNA CNTRL
siRNA DGKα
siRNA CNTRL
siRNA DGKα
PKCθ-CRD
Phase contrast
B
****
**
**
PKCθ-CRD IS/perimeter
1.25
1.15
1.05
0.95
0.85
0.0
siRNA
CNTRL
DGKα
CNTRL
DGKα
shCNTRL
shSAP
C
shCNTRL
shSAP
DMSO
DMSO
R59949
PKCθ-CRD
Phase contrast
D
**
***
PKCθ-CRD IS/perimeter
1.50
1.25
1.00
0.75
0.3
0.0
DMSO
DMSO
R59949
shCNTRL
shSAP
E
shCNTRL
shSAP
siRNA CNTRL
siRNA DGKα
siRNA CNTRL
siRNA DGKα
Lifeact-GFP
Lifeact-GFP
Raji (SEE loaded)
F
****
****
Lifeact-GFP IS/perimeter
1.75
1.50
1.25
1.00
0.75
0.0
siRNA
CNTRL
DGKα
CNTRL
DGKα
shCNTRL
shSAP
G
shCNTRL
shSAP
DMSO
R59949
DMSO
R59949
Lifeact-GFP
Lifeact-GFP
Raji (SEE loaded)
H
****
**
Lifeact-GFP IS/perimeter
1.75
1.50
1.25
1.00
0.75
0.0
DMSO
R59949
DMSO
R59949
shCNTRL
shSAP
I
shCNTRL
shSAP
DMSO
R59949
DMSO
R59949
GFP-tubulin
GFP-tubulin
Raji (SEE loaded)
J
****
**
Polarization index
(μm distance MTOC – IS)
0.8
0.6
0.4
0.2
0.0
DMSO
R59949
DMSO
R59949
shCNTRL
shSAP

We next investigated whether inhibition of DGKα restores DAG-mediated signaling downstream of the TCR in SAP-silenced primary human T cells. PKCθ and RasGRP1 are recruited to the IS in a DAG-dependent manner (2; 49), and are required for induction of RICD (93; 105). Consistent with our hypothesis, SAP-silenced primary T cells exhibited defective recruitment of PKCθ and RasGRP1 to the IS, which was fully restored upon DGKα silencing (Fig. 4A-B, E-F) or pharmacological inhibition (Fig. 4C-D, G-H). Considering inhibition of DGKα also rescues defective ERK1/2 activation in SAP-deficient T cells (9), these data underscore the importance of the SAP/DGKα axis in regulating DAG-dependent signaling.

Figure 4. DGKα silencing or inhibition restores PKCθ and RasGRP1 recruitment to the IS in SAP-deficient cells.

(A, C, E, G) Activated T cells were transfected with the indicated siRNA and after 72 hours incubated with SEE-loaded Raji B cells (denoted with *) for 15 minutes, fixed and stained for PKCθ (A,C) or RasGRP1(E,G). Top rows: target protein (green), bottom rows also show phase contrast. Scale bar 5 μm. (B) Percentage of cells displaying PKCθ at the IS. Data are mean ± SEM of 6 replicates from 2 independent experiments. (D) Percentage of cells displaying PKCθ at the IS. Data are mean ± SEM of 3 experiments. (F) Percentage of cells with RasGRP1 at the IS. Data are mean ± SD of 1 representative experiment performed in quadruplicate. (H) Percentage of cells displaying RasGRP1 at the IS. Data are mean ± SEM of 3 experiments. Asterisks in all panels denote statistical significance by two-way ANOVA + Sidak correction.

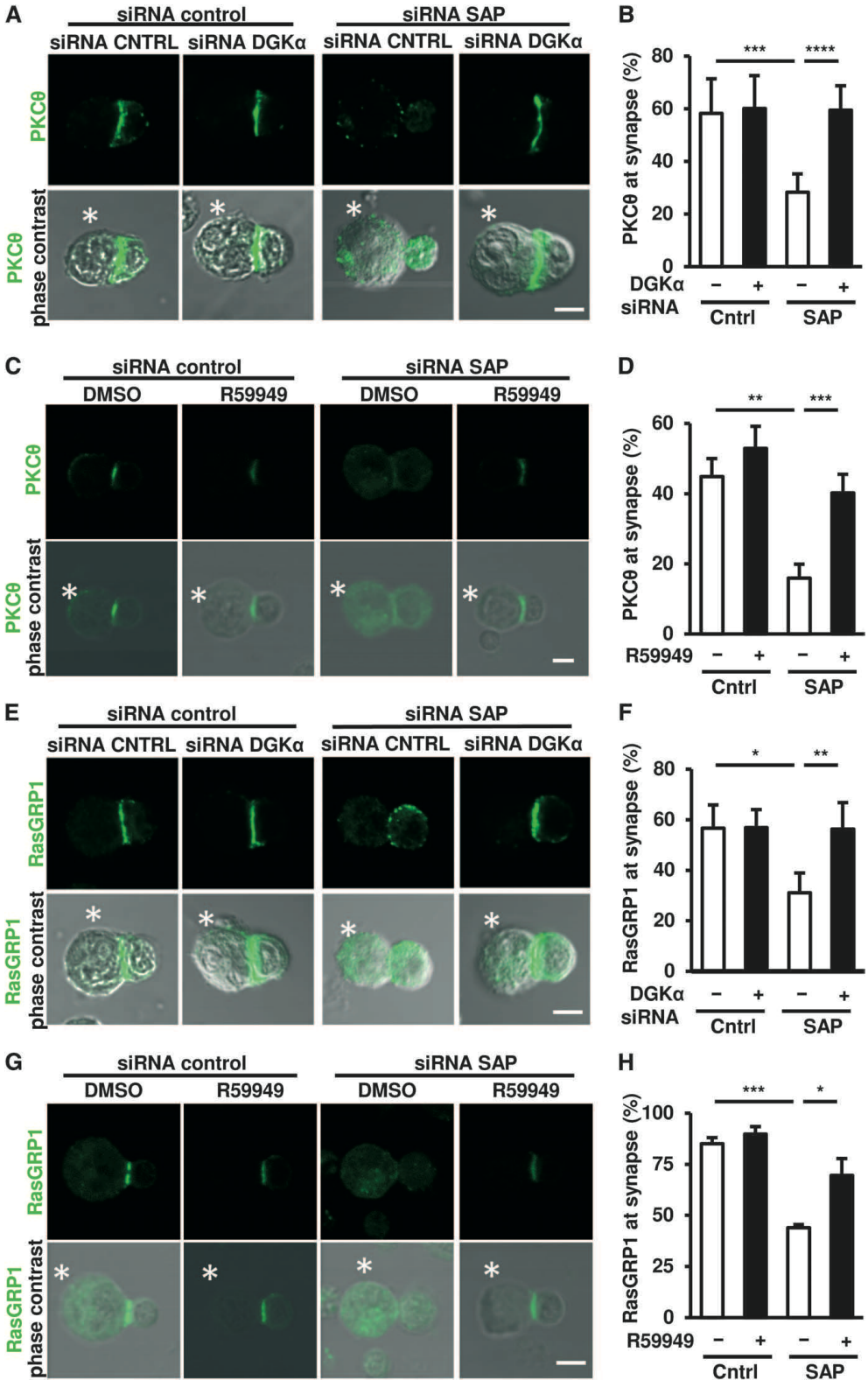
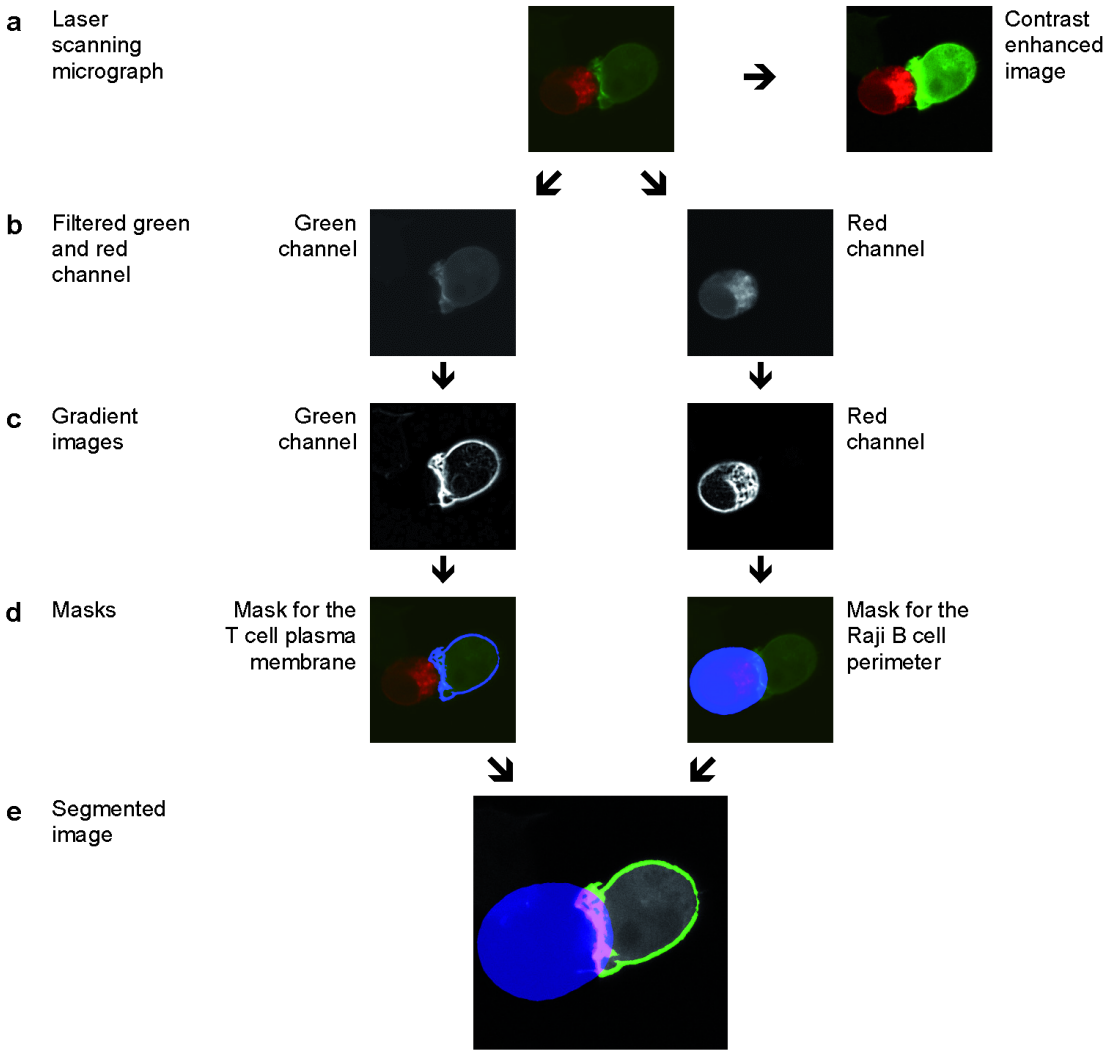

A
siRNA control
siRNA SAP
siRNA CNTRL
siRNA DGKα
siRNA CNTRL
siRNA DGKα
PKCθ
PKCθ phase contrast
B
PKCθ at synapse (%)
80
60
40
20
0
***
****
DGKα siRNA
–
+
–
+
Cntrl
SAP
C
siRNA control
siRNA SAP
DMSO
R59949
DMSO
R59949
PKCθ
PKCθ phase contrast
D
PKCθ at synapse (%)
60
40
20
0
**
***
R59949
–
+
–
+
Cntrl
SAP
E
siRNA control
siRNA SAP
siRNA CNTRL
siRNA DGKα
siRNA CNTRL
siRNA DGKα
RasGRP1
RasGRP1 phase contrast
F
RasGRP1 at synapse (%)
80
60
40
20
0
*
**
DGKα siRNA
–
+
–
+
Cntrl
SAP
G
siRNA control
siRNA SAP
DMSO
R59949
DMSO
R59949
RasGRP1
RasGRP1 phase contrast
H
RasGRP1 at synapse (%)
100
75
50
25
0
***
*
R59949
–
+
–
+
Cntrl
SAP

Figure S4. Major steps of the automated segmentation and fluorescence quantification algorithm.

(A) Original image and contrast enhanced image of a Jurkat T cell and a Raji B cell. The green channel was used to record LifeAct GFP fluorescence whereas CellTracker Red fluorescence was recorded in the red channel. (B) Filtered images. To reduce noise but to preserve edges, images were filtered by a two-dimensional median filtering algorithm. (C) Gradient image. To detect the plasma membrane pixels were identified, where the gradient of the filtered image was steepest. (D) Masks for the plasma membrane of the T cell and the periphery of the Raji B cell. The gradient images were used to create the masks for the plasma membrane of the T cell (blue region in the left panel) and the Raji B cell. A perimeter of 2 μm around the plasma membrane of the Raji B cell (blue region in the right panel) was chosen to identify structures being in contact with the Raji B cell. (E) Segmentation and quantification. Regions of the plasma membrane of the T cell (red) that overlap with the mask for the Raji B cell perimeter (blue) are assumed to be part of the contact site. Remaining parts of the T cell plasma membrane (green) are supposed not to be in contact with the Raji B cell. Fluorescence intensities in the two regions were quantified and their ratio was calculated. In the example shown fluorescence intensities in the contact site were 35% higher than in the remaining regions.


a
Laser scanning micrograph
Contrast enhanced image
b
Filtered green and red channel
Green channel
Red channel
c
Gradient images
Green channel
Red channel
d
Masks
Mask for the T cell plasma membrane
Mask for the Raji B cell perimeter
e
Segmented image

To test if inhibition of DGKα rescues RICD in SAP-deficient T cells by restoring specific DAG-mediated signaling pathways, we examined whether the rescue of RICD requires the activity of PKCθ or RasGRP1. Silencing of PKCθ (Fig. 5A) or RasGRP1 (Fig 5B) reduced RICD in control siRNA transfected T cells, and completely abrogated the rescue of RICD in SAP and DGKα siRNA transfected cells. Moreover, pharmacological inhibition of PKC or MEK/ERK enzymatic activity also prevented the restoration of RICD noted following DGKα silencing in SAP-deficient T cells (Fig. S2).

TCR activation stimulates DAG-dependent induction of IL-2 and the high-affinity IL-2 receptor CD25 (38; 178), which are both required for RICD (94). Indeed, inhibition or silencing of DGKα restored induction of CD25 in SAP-silenced T cells after TCR restimulation, and a similar trend was observed with IL-2 expression (Fig. 5C-E). These findings further establish the SAP/DGKα signaling axis as a critical regulator of DAG signaling potency. Collectively, these findings underscore the vital role of SAP-dependent inhibition of DGKα in sustaining DAG signaling, leading to the activation of PKCθ and Ras-ERK and RICD (Fig. 5F).

Figure 5. DGKα silencing restores TCR-induced PKCθ and Ras-mediated signaling pathways to drive RICD in SAP-deficient cells.

(A-B) Activated normal donor T cells were transfected with the indicated siRNA and restimulated 4 days later with OKT3 Ab (10 ng/ml). After 24 hours, % cell loss was evaluated by PI staining. Data are mean ± SEM of 7 (A) or 6 (B) experiments performed in triplicate. Right panels: expression of PKCθ (A) or RasGRP1 (B) was measured by Western blotting, with actin as a loading control. (C-D) Quantitative RT-PCR for *IL2* mRNA in T cells pre-treated with R59949 (10 μM) (C) or transfected with DGKa siRNA (D) after restimulation with OKT3 (10 μg/ml, 4 hours) *GUSB* served as the reference gene. Graphs represent mean ± SEM of 6 (C) or 7 (D) experiments. (E) Left: Representative flow cytometric histograms showing CD25 surface expression on siRNA-transfected T cells from (A) ± OKT3 restimulation (24 hours). Right: graph depicts mean fluorescence intensity (MFI) of CD25 expression. Data are mean ± SEM of 4 experiments. Asterisks in all panels denote statistical significance by two-way ANOVA with Sidak correction. (F) Schematic cartoon: SAP-mediated inhibition of DGKα activity ensures a sufficient pool of DAG required for proper IS organization and recruitment of PKCθ and RasGRP, which mediates downstream signaling for RICD.

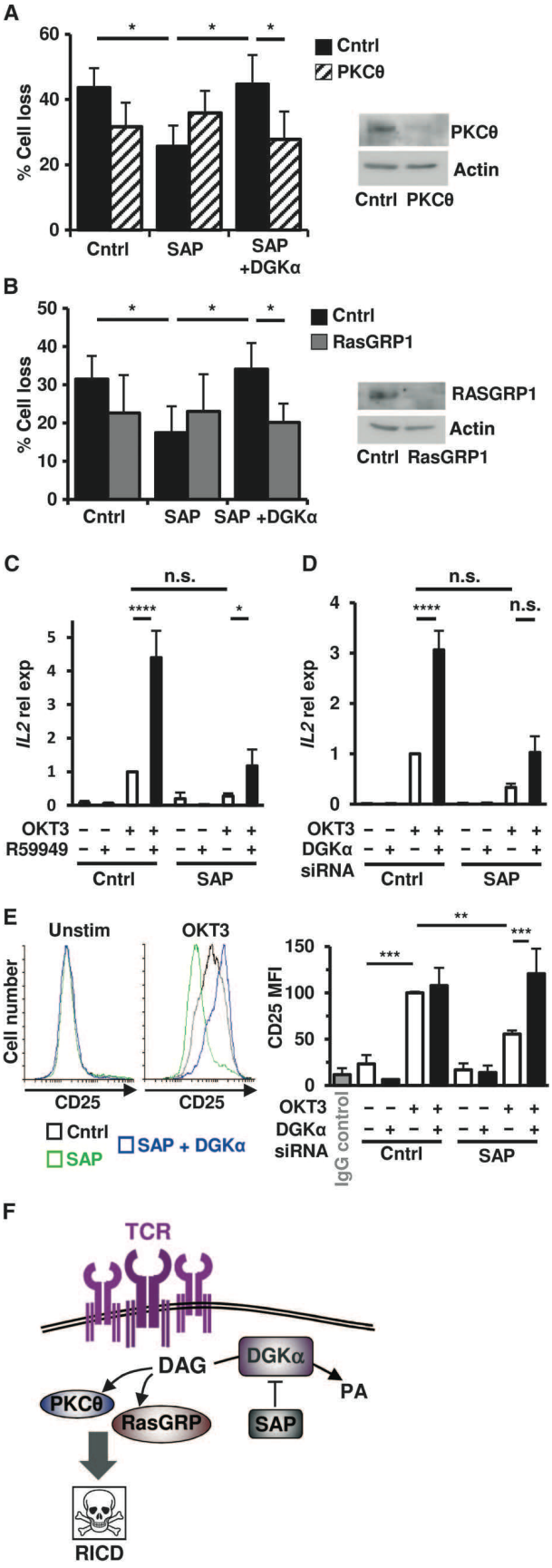
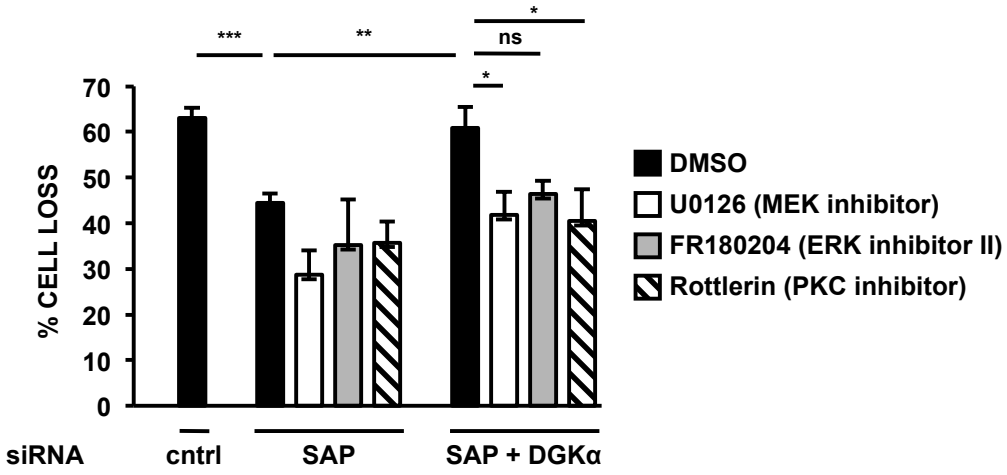

A
% Cell loss
Cntrl
PKCθ
PKCθ
Actin
Cntrl PKCθ
Cntrl
SAP
SAP +DGKα
B
% Cell loss
Cntrl
RasGRP1
RASGRP1
Actin
Cntrl RasGRP1
Cntrl
SAP
SAP +DGKα
C
n.s.
IL2 rel exp
OKT3
R59949
Cntrl
SAP
D
n.s.
IL2 rel exp
OKT3
DGKα siRNA
Cntrl
SAP
E
Unstim
OKT3
Cell number
CD25
CD25
Cntrl
SAP
SAP + DGKα
CD25 MFI
OKT3
DGKα siRNA
IgG control
Cntrl
SAP
F
TCR
DAG
DGKα
PA
PKCθ
RasGRP
SAP
RICD

Figure S2. DGKα silencing restores RICD in SAP-deficient cells through PKCθ and Ras-mediated signaling pathways.

Activated normal donor T cells were transfected with the indicated siRNA. Four days later, cells were pre-treated for 30 min with U0126 (5 μM), FR180204 (10 μM), rottlerin (6 μM), or DMSO and restimulated with OKT3 Ab (100 ng/ml). After 24 hours, % cell loss was evaluated by PI staining. Data are mean ± SEM of 6 experiments performed in triplicate. Asterisks denote significance by 2-way ANOVA + Sidak correction for multiple comparisons.

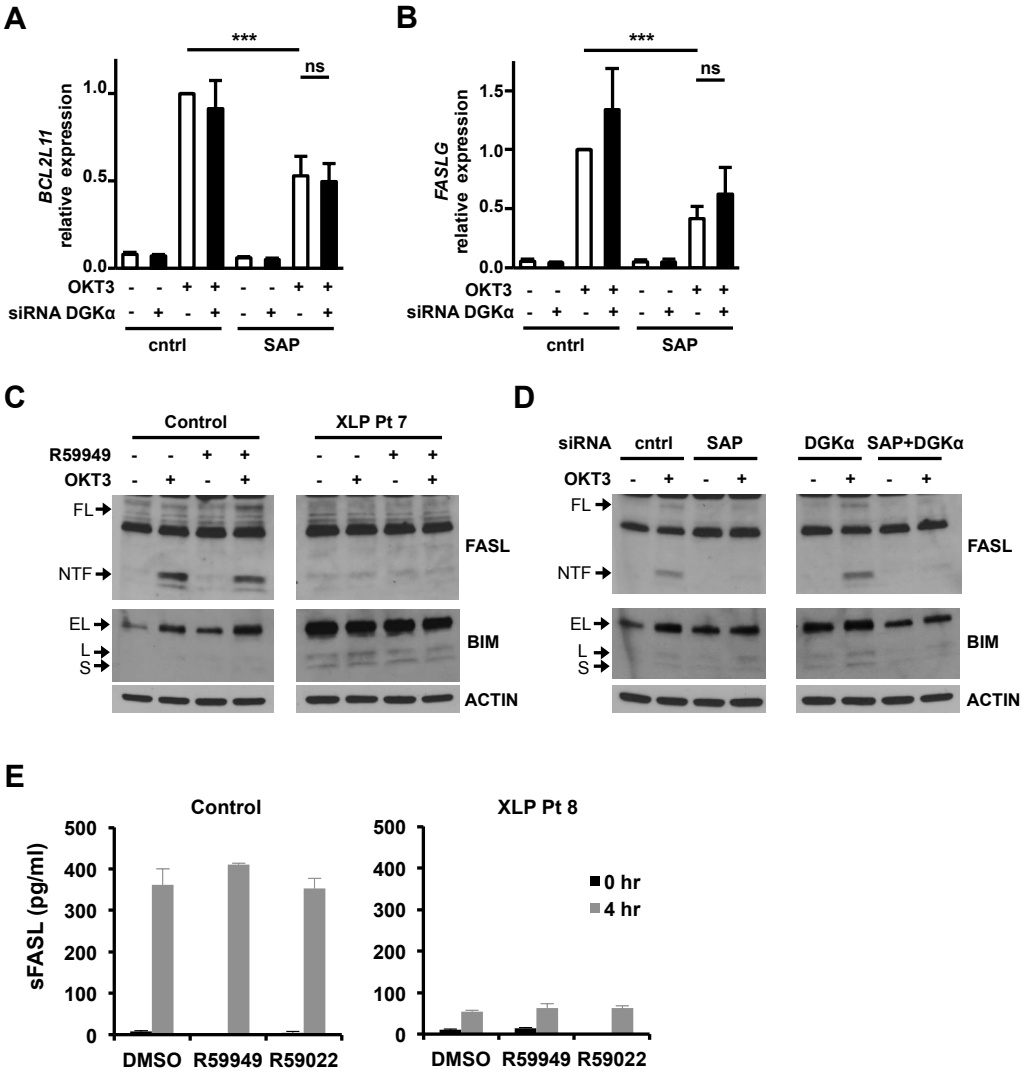

***
**
*
ns
*
70
60
50
40
30
20
10
0
% CELL LOSS
siRNA
cntrl
SAP
SAP + DGKα
DMSO
U0126 (MEK inhibitor)
FR180204 (ERK inhibitor II)
Rottlerin (PKC inhibitor)

NUR77 and NOR1 mediate the rescue of RICD that is induced by DGKα inhibition in SAP-deficient T cells

We next investigated the mechanism by which the enhancement of DAG signaling obtained following inhibition of DGKα restores RICD sensitivity in SAP-deficient T cells. We previously showed that in SAP-deficient T cells, TCR-induced expression of key pro-apoptotic genes such as *FASLG* and *BCL2L11* is impaired (174). Surprisingly, we observed that silencing or inhibition of DGKα failed to rescue *FASLG* or *BCL2L11* expression following TCR restimulation of SAP-silenced T cells (Fig. S3A, B). Similarly, DGKα blockade failed to restore the induction of all three major isoforms of BIM protein (extra-long EL, long L, and short S), as well as full-length and soluble FASL protein in SAP-silenced and XLP-1 patient T cells following restimulation (Fig. S3C-E). These observations imply that DGKα inhibition does not restore all SAP-dependent, pro-apoptotic effector functions that contribute to RICD sensitivity.

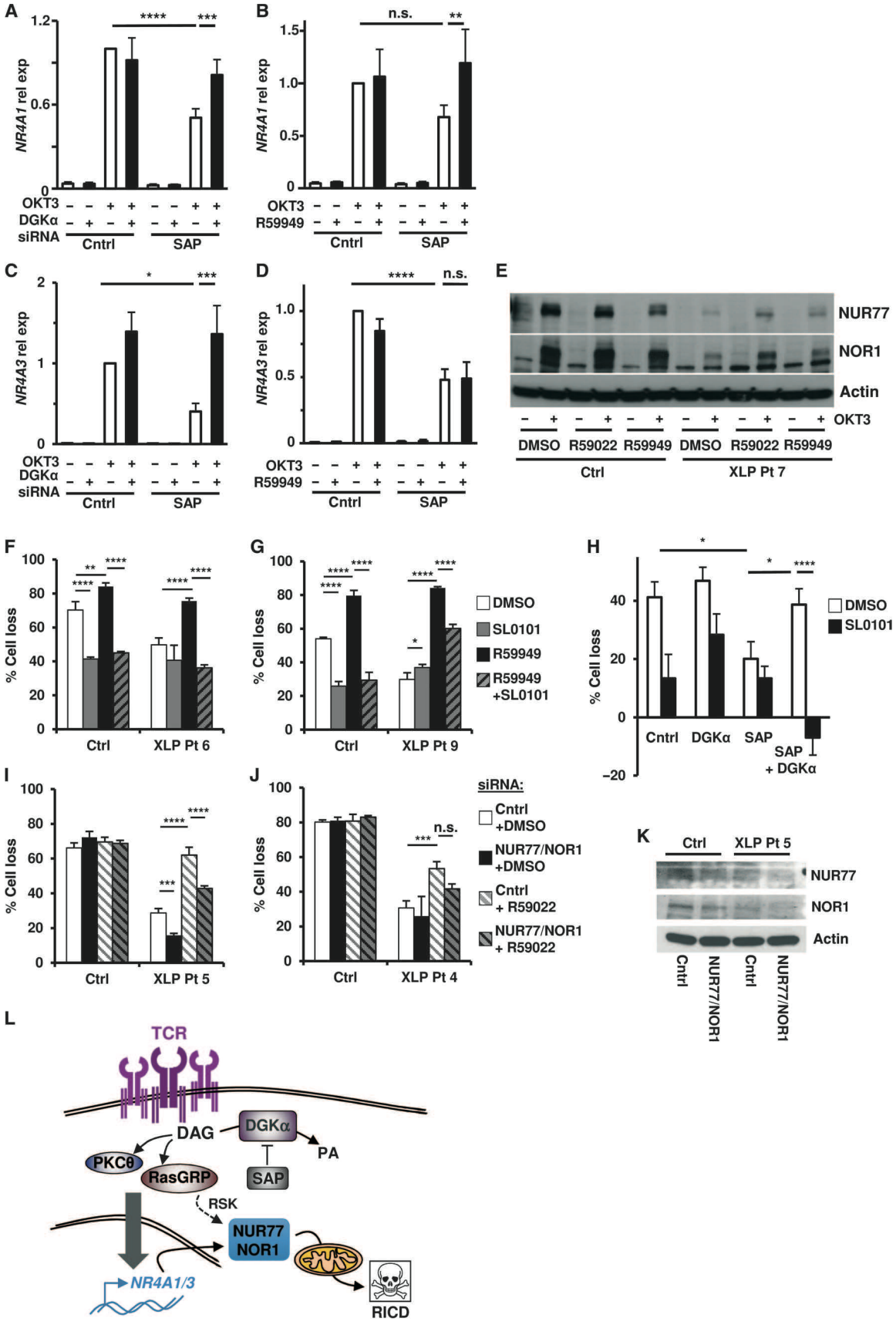
Figure S3. DGKα blockade fails to rescue TCR-induced upregulation of pro-apoptotic mediators FASL and BIM in SAP-deficient cells.

(A-B) Activated normal donor T cells were transfected with the indicated siRNA and restimulated 4 days later with OKT3 (10 μg/ml, 4 hours). *BCL2L11* (A) or FASL (B) mRNA was quantified by quantitative RT-PCR using GUSB as a reference gene. Graph shows the mean ± SEM of 5 independent experiments. Asterisks denote significance based on 2-way ANOVA + Sidak correction for multiple comparisons (*** $P < 0.001$). (C) Activated T cells derived from a normal donor (Ctrl) or XLP-1 patient 7 were pretreated with R59949 (1 μM, 30 minutes) and restimulated with OKT3 (100 ng/ml, 0 or 4 hrs). Cell lysates were separated by SD-PAGE Expression of FASL (FL = full-length, NTF = N-terminal fragment), BIM (EL = extra long, L = long, S = short isoforms), and β-actin expression was assessed by Western blotting. (D) Activated normal donor T cells were transfected with SAP or DGKα-specific siRNA. After 4 days, cells were treated with OKT3 (100 ng/ml, 0 or 4 hrs). Cells were lysed and analyzed by Western blotting as above. (E) Activated T cells derived from a normal donor (Ctrl) or XLP-1 patient 8 were treated with R59949 or R599022 (10 μM) and restimulated with OKT3 (100 ng/ml) for 4 hours. Soluble FASL in cell supernatants was measured by ELISA. Data in (C - E) are representative of 3 independent experiments using different donors.


A
***
ns
BCL2L11 relative expression
1.0
0.5
0.0
OKT3 - - + + - - + +
siRNA DGKα - + - + - + - +
cntrl
SAP
B
***
ns
FASLG relative expression
1.5
1.0
0.5
0.0
OKT3 - - + + - - + +
siRNA DGKα - + - + - + - +
cntrl
SAP
C
Control
XLP Pt 7
R59949 - - + + - - + +
OKT3 - + - + - + - +
FL
NTF
FASL
EL
L
S
BIM
ACTIN
D
siRNA cntrl SAP DGKα SAP+DGKα
OKT3 - + - + - + - +
FL
NTF
FASL
EL
L
S
BIM
ACTIN
E
Control
XLP Pt 8
sFASL (pg/ml)
500
400
300
200
100
0
0 hr
4 hr
DMSO R59949 R59022
DMSO R59949 R59022

Instead, we found that SAP-deficient T cells exhibit a previously unrecognized defect in TCR restimulation-induced upregulation of *NR4A1* (NUR77) and *NR4A3* (NOR1), two nuclear receptors involved in negative selection of thymocytes and RICD of mature T cells (36). Importantly, DGKα silencing or inhibition selectively restored TCR-dependent induction of both *NR4A1* and *NR4A3* in SAP-silenced activated T cells (Fig. 6A-D). DGKα inhibition also partially rescued NUR77 and NOR1 protein induction in XLP-1 T cells following TCR restimulation (Fig. 6E). Upon TCR engagement, NUR77 and NOR1 proteins are phosphorylated by the ERK1/2-regulated 90 kD ribosomal S6 kinase (RSK), triggering the intrinsic apoptosis pathway (190). Indeed, the RSK-specific inhibitor SL0101 (173) significantly reduced RICD in control T cells, confirming that phosphorylation of NUR77 and NOR1 is an important component of RICD execution (Fig 6F-H). Importantly, SL0101 significantly blunted the RICD rescue triggered by DGKα inhibition in XLP-1 T cells, as well as in SAP/DGKα-silenced T cells (Fig 6F-H). These data indicate that the rescue of RICD afforded by DGKα blockade in SAP-deficient T cells is dependent on RSK activity. Moreover, concomitant knockdown of NUR77 and NOR1 reduced the rescue of RICD induced by DGKα inhibition in XLP-1 T cells (Fig. 6I-K). Altogether, these observations indicate that inhibition of DGKα boosts RICD in SAP-deficient T cells in part by selectively restoring TCR-induced upregulation and RSK-dependent phosphorylation of NUR77 and NOR1 (Fig. 6L).

Figure 6. Silencing or inhibition of DGKα restores RICD sensitivity in SAP-deficient T cells via induction of pro-apoptotic molecules NUR77 and NOR1.
(A-D) Quantitative RT-PCR for *NR4A1* (A-B) or *NR4A3 (C-D)* from activated normal donor T cells transfected with control or SAP-specific siRNA ± DGKa-specific siRNA (A,C) or 5 μM R59949 (B,D) and restimulated with OKT3 (10 μg/ml) for 4 hours. *GUSB* served as the reference gene. Data are mean ± SEM of 8 (A), 5 (B), 7 (C) or 6 (D) experiments. (E) Activated T cells from normal donor (Ctrl) or XLP-1 patient 7 were pretreated for 30 minutes with R59022 or R59949 (10 μM), then restimulated with 100 ng/ml OKT3. Cells lysates were analyzed by Western blotting for NUR77, NOR1 and β-actin content. Data are representative of 2 independent experiments using different donors. (F-G) Activated T cells from normal donors (Ctrl) or XLP-1 patients were pretreated for 30 minutes with DMSO, SL0101-1 (90 μM), R59949 (10 μM), or both, followed by restimulation with OKT3 (100 ng/ml). After 24 hours, % cell loss was evaluated by PI staining. Data are mean ± SD of 1 experiment each performed in triplicate using different donors. (H) Activated donor T cells were transfected with the indicated siRNA and treated 4 days later with SL0101-1 (50 μM) for 30 minutes, followed by OKT3 (10 ng/ml). After 24 hours, % cell loss was evaluated by PI staining. Data are mean ± SEM of 5 experiments performed in triplicate. (I-J) Activated T cells from normal donors (Ctrl) or XLP-1 patients were transfected control or NUR77+NOR1 siRNA and treated 4 days later with DMSO or R59022 (10 μM) for 30 minutes, followed by OKT3 (100 ng/ml). After 24 hours, % cell loss was evaluated by PI staining. Data are mean ± SD of 1 experiment each, performed in triplicate using different donors. Asterisks in all panels denote statistical significance by two-way ANOVA with Sidak correction. (K) Western blot for NUR77 and NOR1 expression in OKT3-restimulated, siRNA-transfected T cells from (I). Actin served as a loading control. (L) Schematic cartoon: mechanism of pro-apoptotic TCR signaling governed by SAP-dependent DGKα inhibition in activated T cells.


A
NR4A1 rel exp
OKT3
DGKα
siRNA
Cntrl
SAP
B
NR4A1 rel exp
OKT3
R59949
Cntrl
SAP
n.s.
C
NR4A3 rel exp
OKT3
DGKα
siRNA
Cntrl
SAP
D
NR4A3 rel exp
OKT3
R59949
Cntrl
SAP
n.s.
E
NUR77
NOR1
Actin
OKT3
DMSO
R59022
R59949
Ctrl
XLP Pt 7
F
% Cell loss
Ctrl
XLP Pt 6
G
% Cell loss
DMSO
SL0101
R59949
R59949 +SL0101
Ctrl
XLP Pt 9
H
% Cell loss
DMSO
SL0101
Cntrl
DGKα
SAP
SAP + DGKα
I
% Cell loss
Ctrl
XLP Pt 5
J
% Cell loss
siRNA:
Cntrl +DMSO
NUR77/NOR1 +DMSO
Cntrl + R59022
NUR77/NOR1 + R59022
Ctrl
XLP Pt 4
n.s.
K
Ctrl
XLP Pt 5
NUR77
NOR1
Actin
Cntrl
NUR77/NOR1
Cntrl
NUR77/NOR1
L
TCR
DAG
DGKα
PA
PKCθ
RasGRP
SAP
RSK
NUR77
NOR1
NR4A1/3
RICD

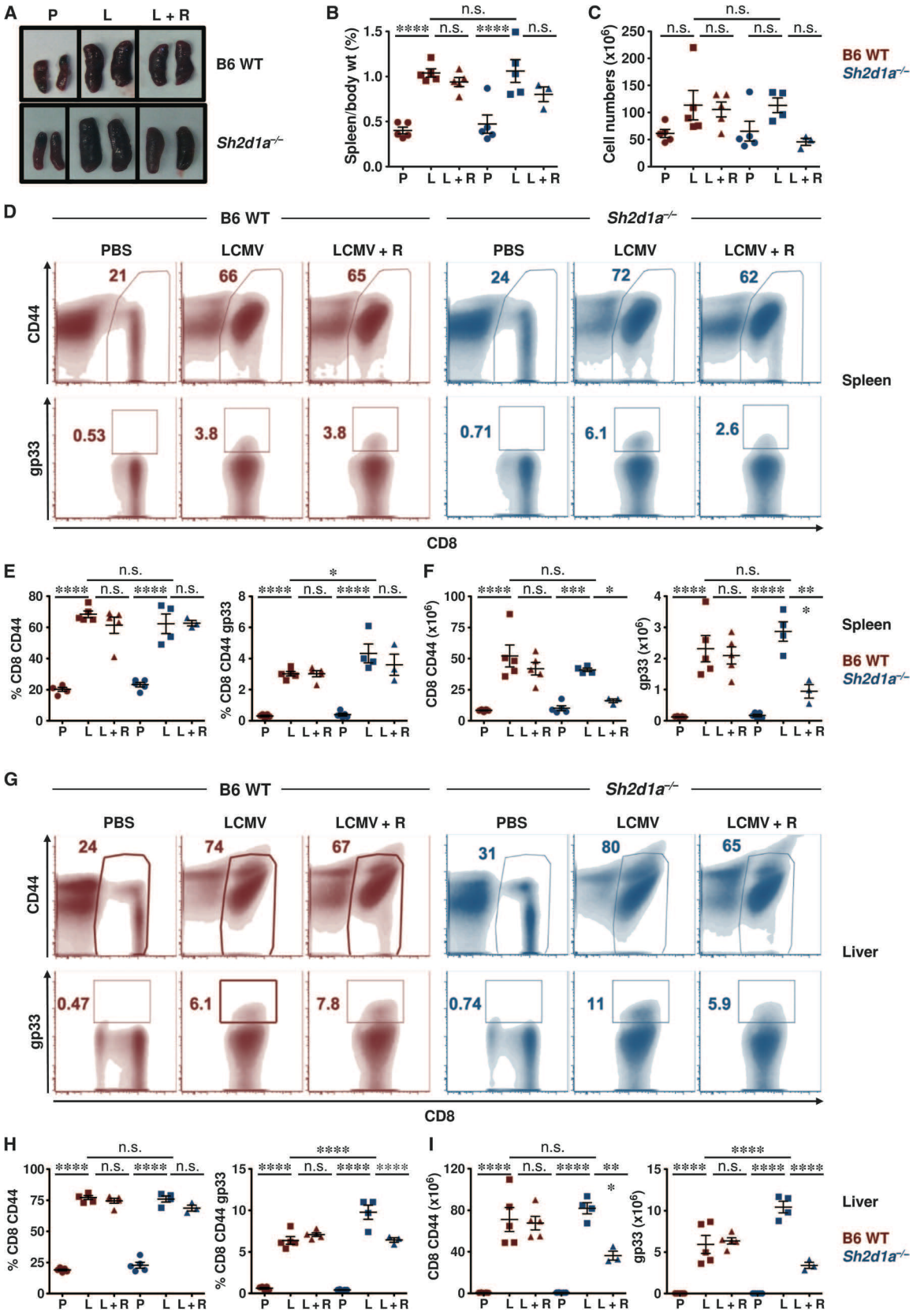
DGKα inhibition reduces CD8$^+$ T cell accumulation and activation in LCMV-infected Sh2d1a -/- mice

Defective RICD is thought to contribute to the aberrant T cell activation and accumulation that occur in EBV-infected XLP-1 patients (53). The demonstration that DGKα silencing or inhibition sensitizes SAP-deficient lymphocytes to RICD *in vitro* prompted us to assess whether DGKα inhibition might influence T cell-mediated immunopathology *in vivo*. Towards this end, we used a murine model in which *Sh2d1a*$^{-/-}$ mice are infected with LCMV. In this model, *Sh2d1a*$^{-/-}$ mice develop many of the cardinal manifestations of FIM, including CD8$^+$ T cell expansion, pro-inflammatory cytokine production and tissue infiltration (40; 201). For these experiments, wild-type (WT; *Sh2d1a*$^{+/+}$) or *Sh2d1a*$^{-/-}$ mice were infected with LCMV-Armstrong and 4 days later, treated with vehicle or R59022 (44). On day 8, the peak of the anti-viral T cell response, mice were euthanized and evaluated for hyper-inflammation.

Following LCMV infection, both WT and S*h2d1a*$^{-/-}$ mice developed marked and comparable splenomegaly (Fig 7A-B) that was associated with an increase in the absolute number of total splenocytes (Fig. 7C). Examination of splenocyte immunophenotype revealed a significant increase in the percentage and absolute number of total as well as LCMV-specific (gp33$^+$) CD8$^+$ T cells, the majority of which exhibited an activated CD44$^+$ phenotype (Fig. 7D-I). Treatment of LCMV-infected WT mice with R59022 did not significantly affect any of these parameters (Fig. 7). Conversely, R59022 treatment of LCMV-infected *Sh2d1a*$^{-/-}$ mice appeared to lessen organomegaly (Fig. 7A-B) and decrease the total splenic lymphocyte count (Fig. 7C). Although R59022 treatment did not affect the percentage of activated splenic CD8$^+$ T cells in either mouse strain, it did

induce a significant decrease in the number of total as well as LCMV-specific $CD8^+$ T cells selectively in the *Sh2d1a*$^{-/-}$ animals (Fig. 7D-I).

Figure 7. R59022 DGK inhibitor reduces the numbers of activated virus- specific $CD8^+$ T cells in LCMV-infected *Sh2d1a*$^{-/-}$ mice.
(A) Images of spleens from uninfected (PBS, "P") and LCMV infected mice without (LCMV, "L") or with R59022 treatment (LCMV+R59022, "L+R"). Representative spleens from each cohort from B6 WT (top panel) and *Sh2d1a*$^{-/-}$ mice (lower panel) are shown. (B) Ratio of spleen over body weight and (C) total splenocyte count for animals in each group are presented. B6 WT mice = red symbols, *Sh2d1a*$^{-/-}$ mice = blue symbols. (D-I) Representative flow cytometric (density) plots showing the percentages of $CD8^+$ $CD44^+$ (top) and LCMV-specific $CD8^+$ $gp33^+$ (bottom) in the spleens (D) and livers (G) of B6 WT and *Sh2d1a*$^{-/-}$ mice. Percentages (E, H) and absolute numbers (F, I) of $CD8^+$ $CD44^+$ and $CD8^+$ $CD44^+$ $gp33^+$ cells in the spleens (E, F) and livers (H, I) of B6 WT (red symbols) and *Sh2d1a*$^{-/-}$ (blue symbols) mice. Data are from 1 of 2 experiments in which a total of 6-10 mice in each cohort was examined. Error bars represent SD. Asterisks denote statistical significance that was determined by two-way ANOVA with Sidak correction. ns: not significant.


A
P
L
L + R
B6 WT
Sh2d1a−/−
B
Spleen/body wt (%)
n.s.
****
C
Cell numbers (x10^6)
B6 WT
Sh2d1a−/−
D
B6 WT
Sh2d1a−/−
PBS
LCMV
LCMV + R
CD44
gp33
CD8
21
66
65
24
72
62
0.53
3.8
3.8
0.71
6.1
2.6
Spleen
E
% CD8 CD44
% CD8 CD44 gp33
F
CD8 CD44 (x10^6)
gp33 (x10^6)
Spleen
B6 WT
Sh2d1a−/−
G
B6 WT
Sh2d1a−/−
PBS
LCMV
LCMV + R
CD44
gp33
CD8
24
74
67
31
80
65
0.47
6.1
7.8
0.74
11
5.9
Liver
H
% CD8 CD44
% CD8 CD44 gp33
I
CD8 CD44 (x10^6)
gp33 (x10^6)
Liver
B6 WT
Sh2d1a−/−

Compared to WT animals, LCMV-infected S*h2d1a*$^{-/-}$ mice also exhibited a trend toward higher serum IFNγ levels (Fig. 8A) and greater degrees of tissue inflammation (Fig 8B-D). To evaluate whether DGKα inhibition affected CD8^{+} T cell functions such as cytokine production or degranulation, splenocytes from LCMV-infected mice were cultured directly *ex vivo* with the MHC class I restricted LCMV peptide gp33 and examined for expression of intracellular TNFα, IFNγ and CD107a. Interestingly, R59022 treatment did not affect the percentage of CD8^{+} T cells that secreted cytokines (TNFα or IFNγ) or degranulated (CD107a exposure) in LCMV-infected WT or *Sh2d1a*$^{-/-}$ mice (Fig 8E-F). In fact, R59022 treatment actually enhanced the cytolytic activity of *Sh2d1a*$^{-/-}$ CD8^{+} T cells against autologous B cell targets *in vitro* (Fig. S5). However, such treatment did reduce the absolute number of cytokine producing and degranulating cells only in the *Sh2d1a*$^{-/-}$ animals (Fig. 8G). Consistent with these findings, only R59022-treated *Sh2d1a*$^{-/-}$ mice exhibited a significant reduction in the serum IFNγ levels (Fig 8A). Finally, R59022 treatment significantly reduced the number and size of hepatic inflammatory infiltrates in LCMV-infected *Sh2d1a*$^{-/-}$ but not WT mice (Fig 8B-D). These findings collectively indicate that inhibition of DGKα selectively decreases the magnitude of the CD8^{+} T cell effector pool in LCMV-infected *Sh2d1a*$^{-/-}$ mice. DGKα inhibition had no adverse effects on viral clearance, as LCMV was efficiently cleared from WT and *Sh2d1a*$^{-/-}$ mice by day 8 with or without R59022 treatment (Fig. S6). These pre-clinical data suggest that pharmacologic inhibition of DGKα might reduce the accumulation of aberrantly activated CD8^{+} T cells and subsequent hypercytokinemia and tissue inflammation that occur in EBV-infected XLP-1 patients, without impairing CD8^{+} T cell activity or viral clearance.

Figure 8. R59022 DGK inhibitor reduces the numbers but not incidence of virus-specific activated $CD8^+$ cytokine producing cells in the spleens of LCMV infected *Sh2d1a*$^{-/-}$ mice.

B6 WT (red symbols) and *Sh2d1a*$^{-/-}$ mice (blue symbols) were either uninfected (PBS, "P") or infected with LCMV without (LCMV, "L") or with R59022 treatment (LCMV+R59022, "L+R"). (A) Serum IFNγ levels were assayed on day 8 post-infection by ELISA. Data are compiled from 2 experiments in which a total of 6-10 mice in each cohort were examined. Error bars represent SEM. (B-D) H&E-stained liver sections from mice in each group were analyzed for the number of inflammatory foci (B) and area of the inflammatory infiltrate (C). For each sample, five random fields were captured at 20X magnification and scored. Histology of livers from representative mice in each group under 20X magnification (top row) is shown (D). Arrows point to the inflammatory foci. Micrographs in the bottom row are the respective analyzed images shown in the top row. (E-G) Splenocytes ($2x10^6$) from PBS (P), LCMV-infected (L) and LCMV-infected mice with R59022 treatment (L+R) groups were left unstimulated or stimulated with 0.4 ng/mL gp33 peptide in the presence of 1000 μg/mL monensin for 5 hours. Cells were then analyzed for intracellular cytokine production and degranulation. Representative flow cytometric (density) plots gated on $CD8^+CD44^+$ splenocytes showing the percentages of $CD8^+IFN\gamma^+$ (top), $IFN\gamma^+TNF\alpha^+$ (middle) and $IFN\gamma^+CD107a^+$ (bottom) cells from B6 WT and *Sh2d1a*$^{-/-}$ mice (E). Percentages (F) and absolute numbers (G) of $CD8^+IFN\gamma^+$, $IFN\gamma^+TNF\alpha^+$ and $IFN\gamma^+CD107a^+$ cells. Absolute numbers were calculated by multiplying the percentages with the respective absolute numbers of $CD8^+gp33^+$ cells. Error bars in B, C, F, and G represent SD. Asterisks denote statistical significance that was determined by two-way ANOVA with Sidak correction. ns: not significant.

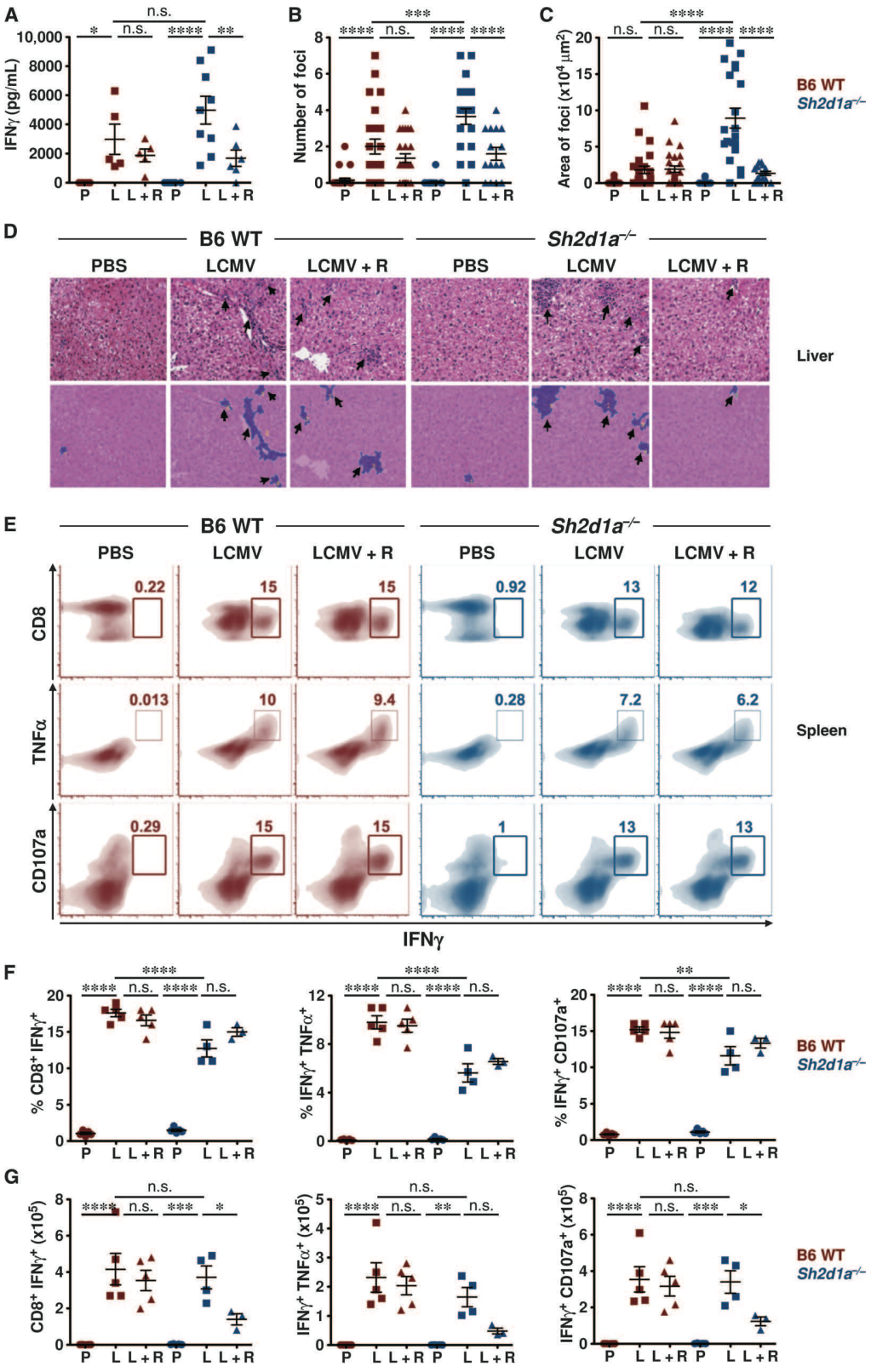

A
IFNγ (pg/mL)
B
Number of foci
C
Area of foci (x10⁴ μm²)
P L L+R P L L+R
B6 WT
Sh2d1a⁻/⁻
D
B6 WT
Sh2d1a⁻/⁻
PBS
LCMV
LCMV + R
Liver
E
CD8
TNFα
CD107a
IFNγ
0.22
15
15
0.92
13
12
0.013
10
9.4
0.28
7.2
6.2
0.29
15
15
1
13
13
Spleen
F
% CD8⁺ IFNγ⁺
% IFNγ⁺ TNFα⁺
% IFNγ⁺ CD107a⁺
G
CD8⁺ IFNγ⁺ (x10⁵)
IFNγ⁺ TNFα⁺ (x10⁵)
IFNγ⁺ CD107a⁺ (x10⁵)

Figure S5. DGKα inhibition enhances SAP-deficient CD8+ T cell cytotoxicity against autologous B cell targets.

In vitro cytolysis of LPS-activated WT B cells targets pulsed with 1μM A4Y peptide by WT P14 (left panel) or $SAP^{-/-}$ P14 (right panel) CTLs treated with DMSO (black) or 10μM R59949 (blue). Graph shows percent target lysis at decreasing CTL:target ratios, and is representative of 2 independent experiments. Bars represent mean ± SD; * indicates $p<0.05$.

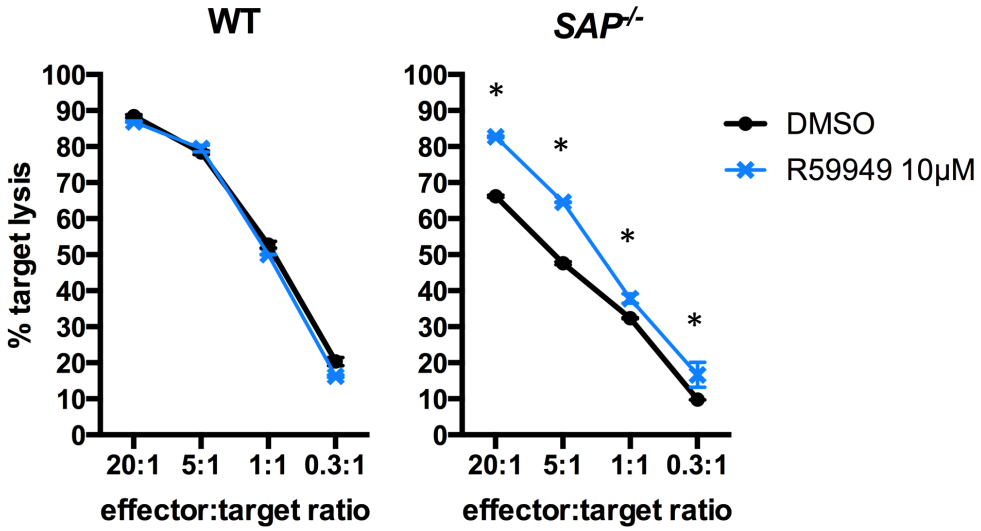
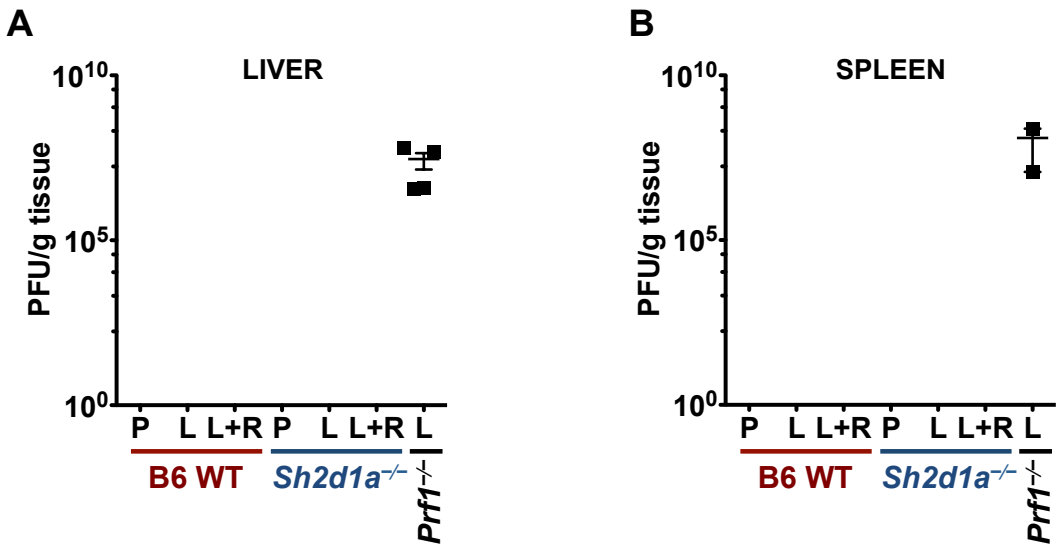

WT
SAP-/-
% target lysis
100
90
80
70
60
50
40
30
20
10
0
20:1
5:1
1:1
0.3:1
effector:target ratio
*
DMSO
R59949 10μM

Figure S6. R59022 DGKα inhibitor does not impair viral clearance in the livers and spleens of LCMV infected *Sh2d1a*$^{-/-}$ mice.

B6 WT and *Sh2d1a*$^{-/-}$ mice were either uninfected (PBS, "P") or infected with LCMV without (LCMV, "L") or with R59022 treatment (LCMV+R59022, "L+R"). As a positive control for impaired viral clearance, *Prf1*$^{-/-}$ mice were infected with LCMV as described. On day 8+, viral titer was determined in the liver **(A)** and spleen **(B)** samples of mice in each group. Data are representative of 2 independent experiments. Error bars denote SD.

Viral Loads


A
LIVER
10^{10}
10^{5}
10^{0}
PFU/g tissue
P L L+R P L L+R L
B6 WT
Sh2d1a−/−
Prf1−/−
B
SPLEEN
10^{10}
10^{5}
10^{0}
PFU/g tissue
P L L+R P L L+R L
B6 WT
Sh2d1a−/−
Prf1−/−

One major limitation of this study is its focus on the role of the SAP/DGKα axis strictly in T cells. It does not address the putative role of DGKα in other SAP-deficient immune cells such as NK or NKT cells, which also likely contribute to the development of various XLP-1 manifestations. In addition, although LCMV-infection of *Sh2d1a*$^{-/-}$ mice is a widely used murine model of FIM, it does not fully recapitulate the pathogenesis of EBV infection in humans. Finally, the translation of these findings to the clinic will require the development and characterization of novel, clinical-grade DGKα specific inhibitors. Nonetheless, our data clearly provide proof of concept that DGKα may be a novel drug target for treating XLP-1-associated FIM.

DISCUSSION

Our results demonstrate that inhibition of DGKα restores sensitivity to RICD in SAP-deficient T cells and reduces hyper-inflammation in LCMV-infected *Sh2d1a*$^{-/-}$ mice. These data support the hypothesis that in SAP-deficient T cells, persistent DGKα activity increases DAG metabolism at the IS, thus reducing DAG signaling and RICD sensitivity, and underscore the role of SAP in modulating DGKα activity (9). In SAP-expressing T cells, further inhibition of DGKα only marginally influenced sensitivity to RICD *in vitro,* and did not dampen the LCMV-induced CD8^{+} T cell response of wild-type mice *in vivo*.

Our finding that inhibition of DGKα restores proper IS organization in SAP-deficient T cells indicates that SAP, through regulation of DGKα, controls DAG polarization at the IS, thus promoting F-actin polymerization and MTOC orientation. Indeed, DGKα is recruited to the pSMAC, where it shapes the DAG gradient responsible for the recruitment of novel PKC isoforms (ε, η and θ), which control MTOC polarization and actin polymerization (Fig. 3) (34; 140). DGKα inhibition also partially rescued

impaired cytolytic activity in SAP-deficient CTLs (Fig. S5), further highlighting the link between SAP-dependent inhibition of DGKa and IS function (209). Altogether, these data indicate that SAP-mediated negative regulation of DGKα controls IS structural organization and function by regulating the TCR-induced gradient of DAG.

Both DGKα and DGKζ regulate TCR-induced DAG-signaling (123; 210). Consistently, inhibition or overexpression of either isoform rendered T cells more or less sensitive to RICD, respectively, confirming that both isoforms regulate DAG signalling in this context (Fig S1). Accordingly, administration of exogenous DAG partially rescued the defective RICD in SAP-deficient T cells (Fig 2F). However, only DGKα is regulated by SAP and shapes the DAG gradient at the IS (9; 34). We speculate that DGKα, which co-localizes with F-actin at the pSMAC, regulates the DAG gradient and F-actin polymerization at the IS, whereas DGKζ, which is more evenly distributed in the IS, metabolizes most of DAG generated there, consistent with proposed models (34; 64). Notably silencing of DGKδ, which is highly expressed in T cells, did not affect RICD, underscoring the specific roles of DGKα and DGKζ in regulating the DAG pool relevant for signalling and RICD onset.

Our finding that inhibition of DGKα restored RasGRP1 and PKCθ recruitment to the IS in SAP-deficient T cells, and subsequent DAG-dependent induction of IL-2 and CD25, illuminates a biochemical link between the SAP/DGKα axis, IS restoration, and downstream signaling events required for RICD (38; 93; 105; 178). Indeed, activation of RasGRP1 and PKCθ was required to rescue RICD in SAP-deficient T cells upon DGKα blockade (Fig. 5A-B, S2). Interestingly, DGKα inhibition cannot recapitulate all SAP-dependent signaling functions, such as TCR-induced expression of *FASLG* or *BCL2L11*,

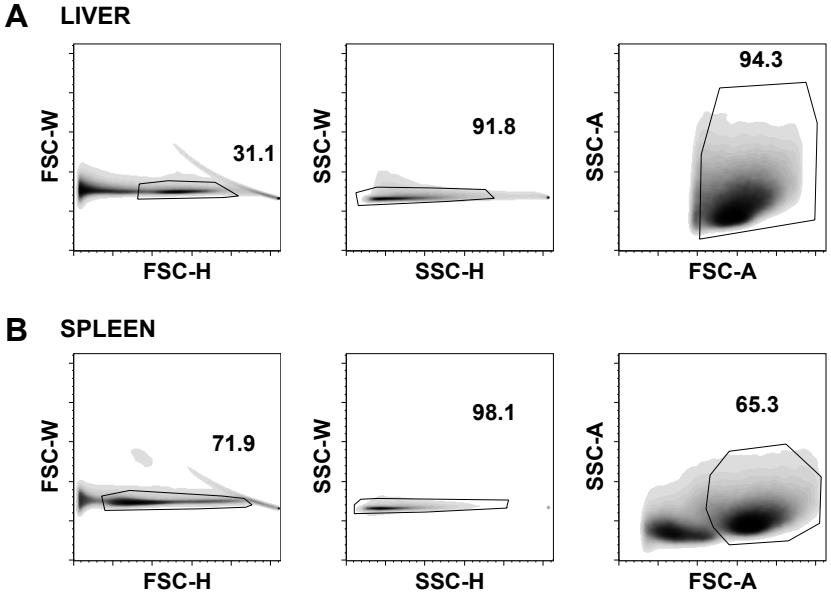
genes previously implicated in SAP-associated induction of RICD (174). This observation suggests that rescue of DAG-mediated signaling activates other pro-apoptotic pathways that partially compensate to boost RICD sensitivity. Here we show that the induction of NUR77 and NOR1 is defective in TCR-restimulated SAP-deficient T cells, and that the expression of these genes is restored by inhibition of DGKα. NUR77 and NOR1 are orphan nuclear receptors known to trigger thymocyte apoptosis during negative selection, and mediate RICD (36; 113). The pro-apoptotic activity of NUR77 and NOR1 depends on their phosphorylation by RSK, an ERK-1/2 dependent kinase, and subsequent translocation to the mitochondria to promote mitochondrial depolarization and apoptosis (36; 190). We observed that ERK and RSK activity, as well as NUR77 and NOR1, were required for RICD rescue triggered by DGKα inhibition in XLP-1 T cells. These observations provide a mechanistic connection between the rescue of DAG signaling and execution of RICD.

EBV-induced FIM is proposed to result from defective RICD of $CD8^+$ T cells and impaired cytotoxic elimination of EBV-infected B cells by $CD8^+$ T cells and NK cells. These events contribute to the excessive accumulation of activated effector $CD8^+$ T cells and life-threating damage to the liver, bone marrow, and other organs (174; 186). Using a murine model of FIM (40; 201), we showed that DGKα inhibition had no significant effect on reducing the activation status or function (e.g. cytokine secretion or degranulation) of effector $CD8^+$ T cells in either WT or *Sh2d1a*$^{-/-}$ mice. These data suggest that treatment with R59022 after LCMV infection does not impair initial lymphocyte activation. However, this treatment did significantly decrease the absolute number of activated $CD8^+$ T cells in *Sh2d1a*$^{-/-}$ mice, leading to fewer and smaller

lymphocytic infiltrates within the liver and marked reductions in the level of IFNγ in the serum. These results suggest that RICD resistance is connected to aberrant DGKα activity and serves as a key driver of virus-induced immunopathology in *Sh2d1a*$^{-/-}$ mice. Remarkably, the apoptosis resistance of activated T cells in LCMV-infected *Sh2d1a*$^{-/-}$ mice can be overcome via DGKα inhibition, even when such inhibition is initiated well after infection is established. These data are relevant to the clinical setting, where patients often present with FIM days to weeks after primary EBV infection.

In conclusion, our findings underscore the importance of SAP-mediated DGKα inhibition in maintaining lymphocyte homeostasis by ensuring sufficient TCR-induced DAG signaling strength for apoptosis. These data provide proof of principle that treatment with a DGKα inhibitor could serve as a novel, reasonable strategy to counteract pathological EBV-driven lymphohistiocytosis that occurs in EBV-infected XLP-1 patients by restoring the RICD sensitivity of activated $CD8^+$ T cells.

Gating strategy for Fig 7.



Gating strategy for Fig 8.

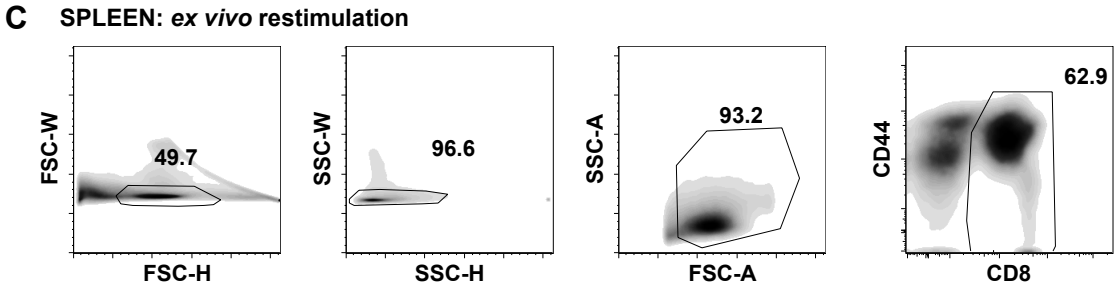


Figure S7. Gating strategies used in Fig 7 and Fig 8 are presented above.

Table S1. siRNA sequences.

Target	Sense	Antisense
SAP	UGUACUGCCUAUGUGUGCUGUAUCA	UGAUACAGCAGACAUAGGCAGUACA
DGKα	CGAGGAUGGCGAGAUGGCUAAAUAU	AUAUUUAGCCAUCUCGCCAUCCUCG
DGKZ	GCCGCUUUCGGAAUAAGAUtt	AUCUUAUUCCGAAAGCGGCtg
DGKD	CCCUAGAGUAUUACACGGATT	UCCGUGUAAUACUCUAGGGTT
PKCθ	CGUUGGAUGAGGUGGAUAAtt	UUAUCCACCUCAUCCAACGga
RasGRP1	CUACGACAAUUACCGGCGAtt	UCGCCGGUAAUUGUCGUAGtt
NR4A1	CCACUUCUCCACACCUUGAtt	UCAAGGUGUGGAGAAGUGGgt
NR4A3	CCUUCCUGCGUGUACCAAAtt	UUUGGUACACGCAGGAAGGct

Table S2. TaqMan gene expression arrays.

Target	Assay ID
GUSB	Hs00939627_m1
DGKA	Hs00176278_m1
DGKZ	Hs01577861_g1
DGKD	Hs01114141_m1
IL2	Hs00174114_m1
SH2D1A	Hs00158978_m1
BCL2L11	Hs01076940_m1
FASLG	Hs00181225_m1
NR4A1	Hs 00374226_m1
NR4A3	Hs 00545007_m1

Table S3. Spot densitometry analysis for western blotting.

Fig 1C

Lane	Sample	tubulin	DGKa	DGKa/tubulin	**DGKa (normalized)**
1	Ctrl siRNA	49723.19	19124.724	0.384623834	**1**
2	DGKa siRNA	51104.078	4969.622	0.097245116	**0.252831747**

Fig 2B

Lane	Sample	actin	SAP	SAP/actin	**SAP (normalized)**
1	Ctrl siRNA	684.2587878	856.5058	1.25172788	**1**
2	SAP siRNA	699.0703311	131.43327	0.188011513	**0.150201586**

Fig 5A

Lane	Sample	actin	PKCq	PKCq/actin	**PKCq (normalized)**
1	Ctrl siRNA	9922.714008	8775.675	0.884402692	**1**
2	PKCq siRNA	9821.410833	1394.2362	0.141958846	**0.160513811**

Fig 5B

Lane	Sample	actin	RASGRP1	RASGRP1/actin	**RASGRP1 (normalized)**
1	Ctrl siRNA	12731.50685	13514.14	1.061472158	**1**
2	RASGRP1 siRNA	11551.55473	2008.3437	0.17385917	**0.163790608**

Fig 6E

Lane	Sample	actin	NOR1	NOR1/actin	**4hr fold change**	NUR77	NUR77/actin	**4h fold change**
1	NC DMSO -	27076.421	6269.004	0.231530009		9062.045	0.334684004	
2	NC DMSO +	30606.007	44562.572	1.456007378	**1**	37220.434	1.21611532	**1**
3	NC+R59022 -	32187.886	8106.51	0.251849718		1542.083	0.0479088	
4	NC+R59022 +	31345.522	47879.936	1.527488871	**1.049094183**	29213.12	0.93197108	**0.766350908**
5	NC+R59949 -	32276.401	4421.276	0.136981691		180.021	0.005577481	
6	NC+R59949 +	31330.815	41607.128	1.327993798	**0.912079031**	21460.2	0.684955051	**0.56323199**
7	XLP DMSO -	30967.986	8858.075	0.286039751		207.263	0.006692815	
8	XLP DMSO +-	30033.229	19808.543	0.659554222	**1**	3176.64	0.105770845	**1**
9	XLP+R59022 -	30336.765	19408.279	0.639760996		205.849	0.006785463	
10	XLP+R59022 +	30188.572	31308.856	1.037109539	**1.572440148**	10916.593	0.361613428	**3.418838422**
11	XLP+R59949 -	28332.501	12996.116	0.458699922		595.92	0.021033088	
12	XLP+R59949 +	29564.203	23038.643	0.779274956	**1.181517652**	6770.631	0.229014494	**2.165194908**

Fig 6K

Lane	Sample	actin	NUR77	NUR77/actin	**NUR77 normalized**	NOR1	NOR1/actin	**NOR1 normalized**
1	NC ctrl	28822.794	20737.057	0.719467273	1	19047.995	0.660865668	1
2	NC NUR77/NOR1	30551.673	7146.815	0.233925487	0.325137079	11800.087	0.386233742	0.584436083
3	XLP ctrl	28896.48	10351.43	0.3582246	1	8721.116	0.301805479	1
4	XLP NUR77/NOR	31145.794	7703.581	0.247339368	0.690458912	3702.43	0.118874157	0.393876735

Fig S3C

Lane	Sample	actin	BIM	BIM/actin	**BIM fold change**	FASL	FASL/actin	**FASL fold change**
1	NC2 DMSO -	13767.589	9963.338	0.723680668	**1**	543.435	0.039472053	**1**
2	NC2 DMSO +	14764.418	23868.613	1.616630808	**2.23390078**	16037.857	1.086250538	**27.51948432**
3	NC2 +R599 -	15502.418	23548.383	1.51901355	**2.099010818**	1349.477	0.087049453	**2.205343942**
4	NC2 +R599 +	15767.489	41663.014	2.642336646	**3.651246695**	15009.694	0.951939399	**24.11679483**
5	XLP DMSO -	18444.146	66690.52	3.615809591	**1**	2468.054	0.133812322	**1**
6	XLP DMSO +	16535.782	61279.893	3.70589628	**1.024914666**	3005.711	0.181770115	**1.358395944**
7	XLP +R599 -	16717.903	63254.257	3.783623879	**1.046411263**	2558.711	0.15305215	**1.143782187**
8	XLP +R599 +	14056.66	48923.488	3.480448983	**0.962564232**	1629.669	0.11593572	**0.866405415**

Fig S3D

Lane	Sample	actin	BIM	BIM/actin	**BIM fold change**	FasL	FASL/actin	**FASL fold change**
1	NS ctrl -	18637.137	8133.581	0.436417943	**1**	483.435	0.025939338	**1**
2	NS ctrl +	17919.581	21229.693	1.184720391	**2.714646381**	8843.48	0.493509307	**19.02551649**
3	SAP KD -	17084.752	16276.007	0.95266276	**2.182913821**	207.021	0.012117296	**0.467139758**
4	SAP KD +	18806.803	19859.35	1.05596629	**2.419621618**	1226.163	0.065197844	**2.513473668**
5	DGKa KD -	19471.681	26726.563	1.372586322	**1**	388.627	0.019958575	**1**
6	DGKa KD +	19366.267	31850.806	1.644653872	**1.198215257**	10875.581	0.561573431	**28.1369506**
7	SAP+DGK KD -	17683.56	16575.915	0.937363008	**0.682917346**	940.92	0.053208743	**2.665959058**
8	SAP+DGK KD +	16688.489	20067.915	1.202500418	**0.876083638**	1608.477	0.096382423	**4.829123524**

Table S4. Statistical analysis.

Figure 1	Statistics performed with PRISM Graphpad software		**alpha: 0.05**		
1A					
2-Way ANOVA with sidak correction for multiple comparisions					
Sidak's multiple comparisons test	**Mean Diff.**	**95% CI of diff.**	**Summary**	**Adjusted P Value**	
Control					
NC ns kd - NC dgkα kd					
1	-5.072	-12.47 to 2.328	ns	0.3163	
5	-6.243	-13.64 to 1.157	ns	0.1355	
10	-2.312	-9.712 to 5.088	ns	0.9274	
50	-8.528	-15.93 to -1.128	*	0.0168	
100	-3.008	-10.41 to 4.392	ns	0.8105	
XLP Pt 4					
XLP ns kd - XLP dgkα kd					
1	-4.893	-11.84 to 2.057	ns	0.2891	
5	-12.04	-18.99 to -5.085	***	0.0001	
10	-11.64	-18.59 to -4.689	***	0.0002	
50	-18.68	-25.63 to -11.73	****	< 0.0001	
100	-22.3	-29.25 to -15.35	****	< 0.0001	
1B					
2-Way ANOVA with sidak correction for multiple comparisions					

Sidak's multiple comparisons test	**Mean Diff.**	**95% CI of diff.**	**Summary**	**Adjusted P Value**	
Control					
NC ns kd - NC dgkα kd					
5	-5.762	-11.48 to -0.04121	*	0.048	
10	-2.872	-8.593 to 2.849	ns	0.5444	
50	-5.193	-10.91 to 0.5280	ns	0.0837	
100	-7.524	-13.25 to -1.804	**	0.0079	
XLP Pt 5					
XLP ns kd - XLP dgkα kd					
5	-22.54	-31.80 to -13.29	***	0.0006	
10	-5.94	-15.19 to 3.315	ns	0.2372	
50	-11.94	-21.19 to -2.681	*	0.016	
100	-14.3	-23.55 to -5.043	**	0.0065	
1C					
Two-tailed paired t test					
siRNA Control vs siRNA DGKα	P value	0.0219			
	P value summary	*			
	t, df	t=4.392 df=3			
1D					
2-Way ANOVA with sidak correction for multiple comparisions					
Sidak's multiple comparisons test	**Mean Diff.**	**95% CI of diff.**	**Summary**	**Adjusted P Value**	
Control					
1					
DMSO vs. R59949 5μM	8.759	-0.08815 to 17.61	ns	0.0527	

DMSO vs. R59949 10µM	0.5371	-8.310 to 9.384	ns	0.9873	
5					
DMSO vs. R59949 5µM	-0.03023	-8.878 to 8.817	ns	> 0.9999	
DMSO vs. R59949 10µM	-14.09	-22.94 to -5.241	**	0.0015	
10					
DMSO vs. R59949 5µM	-2.071	-10.92 to 6.776	ns	0.8283	
DMSO vs. R59949 10µM	-14.2	-23.05 to -5.351	**	0.0014	
50					
DMSO vs. R59949 5µM	-9.849	-18.70 to -1.002	*	0.0271	
DMSO vs. R59949 10µM	-19.35	-28.20 to -10.51	****	< 0.0001	
100					
DMSO vs. R59949 5µM	-8.732	-17.58 to 0.1150	ns	0.0535	
DMSO vs. R59949 10µM	-17.67	-26.52 to -8.827	***	0.0001	
XLP Pt 9					
1					
DMSO vs. R59949 5µM	-6.011	-11.95 to -0.06735	*	0.0472	
DMSO vs. R59949 10µM	3.184	-2.759 to 9.128	ns	0.3662	
5					
DMSO vs. R59949 5µM	-10.29	-16.24 to -4.348	***	0.0007	
DMSO vs. R59949 10µM	-9.891	-15.83 to -3.947	**	0.0011	
10					
DMSO vs. R59949 5µM	-9.544	-15.49 to -3.601	**	0.0016	
DMSO vs. R59949 10µM	-15.76	-21.71 to -9.819	****	< 0.0001	
50					
DMSO vs. R59949 5µM	-20.83	-26.77 to -14.88	****	< 0.0001	
DMSO vs. R59949 10µM	-32.68	-38.62 to -26.73	****	< 0.0001	
100					

DMSO vs. R59949 5μM	-13.8	-19.74 to -7.855	****	< 0.0001	
DMSO vs. R59949 10μM	-23.91	-29.85 to -17.96	****	< 0.0001	
1E					
2-Way ANOVA with sidak correction for multiple comparisions					
Sidak's multiple comparisons test	**Mean Diff.**	**95% CI of diff.**	**Summary**	**Adjusted P Value**	
Control					
1					
DMSO vs. R59949 5μM	-4.246	-19.18 to 10.68	ns	0.706	
DMSO vs. R59949 10μM	-12.96	-27.89 to 1.975	ns	0.0871	
10					
DMSO vs. R59949 5μM	-5.885	-20.82 to 9.046	ns	0.5254	
DMSO vs. R59949 10μM	-10.75	-25.68 to 4.177	ns	0.1602	
100					
DMSO vs. R59949 5μM	-0.7334	-15.66 to 14.20	ns	0.9892	
DMSO vs. R59949 10μM	-0.7238	-15.65 to 14.21	ns	0.9895	
XLP Pt 4					
1					
DMSO vs. R59949 5μM	-19.37	-27.89 to -10.85	***	0.0005	
DMSO vs. R59949 10μM	-2.142	-10.66 to 6.378	ns	0.7598	
10					
DMSO vs. R59949 5μM	-11.17	-19.69 to -2.646	*	0.014	
DMSO vs. R59949 10μM	-10	-18.52 to -1.481	*	0.0243	
100					
DMSO vs. R59949 5μM	-18.14	-26.66 to -9.623	***	0.0008	
DMSO vs. R59949 10μM	-12.87	-21.39 to -4.350	**	0.0065	
1F					

2-Way ANOVA with sidak correction for multiple comparisions					
Sidak's multiple comparisons test	**Mean Diff.**	**95% CI of diff.**	**Summary**	**Adjusted P Value**	
Control					
5					
DMSO vs. R59022 5μM	-14.21	-20.24 to -8.180	****	< 0.0001	
DMSO vs. R59022 10μM	-11.37	-17.41 to -5.343	***	0.0002	
10					
DMSO vs. R59022 5μM	-11.06	-17.09 to -5.024	***	0.0003	
DMSO vs. R59022 10μM	-7.721	-13.75 to -1.689	*	0.0104	
50					
DMSO vs. R59022 5μM	-2.226	-8.258 to 3.806	ns	0.6302	
DMSO vs. R59022 10μM	-2.739	-8.771 to 3.292	ns	0.501	
100					
DMSO vs. R59022 5μM	-8.016	-14.05 to -1.984	**	0.0078	
DMSO vs. R59022 10μM	-8.384	-14.42 to -2.353	**	0.0054	
500					
DMSO vs. R59022 5μM	-6.511	-12.54 to -0.4790	*	0.0327	
DMSO vs. R59022 10μM	-6.516	-12.55 to -0.4845	*	0.0325	
XLP Pt 4					
5					
DMSO vs. R59022 5μM	-5.162	-16.41 to 6.090	ns	0.4942	
DMSO vs. R59022 10μM	-11.24	-22.49 to 0.01384	ns	0.0503	
10					
DMSO vs. R59022 5μM	-13.75	-25.00 to -2.499	*	0.0146	
DMSO vs. R59022 10μM	-18.79	-30.05 to -7.541	***	0.0009	
50					
DMSO vs. R59022 5μM	-3.636	-14.89 to 7.617	ns	0.7006	

DMSO vs. R59022 10µM	-27.81	-39.07 to -16.56	****	< 0.0001	
100					
DMSO vs. R59022 5µM	-22.19	-33.44 to -10.93	***	0.0001	
DMSO vs. R59022 10µM	-37.54	-48.80 to -26.29	****	< 0.0001	
500					
DMSO vs. R59022 5µM	-23.09	-34.34 to -11.84	****	< 0.0001	
DMSO vs. R59022 10µM	-30.2	-41.46 to -18.95	****	< 0.0001	
1G					
	Diff in AnnV+ Cells				
	DMSO	R59949			
	12h	12h			
NC1	24.9	22.6			
NC2	14	9.6			
NC2	31.1	21.5			
NC2	19.3	10.9			
D2	31.9	23.4			
D3	22.3	14.9			
D2	23.2	21.6			
D2	20.8	13.3			
XLP	4.1	3.5			
XLP	6.3	8.7			
XLP	3.3	13			
XLP5	9.3	13.4			
XLP5	11.5	15.7			
XLP9	7.3	11.6			
	AVG			STDEV	
	Diff in AnnV+ Cells			Diff in AnnV+ Cells	
	DMSO	R59949		DMSO	R59949
Ctrls	23.4375	17.225	Ctrls	5.93968193	5.649209806

XLPs	6.966666667	10.98333333	XLPs	3.105264347	4.330088529
DMSO vs. R59949	T-TEST				
Ctrls	0.00066906				
XLPs	0.032602561				

Figure 2	Statistics performed with PRISM Graphpad software		**alpha: 0.05**		
2A					
2-Way ANOVA with sidak correction for multiple comparisions					
Sidak's multiple comparisons test	**Mean Diff.**	**95% CI of diff.**	**Summary**	**Adjusted P Value**	
Control					
n.s. kd - DGKα k.d.					
1	-3.762	-17.32 to 9.800	ns	0.9467	
2	0.3574	-13.20 to 13.92	ns	> 0.9999	
5	0.1165	-13.45 to 13.68	ns	> 0.9999	
10	0.4132	-13.15 to 13.98	ns	> 0.9999	
50	5.792	-7.770 to 19.35	ns	0.7248	
100	5.185	-8.377 to 18.75	ns	0.808	
SAP silenced					
n.s. kd - DGKα k.d.					
1	-10.22	-25.15 to 4.709	ns	0.2623	
2	-19.53	-34.46 to -4.599	**	0.0098	

5	-24.4	-39.33 to -9.471	**	0.002	
10	-19.64	-34.57 to -4.708	**	0.0094	
50	-24.59	-39.52 to -9.660	**	0.0019	
100	-22.01	-36.94 to -7.082	**	0.0043	
2B					
Two-tailed paired t test					
siRNA Control vs siRNA DGKα	P value	0.0096			
	P value summary	**			
	t, df	t=5.919 df=3			
2C					
2-Way ANOVA with sidak correction for multiple comparisions					
Sidak's multiple comparisons test	**Mean Diff.**	**95% CI of diff.**	**Summary**	**Adjusted P Value**	
Control					
1					
DMSO vs. R59949 5μM	-13.43	-24.86 to -2.007	*	0.0241	
DMSO vs. R59949 10μM	-21.59	-33.02 to -10.17	**	0.0017	
10					
DMSO vs. R59949 5μM	-3.155	-14.58 to 8.270	ns	0.7196	
DMSO vs. R59949 10μM	-5.58	-17.00 to 5.845	ns	0.3871	
100					
DMSO vs. R59949 5μM	-7.798	-19.22 to 3.627	ns	0.1865	
DMSO vs. R59949 10μM	-10.22	-21.64 to 1.208	ns	0.0779	
SAP Silenced					

1					
DMSO vs. R59949 5µM	-13.05	-26.85 to 0.7576	ns	0.0629	
DMSO vs. R59949 10µM	-29.89	-43.70 to -16.09	***	0.0007	
10					
DMSO vs. R59949 5µM	-19.14	-32.94 to -5.330	*	0.0104	
DMSO vs. R59949 10µM	-26.24	-40.04 to -12.43	**	0.0016	
100					
DMSO vs. R59949 5µM	-17.23	-31.03 to -3.423	*	0.018	
DMSO vs. R59949 10µM	-26.63	-40.44 to -12.83	**	0.0015	
2D					
2-Way ANOVA with sidak correction for multiple comparisions					
Sidak's multiple comparisons test	**Mean Diff.**	**95% CI of diff.**	**Summary**	**Adjusted P Value**	
Control					
1					
DMSO vs. R59022 5µM	-5.12	-14.99 to 4.751	ns	0.39	
DMSO vs. R59022 10µM	-2.895	-12.77 to 6.976	ns	0.7295	
10					
DMSO vs. R59022 5µM	12.95	3.081 to 22.82	*	0.0103	
DMSO vs. R59022 10µM	14	4.131 to 23.87	**	0.0059	
100					
DMSO vs. R59022 5µM	0.992	-8.879 to 10.86	ns	0.9629	
DMSO vs. R59022 10µM	1.489	-8.382 to 11.36	ns	0.9186	
SAP silenced					
1					
DMSO vs. R59022 5µM	-13.14	-23.21 to -3.078	**	0.0091	

DMSO vs. R59022 10µM	-14.47	-24.53 to -4.406	**	0.0041	
10					
DMSO vs. R59022 5µM	-18.99	-29.05 to -8.925	***	0.0002	
DMSO vs. R59022 10µM	-19.56	-29.62 to -9.492	***	0.0002	
100					
DMSO vs. R59022 5µM	-17.46	-27.52 to -7.391	***	0.0006	
DMSO vs. R59022 10µM	-20	-30.06 to -9.935	***	0.0001	
2E					
	Diff in AnnV+ Cells				
	DMSO	R59949			
	12h	12h			
NS	26.9	25.5			
NS	33.1	30.4			
NS	37.9	34.7			
NS	34.3	23.7			
SAP	7.3	9.7			
SAP	10.5	11.6			
SAP	2.4	4.5			
SAP	20.4	22.6			
	AVG			STDEV	
	Diff in AnnV+ Cells			Diff in AnnV+ Cells	
	DMSO	R59949		DMSO	R599
NS	33.05	28.575	Ctrls	4.579301257	4.968819444
SAP	10.15	12.1	XLPs	7.601973428	7.616210781
DMSO vs.	T-TEST				

R59949					
Ctrls	0.120144873				
XLPs	0.00672217				
2F					
2-Way ANOVA with sidak correction for multiple comparisions					
Sidak's multiple comparisons test	**Mean Diff.**	**95% CI of diff.**	**Summary**	**Adjusted P Value**	
Control					
vehicle - C8-DAG					
10	5.422	0.7701 to 10.07	*	0.0305	
100	2.344	-2.308 to 6.996	ns	0.2847	
SAP silenced					
SAP control - SAP +C8-DAG					
10	-19	-28.82 to -9.177	**	0.0051	
100	-6.766	-16.59 to 3.057	ns	0.1435	

Figure 3	Statistics performed with PRISM Graphpad software		**alpha: 0.05**	
1-Way ANOVA with sidak correction for multiple comparisions				
Sidak's multiple comparisons test	**Mean Diff.**	**95% CI of diff.**	**Summary**	**Adjusted P Value**
3B				
siRNA Control vs. siRNA SAP	0.08706	0.04341 to 0.1307	****	< 0.0001
siRNA Control vs. siRNA DGKα	0.06614	0.01468 to 0.1176	**	0.0049
siRNA Control vs. siRNA SAP and DGKα	0.02849	-0.02037 to 0.07734	ns	0.5387

siRNA SAP vs. siRNA DGKα	-0.02092	-0.06982 to 0.02799	ns	0.8278
siRNA SAP vs. siRNA SAP and DGKα	-0.05857	-0.1047 to -0.01241	**	0.0056
siRNA DGKa vs. siRNA SAP and DGKα	-0.03765	-0.09125 to 0.01595	ns	0.3206
3D				
Control vs. SAP	0.09754	0.02222 to 0.1729	**	0.0066
Control vs. SAP and R59949	-0.03016	-0.1006 to 0.04033	ns	0.6581
SAP vs. SAP and R59949	-0.1277	-0.2109 to -0.04454	***	0.001
3F				
siRNA Control vs.siRNA SAP	0.2396	0.1708 to 0.3084	****	< 0.0001
siRNA Control vs. siRNA DGKα	0.06351	-0.03167 to 0.1587	ns	0.3828
siRNA Control vs. siRNA SAP and DGKα	0.107	0.02523 to 0.1887	**	0.0038
siRNA SAP vs. siRNA DGKα	-0.1761	-0.2692 to -0.08311	****	< 0.0001
siRNA SAP vs. siRNA SAP and DGKα	-0.1327	-0.2119 to -0.05347	****	< 0.0001
siRNA DGKα vs. siRNA SAP and DGKα	0.04345	-0.05951 to 0.1464	ns	0.8389
3H				
siRNA Control vs.siRNA SAP	0.2779	0.1696 to 0.3862	****	< 0.0001
siRNA Control vs.R59949	0.05951	-0.04879 to 0.1678	ns	0.6013
siRNA Control vs. siRNA SAP and R59949	0.1396	0.03265 to 0.2465	**	0.0043
siRNA SAP vs. R59949	-0.2184	-0.3292 to -0.1075	****	< 0.0001

siRNA SAP vs. siRNA SAP and R59949	-0.1383	-0.2478 to -0.02876	**	0.0062
R59949 vs. siRNA SAP and R59949	0.08008	-0.02945 to 0.1896	ns	0.2741
3J				
siRNA Control vs.siRNA SAP	-0.2033	-0.3096 to -0.09690	****	< 0.0001
siRNA Control vs.R59949	-0.03939	-0.1451 to 0.06632	ns	0.9028
siRNA Control vs. siRNA SAP and R59949	-0.0592	-0.1643 to 0.04588	ns	0.5815
siRNA SAP vs. R59949	0.1639	0.06039 to 0.2674	***	0.0003
siRNA SAP vs. siRNA SAP and R59949	0.1441	0.04122 to 0.2469	**	0.0016
R59949 vs. siRNA SAP and R59949	-0.01981	-0.1220 to 0.08236	ns	0.9963

Figure 4	Statistics performed with PRISM Graphpad software		**alpha: 0.05**	
2-Way ANOVA with sidak correction for multiple comparisions				
Sidak's multiple comparisons test	**Mean Diff.**	**95% CI of diff.**	**Summary**	**Adjusted P Value**
4B				
Control - SAP				
Cntrl	29.92	14.96 to 44.88	***	0.0002
DGKα	0.6543	-14.31 to 15.62	ns	0.9931
Cntrl - DGKα				
Control	-1.939	-8.174 to 4.296	ns	0.6786
SAP	-31.21	-37.44 to -24.97	****	< 0.0001
4D				
Control - SAP				
DMSO	29	8.604 to 49.40	**	0.0091
R59949	12.33	-8.063 to 32.73	ns	0.253

DMSO - R59949				
Control	-7.667	-14.28 to -1.051	*	0.0311
SAP	-24.33	-30.95 to -17.72	***	0.0004
4F				
Control - SAP				
Cntrl	25.53	4.967 to 46.10	*	0.028
DGKα	0.6045	-19.96 to 21.17	ns	0.992
Cntrl - DGKα				
Control	-0.3166	-15.70 to 15.07	ns	0.9978
SAP	-25.25	-40.63 to -9.858	**	0.0057
4H				
Control - SAP				
DMSO	41.13	22.52 to 59.73	***	0.0006
R59949	20.12	1.514 to 38.72	*	0.0356
DMSO - R59949				
Control	-4.653	-24.35 to 15.04	ns	0.7051
SAP	-25.66	-45.35 to -5.969	*	0.0209

Figure 5	Statistics performed with PRISM Graphpad software		**alpha: 0.05**	
2-Way ANOVA with sidak correction for multiple comparisions				
Sidak's multiple comparisons test	**Mean Diff.**	**95% CI of diff.**	**Summary**	**Adjusted P Value**
5A				
Control				
Control vs. SAP	17.92	3.247 to 32.60	*	0.0162
Control vs. SAP and DGKα	-1.096	-15.77 to 13.58	ns	0.9959
SAP vs. SAP and DGKα	-19.02	-33.70 to -4.343	*	0.0111
PKC				
Control vs. SAP	-4.248	-18.93 to 10.43	ns	0.8228
Control vs. SAP and	3.838	-10.84 to 18.52	ns	0.8616

DGKα				
SAP vs. SAP and DGKα	8.085	-6.593 to 22.76	ns	0.3922
Control - PKC				
Control	11.95	-2.727 to 26.63	ns	0.1251
SAP	-10.22	-24.90 to 4.456	ns	0.2154
SAP and DGKα	16.88	2.207 to 31.56	*	0.0233
5B				
Control				
Control vs. SAP	14.01	0.03133 to 27.98	*	0.0495
Control vs. SAP and DGKα	-2.635	-16.61 to 11.34	ns	0.9367
SAP vs. SAP and DGKα	-16.64	-30.62 to -2.667	*	0.02
RasGRP1				
Control vs. SAP	-0.4743	-14.45 to 13.50	ns	0.9996
Control vs. SAP and DGKα	2.471	-11.50 to 16.45	ns	0.9469
SAP vs. SAP and DGKα	2.945	-11.03 to 16.92	ns	0.9149
Control - RasGRP1				
Control	8.886	-5.090 to 22.86	ns	0.2686
SAP	-5.596	-19.57 to 8.380	ns	0.6249
SAP and DGKα	13.99	0.01654 to 27.97	*	0.0497
5C				
Control				
no treatment vs. R59949	0.02915	-0.8754 to 0.9337	ns	> 0.9999
no treatment vs. OKT3	-0.9147	-1.819 to -0.01014	*	0.0469
no treatment vs. OKT3 + R59949	-4.258	-5.162 to -3.353	****	< 0.0001
R59949 vs. OKT3	-0.9438	-1.848 to -0.03929	*	0.039
R59949 vs. OKT3 + R59949	-4.287	-5.192 to -3.382	****	< 0.0001
OKT3 vs. OKT3 + R59949	-3.343	-4.248 to -2.439	****	< 0.0001

SAP				
no treatment vs. R59949	0.2064	-0.6981 to 1.111	ns	0.9818
no treatment vs. OKT3	-0.07756	-0.9821 to 0.8270	ns	> 0.9999
no treatment vs. OKT3 + R59949	-1.149	-2.053 to -0.2442	*	0.0107
R59949 vs. OKT3	-0.284	-1.188 to 0.6206	ns	0.92
R59949 vs. OKT3 + R59949	-1.355	-2.260 to -0.4506	**	0.003
OKT3 vs. OKT3 + R59949	-1.071	-1.976 to -0.1667	*	0.0174
Control - SAP				
no treatment	-0.1444	-0.9864 to 0.6976	ns	0.9802
R59949	0.03283	-0.8092 to 0.8748	ns	> 0.9999
OKT3	0.6927	-0.1493 to 1.535	ns	0.1263
OKT3 + R59949	2.965	2.123 to 3.807	****	< 0.0001
5D				
Control				
no treatment vs. DGKα	0.0008571	-0.7457 to 0.7474	ns	> 0.9999
no treatment vs. OKT3	-0.9856	-1.732 to -0.2391	**	0.0063
no treatment vs. OKT3 + DGKα	-3.054	-3.800 to -2.307	****	< 0.0001
DGKα vs. OKT3	-0.9864	-1.733 to -0.2399	**	0.0063
DGKα vs. OKT3 + DGKα	-3.055	-3.801 to -2.308	****	< 0.0001
OKT3 vs. OKT3 + DGKα	-2.068	-2.815 to -1.322	****	< 0.0001
SAP				
no treatment vs. DGKα	-0.006714	-0.7532 to 0.7398	ns	> 0.9999
no treatment vs. OKT3	-0.3206	-1.067 to 0.4259	ns	0.7764
no treatment vs. OKT3 + DGKα	-1.012	-1.759 to -0.2655	**	0.005
DGKα vs. OKT3	-0.3139	-1.060 to 0.4327	ns	0.7922
DGKα vs. OKT3 + DGKα	-1.005	-1.752 to -0.2588	**	0.0053

OKT3 vs. OKT3 + DGKα	-0.6914	-1.438 to 0.05509	ns	0.0789
Control - SAP				
no treatment	-0.0004286	-0.6996 to 0.6987	ns	> 0.9999
DGKα	-0.008	-0.7072 to 0.6912	ns	> 0.9999
OKT3	0.6646	-0.03458 to 1.364	ns	0.0664
OKT3 + DGKα	2.041	1.342 to 2.740	****	< 0.0001
5E				
Control				
No treatment vs. DGKα	16.99	-17.54 to 51.52	ns	0.5772
No treatment vs. OKT3	-76.58	-111.1 to -42.05	***	0.0002
No treatment vs. OKT3 + DGKα	-84.41	-118.9 to -49.88	***	0.0001
DGKα vs. OKT3	-93.57	-128.1 to -59.04	****	< 0.0001
DGKα vs. OKT3 + DGKα	-101.4	-135.9 to -66.87	****	< 0.0001
OKT3 vs. OKT3 + DGKα	-7.829	-42.36 to 26.70	ns	0.977
SAP				
No treatment vs. DGKα	3.111	-31.42 to 37.64	ns	0.9999
No treatment vs. OKT3	-38.45	-72.99 to -3.923	*	0.0278
No treatment vs. OKT3 + DGKα	-103.5	-138.1 to -68.99	****	< 0.0001
DGKα vs. OKT3	-41.57	-76.10 to -7.034	*	0.0176
DGKα vs. OKT3 + DGKα	-106.6	-141.2 to -72.10	****	< 0.0001
OKT3 vs. OKT3 + DGKα	-65.07	-99.60 to -30.53	***	0.0008
Control - SAP				
No treatment	6.345	-25.59 to 38.28	ns	0.9602
DGKα	-7.532	-39.47 to 24.41	ns	0.9288
OKT3	44.47	12.53 to 76.41	**	0.0078
OKT3 + DGKα	-12.77	-44.70 to 19.17	ns	0.6782

Figure 6	Statistics performed with	**alpha:**	

	PRISM Graphpad software		**0.05**	
2-Way ANOVA with sidak correction for multiple comparisions				
Sidak's multiple comparisons test	**Mean Diff.**	**95% CI of diff.**	**Summary**	**Adjusted P Value**
6A				
Control				
unstimulated vs. siRNA DGKα	0.001875	-0.1720 to 0.1758	ns	> 0.9999
unstimulated vs. OKT3	-0.9634	-1.137 to -0.7895	****	< 0.0001
unstimulated vs. OKT3 + DGKα	-0.8815	-1.055 to -0.7076	****	< 0.0001
siRNA DGKα vs. OKT3	-0.9653	-1.139 to -0.7913	****	< 0.0001
siRNA DGKα vs. OKT3 + DGKα	-0.8834	-1.057 to -0.7095	****	< 0.0001
OKT3 vs. OKT3 + DGKα	0.08188	-0.09204 to 0.2558	ns	0.7096
SAP				
unstimulated vs. siRNA DGKα	-0.001375	-0.1753 to 0.1725	ns	> 0.9999
unstimulated vs. OKT3	-0.4818	-0.6557 to -0.3078	****	< 0.0001
unstimulated vs. OKT3 + DGKα	-0.7881	-0.9620 to -0.6142	****	< 0.0001
siRNA DGKα vs. OKT3	-0.4804	-0.6543 to -0.3065	****	< 0.0001
siRNA DGKα vs. OKT3 + DGKα	-0.7868	-0.9607 to -0.6128	****	< 0.0001
OKT3 vs. OKT3 + DGKα	-0.3064	-0.4803 to -0.1325	***	0.0003
Control - SAP				
unstimulated	0.012	-0.1511 to 0.1751	ns	0.9994
siRNA DGKα	0.00875	-0.1544 to 0.1719	ns	0.9998
OKT3	0.4936	0.3305 to 0.6568	****	< 0.0001
OKT3 + DGKα	0.1054	-0.05777 to 0.2685	ns	0.3238
6B				
Control				
unstimulated vs. R59949	-0.01055	-0.3762 to 0.3551	ns	> 0.9999
unstimulated vs. OKT3	-0.9542	-1.320 to -0.5886	****	< 0.0001
unstimulated vs. OKT3	-1.016	-1.382 to -0.6508	****	< 0.0001

+ R59949				
R59949 vs. OKT3	-0.9436	-1.309 to -0.5780	****	< 0.0001
R59949 vs. OKT3 + R59949	-1.006	-1.372 to -0.6403	****	< 0.0001
OKT3 vs. OKT3 + R59949	-0.06227	-0.4279 to 0.3034	ns	0.9961
SAP				
unstimulated vs. R59949	-0.01233	-0.3780 to 0.3533	ns	> 0.9999
unstimulated vs. OKT3	-0.6387	-1.004 to -0.2731	***	0.0008
unstimulated vs. OKT3 + R59949	-1.154	-1.519 to -0.7881	****	< 0.0001
R59949 vs. OKT3	-0.6264	-0.9920 to -0.2608	***	0.001
R59949 vs. OKT3 + R59949	-1.141	-1.507 to -0.7758	****	< 0.0001
OKT3 vs. OKT3 + R59949	-0.515	-0.8806 to -0.1494	**	0.005
Control - SAP				
unstimulated	0.007364	-0.3330 to 0.3477	ns	> 0.9999
R59949	0.005582	-0.3348 to 0.3459	ns	> 0.9999
OKT3	0.3228	-0.01753 to 0.6632	ns	0.0657
OKT3 + R59949	-0.1299	-0.4703 to 0.2105	ns	0.7405
6C				
Control				
unstimulated vs. siRNA DGKα	0.003143	-0.5322 to 0.5385	ns	> 0.9999
unstimulated vs. OKT3	-0.9891	-1.525 to -0.4538	***	0.0002
unstimulated vs. OKT3 + DGKα	-1.383	-1.918 to -0.8475	****	< 0.0001
siRNA DGKα vs. OKT3	-0.9923	-1.528 to -0.4569	***	0.0002
siRNA DGKα vs. OKT3 + DGKα	-1.386	-1.921 to -0.8506	****	< 0.0001
OKT3 vs. OKT3 + DGKα	-0.3937	-0.9291 to 0.1417	ns	0.2342
SAP				
unstimulated vs. siRNA DGKα	0.001571	-0.5338 to 0.5369	ns	> 0.9999
unstimulated vs. OKT3	-0.3959	-0.9312 to 0.1395	ns	0.2293
unstimulated vs. OKT3	-1.352	-1.888 to -0.8171	****	< 0.0001

+ DGKα				
siRNA DGKα vs. OKT3	-0.3974	-0.9328 to 0.1379	ns	0.2258
siRNA DGKα vs. OKT3 + DGKα	-1.354	-1.889 to -0.8186	****	< 0.0001
OKT3 vs. OKT3 + DGKα	-0.9566	-1.492 to -0.4212	***	0.0003
Control - SAP				
unstimulated	0.002571	-0.4988 to 0.5040	ns	> 0.9999
siRNA DGKα	0.001	-0.5004 to 0.5024	ns	> 0.9999
OKT3	0.5959	0.09444 to 1.097	*	0.0163
OKT3 + DGKα	0.033	-0.4684 to 0.5344	ns	0.9996
6D				
siRNA control				
no treatment vs. R59949	-0.003173	-0.1806 to 0.1743	ns	> 0.9999
no treatment vs. OKT3	-0.9917	-1.169 to -0.8142	****	< 0.0001
no treatment vs. R59949+ OKT3	-0.8399	-1.017 to -0.6625	****	< 0.0001
R59949 vs. OKT3	-0.9885	-1.166 to -0.8111	****	< 0.0001
R59949 vs. R59949+ OKT3	-0.8368	-1.014 to -0.6593	****	< 0.0001
OKT3 vs. R59949+ OKT3	0.1518	-0.02568 to 0.3292	ns	0.1173
siRNA SAP				
no treatment vs. R59949	-0.00409	-0.1815 to 0.1733	ns	> 0.9999
no treatment vs. OKT3	-0.4679	-0.6453 to -0.2904	****	< 0.0001
no treatment vs. R59949+ OKT3	-0.4767	-0.6542 to -0.2993	****	< 0.0001
R59949 vs. OKT3	-0.4638	-0.6412 to -0.2863	****	< 0.0001
R59949 vs. R59949+ OKT3	-0.4726	-0.6501 to -0.2952	****	< 0.0001
OKT3 vs. R59949+ OKT3	-0.008868	-0.1863 to 0.1686	ns	> 0.9999
siRNA control - siRNA SAP				
no treatment	-0.004153	-0.1699 to 0.1616	ns	> 0.9999
R59949	-0.00507	-0.1708 to 0.1607	ns	> 0.9999

OKT3	0.5197	0.3539 to 0.6854	****	< 0.0001
R59949+ OKT3	0.359	0.1933 to 0.5248	****	< 0.0001
6F				
Control				
DMSO vs. SL0101-1	28.88	19.42 to 38.33	****	< 0.0001
DMSO vs. R59949	-13.9	-23.35 to -4.443	**	0.0034
DMSO vs. R59949 +SL0101-1	25.22	15.77 to 34.68	****	< 0.0001
SL0101-1 vs. R59949	-42.77	-52.23 to -33.32	****	< 0.0001
SL0101-1 vs. R59949 +SL0101-1	-3.653	-13.11 to 5.802	ns	0.6914
R59949 vs. R59949 +SL0101-1	39.12	29.67 to 48.58	****	< 0.0001
XLP pt 6				
DMSO vs. SL0101-1	9.079	-0.3765 to 18.53	ns	0.0621
DMSO vs. R59949	-25.87	-35.32 to -16.41	****	< 0.0001
DMSO vs. R59949 +SL0101-1	13.45	3.998 to 22.91	**	0.0044
SL0101-1 vs. R59949	-34.94	-44.40 to -25.49	****	< 0.0001
SL0101-1 vs. R59949 +SL0101-1	4.374	-5.081 to 13.83	ns	0.562
R59949 vs. R59949 +SL0101-1	39.32	29.86 to 48.77	****	< 0.0001
Control - XLP pt 6				
DMSO	20.53	11.26 to 29.79	****	< 0.0001
SL0101-1	0.7303	-8.536 to 9.997	ns	0.9991
R59949	8.56	-0.7063 to 17.83	ns	0.0766
R59949 +SL0101-1	8.758	-0.5083 to 18.02	ns	0.0681
6G				
Control				
DMSO vs. SL0101-1	28.04	21.24 to 34.84	****	< 0.0001
DMSO vs. R59949	-25.7	-32.50 to -18.90	****	< 0.0001
DMSO vs. R59949 +SL0101-1	24.44	17.64 to 31.24	****	< 0.0001
SL0101-1 vs. R59949	-53.74	-60.54 to -46.94	****	< 0.0001
SL0101-1 vs. R59949 +SL0101-1	-3.597	-10.40 to 3.203	ns	0.5733
R59949 vs. R59949 +SL0101-1	50.14	43.34 to 56.94	****	< 0.0001

XLP pt 9				
DMSO vs. SL0101-1	-7.068	-13.87 to -0.2676	*	0.0393
DMSO vs. R59949	-54.4	-61.20 to -47.60	****	< 0.0001
DMSO vs. R59949 +SL0101-1	-30.38	-37.18 to -23.58	****	< 0.0001
SL0101-1 vs. R59949	-47.33	-54.13 to -40.53	****	< 0.0001
SL0101-1 vs. R59949 +SL0101-1	-23.31	-30.11 to -16.51	****	< 0.0001
R59949 vs. R59949 +SL0101-1	24.02	17.22 to 30.82	****	< 0.0001
Control - XLP pt 9				
DMSO	24.07	17.71 to 30.43	****	< 0.0001
SL0101-1	-11.04	-17.40 to -4.679	***	0.0007
R59949	-4.632	-10.99 to 1.727	ns	0.2125
R59949 +SL0101-1	-30.75	-37.11 to -24.39	****	< 0.0001
6H				
DMSO				
control vs. DGKα	-5.636	-23.32 to 12.05	ns	0.9147
control vs. SAP	21.08	3.392 to 38.76	*	0.0167
control vs. SAP + DGKα	2.484	-15.20 to 20.17	ns	0.9986
DGKα vs. SAP	26.71	9.028 to 44.40	**	0.0029
DGKα vs. SAP + DGKα	8.12	-9.564 to 25.80	ns	0.6842
SAP vs. SAP + DGKα	-18.59	-36.28 to -0.9076	*	0.0373
SL0101-1				
control vs. DGKα	-15	-32.68 to 2.684	ns	0.1175
control vs. SAP	0.0101	-17.67 to 17.69	ns	> 0.9999
control vs. SAP + DGKα	20.28	2.599 to 37.97	*	0.0216
DGKα vs. SAP	15.01	-2.674 to 32.69	ns	0.1172
DGKα vs. SAP + DGKα	35.28	17.60 to 52.97	***	0.0002
SAP vs. SAP + DGKα	20.27	2.588 to 37.96	*	0.0216
DMSO - SL0101-1				
control	27.82	11.36 to 44.28	**	0.0014
DGKα	18.46	1.997 to 34.92	*	0.0261
SAP	6.757	-9.705 to 23.22	ns	0.6889
SAP + DGKα	45.62	29.16 to 62.08	****	< 0.0001

6I				
Control				
n.s + DMSO vs. NN +DMSO	-6.179	-12.83 to 0.4731	ns	0.0769
n.s + DMSO vs. ns + R59022	-3.51	-10.16 to 3.141	ns	0.5757
n.s + DMSO vs. NN +R59022	-2.693	-9.344 to 3.959	ns	0.811
NN +DMSO vs. ns + R59022	2.668	-3.983 to 9.320	ns	0.8171
NN +DMSO vs. NN +R59022	3.486	-3.166 to 10.14	ns	0.5831
ns + R59022 vs. NN +R59022	0.8177	-5.834 to 7.469	ns	0.9995
XLP pt 5				
n.s + DMSO vs. NN +DMSO	12.77	6.120 to 19.42	***	0.0002
n.s + DMSO vs. ns + R59022	-33.4	-40.06 to -26.75	****	< 0.0001
n.s + DMSO vs. NN +R59022	-14.26	-20.91 to -7.610	****	< 0.0001
NN +DMSO vs. ns + R59022	-46.18	-52.83 to -39.53	****	< 0.0001
NN +DMSO vs. NN +R59022	-27.03	-33.69 to -20.38	****	< 0.0001
ns + R59022 vs. NN +R59022	19.14	12.49 to 25.79	****	< 0.0001
Control - XLP pt 5				
n.s + DMSO	37.45	31.23 to 43.68	****	< 0.0001
NN +DMSO	56.41	50.18 to 62.63	****	< 0.0001
ns + R59022	7.561	1.340 to 13.78	*	0.0143
NN +R59022	25.89	19.67 to 32.11	****	< 0.0001
6J				
Control				
n.s + DMSO vs. NN +DMSO	-0.7795	-12.68 to 11.12	ns	> 0.9999
n.s + DMSO vs. ns + R59022	-0.6119	-12.51 to 11.29	ns	> 0.9999
n.s + DMSO vs. NN +R59022	-2.887	-14.78 to 9.011	ns	0.9796

NN +DMSO vs. ns + R59022	0.1676	-11.73 to 12.07	ns	> 0.9999
NN +DMSO vs. NN +R59022	-2.107	-14.00 to 9.790	ns	0.9961
ns + R59022 vs. NN +R59022	-2.275	-14.17 to 9.623	ns	0.9941
XLP pt 4				
n.s + DMSO vs. NN +DMSO	4.765	-7.133 to 16.66	ns	0.8182
n.s + DMSO vs. ns + R59022	-22.72	-34.62 to -10.82	***	0.0002
n.s + DMSO vs. NN +R59022	-11.09	-22.99 to 0.8043	ns	0.0753
NN +DMSO vs. ns + R59022	-27.49	-39.38 to -15.59	****	< 0.0001
NN +DMSO vs. NN +R59022	-15.86	-27.76 to -3.960	**	0.0062
ns + R59022 vs. NN +R59022	11.63	-0.2700 to 23.52	ns	0.0574
Control - XLP pt 4				
n.s + DMSO	49.54	38.42 to 60.67	****	< 0.0001
NN +DMSO	55.09	43.96 to 66.21	****	< 0.0001
ns + R59022	27.44	16.31 to 38.56	****	< 0.0001
NN +R59022	41.34	30.21 to 52.46	****	< 0.0001

Figure 7	Statistics performed with PRISM Graphpad software		**alpha: 0.05**	
2-Way ANOVA with sidak correction for multiple comparisions				
Sidak's multiple comparisons test	**Mean Diff.**	**95% CI of diff.**	**Summary**	**Adjusted P Value**
7B	Spleen/Body Wt %			
B6				
P vs. L	-0.636	-0.9231 to -0.3489	****	< 0.0001
P vs. L+R	-0.536	-0.8231 to -0.2489	***	0.0002
L vs. L+R	0.1	-0.1871 to 0.3871	ns	0.7593

Sh2d1a KO				
P vs. L	-0.586	-0.8731 to -0.2989	****	< 0.0001
P vs. L+R	-0.3293	-0.6609 to 0.002185	ns	0.0519
L vs. L+R	0.2567	-0.07485 to 0.5882	ns	0.164
B6 - Sh2d1a KO				
P	-0.072	-0.3591 to 0.2151	ns	0.892
L	-0.022	-0.3091 to 0.2651	ns	0.9963
L+R	0.1347	-0.1969 to 0.4662	ns	0.6648
7C	Spl Cell number			
B6				
P vs. L	-52.52	-113.6 to 8.527	ns	0.1061
P vs. L+R	-44.52	-105.6 to 16.53	ns	0.202
L vs. L+R	8	-53.05 to 69.05	ns	0.9819
Sh2d1a KO				
P vs. L	-47.85	-112.6 to 16.90	ns	0.193
P vs. L+R	19.73	-50.76 to 90.22	ns	0.856
L vs. L+R	67.58	-6.138 to 141.3	ns	0.0788
B6 - Sh2d1a KO				
P	-4.32	-65.37 to 56.73	ns	0.997
L	0.35	-64.40 to 65.10	ns	> 0.9999
L+R	59.93	-10.56 to 130.4	ns	0.1117
7E	%CD8+CD44+ (SPL)			
B6				
P vs. L	-48.2	-60.61 to -35.79	****	< 0.0001
P vs. L+R	-41.2	-53.61 to -28.79	****	< 0.0001
L vs. L+R	7	-5.407 to 19.41	ns	0.4035
Sh2d1a KO				

P vs. L	-39.05	-52.21 to -25.89	****	< 0.0001
P vs. L+R	-39.47	-53.79 to -25.14	****	< 0.0001
L vs. L+R	-0.4167	-15.40 to 14.57	ns	0.9998
B6 - Sh2d1a KO				
P	-3	-15.41 to 9.407	ns	0.901
L	6.15	-7.010 to 19.31	ns	0.5592
L+R	-1.267	-15.59 to 13.06	ns	0.9942
7E	%CD8+CD44+ gp33+ (SPL)			
B6				
P vs. L	-2.716	-3.762 to -1.670	****	< 0.0001
P vs. L+R	-2.716	-3.762 to -1.670	****	< 0.0001
L vs. L+R	-4.768E-08	-1.046 to 1.046	ns	> 0.9999
Sh2d1a KO				
P vs. L	-3.937	-5.046 to -2.828	****	< 0.0001
P vs. L+R	-3.212	-4.420 to -2.004	****	< 0.0001
L vs. L+R	0.725	-0.5380 to 1.988	ns	0.3889
B6 - Sh2d1a KO				
P	-0.084	-1.130 to 0.9619	ns	0.9957
L	-1.305	-2.414 to -0.1957	*	0.0181
L+R	-0.58	-1.788 to 0.6277	ns	0.5375
7F	Absolute numbers CD8+CD44+ (SPL)			
B6				
P vs. L	-43.7	-60.40 to -27.00	****	< 0.0001

P vs. L+R	-33.5	-50.20 to -16.80	***	0.0001
L vs. L+R	10.2	-6.505 to 26.90	ns	0.3374
Sh2d1a KO				
P vs. L	-30.86	-48.57 to -13.14	***	0.0006
P vs. L+R	-6.013	-25.30 to 13.28	ns	0.8127
L vs. L+R	24.84	4.669 to 45.01	*	0.013
B6 - Sh2d1a KO				
P	-1.76	-18.46 to 14.94	ns	0.9904
L	11.09	-6.633 to 28.80	ns	0.3176
L+R	25.73	6.438 to 45.02	**	0.007
7F	Absolute numbers CD8+CD44+ gp33+ (SPL)			
B6				
P vs. L	-2.196	-3.114 to -1.278	****	< 0.0001
P vs. L+R	-1.976	-2.894 to -1.057	****	< 0.0001
L vs. L+R	0.2206	-0.6976 to 1.139	ns	0.9026
Sh2d1a KO				
P vs. L	-2.699	-3.672 to -1.725	****	< 0.0001
P vs. L+R	-0.7736	-1.834 to 0.2866	ns	0.2016
L vs. L+R	1.925	0.8162 to 3.034	***	0.0006
B6 - Sh2d1a KO				
P	-0.0488	-0.9670 to 0.8694	ns	0.9987
L	-0.5512	-1.525 to 0.4227	ns	0.4008
L+R	1.153	0.09300 to 2.213	*	0.0304

7H	%CD8+CD44+ (LIV)			
B6				
P vs. L	-58.2	-64.91 to -51.49	****	< 0.0001
P vs. L+R	-55.6	-62.31 to -48.89	****	< 0.0001
L vs. L+R	2.6	-4.111 to 9.311	ns	0.6944
Sh2d1a KO				
P vs. L	-53.2	-60.32 to -46.08	****	< 0.0001
P vs. L+R	-45.87	-53.62 to -38.12	****	< 0.0001
L vs. L+R	7.333	-0.7705 to 15.44	ns	0.084
B6 - Sh2d1a KO				
P	-3.8	-10.51 to 2.911	ns	0.4004
L	1.2	-5.918 to 8.318	ns	0.9629
L+R	5.933	-1.815 to 13.68	ns	0.1701
7H	%CD8+CD44+ gp33+ (LIV)			
B6				
P vs. L	-5.758	-7.113 to -4.403	****	< 0.0001
P vs. L+R	-6.458	-7.813 to -5.103	****	< 0.0001
L vs. L+R	-0.7	-2.055 to 0.6552	ns	0.4777
Sh2d1a KO				
P vs. L	-9.365	-10.80 to -7.928	****	< 0.0001
P vs. L+R	-6.023	-7.588 to -4.459	****	< 0.0001
L vs. L+R	3.342	1.705 to 4.978	****	< 0.0001
B6 - Sh2d1a KO				
P	0.212	-1.143 to 1.567	ns	0.9699
L	-3.395	-4.832 to -1.958	****	< 0.0001

L+R	0.6467	-0.9181 to 2.211	ns	0.651
7I	Absolute numbers CD8+CD44+ (LIV)			
B6				
P vs. L	-70.56	-93.15 to -47.97	****	< 0.0001
P vs. L+R	-67.14	-89.73 to -44.55	****	< 0.0001
L vs. L+R	3.42	-19.17 to 26.01	ns	0.9726
Sh2d1a KO				
P vs. L	-81.27	-105.2 to -57.31	****	< 0.0001
P vs. L+R	-35.67	-61.75 to -9.593	**	0.0057
L vs. L+R	45.59	18.32 to 72.87	***	0.0009
B6 - Sh2d1a KO				
P	-0.12	-22.71 to 22.47	ns	> 0.9999
L	-10.83	-34.78 to 13.13	ns	0.5854
L+R	31.35	5.267 to 57.43	*	0.0155
7I	Absolute numbers CD8+CD44+gp33+ (LIV)			
B6				
P vs. L	-5.906	-7.954 to -3.858	****	< 0.0001
P vs. L+R	-6.336	-8.384 to -4.288	****	< 0.0001
L vs. L+R	-0.43	-2.478 to 1.618	ns	0.932
Sh2d1a KO				
P vs. L	-10.42	-12.59 to -8.244	****	< 0.0001
P vs. L+R	-3.385	-5.750 to -1.020	**	0.0039

L vs. L+R	7.032	4.558 to 9.505	****	< 0.0001
B6 - Sh2d1a KO				
P	0.0078	-2.041 to 2.056	ns	> 0.9999
L	-4.503	-6.676 to -2.330	****	< 0.0001
L+R	2.959	0.5934 to 5.324	*	0.0116

Figure 8	Statistics performed with PRISM Graphpad software		**alpha: 0.05**	
2-Way ANOVA with sidak correction for multiple comparisions				
Sidak's multiple comparisons test	**Mean Diff.**	**95% CI of diff.**	**Summary**	**Adjusted P Value**
8A	Serum IFNγ levels			
B6				
P vs. L	-2980	-5770 to -191.2	*	0.0332
P vs. L+R	-1880	-4669 to 908.9	ns	0.2701
L vs. L+R	1100	-1689 to 3889	ns	0.6978
Sh2d1a KO				
P vs. L	-5207	-7233 to -3180	****	< 0.0001
P vs. L+R	-1682	-4006 to 642.3	ns	0.2162
L vs. L+R	3525	1247 to 5802	**	0.0013
B6 - Sh2d1a KO				
P	-0.00001091	-2460 to 2460	ns	> 0.9999
L	-2226	-4642 to 189.2	ns	0.0783
L=R	198.2	-2472 to 2869	ns	0.9968
8B	Number of Infiltrates			
B6				
P vs. L	-1.84	-2.766 to -0.9141	****	< 0.0001
P vs. L+R	-1.2	-2.126 to -	**	0.0064

		0.2741		
L vs. L+R	0.64	-0.2859 to 1.566	ns	0.2635
Sh2d1a KO				
P vs. L	-3.61	-4.592 to -2.628	****	< 0.0001
P vs. L+R	-1.56	-2.629 to -0.4908	**	0.0017
L vs. L+R	2.05	0.9318 to 3.168	****	< 0.0001
B6 - Sh2d1a KO				
P	0.12	-0.8059 to 1.046	ns	0.9852
L	-1.65	-2.632 to -0.6679	***	0.0002
L+R	-0.24	-1.309 to 0.8292	ns	0.9301
8C	Area of Infiltrates			
B6				
P vs. L	-1.734	-3.645 to 0.1764	ns	0.087
P vs. L+R	-1.825	-3.735 to 0.08588	ns	0.0659
L vs. L+R	-0.09049	-2.001 to 1.820	ns	0.9992
Sh2d1a KO				
P vs. L	-8.857	-10.88 to -6.831	****	< 0.0001
P vs. L+R	-1.265	-3.471 to 0.9408	ns	0.4234
L vs. L+R	7.592	5.285 to 9.899	****	< 0.0001
B6 - Sh2d1a KO				
P	0.01444	-1.896 to 1.925	ns	> 0.9999
L	-7.109	-9.135 to -5.082	****	< 0.0001
L+R	0.5738	-1.632 to 2.780	ns	0.8964
8F	% CD8+ IFNγ			

	+			
B6				
P vs. L	-16.54	-18.69 to -14.38	****	< 0.0001
P vs. L+R	-15.54	-17.69 to -13.38	****	< 0.0001
L vs. L+R	1	-1.153 to 3.153	ns	0.5641
Sh2d1a KO				
P vs. L	-11.27	-13.55 to -8.986	****	< 0.0001
P vs. L+R	-13.52	-16.01 to -11.03	****	< 0.0001
L vs. L+R	-2.25	-4.850 to 0.3502	ns	0.1034
B6 - Sh2d1a KO				
P	-0.418	-2.571 to 1.735	ns	0.9451
L	4.85	2.566 to 7.134	****	< 0.0001
L+R	1.6	-0.8862 to 4.086	ns	0.2949
8F	% IFNγ + TNFα+			
B6				
P vs. L	-9.701	-11.26 to -8.145	****	< 0.0001
P vs. L+R	-9.421	-10.98 to -7.865	****	< 0.0001
L vs. L+R	0.28	-1.277 to 1.837	ns	0.9555
Sh2d1a KO				
P vs. L	-5.456	-7.107 to -3.805	****	< 0.0001
P vs. L+R	-6.398	-8.195 to -4.600	****	< 0.0001
L vs. L+R	-0.9417	-2.822 to 0.9382	ns	0.5032
B6 - Sh2d1a KO				
P	-0.0704	-1.627 to 1.486	ns	0.9992
L	4.175	2.524 to 5.826	****	< 0.0001
L+R	2.953	1.156 to 4.751	**	0.001

8F	%IFNγ+CD107a+			
B6				
P vs. L	-14.42	-16.63 to -12.21	****	< 0.0001
P vs. L+R	-14.02	-16.23 to -11.81	****	< 0.0001
L vs. L+R	0.4	-1.805 to 2.605	ns	0.9544
Sh2d1a KO				
P vs. L	-10.49	-12.82 to -8.147	****	< 0.0001
P vs. L+R	-12.22	-14.77 to -9.673	****	< 0.0001
L vs. L+R	-1.733	-4.396 to 0.9295	ns	0.2859
B6 - Sh2d1a KO				
P	-0.334	-2.539 to 1.871	ns	0.9726
L	3.6	1.261 to 5.939	**	0.002
L+R	1.467	-1.080 to 4.013	ns	0.386
8G	Absolute numbers CD8+IFNγ +			
B6				
P vs. L	-4.148	-5.993 to -2.302	****	< 0.0001
P vs. L+R	-3.526	-5.371 to -1.680	***	0.0002
L vs. L+R	0.622	-1.224 to 2.468	ns	0.7752
Sh2d1a KO				
P vs. L	-3.684	-5.641 to -1.726	***	0.0002
P vs. L+R	-1.377	-3.508 to 0.7539	ns	0.2916
L vs. L+R	2.307	0.07787 to 4.535	*	0.0411
B6 - Sh2d1a KO				
P	-0.01372	-1.859 to 1.832	ns	> 0.9999

L	0.45	-1.508 to 2.408	ns	0.9133
L+R	2.135	0.003525 to 4.266	*	0.0495
8G	Absolute numbers IFNγ + TNFα+			
B6				
P vs. L	-2.319	-3.360 to -1.278	****	< 0.0001
P vs. L+R	-2.039	-3.080 to -0.9982	***	0.0001
L vs. L+R	0.28	-0.7610 to 1.321	ns	0.8697
Sh2d1a KO				
P vs. L	-1.642	-2.746 to -0.5377	**	0.0027
P vs. L+R	-0.4769	-1.679 to 0.7252	ns	0.6789
L vs. L+R	1.165	-0.09215 to 2.422	ns	0.0747
B6 - Sh2d1a KO				
P	-0.002332	-1.043 to 1.039	ns	> 0.9999
L	0.675	-0.4292 to 1.779	ns	0.3365
L+R	1.56	0.3579 to 2.762	**	0.0087
8G	Absolute numbers IFNγ + CD107a+			
B6				
P vs. L	-3.533	-5.151 to -1.915	****	< 0.0001
P vs. L+R	-3.163	-4.781 to -1.545	***	0.0002
L vs. L+R	0.37	-1.248 to 1.988	ns	0.9145
Sh2d1a KO				
P vs. L	-3.381	-5.097 to -	***	0.0001

		1.665		
P vs. L+R	-1.217	-3.086 to 0.6510	ns	0.2851
L vs. L+R	2.163	0.2094 to 4.117	*	0.0271
B6 - Sh2d1a KO				
P	-0.01034	-1.628 to 1.608	ns	> 0.9999
L	0.142	-1.574 to 1.858	ns	0.9953
L+R	1.935	0.06705 to 3.804	*	0.0409

Figure S1	Statistics performed with PRISM Graphpad software		**alpha: 0.05**	
S1A				
2-Way ANOVA with sidak correction for multiple comparisions				
Sidak's multiple comparisons test	**Mean Diff.**	**95% CI of diff.**	**Summary**	**Adjusted P Value**
Control - DGKζ				
0	0	-8.740 to 8.740	ns	> 0.9999
1	-8.062	-16.80 to 0.6786	ns	0.0786
10	-3.971	-12.71 to 4.769	ns	0.6478
100	-3.222	-11.96 to 5.519	ns	0.7948
SAP - SAP + DGKζ				
0	0	-7.925 to 7.925	ns	> 0.9999
1	-17.82	-25.74 to -9.893	****	< 0.0001
10	-15.7	-23.63 to -7.778	****	< 0.0001
100	-10.5	-18.43 to -	**	0.0066

		2.575		
S1B				
Two-tailed paired t test				
siRNA Control vs siRNA DGKζ	P value	0.0016		
	P value summary	**		
	t. df	t=25.01 df=2		
S1C				
2-Way ANOVA with sidak correction for multiple comparisions				
Sidak's multiple comparisons test	**Mean Diff.**	**95% CI of diff.**	**Summary**	**Adjusted P Value**
Control - DGKδ				
0	0	-9.675 to 9.675	ns	> 0.9999
1	4.248	-5.428 to 13.92	ns	0.6041
10	1.67	-8.005 to 11.35	ns	0.9758
100	3.345	-6.330 to 13.02	ns	0.7758
SAP - SAP + DGKδ				
0	0	-7.861 to 7.861	ns	> 0.9999
1	7.718	-0.1436 to 15.58	ns	0.0547
10	-3.488	-11.35 to 4.374	ns	0.5953
100	-1.41	-9.271 to 6.451	ns	0.9722
S1D				
Two-tailed paired t test				
siRNA Control vs siRNA DGKδ	P value	0.0004		

	P value summary	***		
	t. df	t=51.10 df=2		
S1E				
2-Way ANOVA with sidak correction for multiple comparisions				
Sidak's multiple comparisons test	**Mean Diff.**	**95% CI of diff.**	**Summary**	**Adjusted P Value**
5 ng/mL OKT3				
GFP vs. DGKα	5.111	-1.986 to 12.21	ns	0.1758
GFP vs. DGKζ	4.033	-3.064 to 11.13	ns	0.3326
DGKα vs. DGKζ	-1.078	-8.175 to 6.020	ns	0.9608
50 ng/mL OKT3				
GFP vs. DGKα	10.16	3.058 to 17.25	**	0.0078
GFP vs. DGKζ	8.322	1.225 to 15.42	*	0.0232
DGKα vs. DGKζ	-1.833	-8.931 to 5.264	ns	0.8425
500 ng/mL OKT3				
GFP vs. DGKα	10.81	3.714 to 17.91	**	0.0054
GFP vs. DGKζ	7.478	0.3804 to 14.58	*	0.0393
DGKα vs. DGKζ	-3.333	-10.43 to 3.764	ns	0.4801

Figure S2	Statistics performed with PRISM Graphpad software		**alpha 0.05**	
2-Way ANOVA with sidak correction for multiple comparisions				
Sidak's multiple comparisons test	**Mean Diff.**	**95% CI of diff.**	**Summary**	**Adjusted P Value**

DMSO				
Control vs. SAP	18.67	8.059 to 29.28	***	0.0003
Control vs. SAP and DGKα	2.241	-8.372 to 12.85	ns	0.9347
SAP vs. SAP and DGKα	-16.43	-27.04 to -5.818	**	0.0014
Inhibitors				
SAP				
DMSO vs. MEK inhibitor	15.74	-3.049 to 34.52	ns	0.1297
DMSO vs. ERK inhibitor II	9.235	-9.550 to 28.02	ns	0.6426
DMSO vs. Rottlerin	8.754	-10.03 to 27.54	ns	0.6936
MEK inhibitor vs. ERK inhibitor II	-6.501	-25.29 to 12.28	ns	0.8936
MEK inhibitor vs. Rottlerin	-6.982	-25.77 to 11.80	ns	0.8588
ERK inhibitor II vs. Rottlerin	-0.4812	-19.27 to 18.30	ns	> 0.9999
SAP and DGKα				
DMSO vs. MEK inhibitor	19.06	0.2720 to 37.84	*	0.0458
DMSO vs. ERK inhibitor II	14.47	-4.316 to 33.25	ns	0.1881
DMSO vs. Rottlerin	20.38	1.595 to 39.17	*	0.0298
MEK inhibitor vs. ERK inhibitor II	-4.588	-23.37 to 14.20	ns	0.9782
MEK inhibitor vs. Rottlerin	1.323	-17.46 to 20.11	ns	> 0.9999
ERK inhibitor II vs. Rottlerin	5.911	-12.87 to 24.70	ns	0.9288

Figure S3	Statistics performed with PRISM Graphpad software		**alpha: 0.05**	
2-Way ANOVA with sidak correction for multiple comparisions				
Sidak's multiple comparisons test	**Mean Diff.**	**95% CI of diff.**	**Summary**	**Adjusted P Value**
S3A				
Control				

siRNA Control vs. siRNA DGKα	0.0102	-0.2614 to 0.2818	ns	> 0.9999
siRNA Control vs. siRNA Control + OKT3	-0.9204	-1.192 to -0.6488	****	< 0.0001
siRNA Control vs. siRNA DGKα + OKT3	-0.8342	-1.106 to -0.5626	****	< 0.0001
siRNA DGKα vs. siRNA Control + OKT3	-0.9306	-1.202 to -0.6590	****	< 0.0001
siRNA DGKα vs. siRNA DGKα + OKT3	-0.8444	-1.116 to -0.5728	****	< 0.0001
siRNA Control + OKT3 vs. siRNA DGKα + OKT3	0.0862	-0.1854 to 0.3578	ns	0.9162
SAP				
siRNA Control vs. siRNA DGKα	0.009	-0.2626 to 0.2806	ns	> 0.9999
siRNA Control vs. siRNA Control + OKT3	-0.47	-0.7416 to -0.1984	***	0.0009
siRNA Control vs. siRNA DGKα + OKT3	-0.4382	-0.7098 to -0.1666	**	0.0017
siRNA DGKα vs. siRNA Control + OKT3	-0.479	-0.7506 to -0.2074	***	0.0008
siRNA DGKα vs. siRNA DGKα + OKT3	-0.4472	-0.7188 to -0.1756	**	0.0014
siRNA Control + OKT3 vs. siRNA DGKα + OKT3	0.0318	-0.2398 to 0.3034	ns	0.9995
Control - SAP				
siRNA Control	0.02	-0.2328 to 0.2728	ns	0.999
siRNA DGKα	0.0188	-0.2340 to 0.2716	ns	0.9992
siRNA Control + OKT3	0.4704	0.2176 to 0.7232	***	0.0006
siRNA DGKα + OKT3	0.416	0.1632 to 0.6688	**	0.0017
S3B				
Control				
siRNA Control vs. siRNA DGKα	0.0138	-0.3332 to 0.3608	ns	> 0.9999
siRNA Control vs. siRNA Control + OKT3	-0.945	-1.292 to -0.5980	****	< 0.0001
siRNA Control vs. siRNA	-1.285	-1.632 to -	****	< 0.0001

DGKα + OKT3		0.9378		
siRNA DGKα vs. siRNA Control + OKT3	-0.9588	-1.306 to -0.6118	****	< 0.0001
siRNA DGKα vs. siRNA DGKα + OKT3	-1.299	-1.646 to -0.9516	****	< 0.0001
siRNA Control + OKT3 vs. siRNA DGKα + OKT3	-0.3398	-0.6868 to 0.007165	ns	0.0563
SAP				
siRNA Control vs. siRNA DGKα	-0.0014	-0.3484 to 0.3456	ns	> 0.9999
siRNA Control vs. siRNA Control + OKT3	-0.3666	-0.7136 to -0.01964	*	0.0362
siRNA Control vs. siRNA DGKα + OKT3	-0.5748	-0.9218 to -0.2278	**	0.0013
siRNA DGKα vs. siRNA Control + OKT3	-0.3652	-0.7122 to -0.01824	*	0.037
siRNA DGKα vs. siRNA DGKα + OKT3	-0.5734	-0.9204 to -0.2264	**	0.0014
siRNA Control + OKT3 vs. siRNA DGKα + OKT3	-0.2082	-0.5552 to 0.1388	ns	0.4088
Control - SAP				
siRNA Control	0.0046	-0.3184 to 0.3276	ns	> 0.9999
siRNA DGKα	-0.0106	-0.3336 to 0.3124	ns	> 0.9999
siRNA Control + OKT3	0.583	0.2600 to 0.9060	***	0.0008
siRNA DGKα + OKT3	0.7146	0.3916 to 1.038	***	0.0001
S3E				
2-Way ANOVA with sidak correction for multiple comparisions				
Sidak's multiple comparisons test	**Mean Diff.**	**95% CI of diff.**	**Summary**	**Adjusted P Value**
Control				
0 hr				
DMSO vs. R59949	7.799	-53.90 to 69.50	ns	0.9712
DMSO vs. R59022	2.668	-59.03 to 64.37	ns	0.9987
R59949 vs. R59022	-5.131	-66.83 to 56.57	ns	0.9913

4 hr				
DMSO vs. R59949	-48.18	-109.9 to 13.52	ns	0.1239
DMSO vs. R59022	8.456	-53.24 to 70.15	ns	0.9639
R59949 vs. R59022	56.63	-5.067 to 118.3	ns	0.0699
0 hr - 4 hr				
DMSO	-353.5	-415.2 to -291.8	****	< 0.0001
R59949	-409.5	-471.2 to -347.8	****	< 0.0001
R59022	-347.7	-409.4 to -286.0	****	< 0.0001
XLP Pt 8				
0 hr				
DMSO vs. R59949	-3.389	-19.52 to 12.75	ns	0.8876
DMSO vs. R59022	10.44	-5.695 to 26.58	ns	0.2174
R59949 vs. R59022	13.83	-2.306 to 29.97	ns	0.0899
4 hr				
DMSO vs. R59949	-9.698	-25.83 to 6.438	ns	0.2629
DMSO vs. R59022	-8.606	-24.74 to 7.530	ns	0.3447
R59949 vs. R59022	1.092	-15.04 to 17.23	ns	0.9953
0 hr - 4 hr				
DMSO	-42.9	-59.03 to -26.76	***	0.0004
R59949	-49.21	-65.34 to -33.07	***	0.0002
R59022	-61.95	-78.08 to -45.81	****	< 0.0001

S5					
Two-way ANOVA	Ordinary				
Alpha	0.05				
EXPERIMENT 1					
Two-way ANOVA	Ordinary				
Alpha	0.05				
Source of Variation	% of total variation	P value	P value summary		
Interaction	0.1106	0.0044	**		
e:t ratio	99.79	< 0.0001	****		
WT v WT+inhib	0.01112	0.1801	ns		
ANOVA table	SS	DF	MS	F (DFn. DFd)	P value

Interaction	25.86	3	8.622	F (3. 16) = 6.513	P = 0.0044
e:t ratio	23337	3	7779	F (3. 16) = 5877	P < 0.0001
WT v WT+inhib	2.6	1	2.6	F (1. 16) = 1.964	P = 0.1801
Residual	21.18	16	1.324		
Two-way ANOVA	Ordinary				
Alpha	0.05				
Two-way ANOVA	Ordinary				
Alpha	0.05				
Source of Variation	% of total variation	P value	P value summary		
Interaction	1.938	< 0.0001	****		
e:t ratio	94.6	< 0.0001	****		
SAP v SAP+inhib	3.35	< 0.0001	****		
ANOVA table	SS	DF	MS	F (DFn. DFd)	P value
Interaction	192.6	3	64.22	F (3. 16) = 88.67	P < 0.0001
e:t ratio	9404	3	3135	F (3. 16) = 4329	P < 0.0001
SAP v SAP+inhib	333	1	333	F (1. 16) = 459.9	P < 0.0001
Residual	11.59	16	0.7242		
EXPERIMENT 2					
Source of Variation	% of total variation	P value	P value summary	Significant ?	
Interaction	0.1236	< 0.0001	****	Yes	
e:t ratio	99.73	< 0.0001	****	Yes	
WT v WT+inhib	0.1092	< 0.0001	****	Yes	
ANOVA table	SS	DF	MS	F (DFn.	P value

				DFd)	
Interaction	21.8	3	7.267	F (3. 16) = 16.38	P < 0.0001
e:t ratio	17584	3	5861	F (3. 16) = 13209	P < 0.0001
WT v WT+inhib	19.26	1	19.26	F (1. 16) = 43.40	P < 0.0001
Residual	7.1	16	0.4438		
Source of Variation	% of total variation	P value	P value summary	Significant ?	
Interaction	1.239	< 0.0001	****	Yes	
e:t ratio	92.77	< 0.0001	****	Yes	
SAP v SAP+inhib	5.781	< 0.0001	****	Yes	
ANOVA table	SS	DF	MS	F (DFn. DFd)	P value
Interaction	168.2	3	56.05	F (3. 16) = 31.70	P < 0.0001
e:t ratio	12586	3	4195	F (3. 16) = 2372	P < 0.0001
SAP v SAP+inhib	784.3	1	784.3	F (1. 16) = 443.5	P < 0.0001
Residual	28.29	16	1.768		

CHAPTER 3: Sensitivity to restimulation-induced cell death is linked to glycolytic metabolism in human T cells

Submitted as: **Sasha E. Larsen[*#], Abegail Bilenkin[#], and Andrew L. Snow[#]. 2016.** To the Journal of Immunology: Cutting Edge.

Department of Pharmacology & Molecular Therapeutics, Uniformed Services University of the Health Sciences, Bethesda, MD

The work presented in this chapter is the sole work of S E Larsen, with the assistance of A Bilenkin for L-lactate analysis on the first three donors represented in Fig. 1B.

ABSTRACT

Restimulation-induced cell death (RICD) regulates immune responses by restraining effector T cell expansion and limiting nonspecific damage to the host. RICD is triggered by re-engagement of the T cell receptor (TCR) on a cycling effector T cell, resulting in apoptosis. It remains unclear how RICD sensitivity is calibrated in T cells derived from different individuals or subsets. Here we show that aerobic glycolysis strongly correlates with RICD sensitivity in human $CD8^+$ effector T cells. Reducing glycolytic activity or glucose availability rendered effector T cells significantly less sensitive to RICD. We found that active glycolysis specifically facilitates the induction of pro-apoptotic Fas ligand upon TCR restimulation, accounting for enhanced RICD sensitivity in highly glycolytic T cells. Collectively, these data indicate that RICD susceptibility is linked to

metabolic reprogramming, and that switching back to metabolic quiescence may help shield T cells from RICD as they transition into the memory pool.

INTRODUCTION

Dynamic changes in cellular metabolism are vital during the course of an effective $CD8^+$ T cell response. Like most somatic cells, naïve and memory T cells operate in a generally quiescent metabolic state and utilize mitochondrial oxidative phosphorylation (OXPHOS) for ATP generation (189). Following T cell receptor (TCR) stimulation, however, responding T cells rapidly switch to using glycolysis even in the presence of oxygen (Warburg effect) (33; 63; 68; 70; 100; 126; 129). Activated T cells proliferate and acquire potent effector functions (e.g IFN-γ production) which have been linked to glycolytic metabolism (23; 30; 31; 33; 63; 101; 126; 129; 192). Recent reports demonstrate that changes in cellular metabolism over the course of a T cell response profoundly influence cell survival and differentiation, including the generation of memory (4; 5; 63; 69; 115; 128; 129; 135; 191; 192; 199). Interestingly, it is precisely during this window of expansion and aerobic glycolysis that effector T cells become sensitive to activation-/restimulation-induced cell death (AICD/RICD).

Restimulation induced cell death (RICD) is a critical apoptotic program that ultimately sets an upper limit for effector T cell expansion during an infection. RICD sensitivity is dependent on prior activation, cell cycle induction via interleukin-2 (IL-2), and a subsequent, strong restimulation signal propagated through the TCR which induces apoptosis in a subset of effectors (94; 154; 176). Unlike effector T cells, naïve and resting memory T cells are relatively resistant to RICD. By constraining effector T cell numbers during the antigen-induced expansion phase, this self-regulatory death pathway helps to maintain immune homeostasis by precluding excessive, non-specific immunopathological damage to the host. Indeed, our lab previously demonstrated that a

defect in RICD contributes to excessive T cell accumulation and lethal damage to host tissues, as noted in patients with X-linked lymphoproliferative disorder (153; 174).

Although RICD was first described over 25 years ago (7; 24; 67; 97; 154; 167) the molecular components that convert TCR signaling from pro-proliferative in naïve cells to pro-apoptotic in restimulated, activated T cells have yet to be fully defined. Additionally, it remains unclear why RICD sensitivity varies for T cells from different normal human donors, and why only a proportion of expanded effector T cells are rendered competent to die after TCR restimulation. Although robust glycolytic metabolism overlaps closely with the window of RICD susceptibility in effector T cells, it is not known whether metabolic reprogramming influences RICD directly. We hypothesized that glycolytic metabolism promotes the sensitization of effector T cells to RICD. Here we show for the first time that active glycolysis enhances RICD in effector $CD8^+$ T cells, specifically by enabling robust induction of Fas ligand (FASL) after TCR restimulation. Our findings suggest that restricting glucose availability and/or reducing glycolysis may prolong the survival of activated T cells by protecting them from RICD.

MATERIALS AND METHODS

Isolation, activation and culture of primary human CD8$^+$ T cells

Blood from anonymous healthy donors (buffy coats) was generously provided by Dr. Michael Lenardo and the National Institutes of Health Blood Bank. PBMC were isolated using Ficoll density gradient centrifugation, and CD8$^+$ T cells were purified from PBMC using the EasySep Human CD8$^+$ T cell enrichment kit (Stem Cell Technologies). T cells were activated 1:1 with beads coated with anti-CD3/CD2/CD28 antibodies (Human T cell Activation/Expansion Kit, Miltenyi) in glucose-free RPMI 1640 (Life Technologies) + 10% fetal calf serum (FCS) (Lonza) + 1mM sodium pyruvate (Cellgro) + 1% penicillin/streptomycin (Lonza) and either 10 mM D-galactose or D-glucose (Sigma) for 3 days. Activated T cells were washed in PBS and subsequently cultured in glucose- or galactose-containing media as described above with 100 U/mL rIL-2 (PeproTech) at 1x10^6 cells/mL for ≥13 days, changing media every 3 days. In some experiments, cells on days 9-12 were washed 2x in PBS and swapped into media containing the opposite sugar as described in the Figure Legends. Additionally, cells grown in galactose were washed 2x in PBS and resuspended in media supplemented with 10-fold titrations of glucose prior to RICD assays as described. For conditioned media experiments, Glu and Gal T cell cultures were spun down on day 14 of culture in IL-2 and cells were resuspended in the opposite conditioned culture media with additional IL-2. These cells were incubated for 30 minutes and then assayed for RICD as described below.

Apoptosis assays and flow cytometry

RICD assays were performed as previously described (85). Briefly, activated T cells (days 13-15) were treated in triplicate with anti-CD3ε mAb OKT3 (5–500 ng/ml;

Biogems), and plated at $7.5x10^5$ cells/mL in 96-well round bottom plates. For some assays, cells were pretreated for 30 min with 2 mM 2-deoxy-glucose, 5 mM rapamycin, 1 mM oligomycin A, 10 mM metformin, 5 mM rotenone, 10 ng/mL rIFNγ, 5 μg/mL concanamycin A, 20 mM D-glucose (Sigma-Aldrich) or 1 mg/mL anti-FAS antagonistic antibody SM1/23 (Enzo) versus DMSO or ddH_20 solvent control. At 24h after TCR restimulation, cells were stained with 5 μg/mL propidium iodide (Sigma-Aldrich) and collected for constant time on an Accuri C6 flow cytometer (BD Biosciences). Cell death was quantified as percentage cell loss = (1 – [number of viable cells (treated) / number of viable cells (untreated)]) x 100. For some assays, T cells were stained with Annexin V-FITC (Biolegend) 4 hours after restimulation. Surface expression of FAS (CD95) and CD3 were assessed using anti-CD95-APC and anti-CD3-PE antibodies respectively (BioLegend). Surface expression of IL-2Rα was measured by flow cytometry after 3 days of bead activation, using an anti-CD25-PE antibody (BioLegend). DNA content was used to evaluate cell cycle status -/+ 4 hours of anti-CD3 restimulation using methanol fixation and staining with PI and RNAse A (Sigma). All flow cytometric assays were performed on an Accuri C6 flow cytometer (BD Biosciences).

Western blotting

Activated $CD8^+$ T cells ($1x10^6$ per time point) were restimulated with 500 ng/ml OKT3 (0–4hr), washed in cold PBS, and lysed in 1% Nonidet P-40 (NP-40) lysis buffer (50 mM Tris [pH 7.4], 150 mM NaCl, 0.5 mM EDTA, 1% NP-40, 0.5% sodium deoxycholate, 1 mM Na_3VO_4, 1 mM NaF) containing complete protease inhibitors (Roche) for 30 min on ice. Cleared lysates were boiled in 2x reducing sample buffer, and resolved on Any kD SDS-PAGE gels (Bio-Rad). Proteins were transferred to nitrocellulose on a Trans-Blot

Turbo system (Bio-Rad), blocked in 2% Tropix I-Block (Applied Biosystems) in TBS/0.1% Tween, and probed with the following Abs: anti-FASL (Ab3; EMD Millipore); anti-BIM (Enzo); anti-cleaved caspase 9, anti-cleaved caspase 3, anti-NUR77 (Biolegend); anti-geminin; anti-Cdt1 (Santa Cruz Biotechnology) and anti–β-actin (Sigma-Aldrich). Bound Abs were detected using HRP-conjugated secondary Abs (Southern Biotech, eBioscience) and ECL (Thermo Scientific).

ELISA

Detection of soluble/cleaved FASL in cell supernatants from T cells -/+ anti-CD3 restimulation (-/+ inhibitor pre-treatment as described above) was performed using the Quantikine Human Fas Ligand/TNFSF6 Immunoassay Kit (R&D Systems). L-lactate levels were measured in cell supernatants using a Glycolysis Cell-based Assay kit (Cayman Chemical). ELISA plates were read using a Synergy H1 Hybrid Reader (BioTek); concentrations of sFASL (pg/ml) or L-lactate (mM) were calculated using Gen5 data analysis software (BioTek).

Statistics

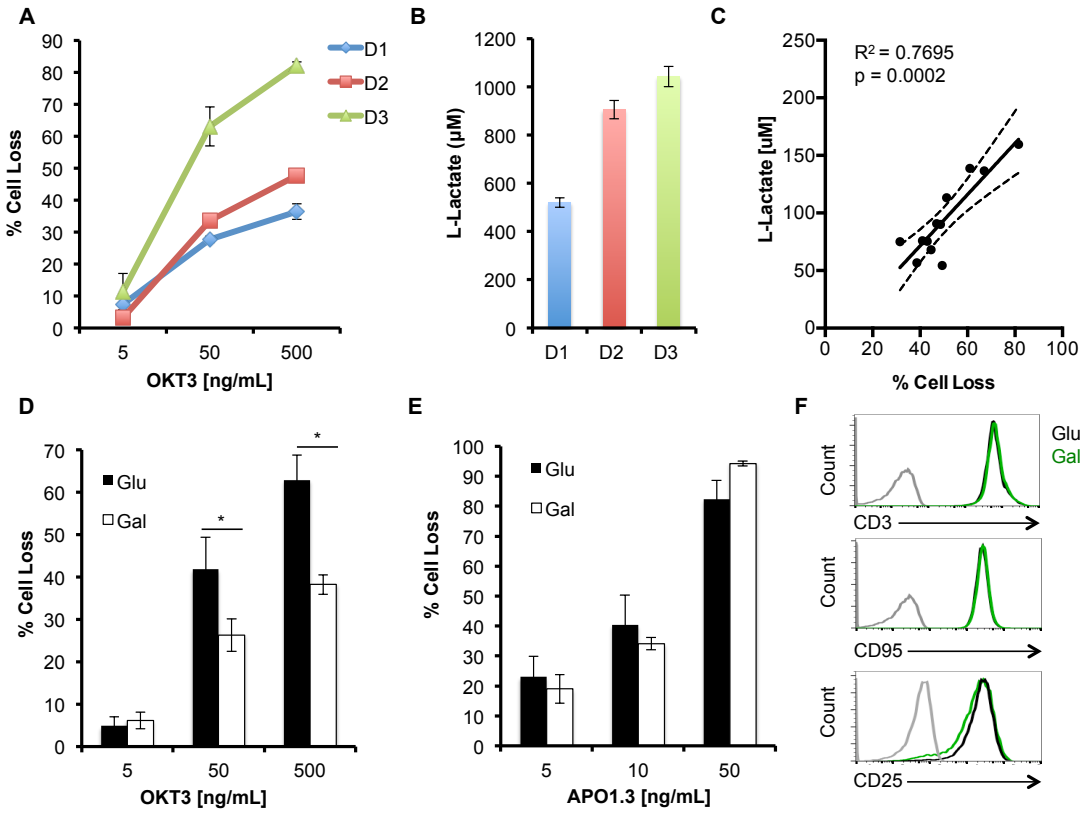
In vitro cell death assays were evaluated using two-way ANOVA (α=0.05) with Sidak correction for multiple comparisons or students T-Test where appropriate. L-lactate, % cell loss and sFASL values were correlated using Pearson's comparison analysis and graphs were generated using linear regression. All statistical analyses were performed using GraphPad PRISM software. Error bars are defined in the figure legends as ± SEM or ± SD where appropriate. Asterisks denote statistical significance and p-values are reported in figure legends.

RESULTS

To investigate whether donor-dependent variability in RICD sensitivity is associated with glycolytic metabolism, we first measured RICD and L-lactate production in $CD8^+$ effector T cells derived from three human donors after restimulation with the agonistic anti-CD3 antibody OKT3. Donor T cells that displayed higher RICD sensitivity also produced more L-lactate, a product of glycolysis, after 4 hours of restimulation (Fig. 9A,B). Indeed, when data collected from 12 donors were subjected to linear regression analysis, we found a significant correlation existed between RICD sensitivity and L-lactate measured in the supernatant, (Fig. 9C, Pearson R^2=0.7695). These data suggest that greater RICD sensitivity correlates with glycolytic activity in human $CD8^+$ T cells.

To establish a causal link between glycolytic metabolism and RICD, we next expanded effector T cells from single donors in glucose- versus galactose-containing culture medium. Substituting galactose for glucose severely restricts glycolysis and forces T cells to predominantly use oxidative phosphorylation (OXPHOS) (33; 46; 65). Interestingly, donor T cells cultured in galactose (Gal) culture media were significantly less sensitive to RICD compared to T cells cultured in glucose (Glu) containing media (Fig 9D). This difference could not be explained by a broader defect in programmed cell death, as both Glu- and Gal-cultured T cells were equally sensitive to direct FAS ligation (Fig. 9E). Glu and Gal-cultured T cells also displayed equivalent cell surface expression of T cell receptor (CD3) and FAS (CD95) on day 14 (Fig. 9F). Glu and Gal-cultured T cells also displayed similar expression of CD25 after three days of bead stimulation (Fig.9F), demonstrating they were similarly activated. These data imply that RICD susceptibility is specifically influenced by metabolic status in effector T cells.

Figure 9. Increased RICD sensitivity in glycolytic $CD8^+$ T cells.
(A) Activated T cells from three normal donors (D1-D3) were restimulated with OKT3 Ab. Percent cell loss was measured 24 hrs later by PI staining and flow cytometry. (B) L-Lactate was measured in T cell supernatants by ELISA after 4 hours of OKT3 restimulation. (C) Linear regression analysis comparing maximum % cell loss versus L-lactate production for 12 independent donors, including 95% confidence interval (dashed line). Pearson correlation R^2=0.7695 and p=0.0002. (D) Activated T cells cultured in glucose (Glu) or galactose (Gal)-containing media for ~14 days were restimulated and analyzed as in (A). Data represent % cell loss (avg ± SEM) for 5 individual donors for a 24h RICD assay. Glu and Gal T cells were compared by two-way ANOVA: OKT3 [5] n.s, [50] p=0.0057, [500] p=0.0003. (E) Activated T cells as in (D) were stimulated with anti-FAS agonistic Ab APO1.3 for 24 hrs to trigger FAS-induced apoptosis. Data represent % cell loss (avg ± SEM) for 3 individual donors. Two-way ANOVA analysis showed no significant differences for all doses of APO1.3. (F) Representative surface staining of CD3 (upper panel), CD95 (middle panel) and CD25 (lower panel) between Glu (black) and Gal (green) T cells versus isotype control (grey) by flow cytometry.


A
% Cell Loss
OKT3 [ng/mL]
D1
D2
D3
B
L-Lactate (µM)
C
L-Lactate [uM]
% Cell Loss
R² = 0.7695
p = 0.0002
D
% Cell Loss
OKT3 [ng/mL]
Glu
Gal
E
% Cell Loss
APO1.3 [ng/mL]
F
Count
CD3
CD95
CD25
Glu
Gal

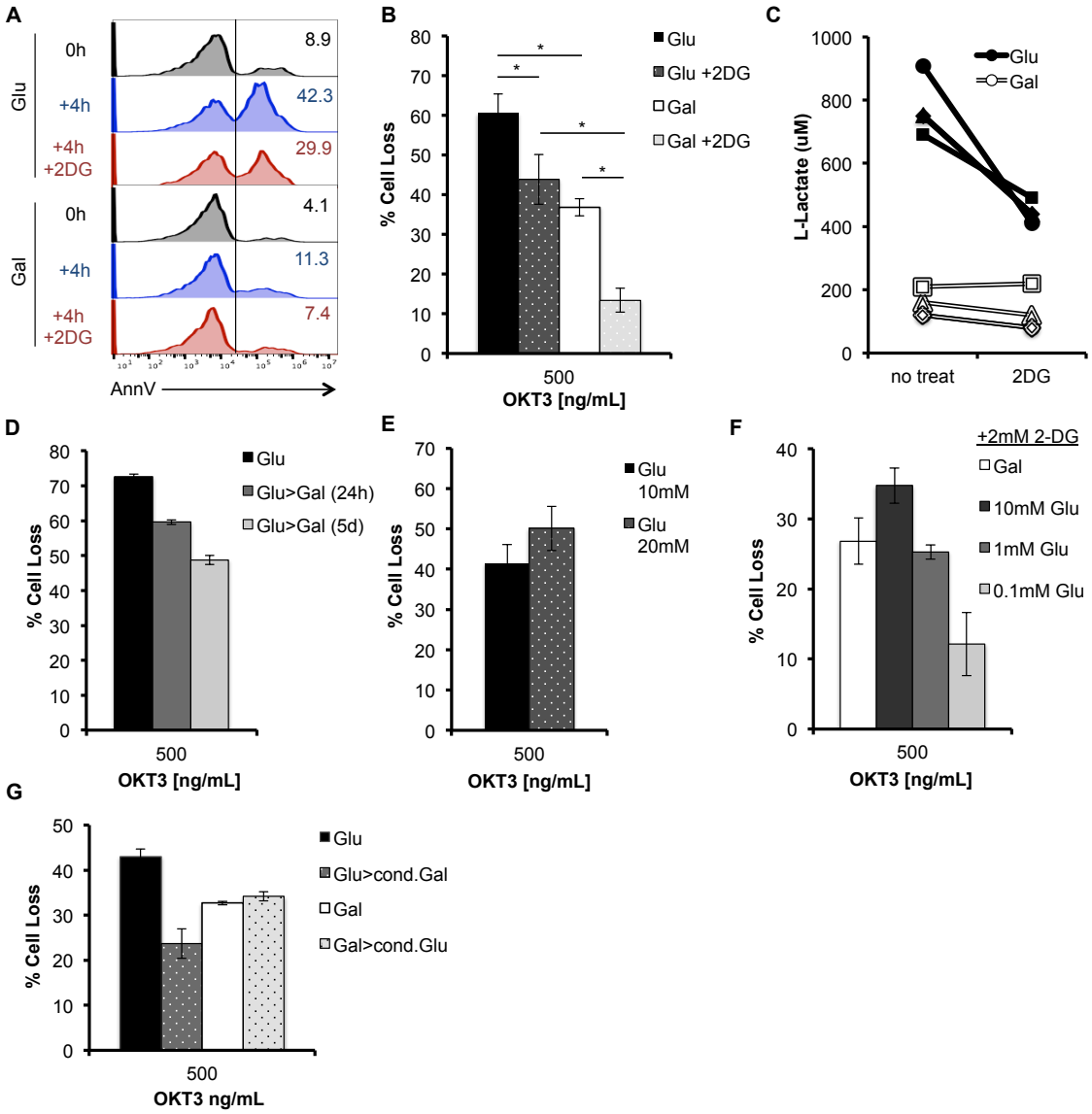
To further explore the link between glycolysis and RICD, we conducted further apoptosis assays comparing Glu versus Gal T cells in the presence of the competitive glucose analog 2-deoxyglucose (2-DG) (31). Brief pre-treatment with 2-DG substantially reduced the number of Glu T cells staining with Annexin V at 4 hours post TCR restimulation, an early marker of apoptosis commitment, and significantly reduced RICD sensitivity at 24 hours (Fig. 10A,B). Indeed, Glu T cells treated with 2-DG showed a dramatic reduction in L-lactate production after 4 hours of restimulation, confirming decreased glycolysis (Fig. 10C). Although Gal T cells primarily utilize OXPHOS, galactose can be used for glycolysis, albeit at much lower efficiency than glucose (30; 46) (Fig. 10C). Indeed, 2-DG also reduced RICD sensitivity in Gal T cells (Fig. 10B), associated with a detectable decrease in lactate production in most donors tested (Fig. 10C). These results indicate that acute inhibition of glycolysis renders T cells less sensitive to RICD.

We next asked whether RICD sensitivity of effector T cells relying primarily on glycolysis versus OXPHOS could be altered by acute changes in glucose availability. Interestingly, we could generate a step-wise reduction in Glu T cell RICD sensitivity by swapping cells into Gal-containing media for 1-5 days of culture prior to restimulation (Fig. 10D). Conversely, supplementing normal culture media with additional glucose further increased RICD of Glu T cells slightly, reaching maximum sensitivity at 20 mM (Fig. 10E). RICD sensitivity of Gal T cells was also titratable depending on glucose availability. Gal T cells swapped into 10 mM glucose-containing media for just 30 minutes were notably more sensitive to RICD (Fig. 10F). However, RICD sensitivity decreased with serial 10-fold dilutions of glucose in the media; the addition of 2-DG

helped accentuate these differences, presumably by impeding hexokinase activity and restricting the entry of freshly added glucose into the glycolytic cycle (Fig. 10F). Since Gal T cells preferentially use pyruvate for the TCA cycle, they lack excess pyruvate for subsequent conversion to secreted L-lactate. We next asked whether extracellular L-lactate was 'priming' Glu T cells for greater RICD sensitivity by swapping Glu T cells into galactose-conditioned culture media and similarly placing Gal T cells into glucose-conditioned culture media. We saw no increase in Gal RICD sensitivity in the glucose-conditioned media compared to Gal T cells in galactose-containing media, suggesting that (a) excess L-lactate was not providing a sensitizing feedback signal to Glu T cells, and (b) there was little to no glucose remaining in the culture media (Fig. 10G). Collectively, these data imply that acute glucose availability, and not L-lactate, indeed helps set the threshold for RICD sensitivity in $CD8^+$ effector T cells.

Figure 10. Acute glucose availability governs RICD sensitivity.

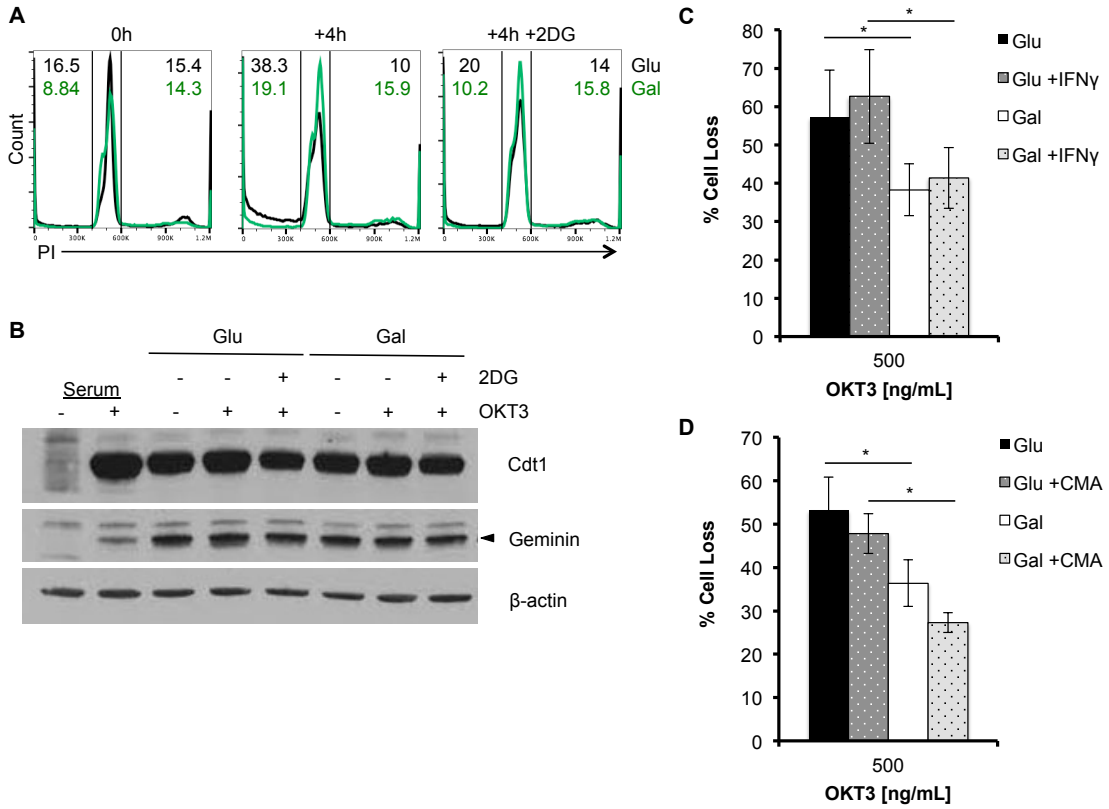
(A) Annexin V binding to Glu or Gal T cells at baseline, or after 4 hr OKT3 restimulation ± 2-DG (2 mM) analyzed by flow cytometry. Numbers denote % of AnnexinV^{+} T cells. (B) Glu or Gal T cells were restimulated with 500 ng/ml OKT3 for 24 hrs ± 2 mM 2-DG pre-treatment, and analyzed for RICD as in Fig 1D. Data represent % cell loss (avg ± SEM) for 6 individual donors. Treatments were compared by two-way ANOVA: Glu-Gal $p<0.0001$, Glu-Glu+2-DG $p=0.0003$, Glu+2DG-Gal+2-DG $p<0.0001$, Gal-Gal+2DG $p<0.0001$ (C) L-Lactate was measured in T cell supernatants after 4 hours of OKT3 restimulation ± 2-DG, n=4 donors. Lines connect data points for each single donor. (D) Glu T cells were maintained or switched into Gal media on day 9 or day 13 in culture, then assayed for RICD sensitivity on day 14 as in (B). Data (average ± SD of technical replicates) are representative of 3 independent experiments using different donors. (E) Glu T cells were incubated in media with 10 mM or 20 mM glucose for 30 minutes and assayed for RICD sensitivity. Average of 3 donors ± SEM. Treatments compared by T-Test, n.s. (F) Gal T cells were washed and resuspended in media containing titrating doses of glucose (0.1 – 10 mM) and tested for RICD sensitivity as in (B) + 2-DG treatment. 24h RICD assay. Data (avg ± SD of technical replicates) are representative of 3 independent experiments using different donors. (G) Glu T cells were maintained or switched into conditioned Gal media and Gal T cells were maintained or switched into conditioned Glu media on day 14, incubated for 30 minutes, then assayed for RICD. Data (average ± SD of technical replicates) are representative of 2 independent experiments using different donors.


A
Glu
0h
+4h
+4h +2DG
8.9
42.3
29.9
Gal
0h
+4h
+4h +2DG
4.1
11.3
7.4
AnnV
B
% Cell Loss
Glu
Glu +2DG
Gal
Gal +2DG
500
OKT3 [ng/mL]
C
L-Lactate (uM)
Glu
Gal
no treat
2DG
D
% Cell Loss
Glu
Glu>Gal (24h)
Glu>Gal (5d)
500
OKT3 [ng/mL]
E
% Cell Loss
Glu 10mM
Glu 20mM
500
OKT3 [ng/mL]
F
% Cell Loss
+2mM 2-DG
Gal
10mM Glu
1mM Glu
0.1mM Glu
500
OKT3 [ng/mL]
G
% Cell Loss
Glu
Glu>cond.Gal
Gal
Gal>cond.Glu
500
OKT3 ng/mL

To understand how glycolytic metabolism drives RICD sensitivity, we examined several requirements known to render effector T cells competent to die through this pathway. Because only effector T cells that are actively cycling are sensitive to RICD (16; 94; 196), we assessed whether cell cycle progression was specifically enhanced in Glu T cells before or after TCR restimulation, relative to Gal T cells. Using PI cell cycle analysis, we found an equal percentage of cells actively dividing (S + G2/M phases) at baseline in both Glu and Gal T cells (Fig. 11A). After 4 hours of restimulation, we measured a lower percentage of Glu T cells in cycle compared to Gal T cells, which was rescued by pre-treatment with 2-DG (Fig. 11A). Glu T cell cultures displayed a concomitant increase in the proportion of sub-G1/apoptotic cells, consistent with RICD induction (Fig. 11A). To complement our flow cytometric cell cycle profiling, we performed immuoblotting of cell lystates from Glu and Gal T effector cells at baseline, after 4 hours restimulation, or with 2-DG treatment compared to serum starved and serum sufficient synchronized controls. In order to determine the relative proportion of each population actively cycling before or after restimulation, we assayed expression of the key cell cycle checkpoint proteins Cdc10-dependent transcript 1 (Cdt-1), which is expressed solely during G1 and S phases, and geminin, which is expressed only during late S-G2-M phase (184; 204). Immunoblotting showed no marked differences in the expression of either Cdt-1 or geminin between Glu and Gal T cells for each condition tested (Fig. 11B). These data suggest that Glu T cells are not more sensitive to RICD simply because a greater proportion of cells are actively cycling or induced into cell cycle upon TCR restimulation.

IFN-γ has also been implicated in potentiating RICD sensitivity (97; 145). Previous studies demonstrated that T cells cultured in Gal media proliferate but cannot mount sufficient effector functions, including IFN- γ secretion (30; 31; 33). Despite this defect, the addition of exogenous IFN- γ did not boost RICD sensitivity in Gal T cells to levels measured in Glu T cells (Fig. 11C). Moreover, inhibition of lytic granule maturation with concanamycin A (CMA)(83) treatment did not preferentially decrease Glu T cell sensitivity (Fig. 11D). These data suggest that diminished RICD sensitivity of Gal T cells is not explained by deficiencies in IFN- γ production or perforin-mediated cytotoxicity.

Figure 11. Cell cycle progression and differential effector function do not contribute to differential RICD sensitivity in Glu vs. Gal T cells RICD sensitivity in glycolytic $CD8^+$ T cells.
(A) Flow cytometric PI cell cycle analysis of Glu (black) and Gal T cells (green) at baseline and after 4 hours of OKT3 restimulation ± 2-DG. Numbers denote % cells in sub-G1/apoptotic gate (upper left) or S+G2/M (upper right). Data are representative of 3 independent experiments using different donors. (B) Whole cell lysates (WCL) from Glu and Gal T cells at baseline and after 4 hours of restimulation ± 2-DG were separated by SDS-PAGE and immunoblotted for the indicated proteins. β-actin serves as a loading control. Data are representative of 2 independent experiments using different donors. (C-D) Glu and Gal T cells were pretreated with 10 ng/mL IFNγ (C) or 5μg/mL concanamycin A (CMA) (D) for 30 minutes, then assayed for RICD as above. Data represent % cell loss (avg ±SEM) of 3 donors. Treatments were compared by two-way ANOVA: (C) Glu-Gal p=0.0176, Glu+IFNy-Gal+IFNy p= 0.0140, Glu-Glu+IFNy n.s, Gal-Gal+IFNy n.s; (D) Glu-Gal p=0.0366, Glu+CMA-Gal+CMA p=0.0223, Glu-Glu+CMA n.s, Gal-Gal+CMA n.s.


A
0h
+4h
+4h +2DG
16.5
8.84
15.4
14.3
38.3
19.1
10
15.9
20
10.2
14
15.8
Glu
Gal
Count
PI
B
Glu
Gal
Serum
2DG
OKT3
Cdt1
Geminin
β-actin
C
% Cell Loss
OKT3 [ng/mL]
500
Glu
Glu +IFNγ
Gal
Gal +IFNγ
D
% Cell Loss
OKT3 [ng/mL]
500
Glu
Glu +CMA
Gal
Gal +CMA

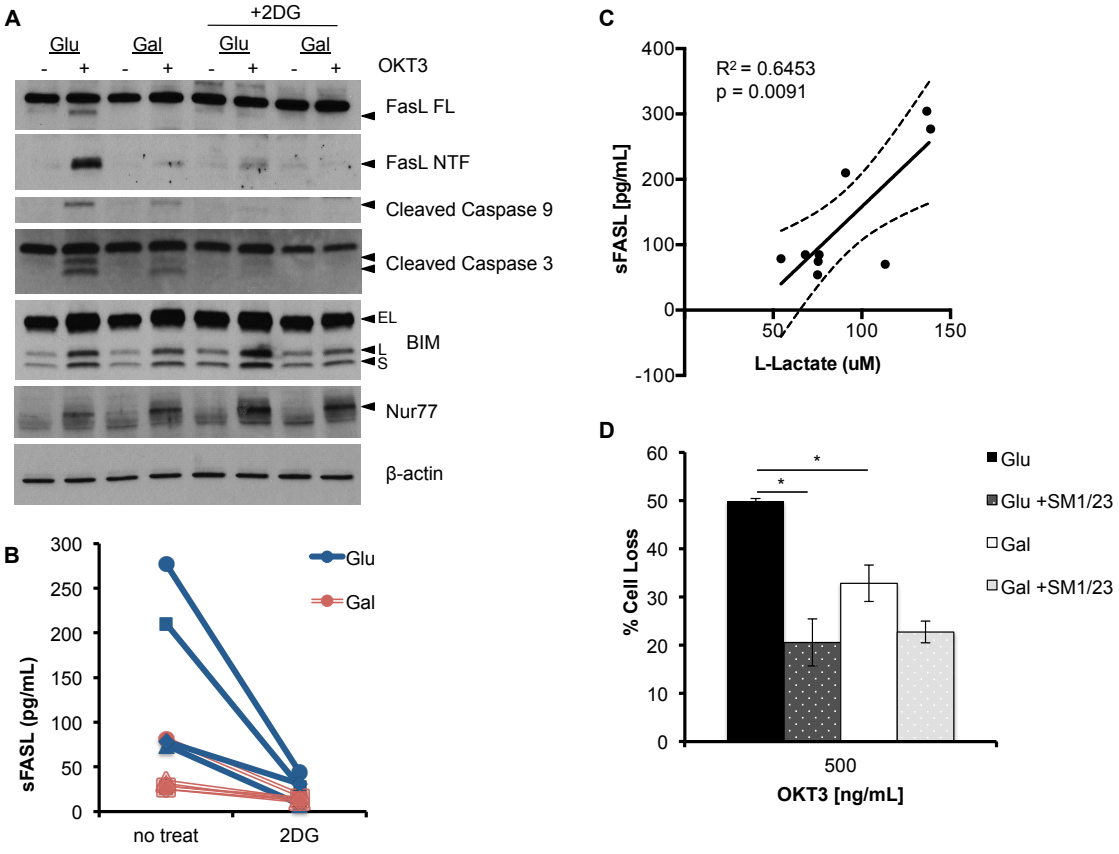
To determine the mechanism by which glycolysis promotes RICD sensitivity, we generated cell lysates from Glu versus Gal T cells pre- and post TCR restimulation to compare expression of critical pro-apoptotic molecules. As reported previously, immunoblotting revealed a robust *de novo* induction of full-length FASL in Glu T cells, some of which is rapidly cleaved at the plasma membrane to generate a prominent N-terminal fragment (Fig 12A) (174). Strikingly, FASL expression was markedly reduced in Gal T cells after 4 hours of restimulation (Fig. 12A). Consistent with a reduction in RICD sensitivity, FASL induction in Glu T cells was almost completely blocked with 2-DG treatment (Fig. 12A). We also noted a concomitant reduction in active caspase-9 and caspase-3 in Gal T cells or with 2-DG treatment (Fig. 12A). In contrast, the induction of other pro-apoptotic proteins important for RICD of $CD8^+$ T cells, including BIM and NUR77, was normal for all culture conditions tested (Fig. 12A) (153; 174). An ELISA confirmed the differential induction of FASL in Glu vs. Gal T cells after restimulation, with more release of soluble FASL (sFASL) in Glu versus Gal T cell supernatants from each donor tested (Fig 12B). Consistent with immunoblotting results, TCR-triggered sFASL release was substantially reduced with 2-DG pre-treatment (Fig. 12B). In fact, linear regression analysis of Glu T cells from 9 separate donors revealed a strong positive correlation between L-lactate and sFASL concentrations in cell supernatants (Fig. 12C, Pearson R^2=0.6453), suggesting a direct association between glycolysis and TCR-induced FASL upregulation in $CD8^+$ effector T cells.

Finally, to test whether differences in FASL induction specifically explained relative RICD sensitivity in Glu vs. Gal T cells, we blocked the death receptor FAS during TCR restimulation. Pretreatment with the antagonistic FAS blocking antibody

SM1/23 reduced RICD sensitivity of Glu T cells to a much greater extent than Gal T cells (Fig. 12D). More importantly, FAS blockade completely abolished any difference in RICD sensitivity between Glu and Gal T cells (Fig. 12D). These data suggest that glycolytic metabolism specifically promotes RICD sensitivity in effector $CD8^+$ T cells through FASL induction and FAS-mediated apoptosis.

Figure 12. Glycolysis enhances RICD specifically by facilitating FASL induction after TCR restimulation.

(A) Lysates of Glu and Gal T cells at baseline or after 4 hr OKT3 restimulation ± 2-DG treatment were separated by SDS-PAGE and immunoblotted for the indicated proteins. β-actin serves as a loading control. Data are representative of 3 independent experiments using different donors. (B) Soluble FASL (sFASL) was measured in Glu (blue) vs. Gal T cell (red) supernatants by ELISA after 4 hours of OKT3 restimulation ± 2-DG by ELISA, n=4 donors. Lines connect data points for each single donor. (C) Linear regression analysis comparing sFASL and L-lactate production in restimulated Glu T cell supernatants for 9 independent donors, including 95% confidence interval (dashed line). Pearson correlation R^2= 0.6453, p=0.0091. (D) Glu and Gal T cells were pretreated with anti-FAS blocking Ab SM1/23 for 30 min, then assayed for RICD as above. Data represent % cell loss (avg ±SEM) for 3 independent donors. Treatments were compared by two-way ANOVA: Glu-Gal p=0.0124, Glu-Glu+SM1/23 p=0.0005, Glu+SM1/23-Gal+SM1/23 n.s, Gal-Gal+SM1/23 n.s.


A
+2DG
Glu
Gal
Glu
Gal
- + - + - + - +
OKT3
FasL FL
FasL NTF
Cleaved Caspase 9
Cleaved Caspase 3
EL
BIM
L
S
Nur77
β-actin
B
sFASL (pg/mL)
300
250
200
150
100
50
0
Glu
Gal
no treat
2DG
C
R² = 0.6453
p = 0.0091
sFASL [pg/mL]
400
300
200
100
0
-100
50
100
150
L-Lactate (uM)
D
% Cell Loss
60
50
40
30
20
10
0
*
*
Glu
Glu +SM1/23
Gal
Gal +SM1/23
500
OKT3 [ng/mL]

DISCUSSION

This study highlights glycolytic metabolism as a novel requirement for licensing the FASL-dependent component of RICD sensitivity in effector $CD8^+$ T cells. Interestingly, we detected no substantial differences in other known requirements for RICD between Glu and Gal T cells, including TCR expression and IL-2-dependent cell cycling. For proliferating T cells, glycolysis is not only employed for macromolecule synthesis, but is also critical for acquiring full effector functions (31; 33; 46; 100; 126). However, our results suggest differences in IFN-γ or cytolytic granule release cannot account for differential RICD between Glu and Gal T cells. We also noted comparable upregulation of TCR-induced pro-apoptotic molecules BIM and NUR77 following restimulation of Glu versus Gal T cells -/+ 2-DG treatment. Unlike SAP-deficient T cells, these data imply that decreased RICD is not caused by a global attenuation of downstream TCR signal strength when glycolysis is restricted.

Instead, our data demonstrate that glucose availability and glycolytic activity enhance RICD specifically through the induction of FASL after TCR restimulation. FASL is one of several pro-apoptotic molecules that contribute to RICD of effector T cells (84; 86). It is not known how specific glycolytic enzymes or responsive signaling intermediates might influence TCR-dependent induction of FASL. Previous work showed that FASL is a TCR-responsive transcriptional target of c-Myc, another crucial driver of glycolytic reprogramming in T cells (22; 86; 133). However, we observed no differences in c-Myc expression for Gal and Glu T cells, and no effect on RICD upon treatment with the c-Myc inhibitor JQ-1 (data not shown). More work is required to pinpoint the exact molecular mechanism connecting glycolysis to FASL induction in effector T cells.

Linking RICD sensitivity to glycolysis provides an elegant control mechanism for maintaining immune homeostasis by precluding the excessive expansion of terminally-differentiated, highly glycolytic effector T cells. It will be important to determine whether certain effector T cells that modulate glycolysis and switch back to OXPHOS, fatty acid oxidation (FAO) or even autophagy can preferentially enter the memory pool in part by escaping RICD (23; 133; 202). Recently identified effector T cell subsets such as short-lived effectors (SLEC) and memory precursor (MPEC) T cells differ in their survival and potential for memory formation (3; 78; 132), which may be influenced by divergences in RICD sensitivity and reliance on glycolysis. Exposure to cytokines such as IL-15 might protect selected effectors from RICD by facilitating a switch from aerobic glycolysis to OXPHOS (3; 106; 155; 203).

In linking glycolysis with susceptibility to a specific self-regulatory apoptosis program, our study complements many recent reports tying T cell survival and memory generation to catabolic metabolism (23; 133; 202). We posit that pharmacological interventions (e.g. rapamycin) that promote memory T cell formation via metabolic reprogramming may work in part by allowing greater numbers of T cells to escape RICD (5; 144). Therefore, agents that alter metabolic programming in T cells may prove useful in regulating the magnitude of any given T cell response specifically by tuning RICD sensitivity, an emerging therapeutic concept for correcting dysregulated immune homeostasis (153).

CHAPTER 4: Differential CWID sensitivity of effector T cells derived from distinct human CD8$^+$ memory subsets

All data presented in this chapter are the sole work of S E Larsen.

ABSTRACT

CD8$^+$ central memory (CM) and effector memory (EM) T cell subsets exhibit well-established differences in proliferative and protective capacity after infectious challenge. However, their relative sensitivity to apoptosis has been largely overlooked, despite the importance of programmed cell death in regulating effector T cell homeostasis. Here we demonstrate that primary human effector T cells derived from the CD8$^+$ EM subset exhibit significantly higher sensitivity to cytokine withdrawal induced cell death (CWID), a critical intrinsic apoptosis program responsible for culling cells once an infection is cleared and interleukin-2 (IL-2) levels diminish. Interestingly, we found no differences in the expression of IL-2 or IL-2 receptor components in cells originating from either subset. Relative to CM-derived effectors, however, EM-derived T cells display more mitochondrial instability and greater basal caspase activation. Indeed, we found that heightened CWID sensitivity in EM-derived effectors is linked to higher expression of the pro-apoptotic Bcl-2 family protein BIM, both at steady state and with *de novo* induction following withdrawal of exogenous IL-2. These data point to "imprinted" differences in BIM protein regulation preserved between CD8$^+$ CM and EM progeny that govern their relative sensitivity to CWID. Additionally, we determined that both subsets demonstrate a burst of autophagy after IL-2 withdrawal. Importantly, autophagy seems to be maintained in CmE over that of EmE. When we inhibited

autophagy during IL-2 withdrawal with chloroquine (CHQ) both subsets now exhibited equal and increased death sensitivity. These findings offer new insight into why CM-derived T cells display superior effector cell expansion and more persistent memory responses *in vivo* relative to EM-derived T cells, based on differential apoptosis sensitivity.

INTRODUCTION

$CD8^+$ T cell memory is an important record of the adaptive immune response to intracellular pathogens, maintained in order to mount more robust and efficient eradication upon reencounter. The $CD8^+$ central memory (CM) and effector memory (EM) T cell subsets demonstrate equivalent cytotoxic activity and cytokine production upon T cell receptor (TCR) stimulation (156; 193; 197). However, these subsets exhibit well-established differences in longevity and protective capacity after infectious challenge (12; 147; 193; 197). CM T cells are less differentiated, have greater self-renewal potential, and are longer-lived *in vivo*, with greater engraftment capabilities after adoptive transfer than EM T cells (12; 147; 156; 157; 193; 197). Previous literature suggests the greater 'proliferative potential' of CM T cells is responsible for their superior ability to control a viral infection. T cell accumulation is frequently referenced as a measure of proliferation, but T cell accumulation is more accurately defined as proliferation minus cell death. Despite the importance of programmed cell death in effector T cell homeostasis, the respective apoptosis sensitivity of CM and EM T cells and their derived effectors has largely been overlooked. Secondary effectors derived from memory T cells have demonstrated a lower sensitivity to *in vivo* contraction after

pathogen clearance than naïve derived effectors (66). Therefore, it seems likely that the continuum of memory subsets may also contain a hierarchy of cell death sensitivity. Indeed, some reports have demonstrated that the more terminally differentiated EM T cells have higher caspase activity than CM T cells (193), which may suggest EM T cells are "closer" to the threshold for commitment to cell death than CM T cells.

Cytokine-withdrawal induced cell death is the critical apoptosis program responsible for eliminating effector T cells once an infection is cleared and interleukin-2 (IL-2) levels diminish (47). CWID is regulated by pro- and anti-apoptotic members of the B cell lymphoma 2 (Bcl-2) protein family (75; 138; 205). Mitochondria sequester pro-apoptotic proteins such as cytochrome c in their inter-membrane space, and anti-apoptotic proteins such as Bcl-2 and Bcl-xL help to maintain outer membrane integrity (21; 205). In the absence of IL-2 and IL-2R signaling, pro-apoptotic BH3-only proteins such as BIM are de-repressed. Once BIM levels overwhelm Bcl-2 and other anti-apoptotic proteins, Bax and Bak proteins are released and thought to form pores in the mitochondrial membrane, resulting in mitochondrial depolarization and downstream signaling events leading to apoptosis (73; 75; 138; 205). CWID seems to be the main overseer that determines which cells survive contraction and enter the memory pool. As such, it may also influence secondary responses derived from distinct memory subsets.

We hypothesized that CM T cells give rise to quantitatively larger effector T cell responses in part due to a decreased sensitivity to CWID compared to EM T cells. Here we demonstrate that primary human effector T cells derived from the $CD8^+$ CM T cell subset exhibit significantly lower sensitivity to CWID. Our data suggests that this

reduced sensitivity is likely linked to greater induction of protective autophagy in CM T cells, which may contribute to decreased BIM expression upon IL-2 withdrawal.

MATERIALS AND METHODS

Isolation, activation and culture of primary human CD8+ T cells

Blood from anonymous healthy donors (buffy coats) was generously provided by Dr. Michael Lenardo and the National Institutes of Health Blood Bank. PBMC were isolated using Ficoll density gradient centrifugation, and $CD8^+$ T cells were purified from PBMC using the EasySep Human $CD8^+$ T cell enrichment kit (Stem Cell Technologies). Enriched $CD8^+$ T cells were stained for 30 minutes on ice with anti-CD45RO-APC and anti-CD62L-FITC antibodies (BioLegend). Memory subsets were sorted on a BD FACS ARIA cell sorter. CM T cells were gated as $CD45RO^{hi}$ and $CD62L^{hi}$, EM T cells were gated as $CD45RO^{hi}$ and $CD62L^{lo}$. Sorted subsets were activated 1:1 with beads coated with anti-CD3/CD2/CD28 antibodies (Human T cell Activation/Expansion Kit, Miltenyi) in RPMI 1640 (Life Technologies) + 10% fetal calf serum (FCS) (Sigma) and 1% penicillin/streptomycin (Lonza) for 3 days. Activated T cells were washed in PBS and subsequently cultured in media as described above with 100 U/mL rIL-2 (PeproTech) at $1x10^6$ cells/mL for ≥10 days, changing media every 3 days.

Apoptosis assays and flow cytometry

CWID assays were performed as previously described (124). Briefly, expanded activated effector T cells (days 10-12) were washed 3X with PBS and resuspended in fresh complete media as previously described without IL-2. Some cells were treated with 10 μM chloroquine (Sigma) or ddH_20 solvent control. These cells were then plated at $7.5x10^5$ cells/mL in 96-well plates. To test sensitivity to other intrinsic death stimuli, cells were treated with 2 μM staurosporine (STS) (Sigma) or DMSO control and plated in triplicate in 96 well plates. Some cells were subjected to 20,000-80,000 mJ/cm^2 UV

irradiation using a Stratalinker UV crosslinker (Stratagene) and plated in triplicate in 96 well plates. On days 0-3 of IL-2 withdrawal, or 24 hours post STS or UV irradiation, cells were stained with 5 μg/mL propidium iodide (Sigma) and collected for constant time on an Accuri C6 flow cytometer (BD Biosciences). Cell death was quantified as percentage cell loss = (1 – [number of viable cells (treated) / number of viable cells (untreated)]) x 100. For some assays, T cells were stained with Annexin V-FITC (BioLegend) on each day of withdrawal. Surface expression of IL-2 receptor components was assessed using anti-CD25-APC (IL2Rα), anti-CD122-PE (IL2Rβ) and anti-CD132-FITC (common-γ chain receptor) antibodies (BioLegend). Analysis of caspase activity between subsets was performed using FITC- conjugated pan caspase inhibitor ApoStat (R&D Systems) according to the product protocol. Mitochondrial membrane integrity was assessed by staining $5x10^6$ cells with 40nM DiOC6 (EMD Biosciences) for 15 minutes at 37°C followed by flow cytometry analysis. Autophagy activity was monitored on each day of cytokine withdrawal using the Cyto-ID kit (Enzo) according to the manufacturer's protocol, followed by flow cytometry analysis. Intracellular staining was performed using the FOXP3 intracellular staining kit (eBiosciences) per protocol using anti-phospho(235/236)-S6-AlexaFluor 488 (Cell Signaling Technologies); anti-IL-2-APC, anti-phospho(T202/Y204)-ERK-PercP-Cy5.5, and anti-phospho(Y694)-STAT5-AlexaFluor 647 (BD Biosciences). All non-sorting flow cytometric assays were performed on an Accuri C6 flow cytometer (BD Biosciences).

Western blotting

Expanded effector T cells ($1x10^6$ per time point) from each day of IL-2 withdrawal (0-3) were washed in cold PBS, and lysed in 1% Nonidet P-40 (NP-40) lysis buffer (50 mM

Tris [pH 7.4], 150 mM NaCl, 0.5 mM EDTA, 1% NP-40, 0.5% sodium deoxycholate, 1 mM Na_3VO_4, 1 mM NaF) containing complete protease inhibitors (Roche) for 30 min on ice. Cleared lysates were boiled in 2x reducing sample buffer, and resolved on Any kD SDS-PAGE gels (Bio-Rad). Proteins were transferred to nitrocellulose on a Trans-Blot Turbo system (Bio-Rad), blocked in 2% Tropix I-Block (Applied Biosystems) in TBS/0.1% Tween, and probed with the following Abs: anti-BIM (Enzo); anti-Mcl-1 (BD Biosciences); anti-phospho(T32)-FOXO3a (Cell Signaling Technologies); and anti–β-actin (Sigma-Aldrich). Bound Abs were detected using HRP-conjugated secondary Abs (Southern Biotech, eBioscience) and ECL (Thermo Scientific).

ELISA

Secreted IL-2 was measured in the cell culture supernatant on days 0-3 of CWID using the human Ready-Set-Go IL-2 ELISA kit (eBiosciences). ELISA plates were read using a Synergy H1 Hybrid Reader (BioTek); concentrations of IL-2 (pg/mL) were calculated using Gen5 data analysis software (BioTek).

RESULTS

EmE T cells are more sensitive to CWID than CmE T cells

In order to test CWID sensitivity between effectors T cells derived from memory T cell subsets, we first isolated $CD8^+$ T cells from normal healthy human donor blood and sorted CM ($CD62L^{hi}$ $CD45RO^+$) and EM ($CD62L^{lo}$ $CD45RO^{hi}$) subsets (Fig. 13A-B). Activated effector T cells were derived from each subset and cultured in media containing IL-2 for 10-14 days. As expected, donor CM T cells were consistently able to generate a larger effector population over time than EM T cells (Fig. 13C). To establish CWID sensitivity of CM-derived effector T cells (CmE) versus EM-derived effector T cells (EmE), cells were washed and IL-2 was removed from the cell culture medium and not replaced for three days while monitoring cell death. EmE T cells were significantly more sensitive to CWID than CmE at 48hr and 72 hr post IL-2 withdrawal, both by PI exclusion and Annexin V staining as a measure of early apoptosis commitment (Fig. 14A, D-E). EmE T cells consistently demonstrated slightly higher baseline Annexin V staining for each donor tested (Fig. 14D-E). These data indicate that EmE are undergoing more cell death at steady state and may in fact be more poised to die by CWID. However, CmE and EmE demonstrated equivalent sensitivity to other intrinsic apoptotic stimuli, including UV irradiation and treatment with the pan-kinase inhibitor staurosporine (Fig. 14B-C). This result suggests the differential CWID sensitivity is a specific phenomenon and not indicative of a global intrinsic death defect in CmE.

Figure 13. Activated human CM $CD8^+$ T cells give ride to more effectors over time compared to EM T cells.

(A) Study design for deriving effectors from primary human $CD8^+$ CM and EM sorted subsets. (B) Representative example of gating/sorting strategy for CM and EM within the $CD8^+$ T cell population. Sorting CM and EM gating strategy, representative example. (C) Fold change of effector T cell expansion in IL-2 over 14 days. Data represent average expansion ± SEM of 6 independent donors.

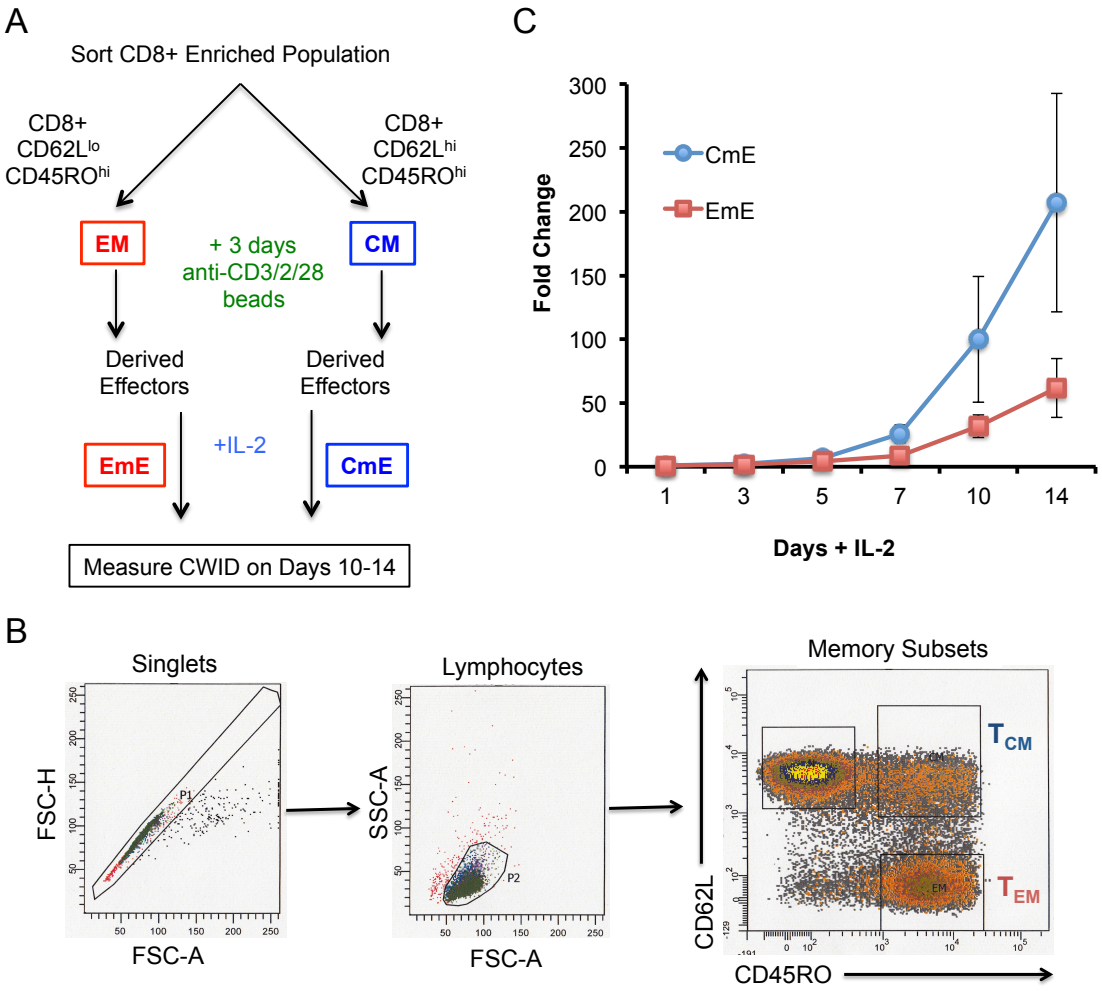
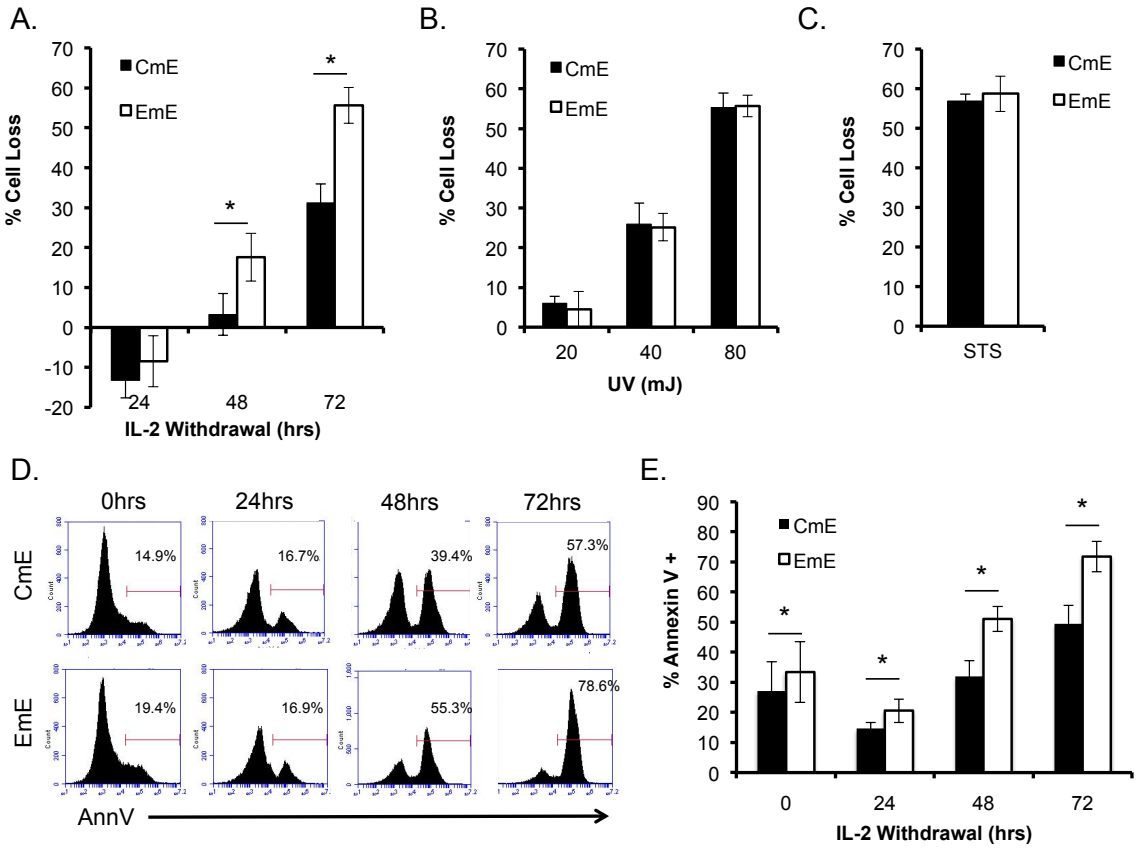

A
Sort CD8+ Enriched Population
CD8+
CD62L^lo
CD45RO^hi
CD8+
CD62L^hi
CD45RO^hi
EM
CM
+ 3 days
anti-CD3/2/28
beads
Derived
Effectors
Derived
Effectors
EmE
+IL-2
CmE
Measure CWID on Days 10-14
C
Fold Change
300
250
200
150
100
50
0
CmE
EmE
1
3
5
7
10
14
Days + IL-2
B
Singlets
FSC-H
FSC-A
P1
Lymphocytes
SSC-A
FSC-A
P2
Memory Subsets
CD62L
CD45RO
T_CM
T_EM

Figure 14. EmE are more sensitive to CWID than CmE.

(A) Activated T cells derived from CM or EM subsets were washed in PBS and resuspended in complete media without IL-2 as described in Materials and Methods. On days 0-3 of IL-2 withdrawal, percent cell loss was measured by PI staining and flow cytometry. Data represent % cell loss (avg ± SEM) for 14 individual donors. Two-way ANOVA analysis showed CmE-EmE 24hrs ns, 48hr $p<0.0001$, 72hr $p<0.0001$. (B) CmE and EmE T cells were treated with increasing doses of UV irradiation as indicated and 24 hours later assayed by PI staining and flow cytometry. Data represent % cell loss (avg ± SEM) for 3 individual donors. Two-way ANOVA analysis showed all doses n.s. (C) CmE and EmE T cells were treated with 2 μM staurosporine and 24 hours later assayed by PI staining and flow cytometry. Data represent % cell loss (avg ± SEM) for 3 individual donors. Student's T-test =n.s. (D-E) CmE and EmE T cells were stained with Annexin V on each day of IL-2 withdrawal and analyzed by flow cytometry. (D) Representative Annexin V staining from a single donor over time. (E) Data represent average ± SEM for 4 individual donors. Two-way ANOVA analysis showed CmE-EmE 0hrs $p=0.0021$, 24hr $p=0.0033$, 48hr $p<0.0001$, 72hr $p<0.0001$.

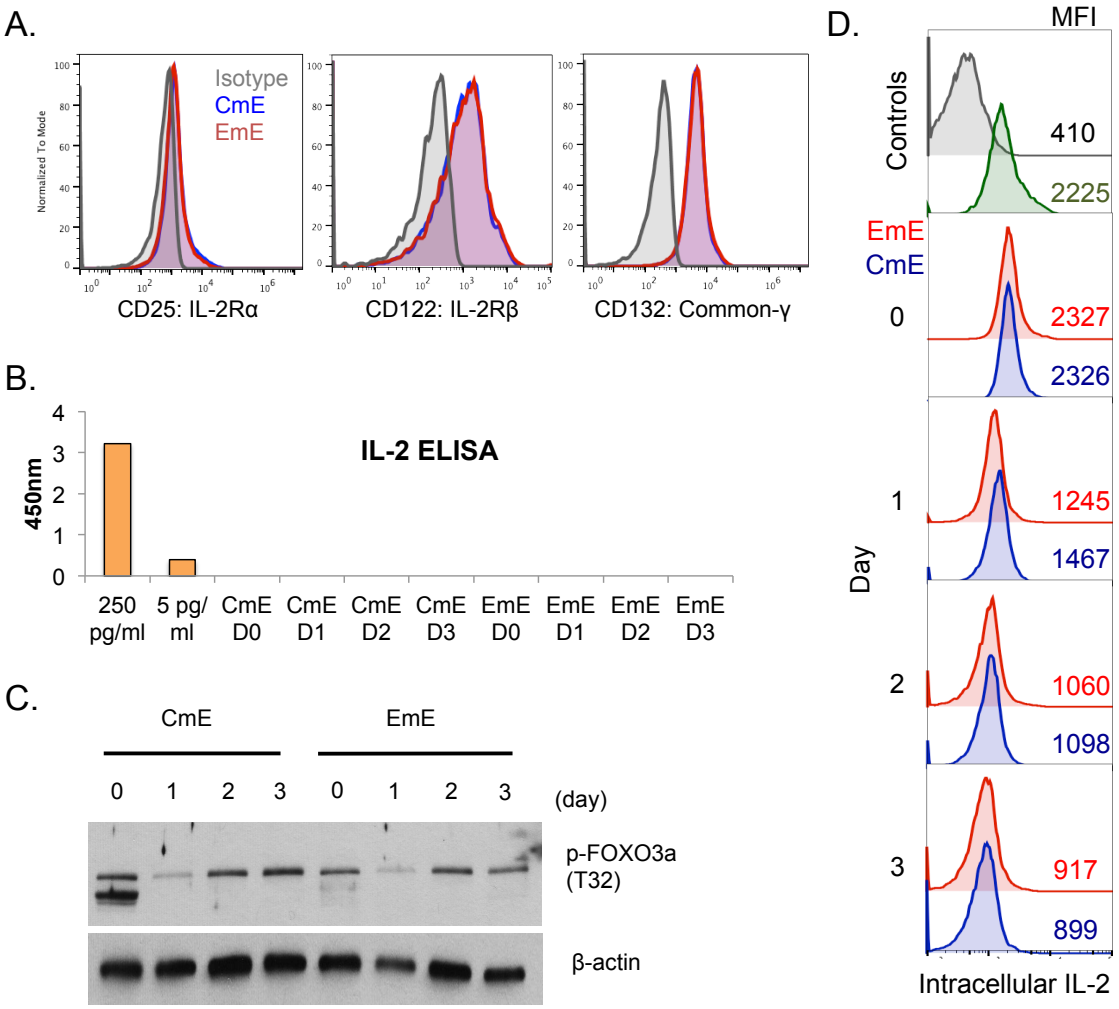

A.
B.
C.
CmE
EmE
% Cell Loss
IL-2 Withdrawal (hrs)
UV (mJ)
STS
D.
0hrs
24hrs
48hrs
72hrs
14.9%
16.7%
39.4%
57.3%
19.4%
16.9%
55.3%
78.6%
AnnV
E.
% Annexin V +

Differential CWID sensitivity is not due to differences in IL-2 production nor IL2R expression

We next compared the expression of IL-2R components and the IL-2 cytokine itself between CmE and EmE. Both subsets showed equal baseline expression of all three subunits of the IL-2R (α, β, γc) (Fig. 15A), suggesting differential receptor expression does not account for differences in death sensitivity. Furthermore, IL-2 was undetectable by ELISA in supernatants on any day following withdrawal of exogenously-added IL-2 (Fig. 15B). Thus either IL-2 was not being secreted and used in an autocrine/paracrine fashion, or IL-2 levels were below the limit of detection by this ELISA. By western blotting, both subsets showed equivalent phosphorylation of the transcription factor FOXO3a at the IL-2 responsive site (T32) (146; 179) on day 0, with a subsequent loss of phosphorylation on day 1 of IL-2 withdrawal (Fig. 15C). This helped to confirm removal of exogenous IL-2 from the media on day 0 and subsequent downregulation of IL-2 signaling. Surprisingly, both CmE and EmE T cells showed a comparable rescue of FOXO3a T32 phosphorylation on days 2 and 3 of IL-2 withdrawal (Fig. 15C). A recent study reported recycling of active IL-2R and IL-2 complexes (182), making it possible that IL-2R on the surface was capturing secreted IL-2 immediately after secretion rendering it undetectable by ELISA. Therefore, we decided to also check IL-2 expression by intracellular flow cytometry. Indeed our analysis did detect some retention of intracellular IL-2, which was roughly equal and progressively lower for both subsets over the course of the assay (Fig.15D). CmE did demonstrate slightly higher intracellular expression of IL-2 on day 1 of cytokine withdrawal (Fig. 15D). Although these data suggest that residual, possibly recycled, IL-2 continues to signal in both subsets, the incremental increase in intracellular IL-2 noted for CmE seems relatively

small compared to the magnitude of death sensitivity difference seen in Fig. 2A. Additionally, the absence of T32 phosphorylation of FoxO3a on day one of IL-2 withdrawal and return of signal on day two suggests that this phosphorylation site may be receiving some alternative feedback activity apart from canonical IL-2 receptor signaling.

Figure 15. Differential CWID sensitivity is not due to different IL-2R expression nor IL-2 autocrine signaling between CmE and EmE.
(A) Representative surface staining of IL-2R components between CmE (blue) and EmE (red) T cells versus isotype control (grey) by flow cytometry. (B) IL-2 was measured in CmE and EmE T cell supernatants from each day of IL-2 withdrawal by ELISA. Data represent average ± SEM for 3 individual donors. (C) Cell lysates from CmE and EmE T cells from each day of IL-2 withdrawal were separated by SDS-PAGE and immunoblotted for phospho-FOXO3a(T32). β-actin serves as a loading control. Data are representative of 3 independent experiments using different donors. (D) Representative intracellular staining of IL-2 between CmE (blue) and EmE (red) T cells versus isotype control (grey) and positive control PBMC stimulated for 2 hours (green) for each day of cytokine withdrawal by flow cytometry. Mean fluorescence intensity reported in each panel.

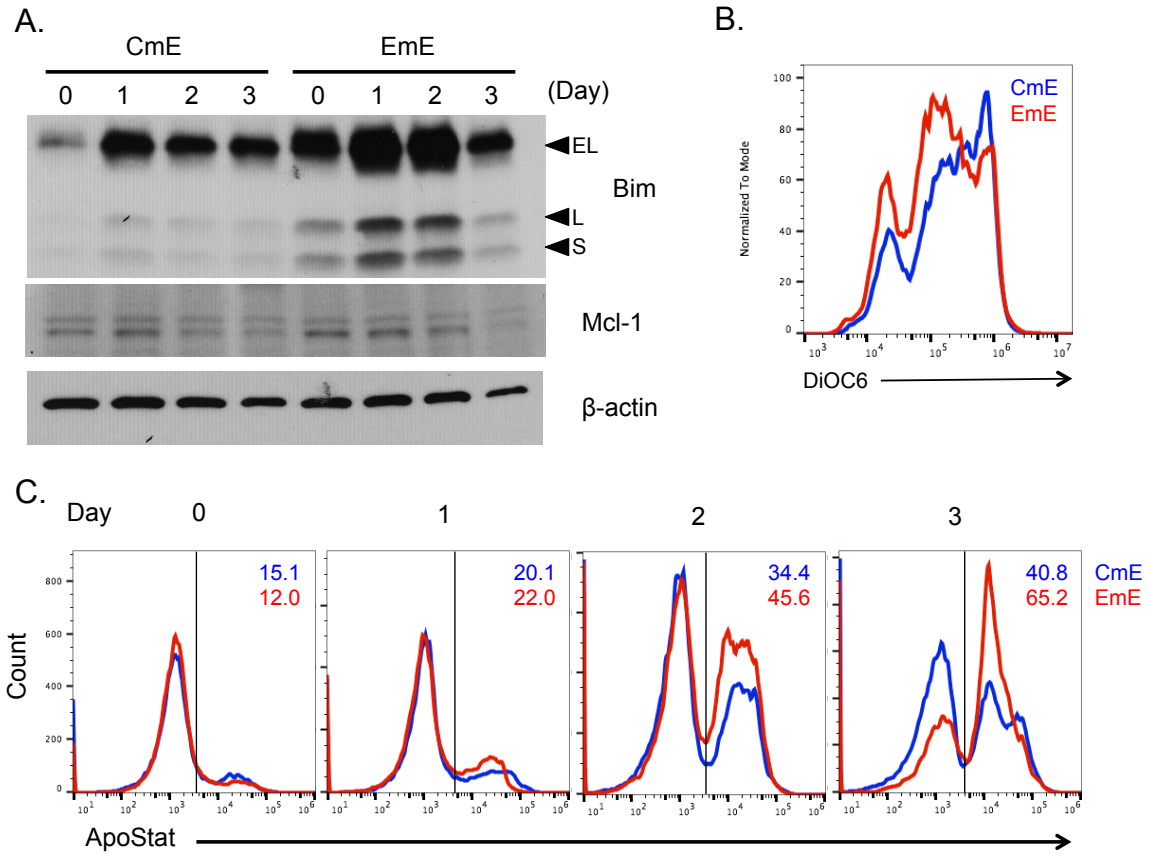

A.
Isotype
CmE
EmE
Normalized To Mode
CD25: IL-2Rα
CD122: IL-2Rβ
CD132: Common-γ
B.
IL-2 ELISA
450nm
250 pg/ml
5 pg/ml
CmE D0
CmE D1
CmE D2
CmE D3
EmE D0
EmE D1
EmE D2
EmE D3
C.
CmE
EmE
0 1 2 3 0 1 2 3
(day)
p-FOXO3a (T32)
β-actin
D.
MFI
Controls
410
2225
EmE
CmE
0
2327
2326
1
1245
1467
2
1060
1098
3
917
899
Day
Intracellular IL-2

Higher basal expression and induction of BIM in EmE T cells

We next investigated the expression of critical Bcl-2 family proteins, including BIM and MCL-1, in $CD8^+$ CmE and EmE over time after IL-2 withdrawal. Strasser and colleagues previously established BIM as the key BH3-only Bcl-2 family protein responsible for initiating CWID in activated T cells (73). Moreover, MCL-1 is a key anti-apoptotic Bcl-2 family protein with the highest binding affinity for BIM (41; 75; 205). Effector T cells derived from both CM and EM subsets expressed relatively similar, tapering levels of MCL-1 during the IL-2 withdrawal time course (Fig.16A). In contrast, EmE revealed a substantially higher basal expression and robust induction of BIM over time after IL-2 withdrawal relative to CmE (Fig. 16A). This marked difference in the BIM:MCL-1 ratio over time is entirely consistent with differential CWID sensitivity observed in Figure 2A. Because an increase in pro vs. anti-apoptotic Bcl-2 family proteins ultimately helps to disrupt mitochondrial membrane integrity, we examined if higher basal expression of BIM in EmE correlated with a reduction in mitochondrial membrane potential versus CmE. Indeed, at baseline EmE T cells demonstrated lower retention of the mitochondrial specific dye $DiOC_6$ compared with CmE T cells (Fig. 16B). Additionally, EmE T cells displayed higher caspase activity during days 2 and 3 of cytokine withdrawal (Fig. 16C). These data suggest that EmE T cells are poised to initiate CWID faster than CmE via the enhanced expression of BIM.

Figure 16. Higher basal expression and induction of BIM make EmE more susceptible to CWID.

(A) Cell lysates from CmE and EmE T cells from each day of IL-2 withdrawal were separated by SDS-PAGE and immunoblotted for BIM and Mcl-1 proteins. β-actin serves as a loading control. Data are representative of 3 independent experiments using different donors. (B) Mitochondrial membrane integrity was compared by DiOC6 staining intensity at baseline between CmE (blue, MFI=353461) and EmE (red, MFI=292880) T cells. Data representative of 3 separate donors. (C) Representative staining intracellular caspase activity (ApoStat) between CmE (blue) and EmE (red) T cells on each day of cytokine withdrawal. Percent of population with positive staining reported in upper right corner for each day.


A.
CmE
EmE
0 1 2 3 0 1 2 3
(Day)
EL
L
S
Bim
Mcl-1
β-actin
B.
CmE
EmE
Normalized To Mode
DiOC6
C.
Day 0 1 2 3
15.1
12.0
20.1
22.0
34.4
45.6
40.8
65.2
CmE
EmE
Count
ApoStat

Differential phosphorylation of S6 between CmE and EmE during IL-2 withdrawal

Since there was seemingly little difference between IL-2R and IL-2 expression in CmE and EmE, we next used intracellular FACS staining to probe key pathways typically associated with IL-2R signaling for discrepancies between CmE and EmE that may help explain the significant difference in BIM expression and CWID (Fig. 2A). Consistent with our IL-2/IL-2R expression analysis, CmE and EmE showed roughly equal levels of phospho-STAT5, a critical proximal indicator of IL-2 signaling (Fig. 17A). We also measured phospho-ERK by intracellular flow as a representative distal kinase in the signaling cascade, and noted equivalent and tapering phosphorylation over the course of IL-2 withdrawal (Fig. 17A). Thus diminishing levels of both phospho-STAT5 and phospho-ERK mirror decreasing levels of intracellular IL-2 (Fig. 15D) seen over the CWID time course.

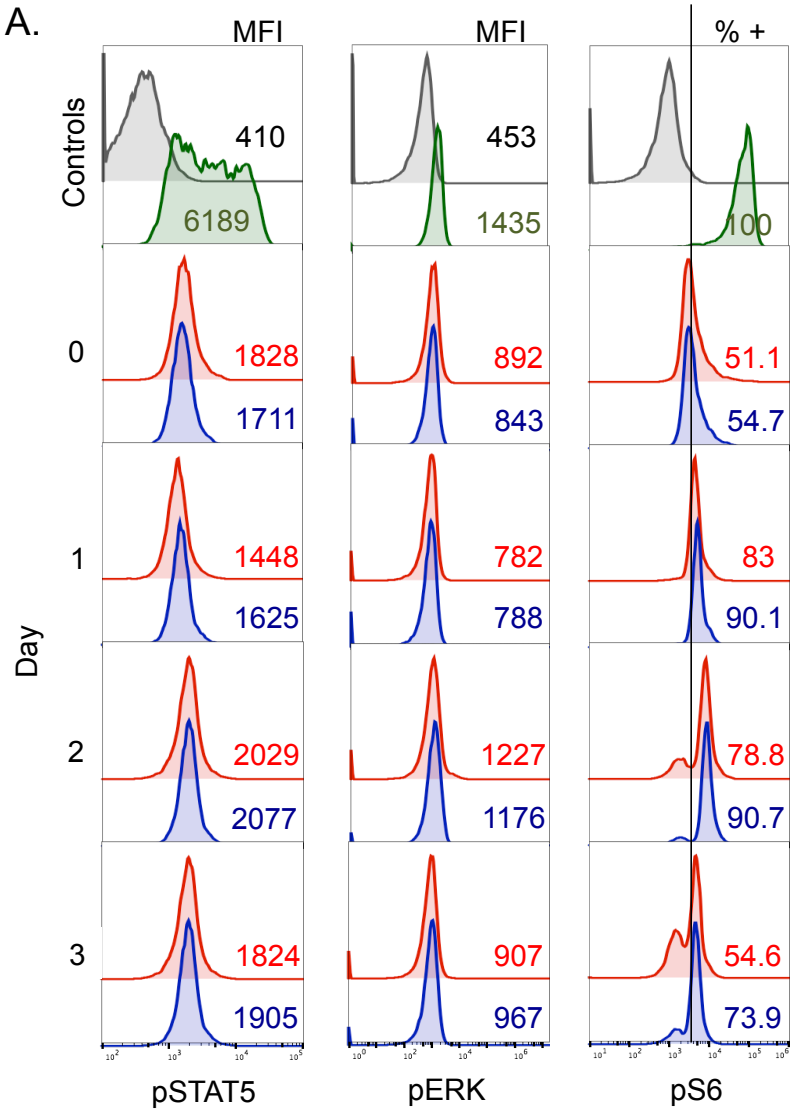
We next decided to interrogate the activity of the mammalian target of rapamycin (mTOR), via phosphorylation of one of its primary targets, ribosomal protein S6. mTOR is an important signaling node that integrates growth factor and nutrient signals from within and around the cell in order to regulate cell growth (5; 37; 102; 135). At times of anabolic metabolism and proliferation, mTOR phosphorylates S6 in order to potentiate protein synthesis required for building new cells. During the course of the CWID assay, nutrients are ostensibly depleted from the culture media in the absence of the major growth factor signal IL-2, which should result in decreasing mTOR activity (165). Surprisingly, effectors derived from both memory subsets displayed a burst of phospho-S6 activity 24hrs after cytokine withdrawal (Fig. 17A). Importantly, CmE demonstrated a sustained phospho-S6 signal while the EmE activity waned over the course of cytokine

withdrawal (Fig. 17A). These results reveal a difference in sustained mTOR signaling induced after 24 hours of IL-2 withdrawal, congruent with the timepoint at which CWID sensitivity diverges between CmE and EmE.

It seemed counter intuitive that effector T cells would demonstrate an abrupt increase in S6 phosphorylation under conditions of growth factor withdrawal. However, mTOR is also responsive to increasing levels of free cellular amino acids, a major product of autophagy (48; 52; 206). Autophagy is a catabolic program induced to adapt to starvation conditions and maintain cellular homeostasis. Autophagy has long held a seemingly conflicting influence on both cell survival and programmed cell death (50). Indeed, active autophagy seems to promote T_H2 T cell sensitivity to CWID (95), yet has been shown to be required for both $CD8^+$ T effector T cell activation and memory formation (89; 111; 202). The contribution of autophagy in promoting or delaying programmed cell death during cytokine withdrawal in $CD8^+$ T cells is less well studied. We hypothesized that the observed burst of S6 phosphorylation beginning on day 1 of CWID reflected feedback mTOR activation via amino acids released by autophagy.

Figure 17. Differential phosphorylation of S6 between CmE and EmE T cells during IL-2 withdrawal.

(A) Representative intracellular staining of phospho-STAT5 (left), phospho-ERK (middle) and phospho-S6 (right) between CmE (blue) and EmE (red) T cells for each day of cytokine withdrawal by flow cytometry versus isotype control (grey) and positive control PBMC stimulated for 2 hours with IL-2 and PMA (green). Mean fluorescence intensity reported in each panel for p-STAT5 and p-ERK. Percent of population with positive p-S6 staining reported in right column.

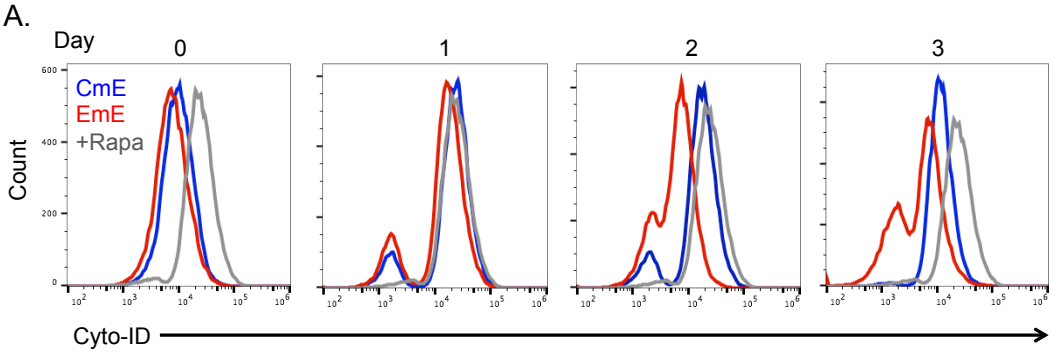

A.
MFI
MFI
% +
Controls
410
6189
453
1435
100
0
1828
1711
892
843
51.1
54.7
1
1448
1625
782
788
83
90.1
Day
2
2029
2077
1227
1176
78.8
90.7
3
1824
1905
907
967
54.6
73.9
pSTAT5
pERK
pS6

CmE T cells demonstrate greater protective autophagy during CWID than EmE T cells

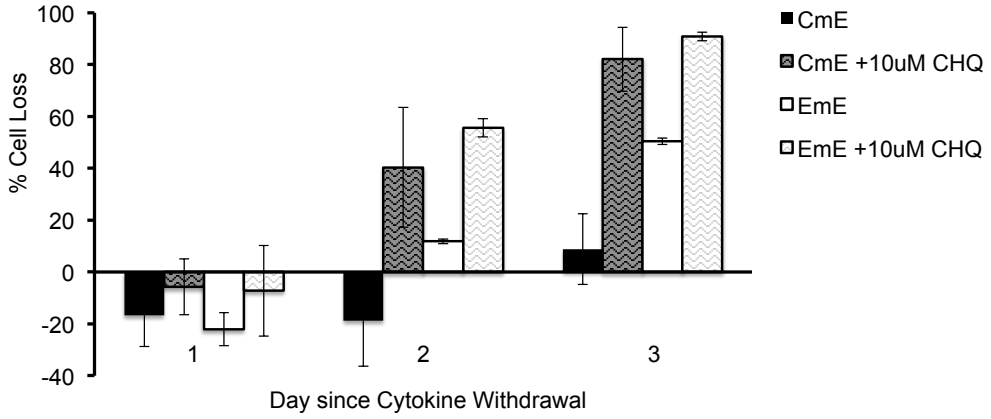
Based on this hypothesis, we next investigated whether CmE and EmE exhibited differential autophagic activity during the course of the IL-2 withdrawal death assay via staining with CytoID, a dye that labels autophagic vacuoles. At baseline, CmE T cells exhibit slightly higher (albeit lower than rapamycin positive control) levels of autophagy compared to EmE T cells (Fig.18A). Both CmE and EmE exhibited bursts of autophagy activity 24hrs after IL-2 withdrawal (Fig.18A). However, only CmE retained this high level of autophagy on days 2 and 3, while positive autophagic vacuole staining waned in EmE T cells (Fig.18A). Interestingly, this discrepancy in sustained autophagy (and S6 phosphorylation) correlates closely with a difference in CWID in CmE versus EmE, which begins to manifest on day 2 of IL-2 withdrawal (Fig. 14A). In order to determine if higher autophagic flux was in fact protecting CmE T cells from CWID, we pre-treated both subsets with the lysosomal acidification inhibitor chloroquine (CHQ) and analyzed changes in cell death sensitivity during CWID. Indeed, with CHQ treatment, both CmE and EmE exhibited increased sensitivity to CWID. Most importantly, however, CHQ eliminated the difference in CWID sensitivity between the two cell types (Fig. 18B). These data imply a protective role for autophagy during CWID that differs among effectors derived from $CD8^+$ memory T cell subsets.

Figure 18. CmE demonstrate greater protective autophagy during CWID than EmE. (A) Representative intracellular staining of active autophagy (Cyto-ID) between CmE (blue) and EmE (red) T cells versus positive control cells treated with rapamycin (grey) for each day of cytokine withdrawal by flow cytometry. (B) CmE and EmE subsets were washed in PBS and resuspended in complete media without IL-2 as described and treated with 10 μM chloroquine (CHQ) or ddH_20 . On days 0-3 of withdrawal percent cell loss was measured by PI staining and flow cytometry. Data represent average % cell loss ± SD of 2 independent donors.

A.


Day
0
1
2
3
CmE
EmE
+Rapa
Count
Cyto-ID

B.


% Cell Loss
100
80
60
40
20
0
-20
-40
1
2
3
Day since Cytokine Withdrawal
CmE
CmE +10uM CHQ
EmE
EmE +10uM CHQ

DISCUSSION

Many studies have focused on assessing the protective capacity of $CD8^+$ memory T cell subsets via adoptive transfer and subsequent pathogen control upon rechallenge (12; 60; 72; 88; 99; 156; 157; 193; 197). It is clear that less differentiated memory subsets are able to provide quicker clearance of pathogen, presumably via the generation of a larger effector pool (12; 147; 156; 193; 197). Effector T cell accumulation, however, is ultimately determined by a balance of both proliferation and cell death. CWID is the primary cell death program that culls the majority of activated effector T cells after clearance of pathogen. To date, the relative sensitivity of memory-derived effectors to CWID has not been established, despite its major influence on T cell accumulation and homeostasis. We hypothesized that greater T cell accumulation derived from CM T cells versus EM T cells was indicative of differential CWID.

Indeed, this study determined that effectors derived from CM T cells are significantly less sensitive to CWID than EM derived effectors. This differential sensitivity to CWID is not due to an underlying apoptosis defect in CmE since they were highly sensitive to other intrinsic death stimuli. Both subsets demonstrated equal expression of IL-2R signaling components by flow cytometry. Additionally we were unable to detect cell derived IL-2 in the media, suggesting that CmE are not making their own IL-2 in the absence of an exogenous source to preferentially survive better than EmE. In line with recent studies (182), we were able to demonstrate some retained intracellular IL-2 in T cells after IL-2 withdrawal, which waned in both subsets with time. Further studies are needed to determine if in fact a proportion of IL-2R is returning to the cell surface in a complex with IL-2 and actively signaling (182). We suspect such a

phenomenon does not impact CWID in a meaningful way, considering downstream readouts of IL-2R signaling (phospho-STAT5, phospho-ERK) remain relatively low and are comparable between CmE and EmE.

Although we showed no appreciable differences in the IL-2 signaling cascade, we did uncover higher basal expression and induction after IL-2 withdrawal of the pro-apoptotic protein BIM in EmE compared to CmE. These data point to "imprinted" differences in BIM protein regulation preserved between $CD8^+$ CM and EM progeny that predisposes EmE to increased cell death sensitivity through cytokine withdrawal. Indeed, EmE also displayed lower mitochondrial membrane integrity at baseline and induced more caspase activity during CWID than CmE, suggesting a higher propensity for intrinsic apoptosis.

Intriguingly, we also noted a sudden burst of S6 phosphorylation after IL-2 withdrawal in both subsets, with a sustained signal in CmE versus EmE. This data suggested mTOR was receiving a positive growth signal on day 1 of our timecourse, even in the absence of IL-2 and waning media derived nutrients. We hypothesized this signal could be derived from an induction of autophagy, an important catabolic program used to recycle old and or damaged organelles to recover and replenish amino acid reserves (48; 52; 206). Autophagy is a stress-induced pathway used to maintain cellular homeostasis in times of starvation and adaptation, including after withdrawal of critical growth factors. Recent reviews highlight the complex nature of autophagy, in certain instances it promotes survival and memory formation while at other times contributes directly to programmed cell death (50; 120; 195; 202). Here we show a novel, protective role for autophagy in $CD8^+$ memory-derived effectors during CWID. CmE consistently

demonstrated a higher and sustained accumulation of autophagic vacuoles during IL-2 withdrawal, correlating with a lower CWID sensitivity. When autophagy was blocked using CHQ, both CmE and EmE displayed increased sensitivity to CWID, suggesting some amount of autophagy (detected by intracellular FACS) could protect either subset against rapid CWID. However, autophagy blockade increased CWID to comparable levels in both subsets, suggesting CmE T cells are able to induce more protective autophagy than EmE and delay CWID. Our findings offer new insight into why CM-derived T cells may display superior effector cell expansion and persistent memory responses *in vivo* relative to EM-derived T cells, beyond simple proliferation capacity.

Under normal conditions, CmE may preferentially be able to degrade death-inducing levels of BIM via autophagy, as some recent studies have demonstrated that autophagy can degrade cell death associated proteins in order to promote survival (89). More work is required to understand how autophagy governs the accumulation of pro-apoptotic Bcl-2 family proteins to regulate CWID of effector T cells as IL-2 is depleted. For example, it will be important to test if autophagy inhibition boosts the expression or accumulation of BIM and other pro-apoptotic proteins (e.g. PUMA) in effector T cells -/+ IL-2 withdrawal, particularly in CmE. Obviously cross talk between autophagy and apoptosis is quite complex. For example, our work suggests autophagy is protective in effectors derived from $CD8^+$ CM T cells during IL-2 withdrawal. In contrast, an earlier study demonstrated that T_H2 T cells are more resistant to cell death under conditions of serum starvation and cytokine withdrawal when autophagy is blocked (95). Our study of $CD8^+$ effector T cells closely examined the specific role of IL-2 withdrawal, without potentially confounding serum starvation, and like most other studies (50; 89; 111; 195;

202) found a protective role for autophagy. Additional comparisons of T cell subsets may help further unravel the intricacies of autophagy as it relates to CWID sensitivity and memory T cell functions

Activated effector T cells undergo minimal amounts of autophagy during the expansion phase and then demonstrate a rapid upregulation just as pathogen is cleared, IL-2 levels wane and the contraction phase begins (202). It is evident that this switch to autophagy is critical for the transition and survival of memory T cells (89; 111; 202). For example, cells lacking important autophagy machinery (Atg5/7) are competent at producing activated effector T cell but have a compromised ability to generate memory T cells (202). Our study adds to this paradigm, demonstrating a novel imprinted setpoint for autophagy induction on effectors derived from distinct EM and CM T cells. This preferential predisposition for autophagy preserved in memory-derived effectors likely has great influence on both the size and length of the recall response of different memory subsets.

CHAPTER 5: Discussion

DISCUSSION

Despite our ever-increasing understanding of adaptive immunity, the ability to manipulate the magnitude of a T cell response is still woefully incomplete. Many research labs are dedicated to enhancing vaccine responses and deriving larger memory populations. Conversely, others focus on reducing T cell expansion in the context of lymphoproliferative disorders. One common theme is regulation of T cell survival, whether during a primary or secondary immune response. As such, the principal goal of this dissertation was to define and investigate specific molecular and metabolic influences on $CD8^+$ T cell death sensitivity. While there are numerous factors that contribute to pathogen control, effector T cell expansion and memory formation are fundamental. This work uses comparative analysis of primary human T cells as a unique and translational approach to studying apoptosis susceptibility.

Determinants of RICD

Molecular

XLP-1 is a rare genetic disorder in which patients lack the small adaptor protein SAP. This seemingly small change at the TCR has profound effects on signaling. Under normal circumstances, SAP interacts with SLAM family receptors in order to propagate and enhance downstream tyrosine phosphorylation events via recruitment of FYN or LCK (26). In the absence of SAP, proximal TCR signals are attenuated because the same SLAM family receptors now have modulatory activity, primarily through immune tyrosine switch motifs (ITSM) that preferentially recruit phosphatases in the absence of

SAP (84). Consequently, loss of SAP reduces proper immune synapse formation, RICD sensitivity and subsequent control of activated effector T cells (9; 84; 153; 174; 209). Previous reports ascertained that SAP has an additional role in suppressing DGKα, and this suppression was dysregulated in SAP-deficient T cells (9). In Chapter 2, we compared SAP-deficient versus normal healthy T cells to elucidate the potential influence of DGKα activity on RICD sensitivity. We determined that in the absence of SAP, DGKα is overactive and converts more DAG into PA. Depletion of second messenger DAG results in a relatively weaker TCR signal that cannot meet the threshold required to promote expression of specific apoptosis effector molecules. Carrying out RICD is multifactorial process, as evidenced by both Chapters 2 and 3. Previous studies have outlined roles for both BIM and FASL induction in the proper execution of RICD (174; 175). Our work adds to this complexity by revealing a previously unappreciated role for nuclear-orphaned receptors NUR77 and NOR1 downstream of the DAG signaling axis. Excitingly, inhibiting DGKα in SAP-deficient T cells pointedly increased expression of NUR77 and NOR1, explaining restored RICD sensitivity.

Of significance, when applied to the *Sh2d1a*$^{-/-}$ mouse model of XLP-1 (35; 40), DGKα inhibition significantly reduced the amount of inflammatory infiltrates and absolute number of activated effector T cells during LCMV infection. Notably, mice were treated with the DGKα inhibitor post-infection with LCMV. This suggests treating XLP-1 patients with a DGKα inhibitor after they had acquired EBV infections could be successful. Further research may be required to determine the optimal timing of treatment with respect to EBV infections in particular, in order to avoid reaching the devastating consequences of FIM. This research highlights the powerful potential of

defining the molecular determinants of death sensitivity. Our research suggests that inhibiting a single enzyme, DGKα, has the potential to reduce the debilitating lymphoproliferation seen in XLP-1 patients who have very few therapeutic options for EBV-induced FIM to date.

Metabolic

A recent boom in metabolism research has clearly linked metabolic programs to T cell effector functions as well as memory formation (126; 129; 135; 183; 192; 199). We now appreciate that each stage of a T cell response (naïve, effector, memory) utilizes a distinct metabolic profile (70; 101; 126; 128-130; 133; 188). As such, metabolic transitions are critical determinants of effector expansion and memory formation. However, metabolic changes have not been studied for their role in sensitizing T cells to cell death at different phases of the immune response. While naïve and memory T cells have a relatively quiescent metabolism, effector T cells instead make a rapid switch to aerobic glycolysis, affording them robust expansion and proper effector functions (30; 31; 33). Of interest, activated effector T cells represent the singular phase of RICD competency during an adaptive immune response.

In Chapter 3 we implicate aerobic glycolysis used by activated, effector T cells as an "RICD licensing" program. Our approach compared activated effector T cells expanded in glucose versus galactose-containing media to induce glycolysis or primarily OXPHOS, respectively. We showed the two cultures had significantly different sensitivities to RICD and that this was mechanistically connected to a preferential induction of FASL in glycolytic T cells. Indeed, when FASL was blocked during restimulation, sensitivity of glycolytic T cells was dramatically and significantly reduced.

This work represents the first direct link between metabolic programming, FASL induction and cell death sensitivity. Further investigation of distinct T cell phases may reveal previously unappreciated cross talk between metabolism and key apoptosis programs (RICD and CWID).

Metabolic networks and pathways involve numerous steps for generating cellular ATP. If we could identify how metabolic programs influence cell death sensitivity this may generate a myriad of novel enzymatic targets for manipulating T cell responses, much like the inhibition of DGKα described in Chapter 2. Specifically, future studies should investigate if and how glycolytic intermediates feed into the TCR signal. Adding exogenous intermediates to cell cultures may reveal feedback loops related to glycolytic activity. Our results suggest acute glucose availability is a limiting factor for sensitizing cells to RICD, therefore it is probable that a proximal step of glycolysis is critical for influencing RICD. When glucose first enters the cell it is phosphorylated for cellular retention, generating glucose-6-phosphate (G6P). Glucose-6-phosphate can be used for both glycolysis and the pentose phosphate pathway (PPP). The PPP is a critical producer of reducing agents, used for fatty acid synthesis, as well as nucleic acid and aromatic amino acid precursors. Our results demonstrated a direct and meaningful correlation between glycolysis and cell death sensitivity. However, it will be interesting to determine if shunting G6P into the PPP also plays a significant role in rendering cells competent for RICD. Deriving precursors for macromolecules is important for deriving new cells, but components of the PPP may have dual functionality and be the point of crossover between metabolism and RICD.

Of additional interest is whether other metabolic programs (FAO, OXPHOS) influence RICD. For instance, it is possible that memory T cells are protected from RICD by their transition away from glycolytic metabolism and greater reliance on FAO and OXPHOS. Metabolism has long been a target of therapeutic manipulation of a T cell response. There is evidence that treating activated effector T cells *in vitro* with rapamycin increases memory formation 5-fold over non-treated controls (69), which suggests that reducing glycolysis is beneficial for memory formation. Indeed, manipulating metabolism with rapamycin treatment has been actively studied for potential benefits in generating enhanced memory in the context of vaccine immunity (5; 69; 115; 144). Importantly, this aforementioned study determined that rapamycin treated T cells in fact were still somewhat glycolytic but preferentially increased rates of OXPHOS over untreated controls (69). Therefore, increasing OXPHOS may be of more importance when generating a large memory pool than reducing glycolysis. In fact, we found that treating glycolytic effector T cells (Chapter 3) with OXPHOS inhibitors such as rotenone (electron transport inhibitor) or oligomycin A (ATP-synthase inhibitor) does slightly but not significantly increase RICD sensitivity (data not shown). We speculate that it may be difficult to resolve a significant influence of blocking OXPHOS in cycling effector T cells that may have already reached a "maximum capacity" for glycolysis and associated RICD sensitization. Conversely, acute treatment of glycolytic effector T cells with rapamycin also decreases their RICD sensitivity (data not shown). This finding further emphasizes that anabolic metabolism promotes RICD, in part through an mTOR-mediated positive feedback loop that sustains glycolysis. Moreover, it suggests that

forcing T cells to convert to OXPHOS or autophagy (see below) may provide direct or indirect protection from self-regulatory T cell apoptosis.

One key feature of cells entering the memory pool is a switch from aerobic glycolysis to OXPHOS and FAO usage. It will be of interest to examine if "memory" cytokines such as IL-7 and IL-15 influence RICD sensitivity through directly eliciting metabolic changes to promote survival. IL-15 has repeatedly been reported to have protective affects for memory survival during contraction (106; 152; 155; 164; 203), however this protection has yet to be linked to a direct increase of OXPHOS or reduction of glycolysis. Much in the way therapeutic addition of IL-2 helps maintain more memory only if added during the contraction phase (and not before) (15), the timing of metabolic manipulation may be critical. In the case of IL-2, adding exogenous cytokine during contraction presumably protects more transitioning T cells from CWID. In contrast, adding IL-2 during the expansion phase in the presence of antigen could drive more RICD in rapidly proliferating effectors. It is evident that glycolysis is directly linked to potent effector functions (31; 33; 46), so reducing glycolysis during effector expansion may in fact be detrimental for a primary immune response taking place. More research is needed to ascertain if an "ideal glycolytic rate" exists in activated T cells to ensure sufficient effector function while remaining under the threshold of RICD induction. Fine-tuning glycolysis with a glucose analog such as 2-DG, or perhaps by timed addition of IL-15, may help achieve this goal to chaperone more T cells into the memory compartment.

Additional genetic and environmental influences on metabolism may also help to explain intra and inter-donor variability to RICD. For example, an individual carrying an

activity promoting single nucleotide polymorphism (SNP) in a glycolytic enzyme (45) may in turn have a greater sensitivity to RICD. Conversely, individuals with metabolic defects may prove to have some concomitant lymphoproliferative symptoms relating to dysregulated control of effector T cell expansion, set in part by RICD. It will be of great interest to determine if metabolic signatures are discovered for use as determinants of subsequent RICD sensitivity, such as glucose or amino acid transporter surface expression.

Work in Chapter 3 ultimately centered on molecular and metabolic changes that influence extrinsic death signaling via FasL-Fas interactions. However, this newly appreciated role for glycolytic metabolism in licensing RICD sensitivity begs a related yet separate question: does metabolic reprogramming also influence intrinsic apoptosis programs such as CWID? Our preliminary findings, discussed below, suggest that a switch to catabolic metabolism, namely autophagy, helps protect effectors from CWID.

Memory phenotypes linked to cell death sensitivities

Most studies of memory T cell subsets have been accomplished in mouse models where a linear relationship and interchange between CM and EM subsets has been demonstrated (159; 197). The substance of work in this dissertation was conducted in primary human T cells from various subsets. This is an important distinction, because in humans the interchange between subsets is less evident. In fact, human CM T cells have been shown to have shorter telomeres and different TCR repertoires when compared with EM T cells, suggesting they are not merely derived from the EM T cell population (157; 181). Additionally CM T cells are able to derive EM T cells *in vitro* but not vice versa

(157). So although CM and EM T cells are neighboring subsets on a continuum, they may also represent more exclusive populations in humans.

In adoptive transfer models, CM T cells are able to control pathogen upon rechallenge better than similarly transferred EM T cells, likely due to the accumulation of more activated effector T cells (12; 147; 193; 197). As previously mentioned, the size of an effector pool is dependent on both proliferative potential and sensitivity to cell death. Therefore, in Chapter 4 we used memory-derived effectors to determine if preferential resistance to CWID may explain greater T cell accumulation and pathogen control by CM versus EM $CD8^+$ T cells.

We determined that EmE T cells were in fact significantly more sensitive to CWID than CmE T cells. In line with recent reports (182), CmE and EmE both retained a small amount of intracellular IL-2 and signaling downstream of the IL-2R after removal of exogenous IL-2. However, we identified no appreciable difference between CmE and EmE in cell derived IL-2 expression, IL-2R expression nor important signaling components downstream of the IL-2R (pSTAT5 and pERK) that would account for the major difference in CWID sensitivity. EmE T cells did demonstrate higher basal expression and induction of pro-apoptotic BIM over the course of IL-2 withdrawal. This correlated with a preferential decrease in mitochondrial membrane integrity and greater induction of caspase activity in EmE T cells compared to CmE T cells. These data suggest that EM derived T cells are indeed more primed for programmed cell death. However this greater sensitivity to cell death in EmE was pathway specific, as both subsets demonstrated equal sensitivity to UV irradiation, direct FAS ligation and STS treatment. We also tested RICD sensitivity between subset-derived effectors and found

that in a majority of donors EmE were more sensitive than CmE. An intriguing correlation between the relative proportion of each memory subset at the time of isolation and subsequent RICD sensitivity is discussed in Appendix A.

Interestingly, within 24 hours after exogenous IL-2 withdrawal, both sets of effectors rapidly upregulated expression of phospho-S6, which was preferentially sustained over time in CmE. We hypothesized that mTOR phosphorylation of S6 during growth factor withdrawal may be dependent on a burst of free amino acids derived from active autophagy. Indeed, flow cytometry analysis showed both subsets exhibit an increase of autophagic vacuoles after 1 day of IL-2 withdrawal and autophagic vacuole staining was sustained in CmE during the time course of CWID, similar to phospho-S6 activity. When we treated with CHQ both CmE and EmE CWID sensitivity increased, but importantly the difference between subsets was erased. This suggests that although both CmE and EmE rapidly induce autophagy upon IL-2 withdrawal, sustained autophagy better protects CmE over prolonged periods of cytokine deprivation. Further work is necessary to confirm autophagy is in fact sustained in CmE T cells using accepted techniques (e.g. LC3 maturation, p62 degradation, etc.). Complementary experiments using additional autophagy inhibitors are also required to corroborate our finding with CHQ showing an increase in CWID sensitivity, particularly in CmE.

Protective autophagy, i.e. autophagy induction to preclude or delay apoptosis, is not a novel concept (50; 89; 111; 202). However, our data introduce an influential role for autophagy in explaining the discrepancies in effector T cell accumulation and pathogen control between defined memory subsets. The connection between BIM expression, CWID and autophagy requires further investigation. Why do CmE T cells

not upregulate BIM expression in the context of IL-2 withdrawal to the extent of EmE T cells? Recent reports have demonstrated autophagy is able to break down molecules involved in cell death cascades, including pro-caspase 3, pro-caspase 8 and BIM (89). Therefore, one possibility is that greater autophagy in CmE is able to degrade BIM and protect cells from mitochondrial depolarization and subsequent CWID. It will be of interest to determine if BIM accumulates in memory-derived effectors, specifically CmE, under autophagy blocking conditions.

It seems likely that in addition to being a critical component of memory formation (202), autophagy may also directly influence the size of secondary memory responses via CWID sensitivity. Profiling other subsets of memory, such as stem cell memory (SCM) and resident memory (RM) and their derived effectors, may yield additional valuable insights into subset phenotypes. Since SCM are touted for their superior protective immunity and multipotency, giving rise to a larger pool of both effector and memory T cells after adoptive transfer (88), SCM-derived effectors may also induce and sustain autophagy during contraction, similar to (or perhaps better than) CmE.

The molecular mechanisms that allow sustained autophagy in CmE remain to be defined. Furthermore, how are autophagy decisions preprogrammed and preserved in memory subset progeny? Connecting transcriptome studies of memory subsets with newly acquired cell death sensitivity information and correlations with autophagy may help inform some of these unanswered questions.

SUMMARY

This dissertation work yielded valuable new insights into biochemical determinants of the two critical cell death pathways governing immune homeostasis,

RICD and CWID. We have identified and characterized hitherto unknown elements of molecular and metabolic control of RICD in human $CD8^+$ T cells, and how such factors dictate the induction of specific pro-apoptotic executioner molecules. In addition, we have uncovered "imprinted" differences in CWID between effector T cells derived from defined memory $CD8^+$ T cell subsets, illuminating an important function for autophagy in modulating CWID sensitivity. Further comprehensive investigation of these cell death pathways in various T cell subsets may help inform translational efforts to further define and target preferential T cell phenotypes and metabolic states for improved vaccine development and therapeutic adoptive transfer strategies.

REFERENCES

1. Ahmed NN, Grimes HL, Bellacosa A, Chan TO, Tsichlis PN. 1997. Transduction of interleukin-2 antiapoptotic and proliferative signals via Akt protein kinase. *Proc Natl Acad Sci USA* 94:3627-32
2. Altman A, Villalba M. 2003. Protein kinase C-theta (PKCtheta): it's all about location, location, location. *Immunol Rev* 192:53-63
3. Amsen D, Backer RA, Helbig C. 2013. Decisions on the road to memory. *Advances in experimental medicine and biology* 785:107-20
4. Araki K, Ellebedy AH, Ahmed R. 2011. TOR in the immune system. *Current opinion in cell biology* 23:707-15
5. Araki K, Turner AP, Shaffer V, Gangappa S, Keller SA, et al. 2009. mTOR regulates memory CD8 T-cell differentiation. *Nature* 460:108-12
6. Arsenio J, Metz PJ, Chang JT. 2015. Asymmetric Cell Division in T Lymphocyte Fate Diversification. *Trends in immunology* 36:670-83
7. Ashwell JD, Cunningham RE, Noguchi PD, Hernandez D. 1987. Cell growth cycle block of T cell hybridomas upon activation with antigen. *J Exp Med* 165:173-94
8. Ashwell JD, Longo DL, Bridges SH. 1987. T-cell tumor elimination as a result of T-cell receptor-mediated activation. *Science (New York, N.Y.)* 237:61-4
9. Baldanzi G, Pighini A, Bettio V, Rainero E, Traini S, et al. 2011. SAP-mediated inhibition of diacylglycerol kinase α regulates TCR-induced diacylglycerol signaling. *J Immunol* 187:5941-51
10. Bas A, Forsberg G, Hammartrom S, Hammartrom M. 2004. Utility of the housekeeping genes 18S rRNA, beta-actin and glyceraldehyde-3-phosphate-dehydrogenase for normalization in real-time quantitative reverse transcriptase-polymerase chain reaction analysis of gene expression in human T lymphocytes. *Scand J Immunol* 59:566-73
11. Becker TC, Wherry JE, Boone D, Murali-Krishna K, Antia R, et al. 2002. Interleukin 15 is required for proliferative renewal of virus-specific memory CD8 T cells. *J Exp Med* 195:1541-8
12. Berger C, Jensen MC, Lansdorp PM, Gough M, Elliott C, Riddell SR. 2008. Adoptive transfer of effector CD8+ T cells derived from central memory cells establishes persistent T cell memory in primates. *The Journal of clinical investigation* 118:294-305
13. Bevan MJ. 2011. Memory T cells as an occupying force. *Eur J Immunol* 41:1192-5
14. Biasco L, Scala S, Ricci L, Dionisio F, Baricordi C, et al. 2015. In vivo tracking of T cells in humans unveils decade-long survival and activity of genetically modified T memory stem cells. *Sci Transl Med* 7
15. Blattman JN, Grayson JM, Wherry EJ, Kaech SM, Smith KA, Ahmed R. 2003. Therapeutic use of IL-2 to enhance antiviral T-cell responses in vivo. *Nature medicine* 9:540-7
16. Boehme SA, Lenardo MJ. 1993. Propriocidal apoptosis of mature T lymphocytes occurs at S phase of the cell cycle. *Eur J Immunol* 23:1552-60

17. Booth C, Gilmour KC, Veys P, Gennery AR, Slatter MA, et al. 2011. X-linked lymphoproliferative disease due to SAP/SH2D1A deficiency: a multicenter study on the manifestations, management and outcome of the disease. *Blood* 117:53-62
18. Bouillet P, Metcalf D, Huang DC, Tarlinton DM, Kay TW, et al. 1999. Proapoptotic Bcl-2 relative Bim required for certain apoptotic responses, leukocyte homeostasis, and to preclude autoimmunity. *Science* 286:1735-8
19. Brenner D, Krammer PH, Arnold R. 2008. Concepts of activated T cell death. *Crit Rev Oncol Hematol* 66:52-64
20. Brezar V, Tu WJ, Seddiki N. 2015. PKC-theta in regulatory and effector T-cell functions. *Frontiers in immunology*
21. Broome HE, Dargan CM, Krajewski S, Reed JC. 1995. Expression of Bcl-2, Bcl-x, and Bax after T cell activation and IL-2 withdrawal. *J Immunol* 155:2311-7
22. Brunner T, Kasibhatla S, Pinkoski MJ, Frutschi C, Yoo NJ, et al. 2000. Expression of Fas ligand in activated T cells is regulated by c-Myc. *The Journal of biological chemistry* 275:9767-72
23. Buck MD, O'Sullivan D, Pearce EL. 2015. T cell metabolism drives immunity. *J Exp Med* 212:1345-60
24. Budd RC. 2001. Activation-induced cell death. *Current opinion in immunology* 13:356-62
25. Calvo KR, Price S, Braylan RC, Oliveira J, Lenardo M, et al. 2015. JMML and RALD (Ras-associated autoimmune leukoproliferative disorder): common genetic etiology yet clinically distinct entities. *Blood* 125:2753-8
26. Cannons JL, Tangye SG, Schwartzberg PL. 2011. SLAM family receptors and SAP adaptors in immunity. *Annu Rev Immunol* 29:665-705
27. Cannons JL, Yu LJ, Hill B, Mijares LA, Dombroski D, et al. 2004. SAP regulates T(H)2 differentiation and PKC-theta-mediated activation of NF-kappaB1. *Immunity* 21:693-706
28. Carrasco S, Merida I. 2004. Diacylglycerol-dependent binding recruits PKCtheta and RasGRP1 C1 domains to specific subcellular localizations in living T lymphocytes. *Mol Biol Cell* 15:2932-42
29. Cerezo A, Martinez-A C, Gonzalez A, Gomez J, Rebollo A. 1999. IL-2 deprivation triggers apoptosis which is mediated by c-Jun N-terminal kinase 1 activation and prevented by Bcl-2. *Cell Death Differ* 6:87-94
30. Cham CM, Driessens G, O'Keefe JP, Gajewski TF. 2008. Glucose deprivation inhibits multiple key gene expression events and effector functions in CD8+ T cells. *Eur J Immunol* 38:2438-50
31. Cham CM, Gajewski TF. 2005. Glucose availability regulates IFN-gamma production and p70S6 kinase activation in CD8+ effector T cells. *J Immunol* 174:4670-7
32. Chan B, Lanyi A, Song HK, Griesbach J, Simarro-Grande M, et al. 2003. SAP couples Fyn to SLAM immune receptors. *Nat Cell Biol* 5:155-60
33. Chang CH, Curtis JD, Maggi LB, Jr., Faubert B, Villarino AV, et al. 2013. Posttranscriptional control of T cell effector function by aerobic glycolysis. *Cell* 153:1239-51

34. Chauveau A, Le Floc'h A, Bantilan NS, Koretzky GA, Huse M. 2014. Diacylglycerol kinase α establishes T cell polarity by shaping diacylglycerol accumulation at the immunological synapse. *Sci Signal* 7:ra82
35. Chen G, Tai AK, Lin M, Chang F, Terhorst C, Huber BT. 2007. Increased proliferation of CD8+ T cells in SAP-deficient mice is associated with impaired activation-induced cell death. *Eur J Immunol* 37:663-74
36. Cheng LE, Chan FK, Cado D, Winoto A. 1997. Functional redundancy of the Nur77 and Nor-1 orphan steroid receptors in T-cell apoptosis. *EMBO J* 16:1865-75
37. Chi H. 2012. Regulation and function of mTOR signalling in T cell fate decisions. *Nat Rev Immunol* 12:325-38
38. Chuck MI, Zhu M, Shen S, Zhang W. 2010. The role of the LAT-PLC-gamma1 interaction in T regulatory cell function. *J Immunol* 184:2476-86
39. Coffer PJ, Burgering BMT. 2004. Forkhead-box transcription factors and their role in the immune system. *Nature Reviews Immunology* 4:889-99
40. Czar MJ, Kersh EN, Mijares LA. 2001. Altered lymphocyte responses and cytokine production in mice deficient in the X-linked lymphoproliferative disease gene SH2D1A/DSHP/SAP. *Proc Natl Acad Sci USA*
41. Day CL, Chen L, Richardson SJ, Harrison PJ, Huang DC, Hinds MG. 2005. Solution structure of prosurvival Mcl-1 and characterization of its binding by proapoptotic BH3-only ligands. *J Biol Chem* 280:4738-44
42. de Bielke MG, Perez L, Yancoski J, Oliveira JB, Danielian S. 2015. FAS Haploinsufficiency Caused by Extracellular Missense Mutations Underlying Autoimmune Lymphoproliferative Syndrome. *J Clin Immunol* 35:769-76
43. Deng G, Podack ER. 1993. Suppression of apoptosis in a cytotoxic T-cell line by interleukin 2-mediated gene transcription and deregulated expression of the protooncogene bcl-2. *Proc Natl Acad Sci USA* 90:2189-93
44. Dominguez CL, Floyd DH, Xiao A, Mullins GR, Kefas BA, et al. 2013. Diacylglycerol kinase α is a critical signaling node and novel therapeutic target in glioblastoma and other cancers. *Cancer Discov* 3:782-97
45. Dong X, Tang H, Hess KR, Abbruzzese JL, Li D. 2011. Glucose metabolism gene polymorphisms and clinical outcome in pancreatic cancer. *Cancer* 177:480-91
46. Donnelly RP, Finlay DK. 2015. Glucose, glycolysis and lymphocyte responses. *Mol Immunol* 68:513-9
47. Duke RC, Cohen JJ. 1986. IL-2 addiction: withdrawal of growth factor activates a suicide program in dependent T cells. *Lymphokine research* 5:289-99
48. Dunlop EA, Tee AR. 2014. mTOR and autophagy: a dynamic relationship governed by nutrients and energy. *Elsevier* 36:121-9
49. Ebinu JO, Stang SL, Teixeira C, Bottorff DA, Hooton J, et al. 2000. RasGRP links T-cell receptor signaling to Ras. *Blood* 95:3199-203
50. Eisenberg-Lerner A, Bialik S, Simon HUU, Kimchi A. 2009. Life and death partners: apoptosis, autophagy and the cross-talk between them. *Cell Death Differ* 16:966-75
51. Ellery JM, Nicholls PJ. 2002. Alternate signalling pathways from the interleukin-2 receptor. *Cytokine & growth factor reviews* 13:27-40

52. Fader CM, Aguilera MO, Colombo MII. 2015. Autophagy response: manipulating the mTOR-controlled machinery by amino acids and pathogens. *Amino acids* 47:2101-12
53. Filipovich AH, Zhang K, Snow AL, Marsh RA. 2010. X-linked lymphoproliferative syndromes: brothers or distant cousins? *Blood* 116:3398-408
54. Fisher GH, Rosenberg FJ, Straus SE, Dale JK, Middleton LA, et al. 1995. Dominant interfering Fas gene mutations impair apoptosis in a human autoimmune lymphoproliferative syndrome. *Cell* 81:935-46
55. Flynn JK, Gorry PR. 2015. T cell therapies—are T memory stem cells the answer? *Ann Transl Med* 3:251
56. Fortner KA, Bouillet P, Strasser A, Budd RC. 2010. Apoptosis regulators Fas and Bim synergistically control T‐lymphocyte homeostatic proliferation. *Eur J Immunol* 40:3043-53
57. Frost EL, Kersh AE, Evavold BD, Lukacher AE. 2015. Cutting Edge: Resident Memory CD8 T Cells Express High-Affinity TCRs. *J Immunol* 195:3520-4
58. Gaffen SL. 2001. Signaling domains of the interleukin 2 receptor. *Cytokine* 14:63-77
59. Gan YH, Lui SS, Malkovsky M. 2001. Differential susceptibility of naïve and activated human gammadelta T cells to activation-induced cell death by T-cell receptor cross-linking. *Mol Medicine* 7:636-43
60. Gattinoni L, Lugli E, Ji Y, Pos Z, Paulos CM, et al. 2011. A human memory T cell subset with stem cell-like properties. *Nature medicine* 17:1290-7
61. Gattinoni L, Zhong X-SS, Palmer DC, Ji Y, Hinrichs CS, et al. 2009. Wnt signaling arrests effector T cell differentiation and generates CD8+ memory stem cells. *Nature medicine* 15:808-13
62. Gebhardt T, Wakim LM, Eidsmo L, Reading PC, Heath WR, Carbone FR. 2009. Memory T cells in nonlymphoid tissue that provide enhanced local immunity during infection with herpes simplex virus. *Nat Immunol* 10:524-30
63. Gerriets VA, Rathmell JC. 2012. Metabolic pathways in T cell fate and function. *Trends Immunol* 33:168-73
64. Gharbi SI, Rincón E, Avila-Flores A, Torres-Ayuso P, Almena M, et al. 2011. Diacylglycerol kinase ζ controls diacylglycerol metabolism at the immunological synapse. *Mol Biol Cell* 22:4406-14
65. Goffe CLE, Vallette G, Jarry A, Bou-Hanna C, Laboisse C. 1999. The in vitro manipulation of carbohydrate metabolism: a new strategy for deciphering the cellular defence mechanisms against nitric oxide attack. *Biochem J* 15:643-8
66. Grayson JM, Harrington LE, Lanier JG, Wherry EJ, Ahmed R. 2002. Differential sensitivity of naive and memory CD8+ T cells to apoptosis in vivo. *J Immunol* 169:3760-70
67. Green DR, Droin N, Pinkoski M. 2003. Activation-induced cell death in T cells. *Immunol Rev* 193:70-81
68. Gubser PM, Bantug GR, Razik L, Fischer M, Dimeloe S, et al. 2013. Rapid effector function of memory CD8+ T cells requires an immediate-early glycolytic switch. *Nature immunology* 14:1064-72

69. He S, Kato K, Jiang J, Wahl DR, Mineishi S, et al. 2011. Characterization of the metabolic phenotype of rapamycin-treated CD8+ T cells with augmented ability to generate long-lasting memory cells. *PloS one* 6
70. Heiden MG, Cantley LC, Thompson CB. 2009. Understanding the Warburg Effect: The Metabolic Requirements of Cell Proliferation. *Science* 324:1029-33
71. Higuchi M, Takahashi M, Tanaka Y, Fujii M. 2014. Downregulation of proapoptotic Bim augments IL‐2‐independent T‐cell transformation by human T‐cell leukemia virus type‐1 Tax. *Cancer medicine* 3:1605-14
72. Hikono H, Kohlmeier JE, Takamura S, Wittmer ST, Roberts AD, Woodland DL. 2007. Activation phenotype, rather than central– or effector–memory phenotype, predicts the recall efficacy of memory CD8+ T cells. *J Exp Med* 204
73. Hildeman DA, Zhu Y, Mitchell TC, Bouillet P, Strasser A, et al. 2002. Activated T cell death in vivo mediated by proapoptotic bcl-2 family member bim. *Immunity* 16:759-67
74. Ho LP, Yit PS, Ng LH, Linn YC, Zhao Y, et al. 2013. The road to memory: an early rest for the long journey. *J Immunol* 191:5603-14
75. Huang D, Strasser A. 2000. BH3-Only Proteins—Essential Initiators of Apoptotic Cell Death. *Cell* 103:839-42
76. Huster KM, Busch V, Schiemann M, Linkemann K, Kerksiek KM, et al. 2004. Selective expression of IL-7 receptor on memory T cells identifies early CD40L-dependent generation of distinct CD8+ memory T cell subsets. *Proc Natl Acad Sci USA* 101:5610-5
77. Issandou M, Bayard F, Darbon JM. 1988. Inhibition of MCF-7 cell growth by 12-O-tetradecanoylphorbol-13-acetate and 1,2-dioctanoyl-sn-glycerol: distinct effects on protein kinase C activity. *Cancer Res* 48:6943-50
78. Joshi NS, Cui W, Chandele A, Lee HK, Urso DR, et al. 2007. Inflammation directs memory precursor and short-lived effector CD8(+) T cell fates via the graded expression of T-bet transcription factor. *Immunity* 27:281-95
79. Jozwik A, Habibi MS, Paras A, Zhu J, Guvenel A, et al. 2015. RSV-specific airway resident memory CD8+ T cells and differential disease severity after experimental human infection. *Nature Communications* 6:10224
80. Kaech SM, Tan JT, Wherry EJ, Konieczny BT, Surh CD, Ahmed R. 2003. Selective expression of the interleukin 7 receptor identifies effector CD8 T cells that give rise to long-lived memory cells. *Nature immunology* 4:1191-8
81. Kalbasi A, Shrimali RK, Chinnasamy D, Rosenberg S. 2010. Prevention of interleukin-2 withdrawal-induced apoptosis in lymphocytes retrovirally cotransduced with genes encoding an antitumor T-cell receptor and an antiapoptotic protein. *J Immunol* 33:672-83
82. Kalia V, Sarkar S, Subramaniam S, Haining WN, Smith KA, Ahmed R. 2010. Prolonged interleukin-2Ralpha expression on virus-specific CD8+ T cells favors terminal-effector differentiation in vivo. *Immunity* 32:91-103
83. Kataoka T, Shinohara N, Takayama H, Takaku K, Kondo S, et al. 1996. Concanamycin A, a powerful tool for characterization and estimation of contribution of perforin- and Fas-based lytic pathways in cell-mediated cytotoxicity. *J Immunol* 156:3678-86

84. Katz G, Krummey SM, Larsen SE, Stinson JR, Snow AL. 2014. SAP facilitates recruitment and activation of LCK at NTB-A receptors during restimulation-induced cell death. *J Immunol* 192:4202-9
85. Katz G, Snow AL, Lenardo MJ. 2013. Methods in Molecular Biology. *Methods Mol Biol* 979:15-23
86. Kavurma MM, Khachigian LM. 2003. Signaling and transcriptional control of Fas ligand gene expression. *Cell Death Differ* 10:36-44
87. Kelly E, Won A, Refaeli Y, Van Parijs L. 2002. IL-2 and related cytokines can promote T cell survival by activating AKT. *J Immunol* 168:597-603
88. Klebanoff CA, Gattinoni L, Restifo NP. 2012. Sorting through subsets: which T-cell populations mediate highly effective adoptive immunotherapy? *J immunotherapy* 35:651-60
89. Kovacs JR, Li C, Yang Q, Li G, Garcia IG, et al. 2012. Autophagy promotes T-cell survival through degradation of proteins of the cell death machinery. *Cell Death Differ* 19:144-52
90. Kovanen PE, Young L, Al-Shami A, Rovella V, Pise-Masison C, et al. 2005. Global analysis of IL-2 target genes: identification of chromosomal clusters of expressed genes. *Int Immunol* 17:1009-21
91. Kurtulus S, Tripathi P, Moreno-Fernandez ME, Sholl A, Katz JD, et al. 2011. Bcl-2 allows effector and memory CD8+ T cells to tolerate higher expression of Bim. *J Immunol* 186:5729-37
92. Latinis KM, Carr LL, Peterson EJ, Norian LA, Eliason SL, Koretzky GA. 1997. Regulation of CD95 (Fas) ligand expression by TCR-mediated signaling events. *The Journal of Immunology* 158:4602-11
93. Layer K, Lin G, Nencioni A, Hu W, Schmucker A, et al. 2003. Autoimmunity as the consequence of a spontaneous mutation in Rasgrp1. *Immunity* 19:243-55
94. Lenardo MJ. 1991. Interleukin-2 programs mouse alpha beta T lymphocytes for apoptosis. *Nature* 353:858-61
95. Li C, Capan E, Zhao Y, Zhao J, Stolz D, et al. 2006. Autophagy is induced in CD4+ T cells and important for the growth factor-withdrawal cell death. *J Immunol* 177:5163-8
96. Lin W-HWH, Adams WC, Nish SA, Chen Y-HH, Yen B, et al. 2015. Asymmetric PI3K Signaling Driving Developmental and Regenerative Cell Fate Bifurcation. *Cell reports* 13:2203-18
97. Liu Y, Janeway CA. 1990. Interferon gamma plays a critical role in induced cell death of effector T cell: a possible third mechanism of self-tolerance. *J Exp Med* 172:1735-9
98. Lord JD, McIntosh BC, Greenberg PD, Nelson BH. 2000. The IL-2 receptor promotes lymphocyte proliferation and induction of the c-myc, bcl-2, and bcl-x genes through the trans-activation domain of Stat5. *J Immunol* 164:2533-41
99. Lugli E, Dominguez MH, Gattinoni L, Chattopadhyay PK, Bolton DL, et al. 2013. Superior T memory stem cell persistence supports long-lived T cell memory. *The Journal of clinical investigation* 123:594-9
100. Lunt SY, Heiden VMG. 2011. Aerobic glycolysis: meeting the metabolic requirements of cell proliferation. *Annu Rev Cell Dev Biol* 27:441-64

101. MacIver NJ, Jacobs SR, Wieman HL, Wofford JA, Coloff JL, Rathmell JC. 2008. Glucose metabolism in lymphocytes is a regulated process with significant effects on immune cell function and survival. *Journal of Leukocyte Biology* 84:949-57
102. Magnuson B, Ekim B, Fingar DC. 2012. Regulation and function of ribosomal protein S6 kinase (S6K) within mTOR signalling networks. *Biochemical Journal* 441:1-21
103. Mahnke YD, Brodie TM, Sallusto F, Roederer M, Lugli E. 2013. The who's who of T-cell differentiation: human memory T-cell subsets. *European journal of immunology* 43:2797-809
104. Malek T, Castro I. 2010. Interleukin-2 Receptor Signaling: At the Interface between Tolerance and Immunity. *Immunity* 33:153-65
105. Manicassamy S, Sun Z. 2007. The critical role of protein kinase C-theta in Fas/Fas ligand-mediated apoptosis. *J Immunol* 178:312-9
106. Marks-Konczalik J, Dubois S, Losi JM, Sabzevari H, Yamada N, et al. 2000. IL-2-induced activation-induced cell death is inhibited in IL-15 transgenic mice. *Proc Natl Acad Sci USA* 97:11445-50
107. Marsland BJ, Kopf M. 2008. T-cell fate and function: PKC-theta and beyond. *Trends Immunol* 29:179-85
108. Martin MD, Kim MT, Shan Q, Sompallae R, Xue H-HH, et al. 2015. Phenotypic and Functional Alterations in Circulating Memory CD8 T Cells with Time after Primary Infection. *PLoS pathogens* 11
109. Masopust D, Vezys V, Marzo AL, Lefrançois L. 2001. Preferential localization of effector memory cells in nonlymphoid tissue. *Science* 291:2413-7
110. Mattson E, Xu L, Li L, Liu GE, Xiao Z. 2014. Transcriptome profiling of CTLs regulated by rapamycin using RNA-Seq. *Immunogenetics* 66:625-33
111. McLeod IX, Jia W, He YW. 2012. The contribution of autophagy to lymphocyte survival and homeostasis. *Immunol Rev* 249:195-204
112. Metz PJ, Lopez J, Kim SH, Akimoto K, Ohno S, Chang JT. 2016. Regulation of Asymmetric Division by Atypical Protein Kinase C Influences Early Specification of CD8(+) T Lymphocyte Fates. *Scientific reports* 6:19182
113. Moran AE, Holzapfel KL, Xing Y, Cunningham NR, Maltzman JS, et al. 2011. T cell receptor signal strength in Treg and iNKT cell development demonstrated by a novel fluorescent reporter mouse. *J Exp Med* 208:1279-89
114. Mueller SN, Mackay LK. 2016. Tissue-resident memory T cells: local specialists in immune defence. *Nat Rev Immunol* 16:79-89
115. Nam J-HH. 2009. Rapamycin: could it enhance vaccine efficacy? *Expert review of vaccines* 8:1535-9
116. Nanjappa SG, Kim EH, Suresh M. 2011. Immunotherapeutic effects of IL-7 during a chronic viral infection in mice. *Blood* 117:5123-32
117. Nanjappa SG, Walent JH, Morre M, Suresh M. 2008. Effects of IL-7 on memory CD8+ T cell homeostasis are influenced by the timing of therapy in mice. *J Clin Invest* 118:1027-39
118. Nelson DL, Terhorst C. 2000. X-linked lymphoproliferative syndrome. *Clinical and experimental immunology* 122:291-5

119. Nichols KE, Harkin DP, Levitz S, Krainer M, Kolquist KA, et al. 1998. Inactivating mutations in an SH2 domain-encoding gene in X-linked lymphoproliferative syndrome. *Proc Natl Acad Sci U S A* 95:13765-70
120. Nikoletopoulou V, Markaki M, Palikaras K, Tavernarakis N. 2013. Crosstalk between apoptosis, necrosis and autophagy. *Biochimica et biophysica acta* 1833:3448-59
121. Nunez-Cruz S, Yeo WC, Rothman J, Ojha P, Bassiri H, et al. 2008. Differential requirement for the SAP-Fyn interaction during NK T cell development and function. *J Immunol* 181:2311-20
122. O'Reilly LA, Kruse EA, Puthalakath H, Kelly PN, Kaufmann T, et al. 2009. MEK/ERK-mediated phosphorylation of Bim is required to ensure survival of T and B lymphocytes during mitogenic stimulation. *J Immunol* 183:261-9
123. Olenchock BA, Guo R, Carpenter JH, Jordan M, Topham MK, et al. 2006. Disruption of diacylglycerol metabolism impairs the induction of T cell anergy. *Nat Immunol* 7:1174-81
124. Oliveira JB. 2013. Evaluation of IL-2-withdrawal-induced apoptosis in human T lymphocytes. *Methods Mol Biol* 979:25-31
125. Opferman JT, Ober BT, Ashton-Rickardt PG. 1999. Linear differentiation of cytotoxic effectors into memory T lymphocytes. *Science* 283:1745-8
126. Palmer CS, Ostrowski M, Balderson B, Christian N, Crowe SM. 2015. Glucose metabolism regulates T cell activation, differentiation, and functions. *Frontiers in immunology* 6:1
127. Paulsen M, Janssen O. 2011. Pro-and anti-apoptotic CD95 signaling in T cells. *Cell Commun Signal* 9
128. Pearce EL. 2010. Metabolism in T cell activation and differentiation. *Curr Opin Immunol* 22:314-20
129. Pearce EL, Poffenberger MC, Chang CH, Jones R. 2013. Fueling immunity: insights into metabolism and lymphocyte function. *Science* 342:1242-54
130. Pearce EL, Walsh MC, Cejas PJ, Harms GM, Shen H, et al. 2009. Enhancing CD8 T-cell memory by modulating fatty acid metabolism. *Nature* 460:103-7
131. Pinkoski MJ, Green DR. 1999. Fas ligand, death gene. *Cell death and differentiation* 6:1174-81
132. Plumlee CR, Obar JJ, Colpitts SL, Jellison ER, Haining WN, et al. 2015. Early Effector CD8 T Cells Display Plasticity in Populating the Short-Lived Effector and Memory-Precursor Pools Following Bacterial or Viral Infection. *Sci Rep* 5:12264
133. Pollizzi KN, Powell JD. 2014. Integrating canonical and metabolic signalling programmes in the regulation of T cell responses. *Nat Rev Immunol* 14:435-46
134. Poppema S, Maggio E, van den Berg A. 2004. Development of lymphoma in Autoimmune Lymphoproliferative Syndrome (ALPS) and its relationship to Fas gene mutations. *Leukemia & lymphoma* 45:423-31
135. Powell JD, Delgoffe GM. 2010. The Mammalian Target of Rapamycin: Linking T Cell Differentiation, Function, and Metabolism. *Immunity* 33:301-11
136. Poy F, Yaffe MB, Sayos J, Saxena K, Morra M, et al. 1999. Crystal structures of the XLP protein SAP reveal a class of SH2 domains with extended, phosphotyrosine-independent sequence recognition. *Mol Cell* 4:555-61

137. Prado-Garcia H, Romero-Garcia S, Morales-Fuentes J, Aguilar-Cazares D, Lopez-Gonzalez J. 2011. Activation-induced cell death of memory CD8+ T cells from pleural effusion of lung cancer patients is mediated by the type II Fas-induced apoptotic pathway. *Cancer Immunology, Immunotherapy* 61:1065-80
138. Puthalakath H, Strasser A. 2002. Keeping killers on a tight leash: transcriptional and post-translational control of the pro-apoptotic activity of BH3-only proteins. *Cell Death Differ* 9:505-12
139. Qi H, Cannons JL, Klauschen F, Schwartzberg PL, Germain RN. 2008. SAP-controlled T-B cell interactions underlie germinal centre formation. *Nature* 455:764-9
140. Quann EJ, Liu X, Altan-Bonnet G, Huse M. 2011. A cascade of protein kinase C isozymes promotes cytoskeletal polarization in T cells. *Nat Immunol* 12:647-54
141. Quann EJ, Merino E, Furuta T, Huse M. 2009. Localized diacylglycerol drives the polarization of the microtubule-organizing center in T cells. *Nat Immunol* 10:627-35
142. Ramaswamy M, Cruz AC, Cleland SY, Deng M, Price S, et al. 2011. Specific elimination of effector memory CD4+ T cells due to enhanced Fas signaling complex formation and association with lipid raft microdomains. *Cell Death Differ* 18:712-20
143. Ramzan R, Weber P, Linne U, Vogt S. 2013. GAPDH: the missing link between glycolysis and mitochondrial oxidative phosphorylation? *Biochemical Society Transactions* 41:1294-7
144. Rao RR, Li Q, Odunsi K, Shrikant PA. 2010. The mTOR kinase determines effector versus memory CD8+ T cell fate by regulating the expression of transcription factors T-bet and Eomesodermin. *Immunity* 32:67-78
145. Refaeli Y, Van Parijs L, Alexander SI, Abbas AK. 2002. Interferon γ Is Required for Activation-induced Death of T Lymphocytes. *J Exp Med* 196:999-1005
146. Riou C, Yassine-Diab B, Van grevenynghe J, Somogyi R, Greller LD, et al. 2007. Convergence of TCR and cytokine signaling leads to FOXO3a phosphorylation and drives the survival of CD4+ central memory T cells. *J Exp Med* 204:79-91
147. Roberts AD, Ely KH, Woodland DL. 2005. Differential contributions of central and effector memory T cells to recall responses. *J Exp Med* 202:123-33
148. Roberts AD, Ely KH, Woodland DL. 2005. Differential contributions of central and effector memory T cells to recall responses. *The Journal of Experimental Medicine* 202:123-33
149. Röpke C, Gladstone P, Nielsen M, Borregaard N, Ledbetter J, et al. 1996. Apoptosis following interleukin‐2 withdrawal from T cells: evidence for a regulatory role of CD 18 (β2‐integrin) molecules. *Tissue Antigens* 48:127-35
150. Rosas M, Birkenkamp KU, Lammers J-WJ, Koenderman L, Coffer PJ. 2005. Cytokine mediated suppression of TF‐1 apoptosis requires PI3K activation and inhibition of Bim expression. *FEBS Letters* 579:191-8
151. Roychoudhuri R, Lefebvre F, Honda M, Pan L, Ji Y, et al. 2015. Transcriptional profiles reveal a stepwise developmental program of memory CD8(+) T cell differentiation. *Vaccine* 33:914-23

152. Rubinstein MP, Lind NA, Purton JF, Filippou P, Best JA, et al. 2008. IL-7 and IL-15 differentially regulate CD8+ T-cell subsets during contraction of the immune response. *Blood* 112:3704-12
153. Ruffo E, Malacarne V, Larsen SE, Das R, Patrussi L, et al. 2016. Inhibition of diacylglycerol kinase α restores restimulation-induced cell death and reduces immunopathology in XLP-1. *Sci Transl Med* 8
154. Russell JH, White CL, Loh DY, Meleedy-Rey P. 1991. Receptor-stimulated death pathway is opened by antigen in mature T cells. *Proc Natl Acad Sci USA* 88:2151-5
155. Saligrama PT, Fortner KA, Secinaro MA, Collins CC, Russell JQ, Budd RC. 2014. IL-15 maintains T-cell survival via S-nitrosylation-mediated inhibition of caspase-3. *Cell Death Differ* 21:904-14
156. Sallusto F, Geginat J, Lanzavecchia A. 2004. Central memory and effector memory T cell subsets: function, generation, and maintenance. *Ann rev immunol* 22:745-63
157. Sallusto F, Lenig D, Förster R, Lipp M, Lanzavecchia A. 1999. Two subsets of memory T lymphocytes with distinct homing potentials and effector functions. *Nature* 401:708-12
158. Sandalova E, Wei C-H, Masucci MG, Levitsky V. 2004. Regulation of expression of Bcl-2 protein family member Bim by T cell receptor triggering. *Proc Natl Acad Sci USA* 101:3011-6
159. Sarkar S, Teichgraber V, Kalia V, Polley A, Masopust D, et al. 2007. Strength of Stimulus and Clonal Competition Impact the Rate of Memory CD8 T Cell Differentiation. *J Immunol* 179:6704-14
160. Sato M, Liu K, Sasaki S, Kunii N, Sakai H, et al. 2013. Evaluations of the selectivities of the diacylglycerol kinase inhibitors r59022 and r59949 among diacylglycerol kinase isozymes using a new non-radioactive assay method. *Pharmacology* 92:99-107
161. Schenkel JM, Fraser KA, Masopust D. 2014. Cutting edge: resident memory CD8 T cells occupy frontline niches in secondary lymphoid organs. *J Immunol* 192:2961-4
162. Schenkel JM, Fraser KA, Vezys V, Masopust D. 2013. Sensing and alarm function of resident memory CD8+ T cells. *Nature Immunology* 14:509-13
163. Schenkel JM, Masopust D. 2014. Tissue-Resident Memory T Cells. *Immunity* 41:886-97
164. Schluns KS, Lefrançois L. 2003. Cytokine control of memory T-cell development and survival. *Nature rev Immunol* 3:269-79
165. Sengupta S, Peterson TR, Sabatini DM. 2010. Regulation of the mTOR complex 1 pathway by nutrients, growth factors, and stress. *Molecular cell* 40:310-22
166. Seward RJ, von Haller PD, Aebersold R, Huber B. 2003. Phosphorylation of the pro-apoptotic protein Bim in lymphocytes is associated with protection from apoptosis. *Mol Immunol* 39:983-93
167. She J, Matsui K, Terhorst C, Ju ST. 1998. Activation-induced apoptosis of mature T cells is dependent upon the level of surface TCR but not on the presence of the CD3 zeta ITAM. *International immunology* 10:1733-40

168. Sheng W, Wang T. 2009. Proteomic analysis of the differential protein expression reveals nuclear GAPDH in activated T lymphocytes. *PLOS One* 4:e6322
169. Sheridan BS, Lefrançois L. 2011. Regional and mucosal memory T cells. *Nature immunology* 12:485-91
170. Shiota M, Yang X, Kubokawa M, Morishima T, Tanaka K, et al. 2015. Somatic mosaicism for a NRAS mutation associates with disparate clinical features in RAS-associated leukoproliferative disease: a report of two cases. *Journal of clinical immunology* 35:454-8
171. Shlapatska LM, Mikhalap SV, Berdova AG, Zelensky OM, Yun TJ, et al. 2001. CD150 association with either the SH2-containing inositol phosphatase or the SH2-containing protein tyrosine phosphatase is regulated by the adaptor protein SH2D1A. *J Immunol* 166:5480-7
172. Sionov R, Vlahopoulos S, Granot Z. 2015. Regulation of Bim in Health and Disease. *Oncotarget* 6:23058-134
173. Smith JA, Poteet-Smith CE, Xu Y, Errington TM, Hecht SM, Lannigan DA. 2005. Identification of the first specific inhibitor of p90 ribosomal S6 kinase (RSK) reveals an unexpected role for RSK in cancer cell proliferation. *Cancer Res* 65:1027-34
174. Snow AL, Marsh RA, Krummey SM, Roehrs P, Young LR, et al. 2009. Restimulation-induced apoptosis of T cells is impaired in patients with X-linked lymphoproliferative disease caused by SAP deficiency. *J Clin Invest* 119:2976-89
175. Snow AL, Oliveira JB, Zheng L, Dale JK, Fleisher TA, Lenardo MJ. 2008. Critical role for BIM in T cell receptor restimulation-induced death. *Biol Direct* 3:34
176. Snow AL, Pandiyan P, Zheng L, Krummey SM, Lenardo MJ. 2010. The power and the promise of restimulation-induced cell death in human immune diseases. *Immunological reviews* 236:68-82
177. Spitaler M, Emslie E, Wood CD, Cantrell D. 2006. Diacylglycerol and protein kinase D localization during T lymphocyte activation. *Immunity* 24:535-46
178. Springael C, Thomas S, Rahmouni S, Vandamme A, Goldman M, et al. 2007. Rottlerin inhibits human T cell responses. *Biochem Pharmacol* 73:515-25
179. Stahl M, Dijkers PF, Kops G, Lens S, Coffer P, et al. 2002. The forkhead transcription factor FoxO regulates transcription of p27Kip1 and Bim in response to IL-2. *J Immunol* 168:5024-31
180. Steinert EM, Schenkel JM, Fraser KA, Beura LK, Manlove LS, et al. 2015. Quantifying Memory CD8 T Cells Reveals Regionalization of Immunosurveillance. *Cell* 161:737-49
181. Stemberger C, Neuenhahn M, Gebhardt FE, Schiemann M, Buchholz VR, Busch DH. 2009. Stem cell-like plasticity of naïve and distinct memory CD8+ T cell subsets. *Seminars in immunology* 21:62-8
182. Su EW, Moore CJ, Suriano S, Johnson C, Songalia N, et al. 2015. IL-2R α mediates temporal regulation of IL-2 signaling and enhances immunotherapy. *Sci Transl Med* 7
183. Sukumar M, Liu J, Ji Y, Subramanian M, Crompton JG, et al. 2013. Inhibiting glycolytic metabolism enhances CD8+ T cell memory and antitumor function. *Journal of Clinical Investigation* 123:4479-88

184. Tada S. 2007. Cdt1 and geminin: role during cell cycle progression and DNA damage in higher eukaryotes. *Front Biosci* 12:1629-41
185. Takagi M, Shinoda K, Piao J, Mitsuiki N, Takagi M, et al. 2011. Autoimmune lymphoproliferative syndrome-like disease with somatic KRAS mutation. *Blood* 117:2887-90
186. Tangye SG. 2014. XLP: clinical features and molecular etiology due to mutations in SH2D1A encoding SAP. *J Clin Immunol* 34:772-9
187. Tristan C, Shahani N, Sedlak TW, Sawa A. 2011. The diverse functions of GAPDH: Views from different subcellular compartments. *Cellular Signalling* 23:317-23
188. van der Windt GJ, Everts B, Chang C-HH, Curtis JD, Freitas TC, et al. 2012. Mitochondrial respiratory capacity is a critical regulator of CD8+ T cell memory development. *Immunity* 36:68-78
189. van der Windt GJ, O'Sullivan D, Everts B, Huang SC, Buck MD, et al. 2013. CD8 memory T cells have a bioenergetic advantage that underlies their rapid recall ability. *Proc Natl Acad Sci USA* 110:14336-41
190. Wang A, Rud J, Olson CM, Anguita J, Osborne BA. 2009. Phosphorylation of Nur77 by the MEK-ERK-RSK cascade induces mitochondrial translocation and apoptosis in T cells. *J Immunol* 183:3268-77
191. Wang R, Dillon CP, Shi L, Milasta S, Carter R, et al. 2011. The Transcription Factor Myc Controls Metabolic Reprogramming upon T Lymphocyte Activation. *Immunity* 35:871-82
192. Wang R, Green DR. 2012. Metabolic reprogramming and metabolic dependency in T cells. *Immunol Rev* 249:14-26
193. Wang X, Berger C, Wong CW, Forman SJ, Riddell SR, Jensen MC. 2011. Engraftment of human central memory-derived effector CD8+ T cells in immunodeficient mice. *Blood* 117:1888-98
194. Warburg O. 1956. On respiratory impairment in cancer cells. *Science* 124:269-70
195. Warr MR, Binnewies M, Flach J, Reynaud D, Garg T, et al. 2013. FOXO3A directs a protective autophagy program in haematopoietic stem cells. *Nature* 494:323-7
196. Wesselborg S, Kabelitz D. 1993. Activation-driven death of human T cell clones: time course kinetics of the induction of cell shrinkage, DNA fragmentation, and cell death. *Cell Immunol* 148:234-41
197. Wherry EJ, Teichgräber V, Becker TC, Masopust D, Kaech SM, et al. 2003. Lineage relationship and protective immunity of memory CD8 T cell subsets. *Nature immunology* 4:225-34
198. Wherry JE, Becker TC, Boone D, Kaja M-K, Ma A, Ahmed R. 2002. Homeostatic proliferation but not the generation of virus specific memory CD8 T cells is impaired in the absence of IL-15 or IL-15Ralpha. *Advances in experimental medicine and biology* 512:165-75
199. Windt GJW, Pearce EL. 2012. Metabolic switching and fuel choice during T - cell differentiation and memory development. *Immunol Rev* 249:27-42
200. Wojciechowski S, Jordan MB, Zhu Y, White J, Zajac AJ, Hildeman DA. 2006. Bim mediates apoptosis of CD127lo effector T cells and limits T cell memory. *Eur J Immunol* 36:1694-706

201. Wu C, Nguyen KB, Pien GC, Wang N, Gullo C, et al. 2001. SAP controls T cell responses to virus and terminal differentiation of TH2 cells. *Nat Immunol* 2:410-4
202. Xu X, Araki K, Li S, Han J-H, Ye L, et al. 2014. Autophagy is essential for effector CD8+ T cell survival and memory formation. *Nature Immunology* 15:1152-61
203. Yajima T, Yoshihara K, Nakazato K, Kumabe S, Koyasu S, et al. 2006. IL-15 regulates CD8+ T cell contraction during primary infection. *J Immunol* 176:507-15
204. Yang L, Kotomura N, Ho YK, Zhi H, Bixler S, et al. 2011. Complex cell cycle abnormalities caused by human T-lymphotropic virus type 1 Tax. *J Virol* 85:3001-9
205. Youle RJ, Strasser A. 2008. The BCL-2 protein family: opposing activities that mediate cell death. *Nat Rev Mol Cell Biol* 9:47-59
206. Yu L, McPhee CK, Zheng L, Mardones GA, Rong Y, et al. 2010. Termination of autophagy and reformation of lysosomes regulated by mTOR. *Nature* 465:942-6
207. Yuzefpolskiy Y, Baumann FM, Kalia V, Sarkar S. 2015. Early CD8 T-cell memory precursors and terminal effectors exhibit equipotent in vivo degranulation. *Cellular & molecular immunology* 12:400-8
208. Zhang L, Tschumi BO, Lopez-Mejia IC, Oberle SG, Meyer M, et al. 2016. Mammalian Target of Rapamycin Complex 2 Controls CD8 T Cell Memory Differentiation in a Foxo1-Dependent Manner. *Cell reports* 14:1206-17
209. Zhao F, Cannons JL, Dutta M, Griffiths GM, Schwartzberg PL. 2012. Positive and negative signaling through SLAM receptors regulate synapse organization and thresholds of cytolysis. *Immunity* 36:1003-16
210. Zhong XP, Hainey EA, Olenchock BA, Jordan MS, Maltzman JS, et al. 2003. Enhanced T cell responses due to diacylglycerol kinase zeta deficiency. *Nat Immunol* 4:882-90

APPENDIX A: Ratio of memory subsets at the time of isolation predict subsequent RICD sensitivity in derived effector CD8$^+$ T cells.

All data presented in this chapter is the sole work of S E Larsen.

INTRODUCTION

As discussed at length in previous chapters, the identification and characterization of various memory T cell subsets are an active area of research. Memory T cells are being evaluated to determine ideal subset phenotypes for adoptive transfer therapy, and define potential markers of optimal long-lived vaccine responses. CM and EM T cells are two of the most well characterized subsets to date. Upon adoptive transfer and rechallenge, CM- and EM-derived T cells develop equivalent effector potential, but differ greatly in the magnitude of T cell accumulation (193; 197). In Chapter 4, we determined that reduced sensitivity to CWID likely plays a significant role in the ability of CM T cells to maintain a larger effector T cell population after rechallenge. However, CWID is only relevant during the contraction phase of a T cell response when pathogen and antigen are cleared, and IL-2 beings to wane. More rapid control of pathogen by CM-derived T cells is more likely related to enhanced effector T expansion at the peak of the immune response, rather than late stage differences in cell death sensitivity during cytokine withdrawal. The magnitude of a T cell response is intimately controlled by RICD in the effector proliferative phase, as detailed in Chapters 2 and 3. We therefore also compared RICD sensitivity between CmE and EmE human T cells, derived as described in Chapter 4.

We hypothesized that reduced sensitivity to RICD in CM-derived T cells facilitates greater T cell accumulation and pathogen control as compared to EM-derived

T cells, as noted after adoptive transfer in mice. Here we demonstrate that in the majority of donors tested, primary human effector T cells derived from the $CD8^+$ CM T cell subset exhibit significantly lower sensitivity to RICD. However, our data suggests that the relative proportion of each memory subset at the time of isolation is predictive of subsequent RICD sensitivity differences between memory-derived effectors.

MATERIALS AND METHODS

Isolation, activation and culture of primary human CD8+ T cells

Blood from anonymous healthy donors (buffy coats) was generously provided by Dr. Michael Lenardo and the National Institutes of Health Blood Bank. PBMC were isolated using Ficoll density gradient centrifugation, and $CD8^+$ T cells were purified from PBMC using the EasySep Human $CD8^+$ T cell enrichment kit (Stem Cell Technologies). Enriched $CD8^+$ T cells were stained for 30 minutes on ice with anti-CD45RO-APC and anti-CD62L-FITC antibodies (BioLegend). Memory subsets were sorted on a BD FACS ARIA cell sorter. CM T cells were gated as $CD45RO^{hi}$ and $CD62L^{hi}$, EM T cells were gated as $CD45RO^{hi}$ and $CD62L^{lo}$. Sorted subsets were activated 1:1 with beads coated with anti-CD3/CD2/CD28 antibodies (Human T cell Activation/Expansion Kit, Miltenyi) in RPMI 1640 (Life Technologies) + 10% fetal calf serum (FCS) (Sigma) and 1% penicillin/streptomycin (Lonza) for 3 days. Activated T cells were washed in PBS and subsequently cultured in media as described above with 100 U/mL rIL-2 (PeproTech) at $1x10^6$ cells/mL for ≥14 days, changing media every 3 days.

Apoptosis assays and flow cytometry

Death assays were performed as previously described (85). Briefly, activated T cells (days 13-15) were treated in triplicate with either anti-CD3ε mAb OKT3 (5–500 ng/ml; Biogems) to induce RICD or anti-FAS agonistic antibody APO1.3 (1-500 ng/ml; Enzo) to trigger FAS-induced apoptosis, and plated at $7.5x10^5$ cells/mL in 96-well round bottom plates. For some assays, cells were pretreated for 30 min with 2 mM 2-deoxy-glucose (2-DG) or 5 mM rapamycin (Sigma-Aldrich) versus DMSO or ddH_20 solvent control. At 24h after TCR restimulation, cells were stained with 5 μg/mL propidium iodide (Sigma-

Aldrich) and collected for constant time on an Accuri C6 flow cytometer (BD Biosciences). Cell death was quantified as percentage cell loss = (1 – [number of viable cells (treated) / number of viable cells (untreated)]) x 100. For some assays, T cells were stained with Annexin V-FITC (Biolegend) at baseline and up to 8 hours after restimulation. Surface expression of FAS (CD95) and CD3 were assessed using anti-CD95-APC and anti-CD3-PE antibodies respectively (BioLegend). Surface expression of NTB-A was also measured using an anti-NTB-A-PE antibody (R&D). All flow cytometric assays were performed on an Accuri C6 flow cytometer (BD Biosciences).

Western Blotting

Activated $CD8^+$ T cells ($1x10^6$ per time point) were restimulated with 500 ng/ml OKT3 (0–4hr), washed in cold PBS, and lysed in 1% Nonidet P-40 (NP-40) lysis buffer (50 mM Tris [pH 7.4], 150 mM NaCl, 0.5 mM EDTA, 1% NP-40, 0.5% sodium deoxycholate, 1 mM Na_3VO_4, 1 mM NaF) containing complete protease inhibitors (Roche) for 30 min on ice. Cleared lysates were boiled in 2X reducing sample buffer, and resolved on Any kD SDS-PAGE gels (Bio-Rad). Proteins were transferred to nitrocellulose on a Trans-Blot Turbo system (Bio-Rad), blocked in 2% Tropix I-Block (Applied Biosystems) in TBS/0.1% Tween, and probed with the following Abs: anti-SAP (eBiosciences); anti-LCK (Santa Cruz Biotechnology); anti-phospho-Src Family (Tyr416) (Cell Signaling Technology); and anti–β-actin (Sigma-Aldrich). Antibodies bound to the membrane were detected using HRP-conjugated secondary Abs (Southern Biotech, eBioscience) and ECL (Thermo Scientific).

2-dimensional differential gel electrophoresis

CmE and EmE T cells (5x106) were restimulated for 4 hours with 500 ng/ml and cell pellets were flash frozen using liquid nitrogen. Frozen pellets were sent to Applied Biomics for further analysis. Briefly, analysis by 2-dimensional differential gel involves labeling each lysate with a specific dye (CmE-green; EmE-red), and then running the two samples together on a gel that separates proteins by both mass and charge. This allows researchers to identify protein 'spots' that are differentially expressed in the two samples. Spots selected are then identified by mass spectrometry.

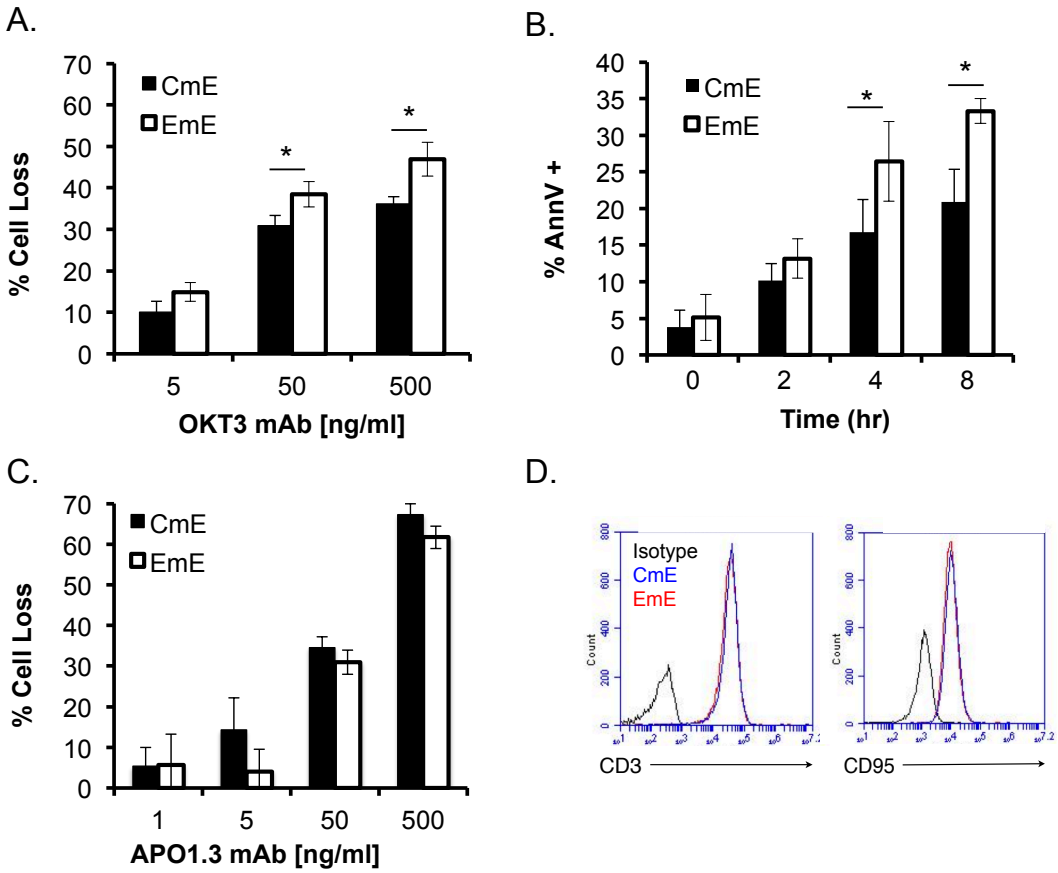
Statistics

In vitro cell death assays were evaluated using two-way ANOVA (α=0.05) with Sidak correction for multiple comparisons or students T-Test where appropriate. All statistical analyses were performed using GraphPad PRISM software. Error bars are defined in the figure legends as ± SEM or ± SD where appropriate. Asterisks denote statistical significance and p-values are reported in figure legends.

RESULTS

Effector T cells derived from CM and EM subsets were prepared and cultured as described in Chapter 4 in order to compare RICD sensitivity. Cells expanded for 13-14 days in IL-2 were restimulated through the TCR using the anti-CD3 antibody OKT3 and assayed for cell death by flow cytometry. Based on analysis of 17 human donors, EmE were significantly more sensitive to RICD than CmE, measured both by 24 hour PI exclusion and a shorter time course of Annexin V staining, an early marker of commitment to apoptosis (Fig. 19A-B). As previously demonstrated in Chapter 4, CmE did not exhibit a global apoptosis defect, as both CmE and EmE were equally sensitive to intrinsic stimuli (e.g. UV, staurosporine in Chapter 4) other extrinsic stimuli, such as direct ligation of the FAS death receptor (Fig. 19C). CmE and EmE T cells also displayed equivalent cell surface expression of T cell receptor (CD3) and FAS (CD95) (Fig. 19D). These data further demonstrate that differences displayed between CmE and EmE are specific to RICD, and likely represent 'imprinted' sensitivities derived from specific memory subsets.

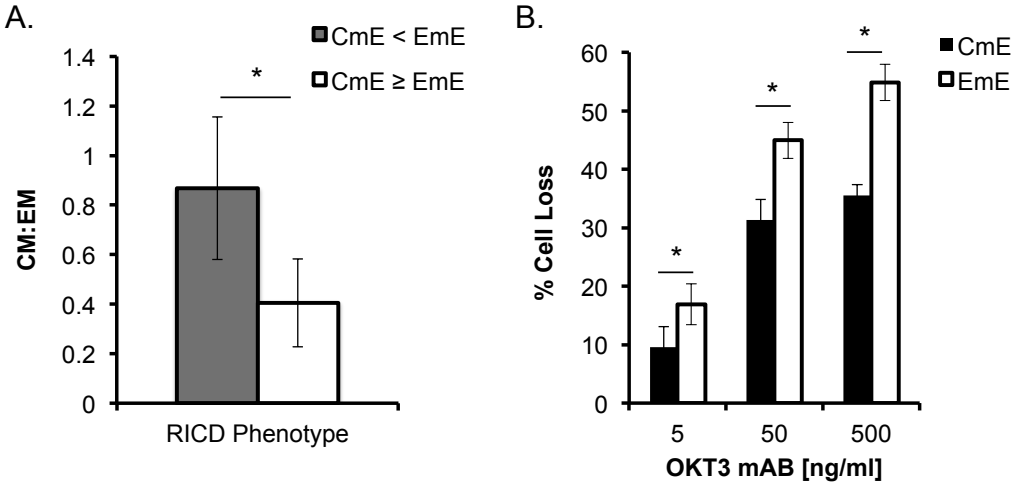
Figure 19. EmE T cells are more sensitive to RICD than CmE T cells. .
(A) Activated T cells were restimulated with OKT3 Ab for 24 hours; death was measured by PI staining and flow cytometry. Data represent % cell loss (avg ± SEM) for 17 individual donors. Two-way ANOVA analysis showed CmE-EmE OKT3 [5] n.s., [50] p=0.0140, [500] p=0.0004 . (B) Annexin V staining over time following OKT3 restimulation; data represent average ± SD for 3 individual donors. Two-way ANOVA analysis showed CmE-EmE 0hr n.s., 2hr n.s., 4hr p=0.0031, 8hr p=0.0008. (C) Activated T cells as in (A) were stimulated with anti-FAS agonistic Ab APO1.3 for 24 hrs to trigger FAS-induced apoptosis. Data represent % cell loss (avg ± SEM) for 3 individual donors. Two-way ANOVA analysis showed no significant differences for all doses of APO1.3. (D) Representative surface staining of CD3 (left) and CD95 (right) between CmE (blue) and EmE (red) T cells versus isotype control Ab (grey), assayed by flow cytometry


A.
% Cell Loss
CmE
EmE
OKT3 mAb [ng/ml]
B.
% AnnV +
Time (hr)
C.
% Cell Loss
APO1.3 mAb [ng/ml]
D.
Isotype
CmE
EmE
CD3
CD95

Interestingly, we noted extensive donor variability in the proportion of memory subsets at the time of isolation from PBMC, before effector T cell expansion was initiated. For example, the ratio of CM to EM at the time of FACS sorting varied from 0.1 to 1.46 (Fig. 20A). Additionally, we observed that not all donor CmE T cells exhibited lower RICD sensitivity when compared to EmE, and in some cases were slightly more sensitive. We decided to test whether the CM:EM ratio predicted a subsequent difference in RICD sensitivity between derived effector subsets. Indeed, when donors were divided based on the phenotypic difference in maximum RICD observed (i.e. CmE < EmE, or vice versa), we exposed a statistically significant difference in the CM:EM ratio at the time of isolation (Fig. 20A). Strikingly, we found that CM:EM ratio of 0.5 constituted a "threshold ratio" that separated and actually predicted the two RICD phenotypes (Fig. 20A). We distinguished this difference after acquiring data for half of our donors, and confirmed in all 8 subsequent donors that the CM:EM ratio predicted RICD outcomes. These results highlight the complexities of working with the outbred human population. Blood from the NIH blood bank is acquired from normal healthy donors and since the donation is anonymous there is minimal health history information available. Other known donor parameters such as age and gender did not segregate with the RICD sensitivity phenotype (data not shown). When we focused on donors with a CM:EM ratio of 0.5 or higher, we found a more profound average reduction in RICD sensitivity for CmE (Fig. 20B). Because our major objective was to identify molecular determinants that influence RICD sensitivity, we concentrated on those donors with a CM:EM ratio > 0.5 to attempt to better expose signaling differences and reduce possible underlying donor confounding factors.

Figure 20. CM:EM ratio predicts the difference in subsequent RICD sensitivity between memory-derived effector T cells.

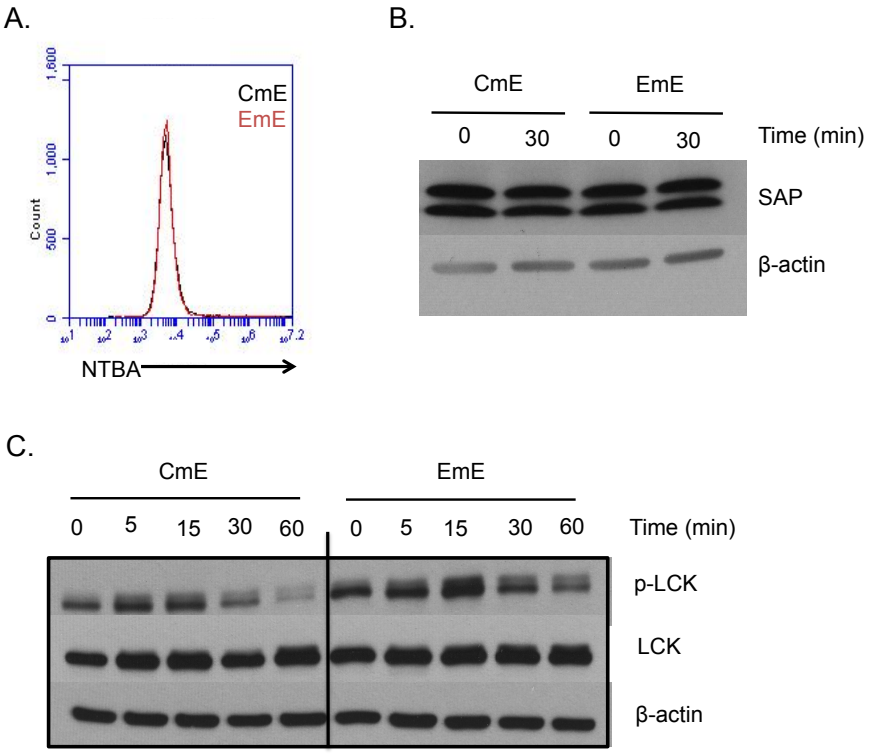
(A) 19 Donors were separated into two categories based on RICD sensitivity phenotypes: CmE < EmE (grey), and CmE ≥ EmE (white). Data represent average CM:EM ratio at the time of PBMC isolation. Student's T-test, p=0.0008. (B) RICD assay: data represent % cell loss (avg ± SEM) for 11 individual donors with a CM:EM ratio 0.5 and above. Two-way ANOVA analysis showed CmE-EmE OKT3 [5] p=0.0009, [50] p<0.0001, [500] p<0.0001.


A.
CmE < EmE
CmE ≥ EmE
CM:EM
1.4
1.2
1
0.8
0.6
0.4
0.2
0
*
RICD Phenotype
B.
CmE
EmE
% Cell Loss
60
50
40
30
20
10
0
*
*
*
5
50
500
OKT3 mAB [ng/ml]

We next examined specific proximal TCR signaling molecules known to influence RICD sensitivity. Our lab previously reported that the small adaptor protein SAP directly promotes RICD through binding to the SLAM family receptor NTB-A and recruiting the kinase LCK in order to propagate a strong TCR signal (84). By immunoblotting and flow cytometry, we noted no difference in the expression of SAP, NTB-A or LCK between CmE and EmE (Fig. 21A-C). However, EmE T cells exhibited greater basal phosphorylation of LCK at tyrosine 394, a marker of the active kinase. In fact, LCK (Y394) phosphorylation was enhanced and sustained over time following TCR restimulation in EmE compared to CmE (Fig. 21C). These results were corroborated with intracellular FACS staining (PhosFlow) for active phospho-LCK (data not shown). Although SAP and NTB-A expression did not differ, higher baseline activity and sustained LCK signaling over time suggests that EmE T cells have a relatively higher 'set point' for TCR signal strength. Because RICD sensitivity directly correlates with TCR signal strength, these data suggest that increased LCK-dependent proximal TCR signaling may preferentially push more EmE T cells past the threshold required to induce RICD.

Figure 21. Higher basal LCK activity and sustained TCR-induced LCK phosphorylation in EmE relative to CmE.

(A) Representative surface staining of NTB-A between CmE and EmE T cells by flow cytometry. (B) Lysates made from CmE and EmE T cells at baseline or after 30 minutes of OKT3 restimulation were separated by SDS-PAGE and immunoblotted for SAP. β-actin serves as a loading control. Data are representative of 3 independent experiments using different donors. (C) Lysates made from CmE and EmE T cells exposed to 0-60 minutes of OKT3 restimulation were separated by SDS-PAGE and immunoblotted for phospho-LCK (Y394) and total LCK. β-actin serves as a loading control. Data are representative of 3 independent experiments using different donors.


A.
B.
C.
CmE
EmE
Count
NTBA
Time (min)
SAP
β-actin
p-LCK
LCK

In order to determine if EmE and CmE T cells differed in their expression of key apoptotic regulators, we analyzed lysates from both subsets for the expression of key pro- and anti-apoptotic proteins using the R&D Apoptosis Proteome Profiler. Surprisingly, we detected no expression differences in the 35 apoptosis-related proteins between CmE and EmE at baseline, nor after 4 hours of OKT3 restimulation (data not shown). However, this array by no means represents the totality of proteins involved in regulating cell death. We therefore subjected lysates from OKT3-restimulated CmE and EmE T cells (4 hours) to an unbiased 2D differential gel electrophoresis (2D-DIGE) experiment (Applied Biosciences). Initial analysis identified ~35 differentially expressed proteins (spots) between CmE and EmE; the top 8 candidate spots were subsequently processed for mass spectrometry identification (Fig. 22A-B). Intriguingly, one protein identified as more highly expressed in EmE T cells was glyceraldehyde 3-phosphate dehydrogenase (GAPDH) (Fig. 22B). GAPDH has been extensively studied for its varied functions in different subcellular compartments (143; 187). Perhaps most importantly, GAPDH is the enzyme that catalyzes the sixth step of glycolysis (143; 187). Although GAPDH is often considered a housekeeping gene, its expression in T cells is dramatically upregulated following antigen stimulation, presumably in part to meet demands for increased glycolysis (10; 168)

Figure 22. Higher GAPDH expression in restimulated EmE T cells.
(A) Restimulated lysates from CmE (green) and EmE (red) T cells were labeled and subjected to 2-dimensional differential gel separation. Top 35 hits were identified based on dye ratio (white circles).

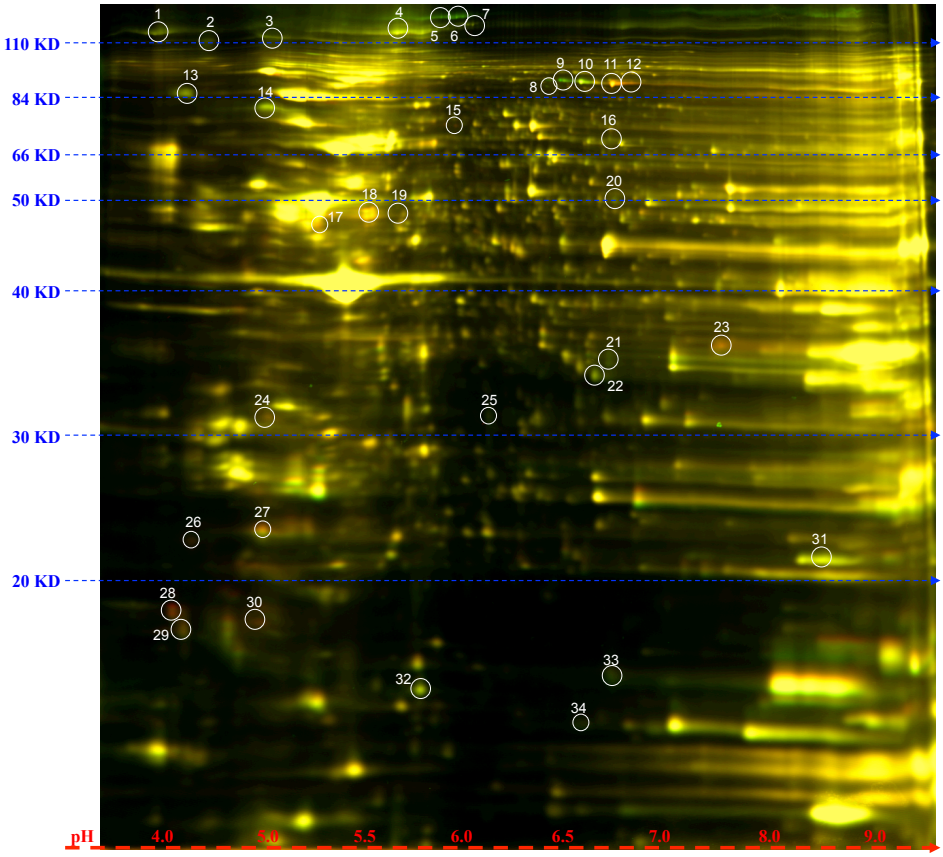
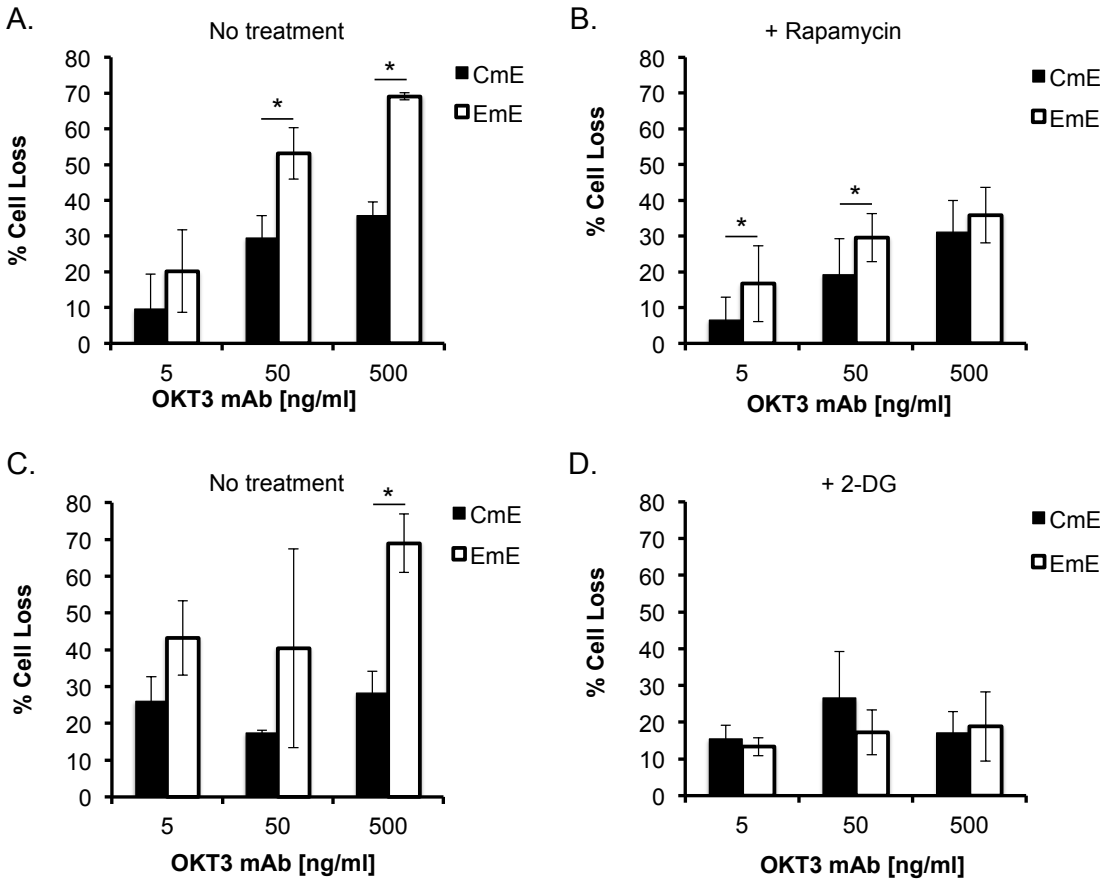

110 KD
84 KD
66 KD
50 KD
40 KD
30 KD
20 KD
pH
4.0
5.0
5.5
6.0
6.5
7.0
8.0
9.0
1
2
3
4
5
6
7
8
9
10
11
12
13
14
15
16
17
18
19
20
21
22
23
24
25
26
27
28
29
30
31
32
33
34

Table 2. MS-MS results from top 8 spots.

Spot Number	EM:CM ratio	Top-Ranked ID	Strength of ID
5	-3.3	Cyclin-dependent kinase 5	Very Poor
6	-3.5	Filamin-A	Great
9	-3.1	Baculoviral IAP repeat-containing protein 6 (BRUCE)	Very Poor
11	1.8	Elongation factor 2	Great
22	-1.4	Calponin-2	Great
23	1.5	Glyceraldehyde-3-phosphate dehydrogenase (GAPDH)	Good
23	1.5	Annexin A1 (ANXA1)	Good
28	2.1	S-phase kinase-associated protein (SKP1)	Good
28	2.1	Acidic leucine-rich nuclear phosphoprotein 32 family (ANP32A)	Good
35	-1.8	Myosin-9	Good

This suggested that EmE T cells might have an altered metabolism, and specifically might be undergoing more glycolysis than CmE T cells. In order to test this notion, we first treated cells with the mTOR inhibitor, rapamycin, and noted that a specific reduction in EmE T cell RICD sensitivity relative to CmE T cells (Fig 23A-B). Additionally, when we treated cells with the competitive glucose analog 2-DG, we again noted a similar reduction in EmE T cell RICD sensitivity that matched the amount of cell death measured for CmE T cells (Fig. 23C-D). These results suggest that a higher glycolytic metabolism in EmE T cells could be partly responsible for greater RICD sensitivity in this subset, compared to CmE.

Figure 23. Greater RICD sensitivity of EmE is linked to glycolytic metabolism. (A-B) CmE and EmE T cells were left untreated (A) or pre-treated with rapamycin (B) and restimulated with OKT3 Ab for 24 hours; cell death was measured by PI staining and flow cytometry. Data represent % cell loss (avg ± SEM) for 3 individual donors. Two-way ANOVA analysis showed (A) CmE-EmE OKT3 [5] n.s., [50] p=0.0193, [500] p=0.0054, (B) CmE-EmE OKT3 [5] p=0.0198, [50] p=0.0184, [500] n.s. (C-D) CmE and EmE T cells were left untreated (C) or pre-treated with 2-DG (D) and restimulated with OKT3 Ab for 24 hours; cell death was measured by PI staining and flow cytometry. Data of a representative donor % cell loss (avg ± SD). Two-way ANOVA analysis showed (C) CmE-EmE OKT3 [5] n.s., [50] n.s., [500] p=0.0062, (D) CmE-EmE OKT3 [5] n.s., [50] n.s., [500] n.s.


A.
No treatment
% Cell Loss
OKT3 mAb [ng/ml]
CmE
EmE
B.
+ Rapamycin
C.
No treatment
D.
+ 2-DG

DISCUSSION

When memory T cells are rechallenged with antigen, they produce a larger effector T cell population than that generated during a primary naïve T cell response, assuring faster removal of the associated pathogen upon second encounter. However, it is well documented that not all memory subsets derive equally sized effector T cell pools and therefore vary in the speed and efficiency with which they are able to control and/or eliminate a pathogen (193; 197). The studies described here, along with Chapter 4, highlight our discovery of important differential cell death sensitivities between memory subset-derived effector T cells. Collectively this work implies that CM T cells are better equipped to generate large effector T populations in part through decreased RICD susceptibility, compared to EM T cells.

Here we determined that both CmE and EmE T cells are equally competent to die via extrinsic apoptosis stimuli, as demonstrated by equally high sensitivity to direct FAS ligation. Yet in a majority of donors, CmE T cells were less sensitive to RICD than EmE T cells. Interestingly, the ratio of CM to EM T cells at the time of isolation became a high fidelity, significant predictor of subsequent RICD sensitivity, such that in donors with a ratio above 0.5, CmE T cells were less sensitive to RICD than EmE T cells. Gender and age, two other known donor parameters, did not segregate RICD phenotypes. More work is required to determine what genetic or environmental factors influence this ratio at any given time in humans. Although blood samples were acquired from normal healthy donors, there is no way of determining the time since an individual's last infection or illness. We believe recent infection history or inflammation may have a significant effect on both the proportion of memory T cell subsets and the relative 'activation status' of

isolated T cells. In support of this theory, earlier studies determined that more rested memory cells, i.e. memory T cells given increased time between primary and secondary challenge, produced more robust recall responses than more recently-generated memory T cells in a mouse model (147). Since CM T cells are more long-lived *in vivo* than EM T cells, we speculate that a larger ratio of CM to EM may also identify donors with more time since a recent infection (103; 108; 148; 193; 197). In other words, CM T cells are able to undergo more homeostatic proliferation and self-renewal, while EM T cells have little to no self-renewal ability. Thus EM numbers may wane with time as CM remain relatively constant. This reduction of EM T cells over time would increase the CM:EM ratio, and as such may identify 'more rested' healthy donors. It will be of interest to corroborate this idea with other markers of recent infection at the time of isolation, such as serum levels of C-reactive protein or active complement components like C3a.

Given our overarching goal of identifying novel molecular determinants that influence RICD sensitivity, we began exploring the mechanism behind our main observation (i.e. RICD in CmE < EmE) using only those donors who had a CM:EM ratio above 0.5. Isolating these donors in this manner helped to both optimize the differential RICD sensitivity between derived effectors, and possibly remove uncontrolled confounding factors like recent infections. CmE and EmE T cells equally expressed proximal signaling proteins we know influence RICD sensitivity, including SAP, NTB-A and LCK. However, we did note that EmE T cells harbored greater basal and TCR-induced LCK phosphorylation on Tyr394, with sustained activity after TCR restimulation compared to CmE. This suggests that EmE T cells might maintain a higher 'activation state' of TCR-associated signaling components. This higher set point likely allows a

greater proportion of EmE T cells to readily reach the threshold required for *de novo* induction of pro-apoptotic molecules and RICD execution following TCR re-engagement. More work is required to determine if CmE are more capable of actively modulating TCR signaling, perhaps via greater expression or activity of known phosphatases (e.g. SHP-1). In addition, it will be of interest to examine donors with CM:EM ratio below 0.5 to determine if these molecular hallmarks are equilibrated or even reversed between CmE and EmE.

Our early survey of pro- and anti-apoptotic protein expression revealed no differences in CmE versus EmE at steady state, although those proteins induced after TCR restimulation remain to be carefully compared. In order to examine differential protein expression between CmE and EmE T cells in a non-biased manner, we subjected lysates from 4 hour restimulated cells to 2-dimensional differential gel electrophoresis (2D-DIGE) analysis. Mass spectrometry profiling uncovered increased expression of GAPDH in EmE T cells, and a possible role for metabolism in differential RICD sensitivity between CmE and EmE. We therefore inhibited mTOR, the major molecular complex involved in integrating and regulating growth signals, and glycolysis to determine if anabolic metabolism was promoting RICD sensitivity in our memory-derived effector T cells. When treated with rapamycin or 2-DG, CmE T cell RICD sensitivity was not dramatically changed, but EmE T cell sensitivity decreased significantly. Importantly, rapamycin and 2-DG treatment reduced EmE T cell RICD sensitivity to the same level measured for CmE. These data suggest that heightened glycolytic metabolism in EmE T cells is responsible for higher RICD sensitivity compared to CmE. Further work is needed to examine downstream consequences of

greater glycolytic metabolism in EmE, employing analyses performed in Chapter 3. For example, greater glycolytic metabolism in EmE may predict more FasL induction after TCR restimulation, at least for donors with a CM:EM ratio >0.5.

In summation, we propose a mechanism whereby EmE T cells maintain higher TCR signaling potential, in turn promoting mTOR activation and glycolysis, which all results in higher RICD sensitivity compared to CmE T cells for most individuals. More importantly, our findings on CmE and EmE T cells represent a translational paradigm for future studies of determinants of RICD sensitivity in humans. Regulating both proliferative and apoptotic checkpoints involved in optimal memory responses may directly influence vaccine strategies, particularly for prime-boost timing. These data further underscore the importance of comprehensively investigating the determinants of differential apoptosis sensitivity in memory T cell subsets.